Introducing height to mechanobiology

Introducing height to mechanobiology
A tissue engineering perspective

ISBN: 978-94-6380-834-7

The work described in this thesis was carried out at the Department of Complex Tissue Engineering of the MERLN institute for Technology-Inspired Regenerative Medicine (Maastricht University, The Netherlands).

This research was funded by the European Research Council starting grant "Cell Hybridge" under the Horizon2020 framework program (Grant #637308).

Lay out: Jip Zonderland
Cover design: Jip Zonderland
Printed by : Gildeprint

Introducing height to mechanobiology
A tissue engineering perspective

Dissertation

To obtain the degree of Doctor at Maastricht University, on the authority of the Rector Magnificus Prof. dr. Rianne M. Letschert in accordance with the decision of the Board of Deans, to be defended in public on Wednesday, 1st of July 2020, at 16:00 hours.

by

Jip Zonderland

Born on the 12th of September 1992 in Delft

Promotor:
Prof. Dr. Lorenzo Moroni

Co-promotor:
Prof. Dr. Clemens van Blitterswijk

Assessment committee:
Prof. Dr. Martijn van Griensven (Chair)
Prof. Dr. Gijsje Koenderink (Technische Universiteit Delft)
Prof. Dr. Boris Kramer
Prof. Dr. Gerjo van Osch (Erasmus MC)
Prof. Dr. Lodewijk van Rhijn

Table of contents

List of abbreviations

AM	Additive manufactured
ASAP	L-Ascorbic acid 2-phosphate
bFGF	Basic fibroblast growth factor
BSA	Bovine serum albumin
CDC42	Cell division control protein 42
CytoD	Cytochalasin D
ECM	Extra cellular matrix
EDC	1-ethyl-(dimethylaminopropyl)-carbodiimide
ES	Embryonic stem cell
ESP	Electrospun
FAK	Focal adhesion kinase
FBS	Fetal bovine serum
FDM	Fused deposition modeling
FGFR1	Fibroblast growth factor receptor 1
GFP	Green fluorescent protein
H&E	Hematoxylin and eosin
HEK	Human embryonic kidney
HFIP	Hexafluoroisopropanol
HIF	Hypoxia-inducible factor
hMSC	Human mesenchymal stromal cell
iPS	Induced pluripotent stem cell
LINC	Linker of nucleoskeleton and cytoskeleton
MES	M 2-(N-morpholino) ethanesulfonic acid (MES)
MLC	Myosin regulatory light chain
MLC2	Myosin light chain 2
MRTF	Myocardin related transcription factor
MT1-MMP	Membrane-type 1 matrix metalloproteinase
NHS	N-hydroxysuccinimide
NM-II	Non-muscle myosin II
OCT	Optimal cutting temperature compound
P/S	Penicillin-streptomycin
PBS	Phosphate-buffered saline
PBT	Poly(butylene terephthalate)
PEG	Poly(ethylene glycol)
PEOT	Poly(ethylene oxide terephthalate)
PPAR-γ	Peroxisome proliferator-activated receptor gamma
PS	Polystyrene

RGD	Arginine-Glycine-Aspartic acid
ROCK	Rho-associated protein kinase
ROS	Reactive oxygen species
SCR	Scrambled
SRF	Serum response factor
STC1	Stanniocalcin-1
TAZ	Transcriptional coactivator with PDZ-binding motif
TBS	Tris-buffered saline
TCP	Tissue culture plastic
VEGF	Vascular endothelial growth factor
VOI	Volume of interest
YAP	Yes-associated protein

Chapter 1

General introduction

Jip Zonderland

The human body has a remarkable ability to regenerate damaged tissues. Even in tissues that regenerate well, such as muscle, bone or skin, regeneration is incomplete when damage is excessive and large volumes of tissue are affected. The field of regenerative medicine develops strategies to aid the body in regenerating damaged tissues, for example through pharmacological approaches or (stem) cell transplantations. Biomaterials can be used as scaffolds with these approaches to fill up sections of empty space in damaged tissues. The most commonly used types of scaffolds are hydrogels, electrospun- (ESP) and additive manufactured scaffolds. Each scaffold can be made from either natural or synthetic materials. Each scaffold type has its own benefits and drawbacks, characterized mainly by the biomaterial of choice and its fabrication method, and their use depending on the specific tissue application.

Hydrogels form a relatively soft structure of hydrated polymers. Cells can easily be distributed throughout the hydrogel and can easily be fit into a specific defect's shape. However, hydrogels can bear little mechanical loading. Electrospinning is a technique where polymers are dissolved in a volatile solvent and attracted to a collector by an electrostatic field. While traveling to the collector, the solvent evaporates and the polymer is stretched out due to an instable jet, and nano- to micro-sized fibers are deposited. The resulting fibrous ESP scaffolds mimic the fibrous nature of ECM and are highly porous, allow cell growth and nutrient diffusion, but cell infiltration is often limited. Additive manufactured scaffolds are often made by melting polymers and depositing these into a specific shape layer by layer. These scaffolds often form relatively strong structures but can be difficult to fully fill with the desired tissue due to the large pores.

Each type of scaffold can be modified in many ways to change scaffold architecture and properties such as the bulk- and local stiffness, surface chemistry and topography. Additionally, proteins can be attached to or released from the scaffolds. Each of these properties influences the cells' behavior, ultimately determining whether new functional tissue will be formed and if regeneration will be successful. It is, therefore, critical to understand how these properties influence cell behavior from a more fundamental perspective, as such knowledge could be funneled back into improved scaffold design and regenerative medicine strategies.

Human mesenchymal stromal cells (hMSCs) have been central in this thesis. hMSCs are the most widely used cells for tissue engineering and their differentiation capacity is highly dependent on mechanobiology[1, 2]. Besides their use in tissue engineering, hMSCs are also utilized for their secretome. The wide range of secreted factors has a beneficial influence on tissue regeneration, modulating the immune-response and angiogenesis, among other effects[3-5]. Hence, the focus of the thesis has been twofold: on one side to increase a fundamental understanding of mechanobiology in 3D, and on the other side to develop novel scaffolds that can be used as tissue engineering scaffolds or to study mechanobiology in 3D.

Mechanobiology can be defined as the process of transducing mechanical signals to biological signals. It is well known that mechanical signals, such as material stiffness, greatly influence cell behavior. Although the underlying biological mechanisms behind mechanobiology are well studied, the research upon which this understanding is built has been mostly done on flat, 2D cell culture surfaces. Increasing evidence demonstrates that the role and regulation of mechanobiological pathways are different when cells are in a 3D matrix[6-8]. For tissue engineering applications, or for other applications where cells are implanted *in vivo*, cells will inevitably be exposed to a 3D environment. For this reason, a deep understanding of mechanobiology in 3D is required. Most of the current literature investigating 3D mechanobiology is done in 3D hydrogels. While hydrogels mimic the hydrated state of extra cellular matrix (ECM)[9, 10], most tissue engineering applications utilize scaffolds made from stiffer materials for their superior mechanical properties, such as ESP- or additive manufactured scaffolds. These stiffer 3D environments remain virtually unexplored in the field of mechanobiology. Hence, in **chapter 2** we summarize the current literature of 3D mechanobiology, focusing on tissue engineering applications of MSCs. We highlight the differences between the influence of matrix properties on MSC differentiation in 2D and 3D. For example, in 2D, stiffness plays a dominant role in guiding MSC differentiation, while in 3D stiffness seems to play a subordinate role, with a dominant role for matrix remodeling. In addition, differences in the role and regulation of some of the key players in the mechanotransduction pathways in 2D and 3D environments are explored.

In **chapters 3-5** of this thesis, I have set out to explore MSC behavior and the underlying mechanobiological mechanisms in common 3D tissue engineering constructs, namely electrospun- (ESP) and additive manufactured scaffolds. Starting with a better understanding of mechanobiology in tissue engineering scaffolds, I studied differentiation, cell survival and proliferation. On top of building fundamental knowledge, in **chapters 6-8**, I have developed different electrospun scaffolds that can be used for tissue engineering as well as to advance fundamental biological research.

Most of the sparse 2D vs 3D mechanobiology research is done in hydrogels, while little has been done in stiffer tissue engineering scaffolds. **Chapter 3** investigates how dimensionality changes the actin network in common 3D tissue engineering scaffolds: additive manufactured- and electrospun scaffolds. We found that the 3D environment reduces focal adhesions, lamin A and C expression, myosin phosphorylation and YAP nuclear localization. In 2D, this is a cellular phenotype of human MSCs (hMSCs) on soft matrices and preferred adipogenic differentiation, but the hMSCs were cultured in stiff materials and exhibited exclusive osteogenic differentiation. This paper highlights the differences in hMSC differentiation and mechanobiology in 2D vs 3D in common tissue engineering scaffolds.

To aid mechanobiology research in 2D and 3D, the **appendix of chapter 3** describes a tool for researchers to investigate the actin distribution in cells. Changes in actin structure and distribution have great effects on cellular tension and a freely available tool to reliably

quantify this in differently shaped cells was not available. We have developed a pipeline using a Fiji macro and R, both freely available software, to easily quantify actin or any other staining distribution in cells.

With a better understanding of the differences in mechanotransduction in 2D vs. 3D, we next investigated role of mechanobiology in cell survival. Stanniocalcin-1 (STC1) plays an important role in cell survival and tissue regeneration, but its regulation is largely unstudied. While most studies looked at STC1 in cell survival conditions, a few researchers demonstrated a change in STC1 secretion in 3D cultures, which triggered us to investigate its regulation more closely. Hence, in **Chapter 4** we show that stanniocalcin-1 secretion is regulated through a mechanosensitive pathway of zyxin, actin-myosin and Rho-associated protein kinase (ROCK). 3D ESP scaffolds and 3D alginate hydrogels also affect the stanniocalcin-1 secretion. As STC1 is involved in MSC survival and proliferation, understanding how this protein is regulated in 3D scaffolds could aid tissue engineering applications.

Besides cells survival, proliferation is important to control in tissue engineering constructs. **Chapter 5** looks at the proliferation of hMSCs and how this is affected by the microfibrillar environment of electrospun scaffolds. We demonstrate a reduction of fibroblast growth factor receptor 1 (FGFR1) in hMSCs cultured on ESP scaffolds, making them irresponsive to basic fibroblast growth factor (bFGF). This was found to be regulated through actin-myosin and the myocardin-related transcription factor/serum response factor (MRTF/SRF) pathway in hMSCs, fibroblasts and cancer cells. Proliferation and cell density are crucial for tissue engineering approaches and 7% of all cancers have FGFR aberrations[11], making this research interesting for both fields.

Besides building fundamental biological knowledge, in the last three chapters I set out to develop novel scaffolds for both tissue engineering purposes and as tools to study 3D cell biology. After exploring cell survival and proliferation, we looked at cell migration. Cell migration is important for tissue regeneration and tissue engineering to get the cells in the right location and to fill 3D scaffolds with cells and *de novo* tissue. Cell migration has been widely studied in 2D, and to a lesser extend in 3D hydrogels, but very little research has been done in other 3D scaffolds. ESP scaffolds exhibit notoriously little cell infiltration due generally small pores. In **Chapter 6**, we developed an ESP scaffold that allows robust cell infiltration. We optimized the ESP scaffold by tweaking fiber diameter and co-spinning sacrificial polymers, which yielded a thick ESP scaffold that was fully infiltrated *in vivo*. Using a transwell system, we developed a platform in which guided, cellular migration through a 3D fibrous mesh can easily be investigated. This research can therefore directly contribute to both tissue engineering applications and fundamental research on 3D cell migration.

Guided migration follows gradients and tissues are full of biological and physical gradients. **Chapter 7** further utilizes electrospinning to create ESP scaffolds with a gradient of functional groups or pore size and fiber diameter. As in chapter 6, these scaffolds could be used to improve tissue engineering and study biological processes such as 3D cell migration.

Having investigated 3D mechanobiology, cell survival, proliferation and developed new scaffolds to study migration in ESP scaffolds, we lastly used ESP scaffolds for *in vivo* delivery of hMSCs. **Chapter 8** describes the development and testing of the hydrocup: a hollow, cup shaped, ESP scaffold that can be used to fix implanted hydrogels in place. hMSCs are utilized here for their secretome and we show that the hydrocup allows for functional cytokines to be secreted. Six weeks after *in vivo* implantation, the soft hydrogels are still found in place inside the hydrocup. The hydrocups could be used for specific on-site delivery of cytokine secreting cell, or drug-releasing hydrogels. Similar to chapter 6 and 7, the scaffold developed in chapter 8 could be used both for regenerative medicine purposes and for fundamental research about environmental influences on hMSC cytokine release *in vivo*.

Chapter 9 puts the results of this thesis into perspective of the current literature and future directions are discussed.

In **Chapter 10**, the possibilities to valorize the research in this thesis are explored, with a specific focus on the hydrocup of chapter 8. As the hydrocup is the first hydrogel-delivery scaffold and shows promising preliminary results, it is a potential product with applications in a wide range of injuries and diseases.

References

1. J. Hao, Y. Zhang, D. Jing, Y. Shen, G. Tang, S. Huang, and Z. Zhao, Mechanobiology of mesenchymal stem cells: Perspective into mechanical induction of MSC fate. Acta Biomater, 2015. 20: p. 1-9.
2. A.B. Castillo and C.R. Jacobs, Mesenchymal Stem Cell Mechanobiology. Current Osteoporosis Reports, 2010. 8(2): p. 98-104.
3. J. Xi, X. Yan, J. Zhou, W. Yue, and X. Pei, Mesenchymal stem cells in tissue repairing and regeneration: Progress and future. Burns Trauma, 2013. 1(1): p. 13-20.
4. Y. Zhou, Y. Yamamoto, Z. Xiao, and T. Ochiya, The Immunomodulatory Functions of Mesenchymal Stromal/Stem Cells Mediated via Paracrine Activity. J Clin Med, 2019. 8(7).
5. S. Meirelles Lda, A.M. Fontes, D.T. Covas, and A.I. Caplan, Mechanisms involved in the therapeutic properties of mesenchymal stem cells. Cytokine Growth Factor Rev, 2009. 20(5-6): p. 419-27.
6. S.R. Caliari, S.L. Vega, M. Kwon, E.M. Soulas, and J.A. Burdick, Dimensionality and spreading influence MSC YAP/TAZ signaling in hydrogel environments. Biomaterials, 2016. 103: p. 314-323.
7. Y. Tang, R.G. Rowe, E.L. Botvinick, A. Kurup, A.J. Putnam, M. Seiki, V.M. Weaver, E.T. Keller, S. Goldstein, J. Dai, D. Begun, T. Saunders, and S.J. Weiss, MT1-MMP-dependent control of skeletal stem cell commitment via a beta1-integrin/YAP/TAZ signaling axis. Dev Cell, 2013. 25(4): p. 402-16.
8. S. Khetan, M. Guvendiren, W.R. Legant, D.M. Cohen, C.S. Chen, and J.A. Burdick, Degradation-mediated cellular traction directs stem cell fate in covalently crosslinked three-dimensional hydrogels. Nat Mater, 2013. 12(5): p. 458-65.
9. K.A. Kyburz and K.S. Anseth, Synthetic mimics of the extracellular matrix: how simple is complex enough? Annals of biomedical engineering, 2015. 43(3): p. 489-500.
10. H. Geckil, F. Xu, X. Zhang, S. Moon, and U. Demirci, Engineering hydrogels as extracellular matrix mimics. Nanomedicine (London, England), 2010. 5(3): p. 469-484.
11. T. Helsten, S. Elkin, E. Arthur, B.N. Tomson, J. Carter, and R. Kurzrock, The FGFR Landscape in Cancer: Analysis of 4,853 Tumors by Next-Generation Sequencing. Clin Cancer Res, 2016. 22(1): p. 259-67.

Chapter 2

Steering cell behavior through mechanobiology in 3D: a regenerative medicine perspective

Jip Zonderland, Lorenzo Moroni

Complex Tissue Regeneration Department, MERLN Institute for Technology-Inspired Regenerative Medicine, Maastricht University, Maastricht, the Netherlands.

Abstract

Mechanobiology, translating mechanical signals into biological ones, greatly affects cellular behavior. Steering cellular behavior for cell-based regenerative medicine approaches requires a thorough understanding of the orchestrating molecular mechanisms, among which mechanotransducive ones are being more and more elucidated. Differentiation and proliferation of the most widely used stem cells for tissue engineering applications, mesenchymal stromal cells, is highly mechanotransduction dependent. While the mechanotransduction pathways are relatively well-studied in 2D, much remains unknown of the role and regulation of these pathways in 3D. Ultimately, cells need to be cultured in a 3D environment to create functional *de novo* tissue. In this review, we explore the literature on the roles of different material properties on cellular behavior and mechanobiology in 2D and 3D. For example, while stiffness plays a dominant role in 2D MSC differentiation, it seems to be of subordinate importance in 3D MSC differentiation, where matrix remodeling seems to be key. Also, the role and regulation of some of the main mechanotransduction players are discussed, focusing on mesenchymal stromal cells.

Introduction

Mechanobiology is an emerging field investigating the translation of physical forces into molecular biological signals. These forces can greatly impact cell behavior, countering or synergizing with other cellular signals from soluble factors. A fundamental understanding of mechanobiology is of importance for many different research areas. In the fields of tissue engineering and regenerative medicine, this fundamental understand is being translated to practical applications, but many challenges still remain. One of the hurdles is that the basic machinery of this system is fairly well established in 2D, but research in 3D is still in its early stages. In order to create functional tissues, cells need to be in a 3D environment. Recent studies illustrate the differences in cell behavior and mechanobiology in 2D vs 3D, which will be discussed in detail in this review. To design smart materials for tissue engineering, a thorough understand of mechanobiology in 3D is critical. In this review, we will briefly go over the current understanding of mechanobiology in 2D and go deeper into how this translates to a 3D environment.

We will focus on the role of mechanobiology in 3D tissue engineering and regenerative medicine. While mesenchymal stromal cells (MSCs) are the most widely used cell-type for tissue engineering, they are also a nice cell-type model for mechanobiological studies because their multi-potent differentiation potential is highly dependent on mechanobiology. For these reasons, MSCs will be take center stage in this review. While well-established in 2D, we will discuss how the extra cellular properties affect cell behavior in 3D and how this is different compared to 2D.

Cell morphology is another well-studied variable in 2D that can greatly influence MSC differentiation. Here, we will explore the influence of cell morphology and cell volume on MSC differentiation in 2D and 3D. Then, we will travel through the cell, discussing integrins, actin-myosin, Rho and ROCK, mechano-sensitive transcription factors and the nuclear lamina, focusing on their role in steering cell behavior in 3D. First, a brief general introduction to mechanobiology will be given, after which we will explore how this is similar or different in 3D environments. The reader is referred to excellent in-depth reviews on these topics that are mentioned throughout the text, for more focused reading on specific sub-sections of this review.

General introduction to mechanobiology

MSCs can differentiate to bone, fat and cartilage and are therefore widely used in tissue engineering applications (for specific MSC reviews the reader is directed to:[1, 2]). In 2D, MSCs are well studied and their lineage commitment and efficiency of differentiation is highly dependent on mechanobiology. Initial studies showed that MSCs on stiff substrates differentiated preferentially to bone, while soft substrates aided adipogenic and chondrogenic differentiation[3, 4]. Since then, a number of material properties besides stiffness have been identified in 2D as potent guiders of cell behavior. These include, among

others, material properties such as chemistry, degradability, stress-relaxation, nano- and microtopography, ligand type and density and externally applied force[5-7]. Besides MSCs, these material properties also influence the proliferation and differentiation of other cell types, such as pluripotent stem cells (induced (iPS), or embryonic (ES)), muscle stem cells, fibroblasts, adipocytes, osteoblasts, chondrocytes, among others[5, 8].

These effects of extra cellular properties are orchestrated by a machinery of mechanosensitive proteins[9]. A cell adheres to the extra cellular matrix using integrins. Different combinations of α and β integrins can recognize different adhesion sides on extra cellular matrix (ECM) proteins, such as the widely used RGD-motif on fibronectin, or to other motives on other ECM proteins (for a specific integrin review the reader is directed to:[10]). When the integrin dimer binds to a ligand and force is applied, early focal adhesion proteins such as focal adhesion kinase (FAK), paxillin and talin, among others, bind to the intracellular part of the integrin subunits. This starts a cascade that will cluster integrins and recruit other proteins to the focal adhesions, including zyxin, vinculin and actin filaments. When enough force is applied, these focal adhesions will mature into large protein complexes, creating a trans-membrane connection from the ECM, through multiple integrin dimers, to the actin cytoskeleton (for focused focal adhesion reviews, the reader is referred to:[10-12]). Force on integrins is applied extracellularly, and/or intra-cellularly. An important force-generating element in cells are actin filaments with incorporated non-muscle myosin II (NM-II). Actin-myosin filaments join together to form large contractile bundles that exert force on the focal adhesions, creating tension in the cell (for a thorough actin-myosin review, we suggest:[13]). The actin-myosin filaments can be connected to two focal adhesions, or a focal adhesion and the nucleus. The actin-myosin filaments connect to the nucleus through the linker of nucleoskeleton and cytoskeleton (LINC) complex[14]. The LINC complex bridges both nuclear membranes and connects to the nuclear lamina. The nuclear lamina is a meshwork of proteins just under that inner nuclear membrane that gives structural integrity to the nucleus[15, 16]. The cellular tension leads to changes in gene expression through a number of different pathways. Mechanosensitive transcription factors such as Yes-associated protein (YAP), transcriptional coactivator with PDZ-binding motif (TAZ), myocardin related transcription factor (MRTF), and serum response factor (SRF), directly affect gene expression when translocated to the nucleus due to mechanical tension in the cell (the reader is referred to detailed reviews on YAP/TAZ[17] and MRTF/SRF[18, 19]). The nuclear lamina can also change gene expression upon force on the nucleus, affecting among others chromosomal organization and histone remodeling. As referred throughout this section, there are plenty of reviews on mechanobiology and the individual proteins and pathways. However, these reviews are mainly based on data from 2D studies. While the behavior of these proteins in different environments and their effect on MSC differentiation and proliferation is fairly well established in 2D, their role and regulation are still vague in 3D. Here, we focus on the differences between 2D and 3D in response to extracellular properties and cell shape and

how important mechanotransduction proteins have a different role and regulation in 3D than in 2D.

Extracellular material properties influence cellular behavior differently in 2D vs 3D

Substrate stiffness in 2D

Stiffness is arguably the most widely researched material property to influence cell proliferation and differentiation. In 2D, stiff substrates allow cells to build up high cellular tension and spread, with pronounced focal adhesions, actin stress fibers and YAP nuclear localization[20-27]. On soft substrates, cells maintain a less spread morphology and display small focal adhesions, few actin stress fibers and cytoplasmic YAP[20-22, 24-28]. This is true for many different cell-types, but in this review we will focus mainly on MSCs, because of their wide use in tissue engineering. MSCs on stiff substrates have increased osteogenic potential, while softer substrates increase adipogenic potential[21, 23, 25-27]. In 2D, MSCs on substrates stiffer than 30-70 kPa undergo efficient osteogenic differentiation, while softer substrates inhibit osteogenesis[20-23, 25-27, 29]. Adipogenesis is optimal around 0.3-3 kPa[21-27]. Although generally inefficient in 2D, chondrogenic differentiation of hMSCs is also influenced by substrate stiffness. Softer substrates with reduced cellular tension increased chondrogenesis at 1kPa [30], in line with results for chondrocytes [31]. Differentiation of other cell types is also dependent on substrate stiffness in 2D, in a similar stiffness range, e.g. muscle stem cells [32-35], induced pluripotent stem cells [36, 37], embryonic stem cells [38], cardiac muscle cells [39] and fibroblasts [40]. Besides differentiation, proliferation is also controlled by substrate stiffness and cellular tension in 2D, in MSCs [29, 41, 42] and other cell types [31, 35, 43-45]. Altogether, the role of substrate stiffness in steering cell behavior in 2D is well established, particularly MSC differentiation and lineage commitment in 2D. However, to form functional tissues, cell behavior needs to be influenced in 3D. In the next section, we will go into the material properties that influence cell behavior in 3D and see how this is different from 2D.

Substrate stiffness in 3D

Similarly to the role of stiffness in 2D, Huebsch et al. showed that for MSCs encapsulated in 3D in RGD-modified alginate, agarose, and PEG hydrogels increasing stiffness led to increased osteogenesis and reduced adipogenesis[46]. The optimal stiffness for osteogenesis was around 20 kPa, whereas ~2.5 kPa for adipogenesis, similar to what was found in 2D. Others have shown a similar effect of matrix stiffness on osteogenesis in 3D gelatin gels[47]. Interestingly, however, stiffnesses of around 100 kPa inhibited osteogenesis in the alginate, agarose and PEG hydrogels[46]. In 2D, there does not seem to be such an upper limit to substrate stiffness, demonstrated by efficient osteogenic differentiation on extremely stiff polystyrene (such as conventional tissue culture plastic dishes) and glass (both in the GPa range) substrates. This upper limit to substrate stiffness in 3D likely arises from a reduced

ability for cells to remodel the matrix and gather adhesive ligands when encapsulated in hydrogels. The importance of matrix remodeling is illustrated in a paper by Khetan et al.[48]. In contrast to Huebsch et al., Khetan et al. showed that irrespective of hydrogel stiffness (~4-91 kPa), only adipogenesis and no osteogenesis occurred in covalently crosslinked hyaluronic acid hydrogels[48]. Khetan et al. elegantly demonstrated that these differences arise from a difference in remodeling of the matrix. Alginate, agarose and PEG hydrogels are relatively dynamic due to non-covalent crosslinks, whereas the covalently crosslinked hyaluronic acid gels are static. Indeed, when 20 kPa alginate (inducing osteogenesis when non-covalently crosslinked) was covalently crosslinked, only adipogenic differentiation occurred[48]. This highlights that matrix stiffness on its own is not enough to guide MSC differentiation in 3D, as it is in 2D. In 3D, it seems that cells need to be able to remodel the matrix sufficiently in order to build up the required cellular tension to undergo efficient osteogenic differentiation. This is likely also the explanation for the upper limit of substrate stiffness in the 3D hydrogels of Huebsch et al.; even though the hydrogels are non-covalently crosslinked, at higher stiffnesses the gels become less dynamic. One strategy to improve the ability of a hydrogel to be remodeled by cells is to make the gels degradable. The next section will discuss the influence of degradability and show how this can be a key aspect in controlling MSC differentiation and proliferation.

Substrate degradability in 3D

While in 2D an increase in stiffness leads to increased cellular tension, Caliari et al. showed that the opposite is true in 3D covalently crosslinked gels[49]. The increased extracellular stiffness in 3D covalently crosslinked gels prevents cell spreading, similar to the results of Huebsch et al.[46]. Indeed, adding degradable motives to the matrix increased spreading and YAP nuclear localization, indicating increased cellular tension. Others have found a similar confining effect of matrix stiffness in 3D[24]. When Khetan et al. added MMP-degradable peptides to covalently crosslinked hydrogels, so that the MSCs could remodel the matrix, almost all cells preferentially differentiated to the osteogenic lineage in 4.4 kPa gels[48]. In line with this, Ferreira et al. also found that inhibiting hyaluronidase in 1 kPa degradable hyaluronic acid hydrogels inhibited osteogenic differentiation[50]. In type-I collagen gels, inhibiting membrane bound membrane-type 1 matrix metalloproteinase (MT1-MMP) (a collagen degrading enzyme) in hMSCs cripples degradation and osteogenic differentiation *in vitro*[51] and *in vivo*[52], while enhancing adipogenic differentiation. Lastly, bone formation is enhanced *in vivo* in MSC-laden degradable alginate hydrogels, as opposed to more slowly degradable gels[53]. On top of 2D collagen gels, however, the lack of MT1-MMP and degradation does not affect adipo- or osteogenic differentiation[52]. Together, these papers demonstrate the importance of matrix degradation in 3D hydrogels to build up cellular tension and undergo osteogenic differentiation. In 2D, this does not seem to be of importance. Also, stiffness seems to be of subordinate importance in 3D, highlighted by

efficient osteogenic differentiation in 1 and 4.4 kPa hydrogels if the gels can be sufficiently degraded[48, 50] (Table 1). Another method to increase the remodeling of hydrogels is by increasing stress-relaxation properties. In the next section, we will discuss how this effects MSC differentiation and how it relates to substrate stiffness. In the section after that, we will go deeper into why this matrix-remodeling is of such important in 3D, and not in 2D.

Stress-relaxation properties in 3D

The studies on matrix degradability highlight the importance of matrix remodeling in 3D. In line with this, Chaudhuri et al. found that with faster stress relaxation in 3D RGD-alginate gels, osteogenesis greatly increased, while adipogenesis decreased[54]. Often used synthetic hydrogels are mostly elastic, whereas natural ECMs derived hydrogels are viscoelastic[54]. By increasing viscoelastic (stress relaxation) properties of the alginate hydrogels, the MSCs are able to harness more RGD than in slower relaxing gels. Indeed, increasing RGD density by 10-fold increases osteogenic potential in the slow and fast relaxing gels. However, MSCs in low-RGD fast relaxing gels still exhibit much greater osteogenic potential than in high-RGD slow relaxing gels[54]. Others have found similar importance of stress relaxation for osteogenesis, where faster stress relaxation greatly enhances osteogenic differentiation of MSCs *in vitro*[55-57]. When implanted *in vivo*, faster stress relaxing hydrogels increases bone formation[56]. In accordance with the differentiation results, proliferation also increases in degradable or fast-relaxing gels for MSCs[55] and other cell types[54, 57-59]. Together, the fast-relaxing and degradable hydrogels demonstrate that for a cell to build cellular tension, it needs to harvest adhesive ligands. While pulling on the ligands, the matrix deforms, and its deformability determines the cellular tension. However, when a cell can harvest enough adhesive ligands, it can build up high (enough) cellular tension even in soft materials. Indeed, it has been shown that the faster stress relaxation in hydrogels allows the cells to gather more adhesive ligands[60]. This brings us to the next section where we discuss the importance of gathering adhesive ligands 3D, and in 2D.

Adhesive ligand gathering in 2D and 3D

In 2D, adhesive ligands are plentiful and in close proximity. This allows easy integrin clustering and large focal adhesion formation, which allows pulling on many ligands and the build-up of cellular tension. If the matrix is soft, the force that can be built-up is low, if the matrix is stiffer, higher cellular tension can be built-up. In 3D, however, adhesive ligands are distributed in three dimensions, and thus the matrix needs to be remodeled in order for the cell to gather many adhesive ligands in close proximity. Research with nanopatterned surfaces in 2D has revealed that to form focal adhesions and spread on thin nanometer adhesive lines, the lines have to be closer than 110 nm apart, or cross with each other[62]. This resembles the situation of the hydrogels, consisting of nanometer sized fibers, and demonstrates the need for close proximity of the ligands. In 2D, a cell can move freely over the surface where adhesive ligands

	Paper	Stiffness	Matrix type	Remodelability
Osteogenesis				
2D	[20-23, 25-27, 29]	>30 kPa	Flat 2D hydrogels	Non-remodelable 2D substrates
3D	Huebsch et al.[46]	12-25 kPa	Alginate-RGD, agarose-RGD or PEG-RGD	Remodelable, non-covalent matrix bounds
	Khetan et al.[48]	4.4 kPa	MMP-degrable hyaluronic acid hydrogels	Remodelable, MMP degradable motives
	Ferreira et al.[50]	1 kPa	Hyaluronic acid hydrogels	Remodelable, degradability
	Chaudhuri et al.[61]	17 kPa	Alginate-RGD hydrogels	Remodelable, fast stress relaxation
	Darnell et al.[56]	18 kPa	Alginate-RGD hydrogels	Remodelable, fast stress relaxation
	Nam et al.[57]	15 kPa	Alginate-RGD hydrogels	Remodelable, fast stress relaxation
	Lee et al.[55]	20 kPa	Alginate-RGD hydrogels	Remodelable, fast stress relaxation
No/Little osteogenesis				
2D	[20-23, 25-27, 29]	<30 kPa	Flat 2D hydrogels	Non-remodelable 2D substrates
3D	Huebsch et al.[46]	>100 kPa	Alginate-RGD, agarose-RGD or PEG-RGD	Non-remodelable, too high stiffness
	Huebsch et al.[46]	2.5-5 kPa	Alginate-RGD, agarose-RGD or PEG-RGD	Remodelable, non-covalent matrix bounds
	Khetan et al.[48]	4-91 kPa	Crosslinked hyaluronic acid hydrogels	Non-remodelable, covalent matrix bounds
	Khetan et al.[48]	20 kPa	Crosslinked alginate-RGD	Non-remodelable, covalent matrix bounds
	Chaudhuri et al.[61]	17 kPa	Alginate-RGD hydrogels	Non-remodelable, slow stress relaxation
	Chaudhuri et al.[61]	9 kPa	Alginate-RGD hydrogels	Remodelable, fast stress relaxation
	Darnell et al.[56]	18 kPa	Alginate-RGD hydrogels	Non-remodelable, slow stress relaxation
	Nam et al.[57]	15 kPa	Alginate-RGD hydrogels	Non-remodelable, slow stress relaxation
	Lee et al.[55]	20 kPa	Alginate-RGD hydrogels	Non-remodelable, slow stress relaxation
Adipogenesis				
2D	[21-27]	0.3-3 kPa	Flat 2D hydrogels	Non-remodelable 2D substrates
3D	Huebsch et al.[46]	2.5-5 kPa	Alginate-RGD, agarose-RGD or PEG-RGD	Remodelable, non-covalent matrix bounds
	Khetan et al.[48]	4-91 kPa	Crosslinked hyaluronic acid hydrogels	Non-remodelable, covalent matrix bounds
	Khetan et al.[48]	20 kPa	Crosslinked alginate-RGD	Non-remodelable, covalent matrix bounds
	Chaudhuri et al.[61]	9 kPa	Alginate-RGD hydrogels	Remodelable, fast stress relaxation

Table 1. Overview of literature investigating the effect of stiffness on MSC differentiation in 2D and 3D, showing the importance of matrix modeling, more than substrate stiffness, in 3D environments.

are presented. When adhesion sites are in close enough proximity, integrin clusters can form to create focal adhesions and build up cellular tension, without the need to remodel the substrate. In 3D, however, adhesive ligands are embedded in a matrix and need to be discovered and gathered before integrin clusters can form to build up cellular tension. To gather multiple adhesive ligands, the matrix needs to be remodeled. This could explain the importance of remodeling the matrix in 3D, which is illustrated elegantly in the degradation and stress-relaxation studies discussed above.

The question then arises whether matrix remodeling is only important in 3D, or also in 2D. When using the right conditions, 2D matrix deformation also plays a role in cellular tension. The effect of stiffness on cellular tension and MSC differentiation in 2D is mostly tested on slow-relaxing or covalently crosslinked gels. Here, significant adhesive ligand clustering is difficult for cells[60], so cellular tension is mostly determined by matrix stiffness and ligand

proximity[62]. However, osteosarcoma cells increase spreading on soft substrates (~1 kPa) with fast stress-relaxation, while cells remain round on soft slow-relaxing substrates[61]. This shows that adhesion ligand gathering can allow cells to build up cellular tension in 2D, like in 3D. The importance for ligand gathering in 2D is also nicely illustrated in a set of studies that use micrometer sized fibers, rather than the nanometer sized fibers of fibrillary hydrogels. These micrometer sized fibers also partially recapitulate the fibrillary ECM *in vivo*, making it an interesting substrate type to study[63-65]. On top of a thin layer of stiff, unmovable electrospun micrometer sized fibers, MSCs and fibroblasts display little cellular tension and proliferation[66]. When fibers were softer and could be displaced more easily, the cells build up more cellular tension and significantly increase proliferation. Similarly, MSCs increase osteogenic differentiation on long, movable collagen fibers (9.3 kPa), while adipogenic differentiation is enhanced on smaller, stiffer, less movable fibers (1.1 kPa)[67]. Bulk stiffness was very low in both conditions (16.4 Pa). On soft, movable fibers, MSCs spread and formed focal adhesions, while no focal adhesion were observed on stiffer, less movable fibers[68]. Similar results have been shown for other cells[69], and this has been further investigated on a variety of different materials. In these studies, thin microfibrillar meshes are used, so cells grow on top and are in a 2D environment. The studies on microfibrillar substrates are interesting because they highlight the importance of ligand gathering and matrix remodeling in a 2D environment and argue against the direct influence of material stiffness. The 2D microfibrillar studies show a similar importance for ligand gathering to build up cellular tension in 2D as in the 3D hydrogel studies. The 3D stiffness, degradation and stress-relaxation studies, together with the 2D stress-relaxation and microfibrillar substrate studies, illustrate the importance for adhesive ligand gathering and the subordinate role for stiffness in both 2D and 3D.

In summary, in most 2D culture substrates, stiffness is very important for cellular tension because adhesive ligands are in close proximity and easily accessible. In 3D, however, adhesive ligands need to be gathered, so the matrix must be remodeled. When adhesive ligands can be gathered sufficiently, cells can build up high cellular tension in 3D even in soft materials (Figure 1). This is nicely demonstrated by the fact that osteogenesis can occur at much lower stiffnesses (1-4 kPa) in 3D when cells are able to remodel the matrix sufficiently, than in 2D[48, 50] (Table 1).

Outlook on extracellular material properties in 2D vs 3D

Now that several individual matrix properties that influence MSC differentiation in 3D have been identified, investigating a combination of these factors could result in superior scaffolds for tissue engineering. For example, even though matrix deformability seems to be more important than stiffness in 3D, stiffness still plays an important role. It is likely that there is an optimal combination of the two to guide MSC differentiation. Combinations of faster stress-relaxation and degradation of a 3D matrix could also result in even further enhancement of

cellular tension, especially when done in a gel of optimal stiffness for a targeted cell differentiation lineage. Whereas adipogenic and osteogenic differentiation are highly influenced by cellular tension, chondrogenesis is also highly dependent on specific protein interactions, such as cadherins[70]. Most MSC mechanobiological studies, therefore, focus on adipogenesis and osteogenesis. However, material properties also influence chrondrogenesis in 3D. Faster stress relaxation hydrogels, for example, allow for the deposition of ECM further away from chondrocytes during chondrogenesis, creating a more interconnected matrix[71]. A deeper investigation of the influence of material properties on chondrogenesis in 3D could advance cartilage tissue engineering approaches. In addition, most of the research on matrix properties and mechanobiology in 3D is done with hydrogels. However, many tissue engineering approaches utilize other scaffold types, such as electrospun- or additive manufactured scaffolds, for their superior structural mechanical properties. Very few articles investigate how MSC differentiation is affected directly by these environments. We have recently shown that cellular tension of MSCs is reduced in 3D electrospun and additive manufactured scaffolds, made up of stiff materials, when compared to the same stiff materials in 2D[72]. Others have also hinted at a decrease in cellular tension in epithelial cells on electrospun scaffolds, showing a decrease in focal adhesions in 3D electrospun scaffolds compared to 2D[73]. This shows that even when using stiff materials, cellular tension can be low and is affected by the properties of the 3D environment. Effects of material properties in 2D cannot be translated directly to 3D, as we've discussed in this section. More research into how different material properties affect MSC proliferation and differentiation is required for more effective design of biomaterials. For example, properties of electrospun scaffolds such as optimal fiber stiffness, diameter and inter-fiber linkage, are yet to be investigated in a comparative manner for their effect on mechanobiology of MSCs. Individual parameters of additive manufactured scaffolds would also be interesting to further investigate and optimize, such as fiber diameter and curvature, pore size and shape and material stiffness. A better understanding of how these individual parameters influence MSC differentiation, and which of these are dominant factors, could greatly aid the design of smart scaffolds for tissue engineering and regenerative medicine strategies. In addition, fundamental knowledge of how MSCs gather adhesive ligands and build up cellular tension in 3D is still lacking. In the sections below, we will go into more detail of the molecular mechanisms that orchestrate cellular tension and MSC differentiation in 3D. First, we will look at the literature of cell morphology and cell volume, and how it influences MSC differentiation in 2D and 3D.

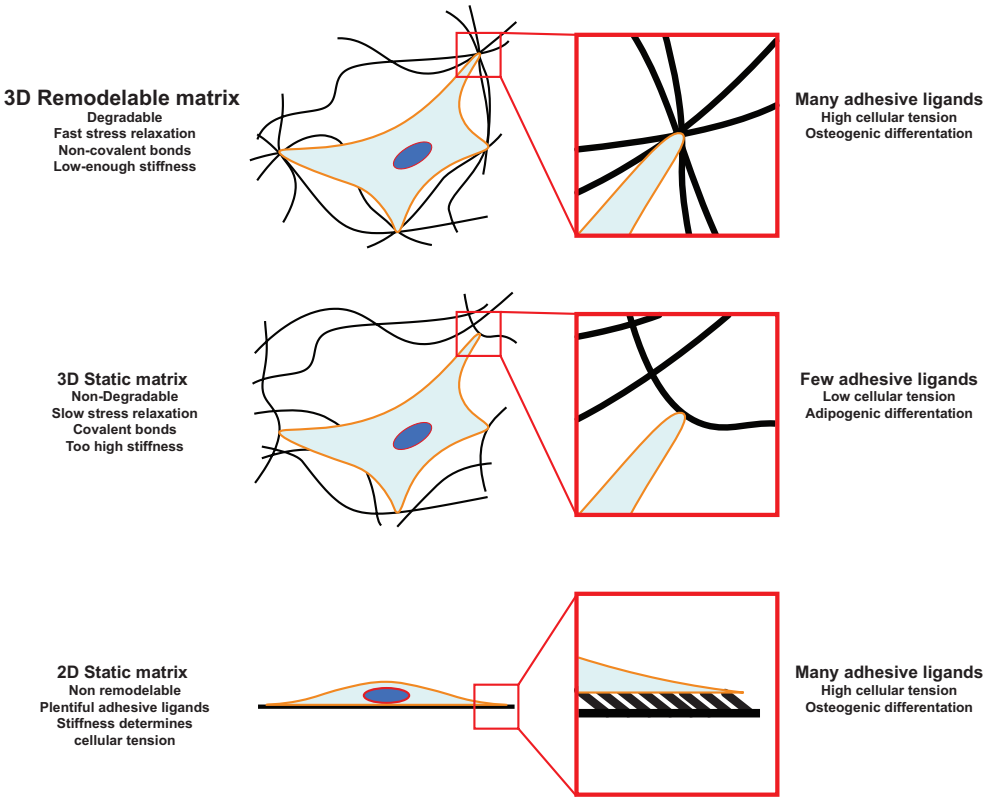

Figure 1. Schematic visualization of differences in adhesive ligand gathering between 2D and 3D. When a 3D matrix is remodelable, due to (a combination of) degradability, fast stress relaxation, non-covalent matrix bounds and a low-enough stiffness, cells can harvest multiple adhesive elements to build up high cellular tension. In a static 3D matrix, which is non-degradable, has slow stress relaxation, is cross-linked covalently and/or too stiff, cells cannot gather enough adhesive ligands to build up high cellular tension. In a classic flat 2D culture setting, the substrate is also static, but there are enough adhesive ligands so that the matrix does not need to be remodeled. In the presence of enough adhesive ligands in 2D, the stiffness of the matrix determines the cellular tension.

Cell morphology and volume in 2D and 3D

Cell morphology

In 2D, MSC osteogenic differentiation is greatly enhanced by cellular tension, marked by actin stress fibers with non-muscle myosin-II, large focal adhesions, a stiff nucleus (high lamin A/C expression) and YAP nuclear translocation[20-27, 29]. The opposite is true for adipogenic differentiation, which is aided by low cellular tension[21-27]. Generally, in 2D stiff substrates such as standard tissue culture plastic, MSCs are allowed to spread and build up high cellular tension. This spread morphology is a good indicator for cellular tension in 2D, and it can also directly influence cellular tension[74], due to an increase in adhesion area[75]. Restriction of MSC spreading by confinement demonstrates that small cells display little cellular tension

and are biased towards adipogenesis, while large cells exhibit increased cellular tension and improved osteogenesis[76]. Also, when MSCs are forced in a specific cell shape, cellular tension and differentiation is influenced. More circular shapes allow less cellular tension and bias MSCs towards adipogenesis, while rectangular shapes increase cellular tension and drive MSCs towards osteogenesis[77]. Cell shape also influences behavior in other cell types in 2D, such as proliferation[78, 79], migration[80, 81], apoptosis[78] and tumorigenicity[82].
Based on these studies, one would expect that cell spreading and morphology in 3D settings also greatly influences differentiation. However, differentiation of MSCs has been fully decoupled from cell morphology in 3D. In hydrogels, both small, circular cells and larger, spread cells have been shown to undergo efficient osteogenesis[46, 48, 50, 54, 55, 83]. Also, both circular and spread cells have been shown to differentiate to adipocytes[46, 48, 54, 55, 83]. In 3D additive manufactured scaffolds, less spread cells more efficiently underwent osteogenic differentiation than more spread cells, contrary to 2D results[84]. This highlights once again that studies performed in 2D can't be expected to directly translate to a 3D setting. Cell morphology doesn't seem to have the same predictive power in 3D as it does in 2D. However, recent studies have demonstrated a role for cell volume in 3D differentiation. In the next section, we will discuss the role of cell volume in 2D and 3D differentiation.

Cell volume in 3D

Rather than cell morphology, a few studies have shown the importance of cell volume as a regulator of cellular tension and differentiation in 3D. Bao et al. investigated cellular tension and differentiation in cells that were confined to different morphologies and volumes in 3D, in specifically shaped wells with lid in hydrogels[85]. They found more actin stress fibers, focal adhesion and YAP nuclear translocation in smaller cells, regardless of cell geometry, up to a certain lower limit. Too little cell volume also decreased cellular tension. Indeed, cells with optimal volume for cellular tension (~3600μm^3) differentiated preferentially towards osteoblasts, while cells with a bigger volume (~6000 or ~9000μm^3) decreased osteogenic differentiation and increased differentiation towards adipocytes. Cells with smaller volumes (~2200μm^3) slightly decreased osteogenesis and showed no difference in adipogenesis. In the cells with optimal volume for osteogenic differentiation, cell morphology influenced differentiation, but to a much smaller extend than cell volume. Seemingly contradictory, Lee et al. later reported that increasing cell volume (by changing stress-relaxation properties or osmotic pressure) increased osteogenesis[55]. However, the investigated cell volumes were in a different range. Cells with a volume of ~1000μm^3 displayed little osteogenic differentiation, while ~2000μm^3 displayed efficient osteogenesis, in accordance with Bao et al. Perhaps a further increase in osteogenesis would be observed if cell volume was increased to 3000-4000μm^3 (the optimal volume for osteogenesis in the Bao et al. study[85]). The increase in osteogenesis in response to volume increase was regulated through TRPV4, actin-myosin and RUNX2. Because faster stress-relaxation increased cell volume and osteogenic

potential, it is likely that other 3D environments that allow matrix remodeling (such as a degradable hydrogel) also increase volume and osteogenesis. This has, however, not yet been investigated. The two studies investigating cellular volume in 3D show the importance of cell volume for MSC differentiation in 3D. Is this a unique attribute of MSC differentiation in 3D, or is this also important in 2D?

Cell volume in 2D

As cells spread and increase their surface area, cell volume decreases[86, 87]. The change in cell volume upon cell spreading is true for a range of cell types, including MSCs. When cell spreading is inhibited, by physical confinement or a decrease in substrate stiffness, cell volume remains larger[86, 87]. When the volume of MSCs cultured on a stiff surface (spread morphology, reduced cell volume) is increased with osmotic pressure to the volume of MSCs on soft surfaces (round morphology, more cell volume), adipogenic differentiation of MSCs is enhanced[87]. Vise-versa, when the volume of MSCs cultured on soft surfaces is decreased with osmotic pressure to the volume of MSCs on stiff surfaces, osteogenic differentiation is improved. The cell volume of MSCs on spread surfaces, where osteogenic differentiation is most efficient, is around 2000μm^3. Round MSCs on a soft surface had a volume of around 2500μm^3. The optimal volume for osteogenic differentiation seems to be different between 2D and 3D (~2000μm^3 in 2D vs ~3600μm^3 in 3D) (Figure 2). This study shows that cell volume can also directly influence differentiation of MSCs in 2D, like in 3D.

Outlook on cell morphology and cell volume in 2D and 3D

The 2D and 3D cell volume studies discussed above question the direct influence of cell morphology on MSC fate. In 2D, when cell morphology was spread, but volume increased, MSCs underwent more efficient adipogenic differentiation, while round cells with decreased volume increased osteogenic potential. As cell volume changes with cell morphology, this questions whether the studies on cell morphology in 2D are not indirectly looking at the effect of cell volume, rather than cell morphology. In 3D cell morphology has also been decoupled from cell volume, and a dominant role for cell volume over morphology was found. Only one study directly investigates cell volume vs cell morphology in MSC differentiation in 2D, and only two studies in 3D. From these studies, many questions arise. The optimal cell volume is still to be determined in both 2D and 3D. Ideally, a comparative study between 2D and 3D could be done, using the same materials and investigating a large range of cell volumes. Chondrogenesis in 3D has also been correlated to a change in cell volume, but direct causality or the underlying mechanisms have not yet been explored[71]. The molecular mechanisms underlying the role of cell volume in MSC differentiation to any of the three lineages is still unclear. Does cell volume induce a change in cellular tension and affect MSC differentiation through that, or is there an independent pathway? Confirming the dominant role of cell volume over cell morphology, determining the optimal cell volume for

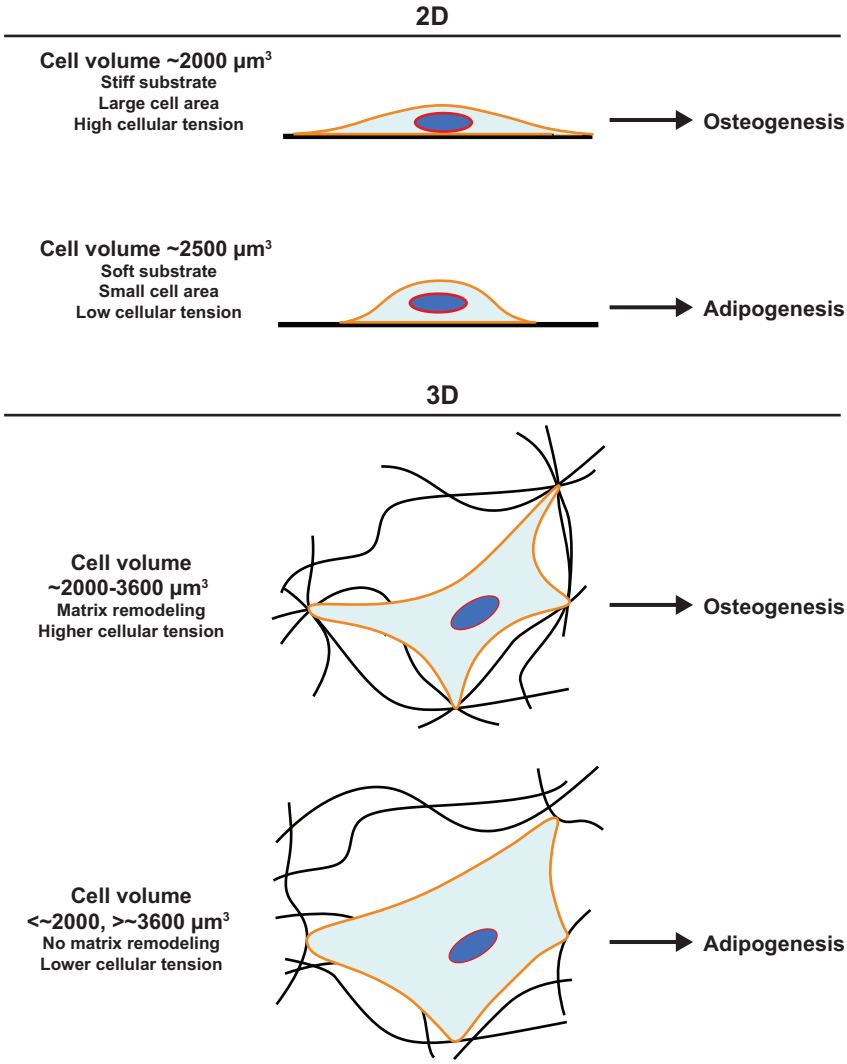

Figure 2. Influence of cell volume, rather than cell morphology, on MSC differentiation. In 2D, MSCs cultured on a stiff substrate have a large surface area, high cellular tension, and a volume of ~2000 µm³. On soft substrate, MSCs spread less and have lower cellular tension with a volume of ~2500 µm³. By changing the volume with different substrates or osmotic pressure, a dominant role for cell volume on MSC differentiation was found[87]. In 3D, MSCs that are able to remodel the matrix sufficiently can build up higher cellar tension, which influences cellular volume. Based on two papers investigating 3D cellular volume, an optimal volume of ~2000-36000 µm³ to induce osteogenesis was found, while larger or smaller volumes drove cells more towards adipogenesis[55, 85].

MSC differentiation, and investigating the molecular pathways could greatly improve understanding and aid design of tissue engineering constructs. In the next section, we will go over some of the main players in mechanosensing and how their role or regulation can be different in 2D vs 3D.

Molecular mechanisms of mechanosensing in 2D and 3D

In this section, we will explore the role and regulation of some key actors in the mechanotransduction pathway. We will focus on their role in 3D mechanobiology and guiding MSC differentiation, and what the differences and similarities are compared to 2D culture systems. Many individual proteins have been shown to play a role in mechanotransduction and MSC differentiation and proliferation. Here we will focus on the most widely studied proteins that play critical roles in MSC mechanotransduction. Starting from the cell membrane and traveling inwards, we will start with integrins, then go to focal adhesions, actin-myosin, RhoA and ROCK, YAP/TAZ, MRTF/SRF and the nuclear lamina.

Integrins

Different combinations of α and β integrin subunits form dimers to bind different ECM proteins and form a physical link between the ECM, through the cell membrane to the cell interior[88]. Clustering of different integrin dimers allows cells to build up cellular tension, driving MSC differentiation towards osteogenesis in 2D. Similarly, in 3D osteogenic differentiation has also been shown to be dependent on integrin clustering[46]. Indeed, inhibiting integrins in 2D inhibits osteogenesis and favors adipogenic differentiation of MSCs[89-92]. Like in 2D, inhibiting integrins in MSCs in 3D also leads to decreased osteogenesis[46, 50, 52, 93-95] and increased adipogenesis[46, 50, 94, 96]. The role of integrins in 3D differentiation of MSCs has been well studied in different 3D environments. As opposed to other proteins discussed later in this review, the role of integrins seems to be very similar in 2D as in 3D.

In 2D, when ligand density is sufficiently high, cellular tension through integrins is mainly dependent on stiffness[97]. In 3D, however, integrin clustering is regulated by local reorganization of the matrix, to gather sufficient adhesive ligands. This is dependent on stress relaxation and degradation in hydrogels[52, 57, 61], and fiber stiffness and movability in fibrous meshes[60, 67]. Increasing the stiffness in 3D reduced integrin bonds, arguably due to a decrease in cells' ability to remodel the matrix[46]. We refer the reader to the 'adhesive ligand gathering in 2D and 3D' section above for a more elaborate discussion on adhesive ligand gathering in 3D. Next, we will discuss the role of focal adhesions in 3D mechanosensing.

Focal adhesions

Focal adhesions are complex structures and consist of more than 60 different proteins that link the ECM-binding integrins to the actin cytoskeleton[98]. Focal adhesions play an important role in transducing mechanical signals from the outside of the cell to the inside. On 2D stiff materials, number and size of focal adhesions vary per cell type, but all adherent cells form many relatively large focal adhesions[98, 99]. On 2D soft materials, fewer and smaller focal adhesions form[99]. Important focal adhesions proteins, such as vinculin[100], focal adhesion kinase (FAK)[101], paxillin[102], talin[103] and zyxin[104], among others, all contribute to mechanotransduction. This contribution is both mechanical, creating the bridge between ECM and actin cytoskeleton, and by signaling, activating other effector proteins.

Focal adhesions increase during osteogenesis of MSCs, while they decrease during adipogenesis[105]. However, surprisingly little is known about the effects of these proteins on lineage commitment of MSCs. Vinculin knockdown decreases osteogenesis and increases adipogenesis[23]. In line with this, FAK inhibits osteogenesis in MSCs, osteoblasts and fibroblasts in 2D[96, 106-109]. Also, proliferation of MSCs[110] and other cells[101] is reduced by FAK inhibition. Interestingly, however, FAK is also required for adipogenesis in MSCs and adipocytes and fibroblasts[111-113], and for the formation of fat tissue *in vivo* in mice[114]. Adipogenesis is inhibited by high cellular tension, but few and small focal adhesions are still present[20-22, 24-28]. This suggests that FAK has a signaling role for FAK in adipogenesis, rather than aiding in the build-up of cellular tension. Other proteins such as paxillin, zyxin and talin remain unexplored in their role in MSC differentiation in both 2D and 3D, even though they are likely to play an important role. More research is required to investigate the specific role of the different focal adhesion proteins in MSC differentiation. Understanding how MSCs convey mechanical signals from outside the cell to the inside, and specifically which proteins are required for the right cellular response, is critical for the smart design of tissue engineering constructs.

In 2D there is a strong correlation between many large focal adhesions and osteogenesis, and few small focal adhesions and adipogenesis[20-22, 24-28]. In 3D, however, there are often very few and small focal adhesions in MSCs and other cell types[115-117], but osteogenesis can still efficiently occur[48, 85, 94]. Fraley et al.[115] have shown that this reduction in focal adhesions is a direct response to the 3D environment. On top of 2D gels, many large focal adhesions formed, but when a gel was pipetted on top of MSCs attached to 2D gels, or when cells were embedded in 3D hydrogels, only few and small focal adhesions were observed. We have recently shown a similar decrease of focal adhesions in stiff 3D electrospun and additive manufactured scaffolds, compared to 2D films of the same stiff material[118, 119]. Rather than forming large protein complexes that tightly anchor the cell to the 2D substrate, the focal adhesion proteins are distributed more diffusely through the cell and regulate protrusion activity and matrix deformation[115, 120]. Creating protrusions and deforming the matrix is required to gather adhesive ligands in 3D, while it does not play a great role on stiff 2D

substrates with plenty closely spaced adhesive ligands. This suggests a critical difference between the role of focal adhesions in 2D and in 3D. This difference is likely to translate more broadly to the build-up of cellular tension, and thus to proliferation and differentiation. Further exploring the role of individual focal adhesion proteins, and the focal adhesion protein complex as a whole in a 3D setting, could greatly aid both fundamental understanding and tissue engineering. This could be investigated in hydrogels, allowing for relatively easy control of properties such as stiffness, stress relaxation and ligand density, among others. However, as most scaffolds exploited for tissue engineering are made up of stiff materials, researching the role of focal adhesion proteins in these settings will also greatly improve understanding of cellular behavior in tissue engineering scaffolds.

Actin-myosin

The actin cytoskeleton is a critical component in the mechanotransduction machinery. Actin monomers polymerize in filaments and multiple filaments come together to form large actin fibers. Non-muscle myosin II (NM-II), consisting of two heavy chains, two essential light chains and two regulatory light chains, incorporates within the actin fibers to create contractile actin-myosin fibers, called stress-fibers. When the actin-myosin elements contract, tension is created between its two attachment points[13]. These two attachment points can be two focal adhesions, or a focal adhesion and the nucleus. On 2D stiff materials, large actin stress fibers are observed in many different cell types. On soft materials, a more diffuse actin network is observed, with fewer stress fibers, thinner actin fibers and more actin around the cell periphery[20-22, 25, 26]. Actin-myosin contractility greatly influences MSC differentiation, as inhibiting NM-II activation by blebbistatin on 2D stiff materials greatly reduces osteogenesis and enhances adipogenesis[20, 24, 121-123]. Actin polymerization inhibitors, such as latrunculin A, also inhibit osteogenesis in MSCs[24, 124]. In 3D, however, pronounced stress fibers as in 2D are often not observed, regardless of stiffness, degradation or stress-relaxation properties of the matrix[42, 46-48, 52, 54, 55, 94, 125]. However, both osteogenesis and adipogenesis can still occur in cells without pronounced stress fibers in 3D[42, 46-48, 50, 54, 55, 118, 125]. Osteogenic differentiation of MSCs without pronounced stress fibers has been extensively shown in hydrogels and we have recently also shown this for MSCs in 3D electrospun and additive manufactured scaffolds[118]. This demonstrates that the actin cytoskeleton doesn't have the same predictive power in 3D as it has in 2D. Yet, consistent with 2D studies, inhibiting myosin activation or actin polymerization in 3D hydrogels results in reduced osteogenesis and increased adipogenesis[48, 54, 55]. This shows that actin-myosin tension is still very important in 3D MSC differentiation, but that thick actin-stress fibers are not required for sufficient cellular tension to induce osteogenesis. One paper, however, has shown no difference in osteogenic differentiation in the presence of myosin II inhibitor blebbistatin[95]. On top of this, surprisingly, the actin polymerization inhibitor latrunculin A increased osteogenic potential. Interestingly, inhibition of integrins did inhibit osteogenesis,

showing that the induced osteogenesis was reliant on cell adhesion to the matrix, but not reliant on actin-myosin contraction. This is contradictory to the above-mentioned papers that found decreased osteogenesis upon blebbistatin inhibition. The concentrations of blebbistatin are the same in the papers (50 μM), but one key difference is the use of osteo-inductive medium supplements. Whereas Khetan et al., Lee et al. and De La Cruz et al. use osteo-inductive factors and show a dependence on actin-myosin for osteogenic differentiation, the hydrogel used by Parekh et al. induces osteogenesis without osteogenic medium. Lee et al. showed that TRPV4 activation can induce osteogenesis even in the presence of blebbistatin by directly regulating cell volume[55]. This shows that there are (at least one) NM-II independent pathways that can induce osteogenesis. Perhaps the hydrogel used by Parekh et al. activates such a pathway. Together, these papers show that actin-myosin tension is required for medium-induced osteogenesis, but that there might be alternative pathways that can bypass the requirement of actin-myosin.

Besides NM-II, smooth muscle myosin has also been suggested to be involved in osteogenic differentiation of MSCs[126], and smooth muscle actin is also important for MSC osteogenesis[22]. Little research has been done to further explore the role of smooth muscle actin and smooth muscle myosin, particularly in 3D. Further research is required to understand the role of other myosins and other actin-modulating proteins in MSC lineage commitment. Also, proteins such as TRPV4, that seem to influence differentiation independent of actin-myosin tension, would also be interesting to further investigate. This could help to better understand results obtained from specific inhibitors, such as blebbistatin. Also, as stress fibers don't seem to have the same predictive power in 3D as they do in 2D, having a profile of proteins that are important for MSC differentiation could greatly aid tissue engineering scaffold optimizations.

RhoA/ROCK

Rho GTPases play important and diverse roles in cell adhesion and cellular tension. RhoA, one of the Rho GTPases, stimulates stress fiber formation and cellular tension mainly, but not exclusively, through ROCK. The reader is referred to an excellent review on Rho GTPases regulation[127]. ROCK phosphorylates myosin regulatory light chain (MLC), which activates the ATPase activity of NM-II, resulting in actin-myosin contraction. In addition, ROCK inhibits MLC phosphatases, and affects a wide range of actin modifying proteins, resulting in the stabilization and formation of actin stress fibers[128]. Other well studied GTPases such as Rac and cell division control protein 42 (CDC42) have different effects on actin and are more involved in the formation of protrusions[129]. In MSCs in 2D, the role of RhoA and ROCK in adipo- and osteogenic differentiation is well studied. In human MSCs, inhibition of either RhoA or ROCK reduces cellular tension[121], promotes adipogenic differentiation and reduces osteogenesis[76, 90, 108, 121, 122, 130-132]. In murine MSCs, ROCK inhibition also increases adipogenesis and decreases osteogenesis[123, 124, 133, 134]. Commonly used ROCK inhibitors such as fasudil and

Y27632 have been shown to also inhibit a wide range of other protein kinases to varying degrees[135, 136]. It is important to understand that the effects ascribed to ROCK inhibition in the above-mentioned papers could also be partially ascribed to other inhibited kinases. Introduced expression of active proteins is a more direct way of measuring the effect of a protein. Supporting these inhibitor studies, constitutive expression of RhoA increases stress fibers[137] and constitutive activity of ROCK increases osteogenic differentiation[132] in human MSCs. Together, these papers demonstrate an important role for RhoA and ROCK in MSC fate-commitment, osteogenic differentiation and mineralization. Other Rho GTPases remain understudied, however, and further research is required to better understand the interplay between the different GTPases, kinases and differentiation of MSCs.

The role of RhoA and ROCK is far less clear in osteoblast differentiation. In rat or murine primary calvaria osteoblasts, inhibition of ROCK increases differentiation and mineralization[138-140], opposite to the effect on MSC osteogenesis. In the murine pre-osteoblast cell line MC3T3-E1, inhibition of ROCK with fasudil led to increased mineralization[141]. In a different paper, but the same cell line, ROCK inhibition with Y27632 decreased mineralization[142]. This suggests a different effect of fasudil and Y27632 on differentiation of this cell line, potentially due to effects on proteins other than ROCK. In murine primary calvaria osteoblasts, however, both Y27632 and fasudil increased mineralization[139]. In the human osteoblast cell line MG63, ROCK inhibition with Y27632 decreases differentiation[143]. Also for RhoA, mixed results have been found. Inhibition of RhoA with C3 toxin reduced mineralization in the MC3T3-E1 cell line,[142] but increased mineralization in murine neonatal calvaria osteoblasts[139]. These conflicting results show an opposite effect of ROCK or RhoA inhibition depending on the specific cell-type and inhibitor that is used. Also, the increased mineralization after ROCK or RhoA inhibition in some of the osteoblast studies is contrary to the results in MSCs. A potential explanation for this is the state of differentiation. ROCK and RhoA may be important for initial differentiation of MSC towards osteoblasts but inhibit further differentiation or mineralization at a more mature osteoblastic stage. Further research into these differences could greatly aid tissue engineering. First, a better understanding of the role of ROCK, RhoA and other GTPases in osteogenic differentiation is required. Then, the ideal timing of activation of these proteins should be studied. If no inhibitors are used, one could think of materials that change properties over time, for example, to inhibit RhoA or ROCK activation after an initial differentiation stage.

In 3D, human MSCs display fewer stress fibers upon RhoA inhibiton[85], illustrating a similar role of actin modulation in 3D as in 2D. In line with this, constitutively active ROCK in human MSCs induces osteogenesis in covalently crosslinked HA gels that normally induce adipogenesis[48]. In degradable HA hydrogels, inhibition of ROCK decreased cellular tension on the matrix and drove cells from osteogenesis to adipogenesis[48]. These results are in line with the results for MSCs in 2D and show a similar role of RhoA and ROCK in driving MSCs

towards osteogenesis. However, one study found no effect of ROCK inhibition on osteogenesis of human MSCs in PEG hydrogels[95]. The hydrogels used in this study induced osteogenesis without the addition of osteogenic factors. Osteogenic differentiation in these hydrogels was independent of actin-myosin tension and ROCK. This study suggests an alternative pathway of osteogenic differentiation, independent of actin-myosin and ROCK, as already discussed above in the actin-myosin section. In mouse MSCs, ROCK inhibition leads to increased ALP activity in slow-stress relaxing 3D alginate gels. In fast-stress relaxing gels, where cellular tension was highest, inhibition of ROCK had no effect[54]. These results are contradictory to the results of human MSCs, where ROCK inhibition decreases osteogenesis. These conflicting results highlight the need for further research. A better understanding of these important proteins and in what situations they are required for osteogenesis and when they are not is needed for a more intelligent design of tissue engineering constructs. Analyzing the effect of ROCK or RhoA inhibition in MSCs in hydrogels with different properties (e.g. stress relaxation, degradability, stiffness) could aid this research. Also, the differences between mouse and human MSCs could be directly compared to exclude a species-specific effect.

The roles of CDC42, Rac1 or other Rho GTPases in MSC differentiation are mostly unstudied in 3D, nor in 2D. CDC42 and Rac1 are more involved in protrusion activity, rather than cell contractility like RhoA and ROCK[129]. One study inhibited Rac1 in 3D hydrogels and found no difference in osteogenesis[61]. This suggests no role for Rac1 in osteogenesis, although it could be worth investigating in different types of hydrogels or other 3D scaffolds. It could be that Rho GTPases other than RhoA are not important for 2D differentiation of MSCs, but are important for 3D osteogenesis. As discussed earlier, MSCs in 3D gather and cluster adhesive ligands by reorganizing the ECM to build up cellular tension. Protrusion activity could play an important role in a cells' ability to sense the surrounding matrix. Studies inhibiting and overexpressing the different Rho GTPases, preferably with knock down/out or specific inhibitors, in different 3D environments would advance fundamental knowledge on 3D MSC differentiation.

YAP/TAZ

YAP and TAZ are a well-studied pair of co-transcription factors that transfer to the nucleus upon high cellular tension in 2D. This nuclear translocation is regulated by two different pathways. One is phosphorylation, which increases nuclear export and degradation by the proteasome. The other is by direct force on the nucleus, opening nuclear pores and allowing YAP to move inside the nucleus by active transport. The reader is referred to an excellent review on YAP regulation[144]. On 2D stiff substrates, where MSCs favor osteogenic differentiation, YAP is located in the nucleus. On soft substrates, YAP is predominantly cytoplasmic and MSCs favor adipogenesis. YAP has been directly involved in the differentiation of MSCs. Expression of non-degradable YAP or activation of TAZ inhibits

adipogenesis and increases osteogenesis[24, 145-147], while knockdown of YAP, TAZ or YAP and TAZ has the opposite effect[145-150]. Also, bone specific YAP/TAZ knockout mice have severely impacted bone formation[151]. Together, these papers clearly show an important role for both YAP and TAZ in differentiation of MSCs.

In 2D YAP and TAZ are regulated by integrin, RhoA, ROCK and actin-myosin tension[24, 144, 145]. In 3D, YAP and TAZ have also been shown to be dependent on integrin[52, 94], ROCK and actin-myosin[52]. However, in 3D, as opposed to 2D, nuclear entry of YAP does not always correlate with adipo- or osteogenic differentiation of MSCs[54, 55, 118], while in other studies it does correlate[24, 52, 85]. In 3D, osteogenic differentiation can still occur without pronounced nuclear translocation of YAP[61, 118], adipogenic differentiation with mainly nuclear YAP[61], and different efficiencies of differentiations don't correlate with different levels of YAP[55, 61]. Similar to 2D, non-degradable YAP reduced adipogenesis in 3D[24]. Also, MSCs expressing non-degradable YAP or TAZ exhibit increased osteogenesis *in vivo*[52]. Another study also found increased osteogenic differentiation and *in vivo* bone formation by pharmacologically activating TAZ in MSCs[146]. In summary, YAP and TAZ are not yet well studied in 3D tissue engineering, but the first results seem to reveal a similar function as in 2D. The studies where YAP and MSC lineage commitment did not correlate, found YAP nuclear localization in gels where MSCs preferred adipogenesis, and more cytoplasmic YAP in gels where MSCs preferred osteogenesis. This shows that YAP alone is not sufficient to guide MSC cell behavior and that other factors also play an important, and sometimes dominant, role. It could be that the low levels of YAP are still sufficient to allow for osteogenesis, and that high levels of YAP alone are not enough to inhibit adipogenesis. Further research into the function of YAP and TAZ in 3D is required to better understand their role in 3D differentiation. Also, in 2D nuclear entry of YAP and TAZ is often used as a read-out of cellular tension (and extrapolated to MSC lineage commitment). As discussed above, this correlation does not always seem to hold true in 3D. More in-depth investigations into the regulation of YAP and TAZ in different 3D environments could shed light on this and help to better interpret YAP and TAZ results in 3D.

MRTF/SRF

The MRTF family of mechanosensitive co-transcription factors (Myocardin, MRTF-A and MRTF-B) are regulated by actin. Myocardin is mostly expressed in cardiac and smooth muscle cells, while MRTF-A and B are more widely expressed. MRTF's bind to G-actin in the cytoplasm and are then prevented from entering the nucleus. When G-actin polymerizes into F-actin, MRTF's release from G-actin and enter the nucleus. Here, they bind to SRF to initiate transcription of a variety of genes[152]. Most, but not all, SRF target genes are MRTF controlled[153]. The MRTF/SRF pathway has been shown to be important in 2D MSC adipogenic and osteogenic differentiation. MRTF-A knock-out murine MSCs exhibit increased adipogenesis and reduced osteogenesis[154]. In line with this, overexpression of either MRTF-A or SRF leads to increased osteogenesis and decreased adipogenesis[134, 154]. Inhibiting the MRTF/SRF pathway with CCG1423 increases adipogenesis in MSCs[134]. Pre-adipocytes also

increase adipogenesis after knockdown of either MRTF-A or -B[155], or SRF[156]. SRF knock-out osteoblasts have reduced osteogenic differentiation capacity[157]. *In vivo*, MRTF-A or SRF knock-out mice display decreased bone-mass[154, 157], illustrating the importance of MRTF/SRF also in 3D settings. However, the MRTF/SRF pathway has not yet been investigated 3D MSC differentiation in tissue-engineering constructs. We have recently shown that the MRTF/SRF pathway influences proliferation of MSCs in 3D ESP scaffolds through the regulation of FGFR1[119]. Given the profound effects of MRTF/SRF on 2D MSC differentiation, investigating their role in a 3D setting would be highly interesting. MRTF's are regulated by G-actin and enter the nucleus when actin polymerizes. In 3D, however, large actin (stress) fibers are mostly absent (see 'actin-myosin' section). Investigating the regulation of MRTF nuclear entry in 3D could shed light on actin dynamics and the role of MRTF in steering MSC behavior. Also, YAP/TAZ nuclear entry does not always correlate with MSC osteogenesis in 3D, as opposed to 2D (see 'YAP/TAZ' section). Understanding a similar correlation for MRTF could help to better unravel the role of the MRTF/SRF pathway in 3D differentiation, and aid in the optimization of biomaterials. Also, we have shown that SRF expression is decreased in 3D ESP scaffold, compared to 2D controls. This is another potential pathway of regulating MRTF/SRF activity and would be interesting to investigate in different 3D biomaterials.

The nuclear lamina

Part of the extra- and intracellular forces are transmitted directly to the nucleus through the cytoskeleton. Forces on the nucleus can directly regulate gene expression through histone modifications and chromatin remodeling[158-161]. These force-induced changes in gene expression can be very rapid and can precede the effects of nuclear translocation of transcription factors such as MRTF-A[161]. The actin cytoskeleton connects to the nuclear lamina through the LINC complex. The LINC complex spans through the inner- and outer nuclear membrane and connects to the nuclear lamina[162, 163]. The nuclear lamina is a meshwork of proteins just under the inner-nuclear membrane that gives structural integrity to the nucleus. It consists of a number of proteins, among which lamin A, -B1, -C and emerin are arguably the most well-studied. Lamin A and C, more than the other nuclear lamina proteins, give the nucleus its mechanical properties[164-166]. In response to force, lamin A and C stiffen the nucleus and emerin plays an important role in regulating this stiffness increase[167]. Besides the mechanical functions, the nuclear lamina plays important roles in gene regulation. The proteins in the nuclear lamina can change the spatial distribution of DNA, impact histone modifications or directly bind to promotor regions[160, 168-171]. In addition, lamin A, -C, emerin and the LINC complex also impact nuclear localization of mechanosensitive transcription factors such as MRTF-A and YAP[21, 149, 172-174].

In 2D, MSCs express more lamin A and C, but not B1, on stiff vs soft surfaces[26]. Also, upon adipogenic differentiation, MSCs[21] and adipocytes[175] reduce lamin A and C expression. During osteogenic differentiation, MSCs increase lamin A and C expression[159, 176]. This

correlation is also functional, as lack of lamin A, C or emerin restricts the transmission of forces to the nucleus[164, 177, 178]. After lamin A and C knock down, MSCs exhibit reduced osteogenic and increased adipogenic potential[21, 174]. In addition, lamin A/C overexpression increases osteogenesis of MSCs[21, 179] and lamin A and C knock-out mice have reduced bone formation and turn-over[180]. Knockdown of MAN1, another nuclear lamina protein, increases osteogenesis and reduces adipogenesis in MSCs in 2D[181]. Lastly, disruption of the LINC complex increases adipogenesis of MSCs[174]. Besides MSCs, differentiation of other cell types is also affected by the nuclear lamina. Lamin A and C or emerin knock down decreases differentiation of, for example, muscle stem cells[163] and osteoblasts[174]. Together, these studies highlight the importance of the nuclear lamina and the LINC complex in transducing forces to the nucleus to guide differentiation of MSCs and other cell-types in 2D.

In 3D, however, very little research has been performed to elucidate the functions of the nuclear lamina in MSC differentiation. We have recently shown that the 3D environment greatly reduces lamin A and C expression, even in stiff materials[118]. We hypothesized that this was due to a difference in force distribution on the nucleus. In 2D, the actin fibers going over the nucleus create indentation sites on the nucleus[182, 183]. Lamin A, -C and LINC proteins accumulate at these indentation sites. At these indentation sites, a change in chromatin[182] and histone acetylation[183] has been observed, showing that these indentation sites can directly affect gene expression. In 2D, actin fibers going over the nucleus push down on the nucleus, creating the indentation sites. On concave surfaces, where the downward force on the nucleus is further increased, lamin A and C expression is higher[184]. In 3D, however, cells adhere in a volumetric manner, with adhesions distributed above and below the nucleus, rather than in a single 2D plane. Indeed, on convex surfaces, where downward force on the nucleus is reduced due to cellular adhesions above the nucleus, lamin A and C expression is lower. This illustrates the importance of force distribution within the cell in regulating lamin A and C expression, greatly influenced by the adhesion sites in all three dimensions (Figure 3). The impact of the change on lamin A and C expression in 3D has not yet been investigated. Actin-myosin has been shown to influence histone acetylation[85] and -methylation[185] in 3D, which it also does in 2D[186]. It has not yet been investigated whether this is coordinated by the nuclear lamina, or through other pathways. Investigating the effect of overexpression or knock-down of nuclear lamina proteins on MSC lineage commitment in different 3D settings could shed light on its role in 3D. In addition, mapping the interaction with- and re-organization of DNA by the nuclear lamina in 3D could elucidate more specific functions in gene regulation. Specifically, a better understanding is required of how forces on the nucleus regulate the expression of individual or groups of genes, and what forces nuclei experience in 3D.

Outlook on molecular mechanisms of mechanobiology in 2D and 3D

Altogether, mechanobiology in 3D remains largely underexplored. The current studies indicate roles of integrins, actin-myosin, ROCK and YAP in 3D MSC differentiation like in 2D. However, there are also conflicting reports for these proteins, hinting at alternative and independent pathways that remain to be described. RhoA and actin-myosin have also been shown to influence chondrogenesis in 2D[187], but remain poorly explored in 3D. Also, some important players in 2D MSC differentiation, such as lamin A and C and MRTF/SRF, remain almost completely unstudied in 3D MSC differentiation. On a more fundamental level, studies using atomic force microscopy and magnetic/optical tweezers to exert forces on isolated nuclei[167] could investigate the precise reaction of chromatin remodeling, histone modification, and other gene regulatory processes, to these forces. With a combination of analysis of what forces nuclei experience in 3D cell cultures, such experiments could help to better understand how the 3D environment can directly regulate gene expression.

A better understanding of the role and regulation of the proteins discussed in this section and how they work together in 3D to guide MSC differentiation could greatly aid tissue engineering. Expanding the research to include chondrogenesis as well as adipo- and osteogenesis, would aid in understanding the trilineage potential of MSCs and how to guide MSCs into a specific lineage. In the next section, we will speculate how a better understanding of cellular response to 3D material properties and the underlying molecular mechanisms could help tissue engineering and where future research could be aimed towards.

Future outlook

On flat 2D substrates, a spread morphology, actin stress fiber, nuclear YAP, among others are fairly good predictors of MSC lineage commitment and osteo- or adipogenic differentiation efficiency. In 3D, however, all of these variables don't have the same predictive power of MSC differentiation as in 2D. Having such a profile of variables that predict differentiation of MSCs in 3D could greatly aid optimization of tissue engineering scaffolds. Differentiation experiments take long (typically at least 21 days), making it difficult to test many different variables and fully explore individual material properties. A profile of variables that accurately predicts MSC differentiation in 3D could greatly reduce the time and costs of experiments. This would allow for the screening of more variables and ease material optimization, before the final scaffold is properly tested for long-term MSC differentiation.

Much research has been done on MSC differentiation into other lineages; MSCs have been proposed to differentiate into lineage of all three germ layers, such as: muscle, heart, liver, and neuronal, to name a few examples (the reader is referred to a number of critical reviews on this topic:[188-190]). This pluripotent differentiation has been proposed to be mechanosensitive[20] and is being investigated in different 3D scaffolds[191, 192].

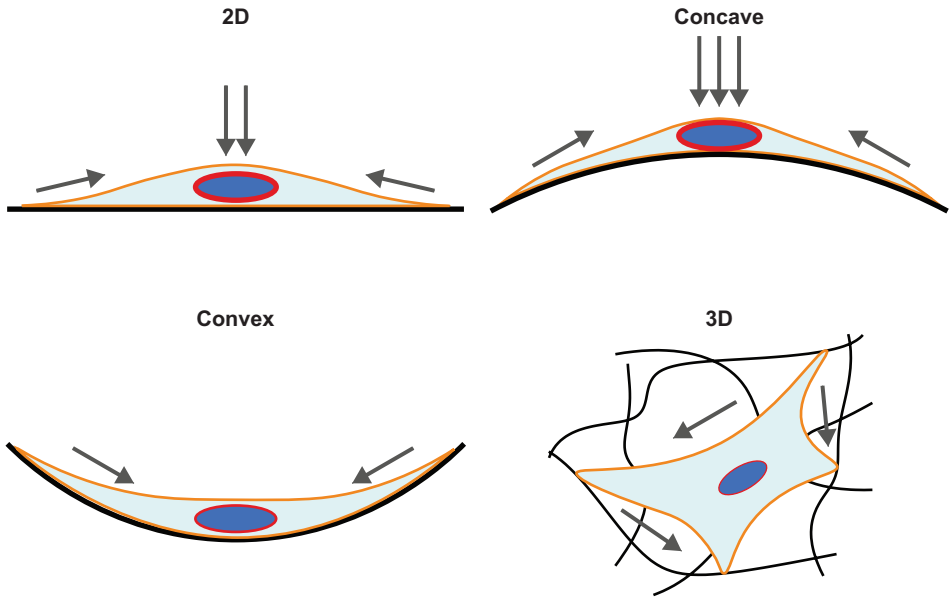

Figure 3. Forces on the nucleus are dependent on the three-dimensional distribution of adhesions. On flat 2D surfaces, adhesions form below the nucleus. Actin fibers attach to these adhesions and attach to- or go over the nucleus, creating downward force on the nucleus. On concave surfaces, this effect is enhanced because many adhesions are even further below the nucleus. On convex surfaces, many the adhesions are above the nucleus, therefore reducing the downward force on the nucleus. In 3D environments, adhesions are distributed equally in all directions, above and below the nucleus, greatly reducing the force on the nucleus.

However, no functional *in vitro* or *in vivo* differentiation of MSCs into lineage other than osteo-, chondro- or adipogenic, has yet been shown. All experiments so far reported are performed by assessing cell morphology and the expression of only a few proteins, thus keeping the possible pluripotent character of MSCs controversial. For these reasons, these studies were not considered in this review. If researchers are to further investigate the effect of materials, scaffolds and mechanobiology on this pluripotent differentiation of MSCs, we argue for the inclusion of functional tests, before strong conclusions are drawn.

With a better understanding of the fundamental process underlying MSC mechanosensing and differentiation, smarter tissue engineering constructs could be developed. As discussed in the RhoA/ROCK section, materials that change properties over time could help to activate specific pathways at specific stages of differentiation. Other proteins, such as lamin A/C or LINC complex proteins because of their key role in gene regulation, could also have an optimal window of activation. Before such materials can sensibly be developed, a thorough understand of the timing and levels of activation is required. Lastly, most 3D mechanobiological studies of MSCs are done in hydrogels. It would be beneficial to the tissue engineering field to extend this research to other 3D tissue engineering constructs, such as

electrospun, additive manufactured, or other types of scaffolds. Individual parameters are more difficult to control when creating more complex tissue engineering scaffolds with stiffer materials, making the investigation of single variables trickier. However, most parameters in these scaffolds (such as fiber size, surface roughness, pore size and shape, fiber interconnectivity, among many others) have been modified. Even though the modification of one variable is likely to change others too, tools are also available to map the different parameters. With in-depth material characterization, smart material design and the development of new materials and techniques, mechanobiology in the more complex 3D materials can surely be properly investigated.

Altogether, many recent developments have shed light on mechanobiology in 3D, but many questions still remain. Even though molecular biological studies are easiest in 2D, we argue for a greater and quicker move towards 3D. Even though more challenging, all the tools and methods are available to study 3D mechanobiology. Even though the focus of many translational tissue engineering and regenerative medicine studies is on the final application, we argue for more research on the fundamental processes that orchestrate the cellular behavior in 3D. A greater fundamental understanding could speed up translational research in the long term and will be crucial in the creation of functional tissue-engineering tissues.

References

1. P. Bianco, *"Mesenchymal" stem cells.* Annu Rev Cell Dev Biol, 2014. 30: p. 677-704.
2. P. Bianco, P.G. Robey, and P.J. Simmons, *Mesenchymal stem cells: revisiting history, concepts, and assays.* Cell stem cell, 2008. 2(4): p. 313-319.
3. J. Hao, Y. Zhang, D. Jing, Y. Shen, G. Tang, S. Huang, and Z. Zhao, *Mechanobiology of mesenchymal stem cells: Perspective into mechanical induction of MSC fate.* Acta Biomater, 2015. 20: p. 1-9.
4. A.B. Castillo and C.R. Jacobs, *Mesenchymal Stem Cell Mechanobiology.* Current Osteoporosis Reports, 2010. 8(2): p. 98-104.
5. A. Kumar, J.K. Placone, and A.J. Engler, *Understanding the extracellular forces that determine cell fate and maintenance.* Development, 2017. 144(23): p. 4261-4270.
6. D. Mohammed, M. Versaevel, C. Bruyère, L. Alaimo, M. Luciano, E. Vercruysse, A. Procès, and S. Gabriele, *Innovative Tools for Mechanobiology: Unraveling Outside-In and Inside-Out Mechanotransduction.* Frontiers in bioengineering and biotechnology, 2019. 7: p. 162-162.
7. L. Li, J. Eyckmans, and C.S. Chen, *Designer biomaterials for mechanobiology.* Nature Materials, 2017. 16(12): p. 1164-1168.
8. J.H.C. Wang and B.P. Thampatty, Chapter 7 Mechanobiology of Adult and Stem Cells, in International Review of Cell and Molecular Biology. 2008, Academic Press. p. 301-346.
9. K.A. Jansen, D.M. Donato, H.E. Balcioglu, T. Schmidt, E.H.J. Danen, and G.H. Koenderink, *A guide to mechanobiology: Where biology and physics meet.* Biochimica et Biophysica Acta (BBA) - Molecular Cell Research, 2015. 1853(11, Part B): p. 3043-3052.
10. J.Z. Kechagia, J. Ivaska, and P. Roca-Cusachs, *Integrins as biomechanical sensors of the microenvironment.* Nature Reviews Molecular Cell Biology, 2019. 20(8): p. 457-473.
11. K. Burridge, Focal adhesions: a personal perspective on a half century of progress. The FEBS Journal, 2017. 284(20): p. 3355-3361.
12. B. Geiger, J.P. Spatz, and A.D. Bershadsky, *Environmental sensing through focal adhesions.* Nature Reviews Molecular Cell Biology, 2009. 10(1): p. 21-33.
13. M. Vicente-Manzanares, X. Ma, R.S. Adelstein, and A.R. Horwitz, *Non-muscle myosin II takes centre stage in cell adhesion and migration.* Nat Rev Mol Cell Biol, 2009. 10(11): p. 778-90.
14. T. Bouzid, E. Kim, B.D. Riehl, A.M. Esfahani, J. Rosenbohm, R. Yang, B. Duan, and J.Y. Lim, *The LINC complex, mechanotransduction, and mesenchymal stem cell function and fate.* Journal of Biological Engineering, 2019. 13(1): p. 68.
15. A. Dobrzynska, S. Gonzalo, C. Shanahan, and P. Askjaer, *The nuclear lamina in health and disease.* Nucleus (Austin, Tex.), 2016. 7(3): p. 233-248.
16. R. de Leeuw, Y. Gruenbaum, and O. Medalia, *Nuclear Lamins: Thin Filaments with Major Functions.* Trends Cell Biol, 2018. 28(1): p. 34-45.
17. T. Panciera, L. Azzolin, M. Cordenonsi, and S. Piccolo, *Mechanobiology of YAP and TAZ in physiology and disease.* Nature Reviews Molecular Cell Biology, 2017. 18(12): p. 758-770.
18. G. Posern and R. Treisman, Actin' together: serum response factor, its cofactors and the link to signal transduction. Trends Cell Biol, 2006. 16(11): p. 588-96.
19. D. Gau and P. Roy, *SRF'ing and SAP'ing – the role of MRTF proteins in cell migration.* Journal of Cell Science, 2018. 131(19): p. jcs218222.
20. A.J. Engler, S. Sen, H.L. Sweeney, and D.E. Discher, *Matrix elasticity directs stem cell lineage specification.* Cell, 2006. 126(4): p. 677-89.
21. J. Swift, I.L. Ivanovska, A. Buxboim, T. Harada, P.C. Dingal, J. Pinter, J.D. Pajerowski, K.R. Spinler, J.W. Shin, M. Tewari, F. Rehfeldt, D.W. Speicher, and D.E. Discher, *Nuclear lamin-A scales with tissue stiffness and enhances matrix-directed differentiation.* Science, 2013. 341(6149): p. 1240104.

22. N.P. Talele, J. Fradette, J.E. Davies, A. Kapus, and B. Hinz, *Expression of alpha-Smooth Muscle Actin Determines the Fate of Mesenchymal Stromal Cells.* Stem Cell Reports, 2015. 4(6): p. 1016-30.
23. M. Kuroda, H. Wada, Y. Kimura, K. Ueda, and N. Kioka, Vinculin promotes nuclear localization of TAZ to inhibit ECM stiffness-dependent differentiation into adipocytes. J Cell Sci, 2017. 130(5): p. 989-1002.
24. J. Oliver-De La Cruz, G. Nardone, J. Vrbsky, A. Pompeiano, A.R. Perestrelo, F. Capradossi, K. Melajova, P. Filipensky, and G. Forte, *Substrate mechanics controls adipogenesis through YAP phosphorylation by dictating cell spreading.* Biomaterials, 2019. 205: p. 64-80.
25. M. Guvendiren and J.A. Burdick, Stiffening hydrogels to probe short- and long-term cellular responses to dynamic mechanics. Nat Commun, 2012. 3: p. 792.
26. A. Galarza Torre, J.E. Shaw, A. Wood, H.T.J. Gilbert, O. Dobre, P. Genever, K. Brennan, S.M. Richardson, and J. Swift, An immortalised mesenchymal stem cell line maintains mechano-responsive behaviour and can be used as a reporter of substrate stiffness. Sci Rep, 2018. 8(1): p. 8981.
27. J. Fu, Y.K. Wang, M.T. Yang, R.A. Desai, X. Yu, Z. Liu, and C.S. Chen, *Mechanical regulation of cell function with geometrically modulated elastomeric substrates.* Nat Methods, 2010. 7(9): p. 733-6.
28. R.J. Pelham, Jr. and Y. Wang, *Cell locomotion and focal adhesions are regulated by substrate flexibility.* Proc Natl Acad Sci U S A, 1997. 94(25): p. 13661-5.
29. M. Sun, G. Chi, P. Li, S. Lv, J. Xu, Z. Xu, Y. Xia, Y. Tan, J. Xu, L. Li, and Y. Li, Effects of Matrix Stiffness on the Morphology, Adhesion, Proliferation and Osteogenic Differentiation of Mesenchymal Stem Cells. Int J Med Sci, 2018. 15(3): p. 257-268.
30. H.J. Kwon and K. Yasuda, Chondrogenesis on sulfonate-coated hydrogels is regulated by their mechanical properties. J Mech Behav Biomed Mater, 2013. 17: p. 337-46.
31. E. Schuh, J. Kramer, J. Rohwedel, H. Notbohm, R. Muller, T. Gutsmann, and N. Rotter, *Effect of matrix elasticity on the maintenance of the chondrogenic phenotype.* Tissue Eng Part A, 2010. 16(4): p. 1281-90.
32. A. Urciuolo, M. Quarta, V. Morbidoni, F. Gattazzo, S. Molon, P. Grumati, F. Montemurro, F.S. Tedesco, B. Blaauw, G. Cossu, G. Vozzi, T.A. Rando, and P. Bonaldo, *Collagen VI regulates satellite cell self-renewal and muscle regeneration.* Nat Commun, 2013. 4: p. 1964.
33. A.J. Engler, M.A. Griffin, S. Sen, C.G. Bonnemann, H.L. Sweeney, and D.E. Discher, Myotubes differentiate optimally on substrates with tissue-like stiffness: pathological implications for soft or stiff microenvironments. J Cell Biol, 2004. 166(6): p. 877-87.
34. P.M. Gilbert, K.L. Havenstrite, K.E. Magnusson, A. Sacco, N.A. Leonardi, P. Kraft, N.K. Nguyen, S. Thrun, M.P. Lutolf, and H.M. Blau, *Substrate elasticity regulates skeletal muscle stem cell self-renewal in culture.* Science, 2010. 329(5995): p. 1078-81.
35. K.J. Boonen, K.Y. Rosaria-Chak, F.P. Baaijens, D.W. van der Schaft, and M.J. Post, *Essential environmental cues from the satellite cell niche: optimizing proliferation and differentiation.* Am J Physiol Cell Physiol, 2009. 296(6): p. C1338-45.
36. L. Macri-Pellizzeri, B. Pelacho, A. Sancho, O. Iglesias-Garcia, A.M. Simon-Yarza, M. Soriano-Navarro, S. Gonzalez-Granero, J.M. Garcia-Verdugo, E.M. De-Juan-Pardo, and F. Prosper, *Substrate stiffness and composition specifically direct differentiation of induced pluripotent stem cells.* Tissue Eng Part A, 2015. 21(9-10): p. 1633-41.
37. I.G. Kim, C.H. Gil, J. Seo, S.J. Park, R. Subbiah, T.H. Jung, J.S. Kim, Y.H. Jeong, H.M. Chung, J.H. Lee, M.R. Lee, S.H. Moon, and K. Park, *Mechanotransduction of human pluripotent stem cells cultivated on tunable cell-derived extracellular matrix.* Biomaterials, 2018. 150: p. 100-111.

38. A. Arshi, Y. Nakashima, H. Nakano, S. Eaimkhong, D. Evseenko, J. Reed, A.Z. Stieg, J.K. Gimzewski, and A. Nakano, *Rigid microenvironments promote cardiac differentiation of mouse and human embryonic stem cells.* Sci Technol Adv Mater, 2013. 14(2).
39. A.J. Engler, C. Carag-Krieger, C.P. Johnson, M. Raab, H.Y. Tang, D.W. Speicher, J.W. Sanger, J.M. Sanger, and D.E. Discher, *Embryonic cardiomyocytes beat best on a matrix with heart-like elasticity: scar-like rigidity inhibits beating.* J Cell Sci, 2008. 121(Pt 22): p. 3794-802.
40. G. Pennarossa, R. Santoro, E.F.M. Manzoni, M. Pesce, F. Gandolfi, and T.A.L. Brevini, Epigenetic Erasing and Pancreatic Differentiation of Dermal Fibroblasts into Insulin-Producing Cells are Boosted by the Use of Low-Stiffness Substrate. Stem Cell Rev Rep, 2018. 14(3): p. 398-411.
41. B. Venugopal, P. Mogha, J. Dhawan, and A. Majumder, Cell density overrides the effect of substrate stiffness on human mesenchymal stem cells' morphology and proliferation. Biomater Sci, 2018. 6(5): p. 1109-1119.
42. Y.H. Zhao, X. Lv, Y.L. Liu, Y. Zhao, Q. Li, Y.J. Chen, and M. Zhang, Hydrostatic pressure promotes the proliferation and osteogenic/chondrogenic differentiation of mesenchymal stem cells: The roles of RhoA and Rac1. Stem Cell Res, 2015. 14(3): p. 283-96.
43. C. Monge, N. DiStasio, T. Rossi, M. Sebastien, H. Sakai, B. Kalman, T. Boudou, S. Tajbakhsh, I. Marty, A. Bigot, V. Mouly, and C. Picart, *Quiescence of human muscle stem cells is favored by culture on natural biopolymeric films.* Stem Cell Res Ther, 2017. 8(1): p. 104.
44. T.A. Ulrich, E.M. de Juan Pardo, and S. Kumar, The mechanical rigidity of the extracellular matrix regulates the structure, motility, and proliferation of glioma cells. Cancer Res, 2009. 69(10): p. 4167-74.
45. H.B. Wang, M. Dembo, and Y.L. Wang, *Substrate flexibility regulates growth and apoptosis of normal but not transformed cells.* Am J Physiol Cell Physiol, 2000. 279(5): p. C1345-50.
46. N. Huebsch, P.R. Arany, A.S. Mao, D. Shvartsman, O.A. Ali, S.A. Bencherif, J. Rivera-Feliciano, and D.J. Mooney, *Harnessing traction-mediated manipulation of the cell/matrix interface to control stem-cell fate.* Nat Mater, 2010. 9(6): p. 518-26.
47. X.T. He, R.X. Wu, X.Y. Xu, J. Wang, Y. Yin, and F.M. Chen, Macrophage involvement affects matrix stiffness-related influences on cell osteogenesis under three-dimensional culture conditions. Acta Biomater, 2018. 71: p. 132-147.
48. S. Khetan, M. Guvendiren, W.R. Legant, D.M. Cohen, C.S. Chen, and J.A. Burdick, *Degradation-mediated cellular traction directs stem cell fate in covalently crosslinked three-dimensional hydrogels.* Nat Mater, 2013. 12(5): p. 458-65.
49. S.R. Caliari, S.L. Vega, M. Kwon, E.M. Soulas, and J.A. Burdick, *Dimensionality and spreading influence MSC YAP/TAZ signaling in hydrogel environments.* Biomaterials, 2016. 103: p. 314-323.
50. S.A. Ferreira, M.S. Motwani, P.A. Faull, A.J. Seymour, T.T.L. Yu, M. Enayati, D.K. Taheem, C. Salzlechner, T. Haghighi, E.M. Kania, O.P. Oommen, T. Ahmed, S. Loaiza, K. Parzych, F. Dazzi, O.P. Varghese, F. Festy, A.E. Grigoriadis, H.W. Auner, A.P. Snijders, L. Bozec, and E. Gentleman, *Bi-directional cell-pericellular matrix interactions direct stem cell fate.* Nat Commun, 2018. 9(1): p. 4049.
51. C. Lu, X.Y. Li, Y. Hu, R.G. Rowe, and S.J. Weiss, *MT1-MMP controls human mesenchymal stem cell trafficking and differentiation.* Blood, 2010. 115(2): p. 221-9.
52. Y. Tang, R.G. Rowe, E.L. Botvinick, A. Kurup, A.J. Putnam, M. Seiki, V.M. Weaver, E.T. Keller, S. Goldstein, J. Dai, D. Begun, T. Saunders, and S.J. Weiss, *MT1-MMP-dependent control of skeletal stem cell commitment via a beta1-integrin/YAP/TAZ signaling axis.* Dev Cell, 2013. 25(4): p. 402-16.
53. H.J. Kong, D. Kaigler, K. Kim, and D.J. Mooney, *Controlling rigidity and degradation of alginate hydrogels via molecular weight distribution.* Biomacromolecules, 2004. 5(5): p. 1720-7.

54. O. Chaudhuri, L. Gu, D. Klumpers, M. Darnell, S.A. Bencherif, J.C. Weaver, N. Huebsch, H.P. Lee, E. Lippens, G.N. Duda, and D.J. Mooney, *Hydrogels with tunable stress relaxation regulate stem cell fate and activity.* Nat Mater, 2016. 15(3): p. 326-34.
55. H.P. Lee, R. Stowers, and O. Chaudhuri, Volume expansion and TRPV4 activation regulate stem cell fate in three-dimensional microenvironments. Nat Commun, 2019. 10(1): p. 529.
56. M. Darnell, S. Young, L. Gu, N. Shah, E. Lippens, J. Weaver, G. Duda, and D. Mooney, *Substrate Stress-Relaxation Regulates Scaffold Remodeling and Bone Formation In Vivo.* Adv Healthc Mater, 2017. 6(1).
57. S. Nam, R. Stowers, J. Lou, Y. Xia, and O. Chaudhuri, Varying PEG density to control stress relaxation in alginate-PEG hydrogels for 3D cell culture studies. Biomaterials, 2019. 200: p. 15-24.
58. J. Patterson and J.A. Hubbell, Enhanced proteolytic degradation of molecularly engineered PEG hydrogels in response to MMP-1 and MMP-2. Biomaterials, 2010. 31(30): p. 7836-45.
59. S. Nam and O. Chaudhuri, Mitotic cells generate protrusive extracellular forces to divide in three-dimensional microenvironments. Nature Physics, 2018. 14(6): p. 621-628.
60. S. Nam, J. Lee, D.G. Brownfield, and O. Chaudhuri, *Viscoplasticity Enables Mechanical Remodeling of Matrix by Cells.* Biophys J, 2016. 111(10): p. 2296-2308.
61. O. Chaudhuri, L. Gu, M. Darnell, D. Klumpers, S.A. Bencherif, J.C. Weaver, N. Huebsch, and D.J. Mooney, *Substrate stress relaxation regulates cell spreading.* Nat Commun, 2015. 6: p. 6364.
62. R. Changede, H. Cai, S.J. Wind, and M.P. Sheetz, *Integrin nanoclusters can bridge thin matrix fibres to form cell–matrix adhesions.* Nature Materials, 2019. 18(12): p. 1366-1375.
63. B.M. Baker and C.S. Chen, Deconstructing the third dimension: how 3D culture microenvironments alter cellular cues. J Cell Sci, 2012. 125(Pt 13): p. 3015-24.
64. A. Pathak and S. Kumar, Biophysical regulation of tumor cell invasion: moving beyond matrix stiffness. Integr Biol (Camb), 2011. 3(4): p. 267-78.
65. J.A. Pedersen and M.A. Swartz, *Mechanobiology in the third dimension.* Ann Biomed Eng, 2005. 33(11): p. 1469-90.
66. B.M. Baker, B. Trappmann, W.Y. Wang, M.S. Sakar, I.L. Kim, V.B. Shenoy, J.A. Burdick, and C.S. Chen, *Cell-mediated fibre recruitment drives extracellular matrix mechanosensing in engineered fibrillar microenvironments.* Nat Mater, 2015. 14(12): p. 1262-8.
67. J. Xie, M. Bao, S.M.C. Bruekers, and W.T.S. Huck, *Collagen Gels with Different Fibrillar Microarchitectures Elicit Different Cellular Responses.* ACS Appl Mater Interfaces, 2017. 9(23): p. 19630-19637.
68. X. Cao, E. Ban, B.M. Baker, Y. Lin, J.A. Burdick, C.S. Chen, and V.B. Shenoy, *Multiscale model predicts increasing focal adhesion size with decreasing stiffness in fibrous matrices.* Proc Natl Acad Sci U S A, 2017. 114(23): p. E4549-E4555.
69. M.D. Davidson, K.H. Song, M.-H. Lee, J. Llewellyn, Y. Du, B.M. Baker, R.G. Wells, and J.A. Burdick, *Engineered Fibrous Networks To Investigate the Influence of Fiber Mechanics on Myofibroblast Differentiation.* ACS Biomaterials Science & Engineering, 2019. 5(8): p. 3899-3908.
70. L. Bian, M. Guvendiren, R.L. Mauck, and J.A. Burdick, *Hydrogels that mimic developmentally relevant matrix and N-cadherin interactions enhance MSC chondrogenesis.* Proc Natl Acad Sci U S A, 2013. 110(25): p. 10117-22.
71. H.P. Lee, L. Gu, D.J. Mooney, M.E. Levenston, and O. Chaudhuri, *Mechanical confinement regulates cartilage matrix formation by chondrocytes.* Nat Mater, 2017. 16(12): p. 1243-1251.
72. J. Zonderland, I. Moldero Lorenzo, C. Mota, and L. Moroni, *Dimensionality changes actin network through lamin A/C and zyxin.* BioRxiv https://doi.org/10.1101/752691, 2019.
73. S.J. Sequeira, D.A. Soscia, B. Oztan, A.P. Mosier, R. Jean-Gilles, A. Gadre, N.C. Cady, B. Yener, J. Castracane, and M. Larsen, *The regulation of focal adhesion complex formation and salivary gland epithelial cell organization by nanofibrous PLGA scaffolds.* Biomaterials, 2012. 33(11): p. 3175-86.

74. C.Y. Tay, Y.-L. Wu, P. Cai, N.S. Tan, S.S. Venkatraman, X. Chen, and L.P. Tan, Bio-inspired micropatterned hydrogel to direct and deconstruct hierarchical processing of geometry-force signals by human mesenchymal stem cells during smooth muscle cell differentiation. NPG Asia Materials, 2015. 7(7): p. e199-e199.
75. X. Wang, X. Hu, I. Dulinska-Molak, N. Kawazoe, Y. Yang, and G. Chen, Discriminating the Independent Influence of Cell Adhesion and Spreading Area on Stem Cell Fate Determination Using Micropatterned Surfaces. Sci Rep, 2016. 6: p. 28708.
76. R. McBeath, D.M. Pirone, C.M. Nelson, K. Bhadriraju, and C.S. Chen, *Cell shape, cytoskeletal tension, and RhoA regulate stem cell lineage commitment.* Dev Cell, 2004. 6(4): p. 483-95.
77. K.A. Kilian, B. Bugarija, B.T. Lahn, and M. Mrksich, *Geometric cues for directing the differentiation of mesenchymal stem cells.* Proc Natl Acad Sci U S A, 2010. 107(11): p. 4872-7.
78. C.S. Chen, M. Mrksich, S. Huang, G.M. Whitesides, and D.E. Ingber, *Geometric control of cell life and death.* Science, 1997. 276(5317): p. 1425-8.
79. N. Minc, D. Burgess, and F. Chang, *Influence of cell geometry on division-plane positioning.* Cell, 2011. 144(3): p. 414-26.
80. X. Jiang, D.A. Bruzewicz, A.P. Wong, M. Piel, and G.M. Whitesides, *Directing cell migration with asymmetric micropatterns.* Proc Natl Acad Sci U S A, 2005. 102(4): p. 975-8.
81. B. Chen, G. Kumar, C.C. Co, and C.C. Ho, *Geometric control of cell migration.* Sci Rep, 2013. 3: p. 2827.
82. J. Lee, A.A. Abdeen, K.L. Wycislo, T.M. Fan, and K.A. Kilian, *Interfacial geometry dictates cancer cell tumorigenicity.* Nat Mater, 2016. 15(8): p. 856-62.
83. A.C. Jimenez-Vergara, R. Zurita, A. Jones, P. Diaz-Rodriguez, X. Qu, K.L. Kusima, M.S. Hahn, and D.J. Munoz-Pinto, *Refined assessment of the impact of cell shape on human mesenchymal stem cell differentiation in 3D contexts.* Acta Biomater, 2019. 87: p. 166-176.
84. G. Kumar, M.S. Waters, T.M. Farooque, M.F. Young, and C.G. Simon, Jr., Freeform fabricated scaffolds with roughened struts that enhance both stem cell proliferation and differentiation by controlling cell shape. Biomaterials, 2012. 33(16): p. 4022-30.
85. M. Bao, J. Xie, A. Piruska, and W.T.S. Huck, *3D microniches reveal the importance of cell size and shape.* Nature Communications, 2017. 8(1): p. 1962.
86. K. Xie, Y. Yang, and H. Jiang, Controlling Cellular Volume via Mechanical and Physical Properties of Substrate. Biophys J, 2018. 114(3): p. 675-687.
87. M. Guo, A.F. Pegoraro, A. Mao, E.H. Zhou, P.R. Arany, Y. Han, D.T. Burnette, M.H. Jensen, K.E. Kasza, J.R. Moore, F.C. Mackintosh, J.J. Fredberg, D.J. Mooney, J. Lippincott-Schwartz, and D.A. Weitz, *Cell volume change through water efflux impacts cell stiffness and stem cell fate.* Proc Natl Acad Sci U S A, 2017. 114(41): p. E8618-E8627.
88. Z. Sun, S.S. Guo, and R. Fassler, *Integrin-mediated mechanotransduction.* J Cell Biol, 2016. 215(4): p. 445-456.
89. Z. Hamidouche, O. Fromigue, J. Ringe, T. Haupl, P. Vaudin, J.C. Pages, S. Srouji, E. Livne, and P.J. Marie, *Priming integrin alpha5 promotes human mesenchymal stromal cell osteoblast differentiation and osteogenesis.* Proc Natl Acad Sci U S A, 2009. 106(44): p. 18587-91.
90. Y.R. Shih, K.F. Tseng, H.Y. Lai, C.H. Lin, and O.K. Lee, Matrix stiffness regulation of integrin-mediated mechanotransduction during osteogenic differentiation of human mesenchymal stem cells. J Bone Miner Res, 2011. 26(4): p. 730-8.
91. Q. Chen, P. Shou, L. Zhang, C. Xu, C. Zheng, Y. Han, W. Li, Y. Huang, X. Zhang, C. Shao, A.I. Roberts, A.B. Rabson, G. Ren, Y. Zhang, Y. Wang, D.T. Denhardt, and Y. Shi, *An osteopontin-integrin interaction plays a critical role in directing adipogenesis and osteogenesis by mesenchymal stem cells.* Stem Cells, 2014. 32(2): p. 327-37.

92. E.M. Morandi, R. Verstappen, M.E. Zwierzina, S. Geley, G. Pierer, and C. Ploner, ITGAV and ITGA5 diversely regulate proliferation and adipogenic differentiation of human adipose derived stem cells. Sci Rep, 2016. 6: p. 28889.
93. Y.P. Lo, Y.S. Liu, M.G. Rimando, J.H. Ho, K.H. Lin, and O.K. Lee, Three-dimensional spherical spatial boundary conditions differentially regulate osteogenic differentiation of mesenchymal stromal cells. Sci Rep, 2016. 6: p. 21253.
94. C. Loebel, R.L. Mauck, and J.A. Burdick, Local nascent protein deposition and remodelling guide mesenchymal stromal cell mechanosensing and fate in three-dimensional hydrogels. Nat Mater, 2019. 18(8): p. 883-891.
95. S.H. Parekh, K. Chatterjee, S. Lin-Gibson, N.M. Moore, M.T. Cicerone, M.F. Young, and C.G. Simon, Jr., Modulus-driven differentiation of marrow stromal cells in 3D scaffolds that is independent of myosin-based cytoskeletal tension. Biomaterials, 2011. 32(9): p. 2256-64.
96. J. Hu, H. Liao, Z. Ma, H. Chen, Z. Huang, Y. Zhang, M. Yu, Y. Chen, and J. Xu, Focal Adhesion Kinase Signaling Mediated the Enhancement of Osteogenesis of Human Mesenchymal Stem Cells Induced by Extracorporeal Shockwave. Sci Rep, 2016. 6: p. 20875.
97. A. Elosegui-Artola, R. Oria, Y. Chen, A. Kosmalska, C. Perez-Gonzalez, N. Castro, C. Zhu, X. Trepat, and P. Roca-Cusachs, *Mechanical regulation of a molecular clutch defines force transmission and transduction in response to matrix rigidity.* Nat Cell Biol, 2016. 18(5): p. 540-8.
98. C. Wu, Focal adhesion: a focal point in current cell biology and molecular medicine. Cell Adh Migr, 2007. 1(1): p. 13-8.
99. M. Gupta, B. Doss, C.T. Lim, R. Voituriez, and B. Ladoux, Single cell rigidity sensing: A complex relationship between focal adhesion dynamics and large-scale actin cytoskeleton remodeling. Cell Adh Migr, 2016. 10(5): p. 554-567.
100. P. Atherton, B. Stutchbury, D. Jethwa, and C. Ballestrem, *Mechanosensitive components of integrin adhesions: Role of vinculin.* Exp Cell Res, 2016. 343(1): p. 21-27.
101. E.G. Kleinschmidt and D.D. Schlaepfer, *Focal adhesion kinase signaling in unexpected places.* Curr Opin Cell Biol, 2017. 45: p. 24-30.
102. A.M. López-Colomé, I. Lee-Rivera, R. Benavides-Hidalgo, and E. López, *Paxillin: a crossroad in pathological cell migration.* Journal of Hematology & Oncology, 2017. 10(1): p. 50.
103. B. Klapholz and N.H. Brown, *Talin – the master of integrin adhesions.* Journal of Cell Science, 2017. 130(15): p. 2435.
104. H. Hirata, H. Tatsumi, and M. Sokabe, *Zyxin emerges as a key player in the mechanotransduction at cell adhesive structures.* Commun Integr Biol, 2008. 1(2): p. 192-5.
105. P.S. Mathieu and E.G. Loboa, Cytoskeletal and focal adhesion influences on mesenchymal stem cell shape, mechanical properties, and differentiation down osteogenic, adipogenic, and chondrogenic pathways. Tissue Eng Part B Rev, 2012. 18(6): p. 436-44.
106. W. Zheng, X. Gu, X. Sun, Q. Wu, and H. Dan, *FAK mediates BMP9-induced osteogenic differentiation via Wnt and MAPK signaling pathway in synovial mesenchymal stem cells.* Artificial Cells, Nanomedicine, and Biotechnology, 2019. 47(1): p. 2641-2649.
107. C. Yuan, X. Gou, J. Deng, Z. Dong, P. Ye, and Z. Hu, FAK and BMP-9 synergistically trigger osteogenic differentiation and bone formation of adipose derived stem cells through enhancing Wnt-beta-catenin signaling. Biomed Pharmacother, 2018. 105: p. 753-757.
108. D. Rajshankar, Y. Wang, and C.A. McCulloch, Osteogenesis requires FAK-dependent collagen synthesis by fibroblasts and osteoblasts. FASEB J, 2017. 31(3): p. 937-953.
109. A.K. Kundu and A.J. Putnam, Vitronectin and collagen I differentially regulate osteogenesis in mesenchymal stem cells. Biochem Biophys Res Commun, 2006. 347(1): p. 347-57.

110. F.Y. Lee, Y.Y. Zhen, C.M. Yuen, R. Fan, Y.T. Chen, J.J. Sheu, Y.L. Chen, C.J. Wang, C.K. Sun, and H.K. Yip, *The mTOR-FAK mechanotransduction signaling axis for focal adhesion maturation and cell proliferation.* Am J Transl Res, 2017. 9(4): p. 1603-1617.
111. J.S. Lee, L. Ha, I.K. Kwon, and J.Y. Lim, *The role of focal adhesion kinase in BMP4 induction of mesenchymal stem cell adipogenesis.* Biochem Biophys Res Commun, 2013. 435(4): p. 696-701.
112. J.J. Li and D. Xie, Cleavage of focal adhesion kinase (FAK) is essential in adipocyte differentiation. Biochem Biophys Res Commun, 2007. 357(3): p. 648-54.
113. C. Schreiber, S. Saraswati, S. Harkins, A. Gruber, N. Cremers, W. Thiele, M. Rothley, D. Plaumann, C. Korn, O. Armant, H.G. Augustin, and J.P. Sleeman, *Loss of ASAP1 in mice impairs adipogenic and osteogenic differentiation of mesenchymal progenitor cells through dysregulation of FAK/Src and AKT signaling.* PLoS Genet, 2019. 15(6): p. e1008216.
114. C.T. Luk, S.Y. Shi, E.P. Cai, T. Sivasubramaniyam, M. Krishnamurthy, J.J. Brunt, S.A. Schroer, D.A. Winer, and M. Woo, *FAK signalling controls insulin sensitivity through regulation of adipocyte survival.* Nat Commun, 2017. 8: p. 14360.
115. S.I. Fraley, Y. Feng, R. Krishnamurthy, D.H. Kim, A. Celedon, G.D. Longmore, and D. Wirtz, *A distinctive role for focal adhesion proteins in three-dimensional cell motility.* Nat Cell Biol, 2010. 12(6): p. 598-604.
116. S.R. Peyton, P.D. Kim, C.M. Ghajar, D. Seliktar, and A.J. Putnam, The effects of matrix stiffness and RhoA on the phenotypic plasticity of smooth muscle cells in a 3-D biosynthetic hydrogel system. Biomaterials, 2008. 29(17): p. 2597-607.
117. A.D. Doyle and K.M. Yamada, *Mechanosensing via cell-matrix adhesions in 3D microenvironments.* Exp Cell Res, 2016. 343(1): p. 60-66.
118. J. Zonderland, I.L. Moldero, C. Mota, and L. Moroni, *Dimensionality changes actin network through lamin A and C and zyxin.* bioRxiv, 2019: p. 752691.
119. J. Zonderland, S. Rezzola, and L. Moroni, *Mechanosensitive regulation of FGFR1 through the MRTF-SRF pathway.* bioRxiv, 2019: p. 782243.
120. S.I. Fraley, Y. Feng, A. Giri, G.D. Longmore, and D. Wirtz, *Dimensional and temporal controls of three-dimensional cell migration by zyxin and binding partners.* Nature Communications, 2012. 3(1): p. 719.
121. Y.K. Wang, X. Yu, D.M. Cohen, M.A. Wozniak, M.T. Yang, L. Gao, J. Eyckmans, and C.S. Chen, Bone morphogenetic protein-2-induced signaling and osteogenesis is regulated by cell shape, RhoA/ROCK, and cytoskeletal tension. Stem Cells Dev, 2012. 21(7): p. 1176-86.
122. R.J. McMurray, N. Gadegaard, P.M. Tsimbouri, K.V. Burgess, L.E. McNamara, R. Tare, K. Murawski, E. Kingham, R.O.C. Oreffo, and M.J. Dalby, *Nanoscale surfaces for the long-term maintenance of mesenchymal stem cell phenotype and multipotency.* Nature Materials, 2011. 10(8): p. 637-644.
123. C.H. Seo, H. Jeong, Y. Feng, K. Montagne, T. Ushida, Y. Suzuki, and K.S. Furukawa, Micropit surfaces designed for accelerating osteogenic differentiation of murine mesenchymal stem cells via enhancing focal adhesion and actin polymerization. Biomaterials, 2014. 35(7): p. 2245-52.
124. X. Yao, R. Peng, and J. Ding, Effects of aspect ratios of stem cells on lineage commitments with and without induction media. Biomaterials, 2013. 34(4): p. 930-9.
125. F.R. Maia, K.B. Fonseca, G. Rodrigues, P.L. Granja, and C.C. Barrias, *Matrix-driven formation of mesenchymal stem cell-extracellular matrix microtissues on soft alginate hydrogels.* Acta Biomater, 2014. 10(7): p. 3197-208.
126. K.P. Bennett, C. Bergeron, E. Acar, R.F. Klees, S.L. Vandenberg, B. Yener, and G.E. Plopper, *Proteomics reveals multiple routes to the osteogenic phenotype in mesenchymal stem cells.* BMC Genomics, 2007. 8: p. 380.
127. R.G. Hodge and A.J. Ridley, *Regulating Rho GTPases and their regulators.* Nature Reviews Molecular Cell Biology, 2016. 17(8): p. 496-510.

128. M. Amano, M. Nakayama, and K. Kaibuchi, *Rho-kinase/ROCK: A key regulator of the cytoskeleton and cell polarity.* Cytoskeleton (Hoboken), 2010. 67(9): p. 545-54.
129. K.M. Riching and P.J. Keely, *Rho family GTPases: making it to the third dimension.* Int J Biochem Cell Biol, 2015. 59: p. 111-5.
130. L. Zhang, G. Jiang, X. Zhao, and Y. Gong, *Dimethyloxalylglycine Promotes Bone Marrow Mesenchymal Stem Cell Osteogenesis via Rho/ROCK Signaling.* Cellular Physiology and Biochemistry, 2016. 39(4): p. 1391-1403.
131. Z. Chen, X. Wang, Y. Shao, D. Shi, T. Chen, D. Cui, and X. Jiang, Synthetic osteogenic growth peptide promotes differentiation of human bone marrow mesenchymal stem cells to osteoblasts via RhoA/ROCK pathway. Molecular and Cellular Biochemistry, 2011. 358(1): p. 221-227.
132. S.A. Ruiz and C.S. Chen, Emergence of patterned stem cell differentiation within multicellular structures. Stem Cells, 2008. 26(11): p. 2921-7.
133. L. Zhang, G. Jiang, X. Zhao, and Y. Gong, Dimethyloxalylglycine Promotes Bone Marrow Mesenchymal Stem Cell Osteogenesis via Rho/ROCK Signaling. Cell Physiol Biochem, 2016. 39(4): p. 1391-403.
134. M.E. McDonald, C. Li, H. Bian, B.D. Smith, M.D. Layne, and S.R. Farmer, *Myocardin-related transcription factor A regulates conversion of progenitors to beige adipocytes.* Cell, 2015. 160(1-2): p. 105-118.
135. S.P. Davies, H. Reddy, M. Caivano, and P. Cohen, *Specificity and mechanism of action of some commonly used protein kinase inhibitors.* The Biochemical journal, 2000. 351(Pt 1): p. 95-105.
136. J. Bain, L. Plater, M. Elliott, N. Shpiro, C.J. Hastie, H. McLauchlan, I. Klevernic, J.S.C. Arthur, D.R. Alessi, and P. Cohen, *The selectivity of protein kinase inhibitors: a further update.* The Biochemical journal, 2007. 408(3): p. 297-315.
137. V.E. Meyers, M. Zayzafoon, J.T. Douglas, and J.M. McDonald, RhoA and cytoskeletal disruption mediate reduced osteoblastogenesis and enhanced adipogenesis of human mesenchymal stem cells in modeled microgravity. J Bone Miner Res, 2005. 20(10): p. 1858-66.
138. P.D. Prowse, C.G. Elliott, J. Hutter, and D.W. Hamilton, Inhibition of Rac and ROCK signalling influence osteoblast adhesion, differentiation and mineralization on titanium topographies. PLoS One, 2013. 8(3): p. e58898.
139. D. Harmey, G. Stenbeck, C.D. Nobes, A.J. Lax, and A.E. Grigoriadis, Regulation of osteoblast differentiation by Pasteurella multocida toxin (PMT): a role for Rho GTPase in bone formation. J Bone Miner Res, 2004. 19(4): p. 661-70.
140. H. Yoshikawa, K. Yoshioka, T. Nakase, and K. Itoh, *Stimulation of ectopic bone formation in response to BMP-2 by Rho kinase inhibitor: a pilot study.* Clin Orthop Relat Res, 2009. 467(12): p. 3087-95.
141. I. Kanazawa, T. Yamaguchi, S. Yano, M. Yamauchi, and T. Sugimoto, Activation of AMP kinase and inhibition of Rho kinase induce the mineralization of osteoblastic MC3T3-E1 cells through endothelial NOS and BMP-2 expression. Am J Physiol Endocrinol Metab, 2009. 296(1): p. E139-46.
142. C.B. Khatiwala, P.D. Kim, S.R. Peyton, and A.J. Putnam, *ECM Compliance Regulates Osteogenesis by Influencing MAPK Signaling Downstream of RhoA and ROCK.* Journal of Bone and Mineral Research, 2009. 24(5): p. 886-898.
143. S.W. Tsai, H.M. Liou, C.J. Lin, K.L. Kuo, Y.S. Hung, R.C. Weng, and F.Y. Hsu, MG63 osteoblast-like cells exhibit different behavior when grown on electrospun collagen matrix versus electrospun gelatin matrix. PLoS One, 2012. 7(2): p. e31200.
144. O. Dobrokhotov, M. Samsonov, M. Sokabe, and H. Hirata, *Mechanoregulation and pathology of YAP/TAZ via Hippo and non-Hippo mechanisms.* Clin Transl Med, 2018. 7(1): p. 23.

145. S. Dupont, L. Morsut, M. Aragona, E. Enzo, S. Giulitti, M. Cordenonsi, F. Zanconato, J. Le Digabel, M. Forcato, S. Bicciato, N. Elvassore, and S. Piccolo, *Role of YAP/TAZ in mechanotransduction.* Nature, 2011. 474(7350): p. 179-183.

146. Y. Zhu, Y. Wu, J. Cheng, Q. Wang, Z. Li, Y. Wang, D. Wang, H. Wang, W. Zhang, J. Ye, H. Jiang, and L. Wang, *Pharmacological activation of TAZ enhances osteogenic differentiation and bone formation of adipose-derived stem cells.* Stem Cell Res Ther, 2018. 9(1): p. 53.

147. Z. Chen, Q. Luo, C. Lin, and G. Song, Simulated microgravity inhibits osteogenic differentiation of mesenchymal stem cells through down regulating the transcriptional co-activator TAZ. Biochem Biophys Res Commun, 2015. 468(1-2): p. 21-6.

148. H. Pan, Y. Xie, Z. Zhang, K. Li, D. Hu, X. Zheng, Q. Fan, and T. Tang, *YAP-mediated mechanotransduction regulates osteogenic and adipogenic differentiation of BMSCs on hierarchical structure.* Colloids Surf B Biointerfaces, 2017. 152: p. 344-353.

149. H.W. Park, Y.C. Kim, B. Yu, T. Moroishi, J.S. Mo, S.W. Plouffe, Z. Meng, K.C. Lin, F.X. Yu, C.M. Alexander, C.Y. Wang, and K.L. Guan, *Alternative Wnt Signaling Activates YAP/TAZ.* Cell, 2015. 162(4): p. 780-94.

150. J.H. Hong, E.S. Hwang, M.T. McManus, A. Amsterdam, Y. Tian, R. Kalmukova, E. Mueller, T. Benjamin, B.M. Spiegelman, P.A. Sharp, N. Hopkins, and M.B. Yaffe, *TAZ, a transcriptional modulator of mesenchymal stem cell differentiation.* Science, 2005. 309(5737): p. 1074-8.

151. C.D. Kegelman, D.E. Mason, J.H. Dawahare, D.J. Horan, G.D. Vigil, S.S. Howard, A.G. Robling, T.M. Bellido, and J.D. Boerckel, *Skeletal cell YAP and TAZ combinatorially promote bone development.* FASEB J, 2018. 32(5): p. 2706-2721.

152. M. Finch-Edmondson and M. Sudol, *Framework to function: mechanosensitive regulators of gene transcription.* Cellular & molecular biology letters, 2016. 21: p. 28-28.

153. C. Esnault, A. Stewart, F. Gualdrini, P. East, S. Horswell, N. Matthews, and R. Treisman, *Rho-actin signaling to the MRTF coactivators dominates the immediate transcriptional response to serum in fibroblasts.* Genes & development, 2014. 28(9): p. 943-958.

154. H. Bian, J.Z. Lin, C. Li, and S.R. Farmer, Myocardin-related transcription factor A (MRTFA) regulates the fate of bone marrow mesenchymal stem cells and its absence in mice leads to osteopenia. Molecular metabolism, 2016. 5(10): p. 970-979.

155. H. Nobusue, N. Onishi, T. Shimizu, E. Sugihara, Y. Oki, Y. Sumikawa, T. Chiyoda, K. Akashi, H. Saya, and K. Kano, *Regulation of MKL1 via actin cytoskeleton dynamics drives adipocyte differentiation.* Nature Communications, 2014. 5(1): p. 3368.

156. T.S. Mikkelsen, Z. Xu, X. Zhang, L. Wang, J.M. Gimble, E.S. Lander, and E.D. Rosen, *Comparative epigenomic analysis of murine and human adipogenesis.* Cell, 2010. 143(1): p. 156-169.

157. J. Chen, K. Yuan, X. Mao, J.M. Miano, H. Wu, and Y. Chen, *Serum response factor regulates bone formation via IGF-1 and Runx2 signals.* Journal of bone and mineral research : the official journal of the American Society for Bone and Mineral Research, 2012. 27(8): p. 1659-1668.

158. Y. Li, J.S. Chu, K. Kurpinski, X. Li, D.M. Bautista, L. Yang, K.L.P. Sung, and S. Li, *Biophysical regulation of histone acetylation in mesenchymal stem cells.* Biophysical journal, 2011. 100(8): p. 1902-1909.

159. E. Makhija, D.S. Jokhun, and G.V. Shivashankar, *Nuclear deformability and telomere dynamics are regulated by cell geometric constraints.* Proceedings of the National Academy of Sciences of the United States of America, 2016. 113(1): p. E32-E40.

160. H.Q. Le, S. Ghatak, C.-Y.C. Yeung, F. Tellkamp, C. Günschmann, C. Dieterich, A. Yeroslaviz, B. Habermann, A. Pombo, C.M. Niessen, and S.A. Wickström, *Mechanical regulation of transcription controls Polycomb-mediated gene silencing during lineage commitment.* Nature cell biology, 2016. 18(8): p. 864-875.

161. A. Tajik, Y. Zhang, F. Wei, J. Sun, Q. Jia, W. Zhou, R. Singh, N. Khanna, A.S. Belmont, and N. Wang, *Transcription upregulation via force-induced direct stretching of chromatin.* Nature materials, 2016. 15(12): p. 1287-1296.

162. G. Uzer, C.T. Rubin, and J. Rubin, *Cell Mechanosensitivity Is Enabled by the LINC Nuclear Complex.* Current Molecular Biology Reports, 2016. 2(1): p. 36-47.

163. R.L. Frock, B.A. Kudlow, A.M. Evans, S.A. Jameson, S.D. Hauschka, and B.K. Kennedy, *Lamin A/C and emerin are critical for skeletal muscle satellite cell differentiation.* Genes & development, 2006. 20(4): p. 486-500.

164. J. Lammerding, J. Hsiao, P.C. Schulze, S. Kozlov, C.L. Stewart, and R.T. Lee, *Abnormal nuclear shape and impaired mechanotransduction in emerin-deficient cells.* J Cell Biol, 2005. 170(5): p. 781-91.

165. J. Lammerding, L.G. Fong, J.Y. Ji, K. Reue, C.L. Stewart, S.G. Young, and R.T. Lee, *Lamins A and C but not lamin B1 regulate nuclear mechanics.* The Journal of biological chemistry, 2006. 281(35): p. 25768-25780.

166. J.D. Pajerowski, K.N. Dahl, F.L. Zhong, P.J. Sammak, and D.E. Discher, *Physical plasticity of the nucleus in stem cell differentiation.* Proceedings of the National Academy of Sciences of the United States of America, 2007. 104(40): p. 15619-15624.

167. C. Guilluy, L.D. Osborne, L. Van Landeghem, L. Sharek, R. Superfine, R. Garcia-Mata, and K. Burridge, *Isolated nuclei adapt to force and reveal a mechanotransduction pathway in the nucleus.* Nature cell biology, 2014. 16(4): p. 376-381.

168. S. Osmanagic-Myers, T. Dechat, and R. Foisner, *Lamins at the crossroads of mechanosignaling.* Genes & development, 2015. 29(3): p. 225-237.

169. E. Lund, A.R. Oldenburg, E. Delbarre, C.T. Freberg, I. Duband-Goulet, R. Eskeland, B. Buendia, and P. Collas, *Lamin A/C-promoter interactions specify chromatin state-dependent transcription outcomes.* Genome research, 2013. 23(10): p. 1580-1589.

170. L. Guelen, L. Pagie, E. Brasset, W. Meuleman, M.B. Faza, W. Talhout, B.H. Eussen, A. de Klein, L. Wessels, W. de Laat, and B. van Steensel, *Domain organization of human chromosomes revealed by mapping of nuclear lamina interactions.* Nature, 2008. 453(7197): p. 948-951.

171. K.K. Lee, T. Haraguchi, R.S. Lee, T. Koujin, Y. Hiraoka, and K.L. Wilson, *Distinct functional domains in emerin bind lamin A and DNA-bridging protein BAF.* Journal of cell science, 2001. 114(Pt 24): p. 4567-4573.

172. A.T. Bertrand, S. Ziaei, C. Ehret, H. Duchemin, K. Mamchaoui, A. Bigot, M. Mayer, S. Quijano-Roy, I. Desguerre, J. Lainé, R. Ben Yaou, G. Bonne, and C. Coirault, *Cellular microenvironments reveal defective mechanosensing responses and elevated YAP signaling in LMNA-mutated muscle precursors.* Journal of cell science, 2014. 127(Pt 13): p. 2873-2884.

173. T.P. Driscoll, B.D. Cosgrove, S.-J. Heo, Z.E. Shurden, and R.L. Mauck, *Cytoskeletal to Nuclear Strain Transfer Regulates YAP Signaling in Mesenchymal Stem Cells.* Biophysical journal, 2015. 108(12): p. 2783-2793.

174. R. Akter, D. Rivas, G. Geneau, H. Drissi, and G. Duque, *Effect of lamin A/C knockdown on osteoblast differentiation and function.* Journal of bone and mineral research : the official journal of the American Society for Bone and Mineral Research, 2009. 24(2): p. 283-293.

175. V.L.R.M. Verstraeten, J. Renes, F.C.S. Ramaekers, M. Kamps, H.J. Kuijpers, F. Verheyen, M. Wabitsch, P.M. Steijlen, M.A.M. van Steensel, and J.L.V. Broers, *Reorganization of the nuclear lamina and cytoskeleton in adipogenesis.* Histochemistry and cell biology, 2011. 135(3): p. 251-261.

176. C. Vidal, S. Bermeo, D. Fatkin, and G. Duque, Role of the nuclear envelope in the pathogenesis of age-related bone loss and osteoporosis. BoneKEy reports, 2012. 1: p. 62-62.

177. M. Zwerger, D.E. Jaalouk, M.L. Lombardi, P. Isermann, M. Mauermann, G. Dialynas, H. Herrmann, L.L. Wallrath, and J. Lammerding, *Myopathic lamin mutations impair nuclear stability in cells and tissue and disrupt nucleo-cytoskeletal coupling.* Human molecular genetics, 2013. 22(12): p. 2335-2349.
178. Y.-C. Poh, S.P. Shevtsov, F. Chowdhury, D.C. Wu, S. Na, M. Dundr, and N. Wang, *Dynamic force-induced direct dissociation of protein complexes in a nuclear body in living cells.* Nature communications, 2012. 3: p. 866-866.
179. S. Bermeo, C. Vidal, H. Zhou, and G. Duque, Lamin A/C Acts as an Essential Factor in Mesenchymal Stem Cell Differentiation Through the Regulation of the Dynamics of the Wnt/β-Catenin Pathway. Journal of cellular biochemistry, 2015. 116(10): p. 2344-2353.
180. W. Li, L.S. Yeo, C. Vidal, T. McCorquodale, M. Herrmann, D. Fatkin, and G. Duque, *Decreased bone formation and osteopenia in lamin a/c-deficient mice.* PloS one, 2011. 6(4): p. e19313-e19313.
181. S. Bermeo, A. Al-Saedi, M. Kassem, C. Vidal, and G. Duque, *The Role of the Nuclear Envelope Protein MAN1 in Mesenchymal Stem Cell Differentiation.* Journal of cellular biochemistry, 2017. 118(12): p. 4425-4435.
182. M. Versaevel, J.-B. Braquenier, M. Riaz, T. Grevesse, J. Lantoine, and S. Gabriele, *Super-resolution microscopy reveals LINC complex recruitment at nuclear indentation sites.* Scientific Reports, 2014. 4(1): p. 7362.
183. D.-H. Kim and D. Wirtz, Cytoskeletal tension induces the polarized architecture of the nucleus. Biomaterials, 2015. 48: p. 161-172.
184. M. Werner, S.B. Blanquer, S.P. Haimi, G. Korus, J.W. Dunlop, G.N. Duda, D.W. Grijpma, and A. Petersen, Surface Curvature Differentially Regulates Stem Cell Migration and Differentiation via Altered Attachment Morphology and Nuclear Deformation. Adv Sci (Weinh), 2017. 4(2): p. 1600347.
185. P. Wang, M. Dreger, E. Madrazo, C.J. Williams, R. Samaniego, N.W. Hodson, F. Monroy, E. Baena, P. Sánchez-Mateos, A. Hurlstone, and J. Redondo-Muñoz, *WDR5 modulates cell motility and morphology and controls nuclear changes induced by a 3D environment.* Proceedings of the National Academy of Sciences of the United States of America, 2018. 115(34): p. 8581-8586.
186. N. Jain, K.V. Iyer, A. Kumar, and G.V. Shivashankar, Cell geometric constraints induce modular gene-expression patterns via redistribution of HDAC3 regulated by actomyosin contractility. Proceedings of the National Academy of Sciences, 2013. 110(28): p. 11349.
187. M.J. Kim, S. Kim, Y. Kim, E.J. Jin, and J.K. Sonn, *Inhibition of RhoA but not ROCK induces chondrogenesis of chick limb mesenchymal cells.* Biochem Biophys Res Commun, 2012. 418(3): p. 500-5.
188. D.G. Phinney and D.J. Prockop, Concise review: mesenchymal stem/multipotent stromal cells: the state of transdifferentiation and modes of tissue repair--current views. Stem Cells, 2007. 25(11): p. 2896-902.
189. P. Bianco, X. Cao, P.S. Frenette, J.J. Mao, P.G. Robey, P.J. Simmons, and C.Y. Wang, *The meaning, the sense and the significance: translating the science of mesenchymal stem cells into medicine.* Nat Med, 2013. 19(1): p. 35-42.
190. N.S. Hwang, C. Zhang, Y.-S. Hwang, and S. Varghese, *Mesenchymal stem cell differentiation and roles in regenerative medicine.* WIREs Systems Biology and Medicine, 2009. 1(1): p. 97-106.
191. R. Ashraf, H.S. Sofi, and F.A. Sheikh, *Experimental Protocol of MSC Differentiation into Neural Lineage for Nerve Tissue Regeneration Using Polymeric Scaffolds.* Methods in molecular biology (Clifton, N.J.), 2019: p. 10.1007/7651_2019_229.
192. K. Quintiliano, T. Crestani, D. Silveira, V.E. Helfer, A. Rosa, E. Balbueno, D. Steffens, G.P. Jotz, D.A. Pilger, and P. Pranke, *Neural Differentiation of Mesenchymal Stem Cells on Scaffolds for Nerve Tissue Engineering Applications.* Cellular reprogramming, 2016. 18(6): p. 369-381.

Chapter 3

Dimensionality changes actin network through lamin A/C and zyxin

Jip Zonderland, Ivan Lorenzo Moldero, Shivesh Anand, Carlos Mota, Lorenzo Moroni

Complex Tissue Regeneration Department, MERLN Institute for Technology-Inspired Regenerative Medicine, Maastricht University, Maastricht, the Netherlands.

Abstract

Mechanosensing proteins have mainly been investigated in 2D culture platforms, while understanding their regulation in 3D environments is critical for tissue engineering. Among mechanosensing proteins, the actin cytoskeleton plays a key role in human mesenchymal stromal cells (hMSCs) activity, but its regulation in 3D tissue engineered scaffolds remains poorly studied. Here, we show that human mesenchymal stromal cells (hMSCs) cultured on 3D electrospun scaffolds made of a stiff material do not form actin stress fibers, contrary to hMSCs on 2D films of the same material. On 3D electrospun- and 3D additive manufactured scaffolds, hMSCs also displayed fewer focal adhesions, lower lamin A and C expression and less YAP1 nuclear localization and myosin light chain phosphorylation. Together, this strongly suggests that dimensionality prevents the build-up of cellular tension, even on stiff materials. Knock down of either lamin A and C or zyxin resulted in fewer stress fibers in the cell center. Zyxin knock down reduced lamin A and C expression, but not vice versa, showing that this signal chain starts from the outside of the cell. Lineage commitment was not affected by the lack of these important osteogenic proteins in 3D, as all cells committed to osteogenesis in bi-potential medium. Our study demonstrates that dimensionality changes the actin cytoskeleton through lamin A and C and zyxin, and highlights the difference in the regulation of lineage commitment in 3D enviroments. Together, these results can have important implications for future scaffold design for both stiff- and soft tissue engineering constructs.

Introduction

Understanding cellular responses, such as differentiation and proliferation, to material properties (e.g. stiffness, chemistry, and topography) are critical endeavors in fields like tissue engineering and regenerative medicine. Unraveling the molecular mechanisms underlying these cellular responses can lead to more intelligent design of tissue engineering constructs. Cells adhere to extracellular matrix (ECM) proteins through integrins, forming focal adhesion complexes that connect the actin cytoskeleton to the ECM[1]. The other end of the actin filament, is attached to either another focal adhesions, or to the nucleus, by binding to the linker of nucleoskeleton and cytoskeleton (LINC) complex, which in turn is linked to lamin A and C[2]. Lamin A and C form a protein meshwork under the nuclear membrane to give structural integrity to the nucleus[3-5]. Lamin B1 and B2 are also part of the lamin protein meshwork. B-type lamins have been shown to influence nuclear integrity, while nuclear stiffness is mainly determined by lamin A and C[4, 6]. The different roles and functions of lamin A and C have not been widely investigated; the reader is referred to an excellent review on this topic[7]. Actin filaments join together to form stress fibers, with incorporated non-muscle myosin to create contractile force between its two attachment points[8]. On stiffer materials, focal adhesions and stress fibers have been shown to be bigger and more abundant than on softer materials[9-12], creating a higher cellular tension[12, 13]. Indeed, lamin A and C expression, indirectly attached to actin stress fibers, has also been shown to increase on stiffer materials[5]. Besides material stiffness, other factors such as material chemistry and topography have also been shown to influence focal adhesions, actin stress fibers and lamin A and C[14-16]. Yes-associated protein 1 (YAP1) is an important mechanosensitive co-transcription factor that translocates to the nucleus at higher cellular tension to transduce these mechanical changes in the cell to changes in gene expression[17].

On stiffer materials and with more cellular tension human mesenchymal stromal cells (hMSCs) show increased osteogenic differentiation, while softer materials and lower cellular tension enhance differentiation to chondro- and adipogenic lineages[18-22]. These changes in hMSC differentiation have been shown to be orchestrated by actin stress fibers[23], focal adhesions[23], lamin A and C[24] and Yes-associated protein 1 (YAP1)[25, 26].

While other material properties are relatively well studied, the dimensionality (2D v. 3D) of a material has not yet been widely studied. All 3D tissue engineering constructs inherently introduce dimensionality, but direct comparison between cells cultured in 2D and 3D, made of the same material, are sparsely reported. It is therefore important to understand the effect of dimensionality on the proteins involved in cellular tension, as they are critical for hMSC differentiation[23-26]. Some studies have investigated the role of the dimensionality on cellular tension in soft hydrogels[27]. While this gives valuable insights for some tissue engineering applications, many 3D tissue engineering constructs are made of stiff materials. Therefore, we investigated the effect of dimensionality in 3D electrospun (ESP) and 3D additive

manufactured (AM) scaffolds and compared to flat films made of the same stiff material (300PEOT55PBT45, 100 MPa[28]) (Fig. 1a). Specifically, we focused on four main parts of the cellular tension machinery: focal adhesions (zyxin and paxillin), actin cytoskeleton, nuclear skeleton (lamin A and C) and a mechanosensitive co-transcription factor (YAP1).
We demonstrate that dimensionality influenced the actin stress fiber formation, focal adhesion formation, lamin A and C expression and YAP1 nuclear localization in these commonly used 3D tissue engineering scaffolds. The 3D scaffolds changed the actin network of hMSCs through a decrease in zyxin expression, which decreases lamin A and C expression and together change the actin cytoskeleton.

Results

Dimensionality prevents formation of actin stress fibers and reduces lamin A and C

To start investigating how dimensionality influences cellular tension in stiff materials, we cultured hMSCs on 300PEOT55PBT45 3D AM and 3D ESP scaffolds, or 2D films, for 7 days (Fig. S1a-b) and looked at the actin cytoskeleton (Fig. 1a). The electrospun scaffolds had a fiber diameter of 0.99 ± 0.18 µm and a thickness of ~50 µm. Cells infiltrated and grew on top of the scaffolds. Using AM, we created stacks of fibers of ~200 µm, with square pores of ~650 µm, in a 0-90 pattern (Supplementary Fig. 1). 300PEOT55PBT45 is a stiff material (100MPa[28]), Young's moduli of the films, AM and ESP scaffolds were: 98±23MPa (tensile), 2.0±0.1MPa (compression) and 1.2±0.2MPa (tensile), respectively (Supplementary Fig. 2a-c). As expected, on 2D films large actin stress fibers formed and F-actin fibers were distributed throughout the whole cell (Fig. 1b). When hMSCs were cultured on ESP 3D scaffolds, we observed far fewer actin stress fibers and a change in F-actin distribution. F-actin fibers were mainly located on the cell periphery and very little F-actin was observed in the cell center or overlapping with the nucleus (Fig. 1c). The lack of many stress fibers and a more pronounced peripheral actin network is a sign of lower cellular tension[29], even though cells were cultured on stiff materials. F-actin distribution of hMSCs in AM 3D scaffolds was attempted but could not be evaluated due to the very high cell density in these 3D constructs. In this high cell density environment, the F-actin distribution of individual cells could not be discriminated from F-actin of surrounding cells.

To understand why few actin fibers were found overlapping with the cell nucleus, we evaluated the expression of lamin A and C, a protein that assists in linking actin filaments to the nucleus[2]. After 7 days of culture, lamin A and C expression were significantly reduced in AM scaffolds, by 30 ± 3.5% ($p<0.001$) and 46 ± 14% ($p<0.05$), respectively, compared to 2D films (Fig. 1d). Lamin A and C expression was even more reduced in hMSCs cultured on the ESP scaffolds, by 85 ± 6.5% ($p<0.01$) and 91 ± 8.0% ($p<0.05$), respectively, compared to those cultured on 2D films. Phosphorylation of Lamin A and C at Ser22 induces dislocalization from the nuclear membrane and later degradation[30, 31]. The ratio between phosphorylated and

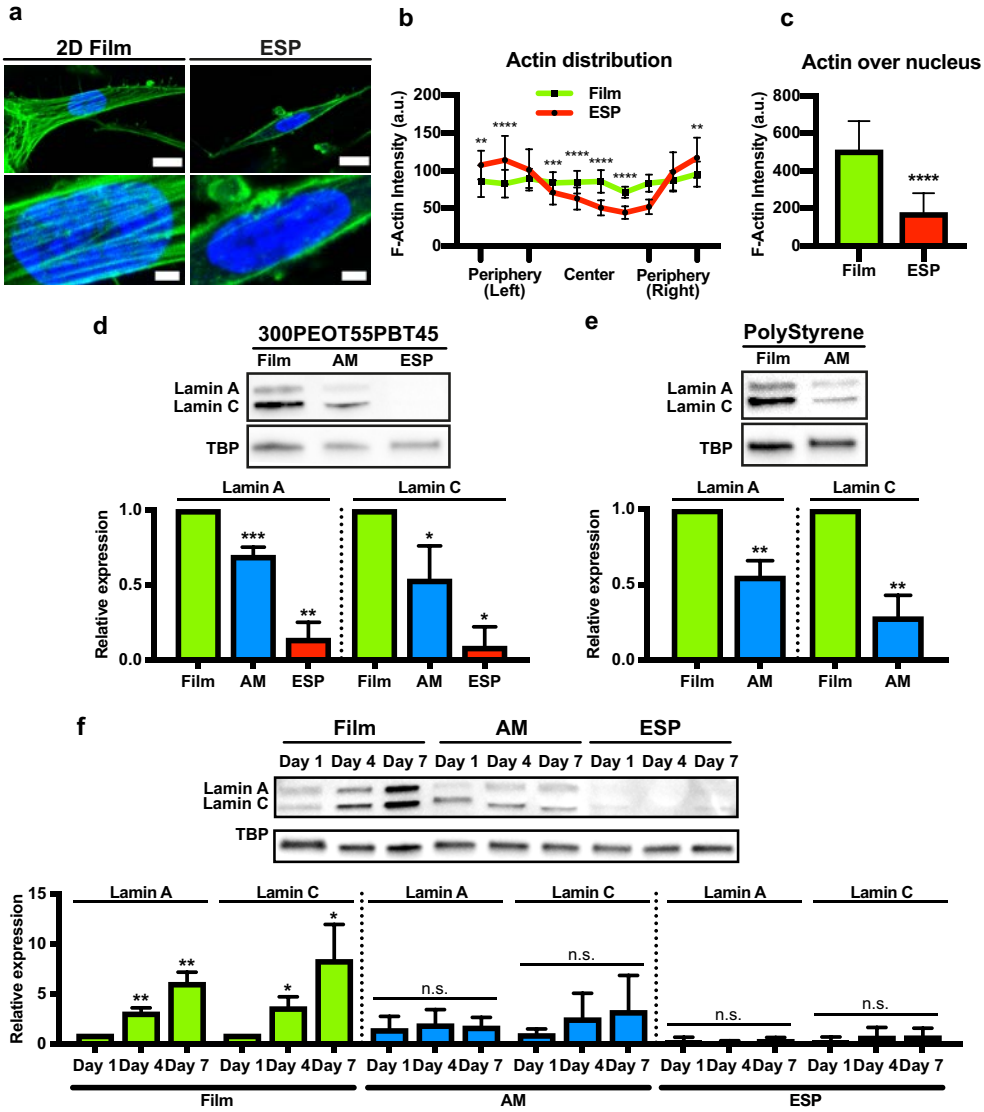

Figure 1. Different actin network organization and lower Lamin A and C in hMSCs cultured on 3D ESP scaffolds. a, hMSCs cultured on 300PEOT55PBT45 2D films and 3D electrospun (ESP) scaffolds stained for F-actin (green) and nuclei (blue). The bottom panels are magnifications (4×) of the respective images above. Scale bars represent 15 μm (top panels) and 3 μm (bottom panels). **b,** Quantification of the F-actin intensity distribution in hMSCs cultured on 300PEOT55PBT45 2D films or 3D ESP scaffolds. n=21 for films and n=23 for ESP from 3 biological replicates. Two-way ANOVA; **p<0.01, ***p<0.001, ****p<0.0001. **c,** Quantification of F-actin intensity that overlaps with the nucleus in hMSCs cultured on 300PEOT55PBT45 2D films or 3D ESP scaffolds. n=12 for films and n=13 for ESP from 3 biological replicates. Student's t-test, ****p<0.0001. **d,** Lamin A and C expression in hMSCs grown on 300PEOT55PBT45 2D films, 3D AM, and ESP scaffolds. TBP shown as loading control in the blots. Graph depicts average expression of lamin A or C/TBP normalized to films, quantified by western blots from 4 independent experiments. One-way ANOVA; * p<0.05, **p<0.01,

***p<0.001 compared with films. **e,** Lamin A and C expression in hMSCs cultured on polystyrene, as 2D films or 3D AM scaffolds. TBP shown as loading control in the blots. Graph shows the average expression of lamin A or C/TBP normalized to films, quantified by western blot from 3 independent experiments. Ratio paired t-test; **p<0.01. **b-e,** Error bars represent mean±95% CI. **f,** Lamin A and C expression on day 1, 4 and 7 after seeding hMSCs on 300PEOT55PBT45 2D films, 3D additive manufactured (AM) or electrospun (ESP) scaffolds. TBP shown as loading controls. Quantification of western blots from 3 independent experiments shows average expression of lamin A or C/TBP normalized to 2D films at day 1. Error bars represent mean±SD. One-way ANOVA; *p<0.05 ** p<0.01 compared with expression on 2D film at day 1.

total lamin A and C was increased in the 3D ESP scaffolds 2.3±0.5x ($p<0.05$) and 5.9±3.5x ($p<0.05$), respectively, compared to films (Supplementary Fig. 3). This shows that the reduction of lamin A and C in 3D ESP scaffolds comes partly from an increase of phosphorylation.
The same trend of lamin A and C expression was observed for polystyrene, another stiff material: cells expressed 44 ± 4.7% ($p<0.01$) less lamin A and 71 ± 6.5% ($p<0.01$) less lamin C when cultured on AM 3D scaffolds, compared to 2D films (Fig. 1e). Young's moduli of the polystyrene films and AM 3D scaffolds were 882±112MPa and 89±33MPa, respectively. From here on, all 2D film, 3D AM and ESP scaffolds will be 300PEOT55PBT45.

To determine how lamin A and C expression changed over the culture period, we measured their expression levels at days 1, 4, and 7 (Fig. 1f). Lamin A and C expression in hMSCs cultured on the 3D ESP or AM scaffolds remained low at all time points. In comparison, lamin A and C steadily increased over time in hMSCs cultured on 2D films. Lamin A was 3.2 ± 0.43 and 6.2 ± 1.0 times higher after day 4 and day 7, respectively, compared to day 1. Lamin C was 3.7 ± 1.0 and 8.4 ± 3.5 times higher on day 4 and day 7, respectively, compared to day 1. These findings show that due to the dimensionality, lamin A and C expression remains low over the culture period, in contrast to 2D, where lamin A and C expression increases over time.

Improved migration through small pores of cells cultured in 3D
Lower lamin A and C expression has been shown to decrease nuclear stiffness and improve migration through small pores[5, 32]. To test whether the change in lamin A and C expression affected this migration capacity, we observed hMSC migration from 2D films or 3D scaffolds, through a transwell with 3 µm or 8 µm pores. Indeed, cells cultured on 2D films and harboring higher lamin A and C expression migrated less well through 3 µm pores than through 8 µm pores ($p<0.05$) (Fig. 2a). Cells migrating from ESP scaffolds migrated equally well through 3 µm or 8 µm pores. The ratio of hMSCs migrating through 3 µm pores to those not migrating was significantly higher from ESP scaffolds than 2D films ($p<0.01$). hMSCs on AM scaffolds did not have sufficient physical contact with the transwells to migrate from the AM scaffold to the transwell membrane (data not shown), so their migration ability could not be evaluated. These data indicate that lower lamin A and C expression from hMSCs in 3D ESP resulted in

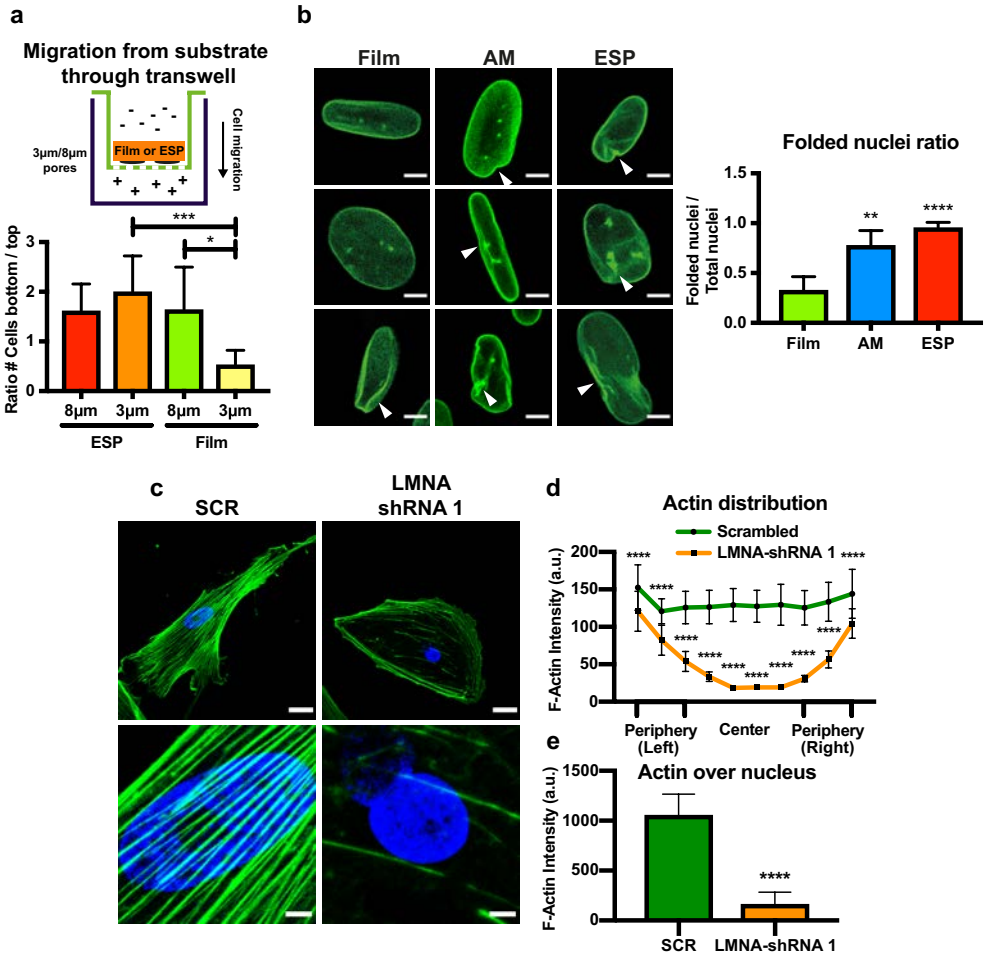

Figure 2. More nuclear folds and improved migration in cells from 3D ESP and Lamin A and C influences F-actin organization. a, Migration of hMSCs from 300PEOT55PBT45 2D films or 3D ESP scaffolds through a transwell with 8 µm or 3 µm pores. 8 µm ESP: n=18 ; 3 µm ESP n=19 ; 8 µm Film n=18 ; 3 µm Film n=19 , from 4 independent experiments. Krusal Wallis test; *p<0.05, ***p<0.001. **b,** Representative images of examples of folded and non-folded nuclei of hMSCs grown on 300PEOT55PBT45 2D films, 3D AM or 3D ESP scaffolds, stained with Lamin A and C (green), scalebars 5 µm. Arrowheads indicate what was considered a nuclear fold. The graph shows the corresponding quantification. Total counted nuclei for films: 491, AM: 159, ESP: 79, in 8, 11 and 10 different images, respectively, from 2 independent experiments. Kruskal Wallis test, ** p<0,01, **** p<0,0001 compared to films. **c,** hMSCs transduced with scrambled- (SCR, left) or LMNA-shRNA (right), cultured on TCP, stained for F-actin (green) and nuclei (blue). The bottom panels are 7× magnifications of the respective images above. Scale bars represent 30 µm (top panels) and 5 µm (bottom panels). **d,** Quantification of the F-actin intensity distribution in hMSCs transduced with scrambled- or LMNA-shRNA, cultured on 2D TCP. n=33 for SCR and n=29 for LMNA-shRNA from 3 biological replicates. Two-way ANOVA; ****p<0.0001. **e,** Quantification of F-actin intensity that overlaps with nuclei staining in hMSCs transduced with scrambled- or LMNA-shRNA. n=25 cells analyzed for SCR and n=22 for LMNA from 3 biological replicates. Mann-Whitney test, ****p<0.0001. **a-e**, Error bars represent mean ± 95% CI.

improved migration through small pores compared to hMSCs grown on 2D films, potentially due to lower nuclear stiffness of the cells.

While a stiff nucleus shows a uniform shape, lower nuclear stiffness results in more heterogeneous shapes and more 'folds'[33, 34]. Indeed, nuclei of cells cultured in 2D showed mostly uniform nuclei, with folds in 33 ± 11% nuclei. From hMSCs on the 3D scaffolds, 76 ± 12% ($p<0.01$) and 96 ± 4% ($p<0.0001$) of nuclei displayed folds from AM and ESP scaffolds, respectively (Fig. 2b).

Together, these observations suggest that lower lamin A and C expression, resulting from the dimensionality of the 3D scaffolds compared to 2D films composed of the same stiff material, reduced nuclear stiffness, an observation not previously reported.

Lamin A and C plays a role in shaping the F-actin network

Actin tension has been shown to influence lamin A and C expression[30], but the role of lamin A and C in shaping the actin network is not known. To investigate this, cells were transduced with LMNA shRNA, knocking down both lamin A and C (Supplementary Fig. 4), and stained for F-actin (Fig. 2c). A large change in actin organization was observed in the LMNA knock down. Similar to the actin organization of hMSCs on 3D ESP scaffolds, the LMNA knock down showed a clear decrease in F-actin in the cell center and over the nucleus (Fig. 2d and e). Thus, lamin A and C plays an important role in shaping the actin network and could be partly responsible for the difference in actin organization in 2D vs 3D.

Cell density does not explain differences in lamin A and C expression observed between 2D and 3D

Because cell density inherently differs between 2D and 3D substrates, we wished to determine whether it was the reason for the differences we observed in lamin A and C expression. To determine the influence of cell density on lamin A and C expression, we cultured hMSCs for 7 days with different cell seeding densities on 2D TCP (Fig. 3a). The different cell densities were chosen to reach confluency after 1 day (20k cells/cm^2), 2 days (10k cells/cm^2), or roughly 40%, 60%, 70%, or 80% confluency after 7 days (1.25k, 2.5k and 5k cells/cm^2, respectively), or little cell-cell contact after 7 days (625 cells/cm^2). Increasing cell seeding density increased lamin A and C expression after 7 days of culture (Fig. 3a). Lamin A was 2.4±0.5x higher at 10k than at 625 cells/cm^2 ($p<0.05$), while lamin C was 5.0±0.6x higher at 20k than at 625 cells/cm^2 ($p<0.05$).

As lamin A and C were influenced by cell density in 2D, we next examined whether this was also true in the 3D scaffolds. For the 3D ESP scaffolds, different cell densities were chosen to have confluency after 1 day (120k cells/scaffold), near confluency after 7 days (30k cells/scaffold), or little cell contact after 7 days (10k cells/scaffold). For 3D AM scaffolds, confluency is more difficult to determine. With 400k cells/scaffold, most pores are filled after 1-2 days of culture. With 200k and 100k cells/scaffold, full pores are attained after 4–5 and 7

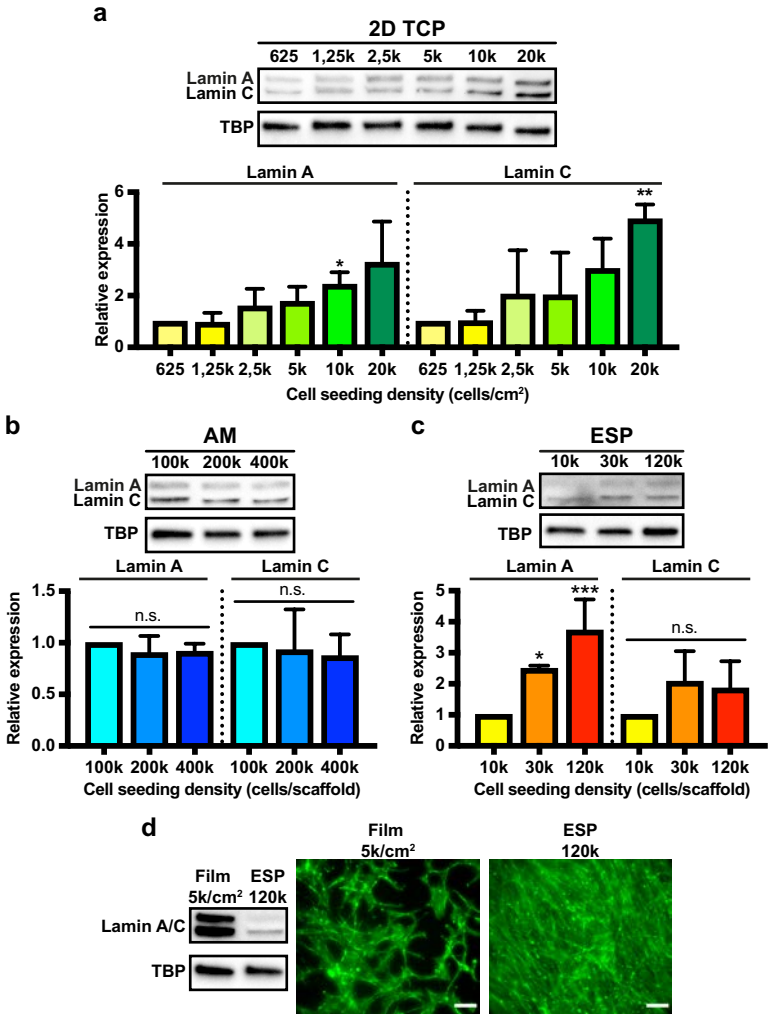

Figure 3. Cell seeding density influences lamin A and C expression. a–c, Lamin A and C expression of hMSCs seeded on 2D TCP (a), 300PEOT55PBT45 3D AM (b), or 300PEOT55PBT45 3D ESP (c) in varying densities. Western blots (top) and quantification of western blots (graphs below) from 3 independent experiments. Error bars represent mean ± SD. Values were normalized to 625 cells/cm^2 (a), 100k cells/scaffold (b), or 10K cells/scaffold (c). One-way ANOVA; *p<0.05 compared with 625 cells/cm^2 (a) or 10k cells/scaffold (c). ***p<0.001, compared to 10k cells/scaffold. TBP shown as a loading control. **d,** Representative western blot (left) of hMSCs cultured on 300PEOT55PBT45 films at a medium cell density, or on 300PEOT55PBT45 3D ESP scaffolds at a high cell density. Representative images of hMSCs on 2D films seeded at 5k cells/cm^2 (left) and on a 3D ESP scaffold seeded with 120k cells (right) show the observed cell density at the time of harvest (day 7), visualized by F-actin staining (green). Scale bars represent 50 µm.

days of culture, respectively. Importantly, little cell proliferation was observed in 3D AM scaffolds (data not shown), thus the increased filling of the scaffold is not related to proliferation, unlike cells on 3D ESP or 2D TCP.
Interestingly, cell density on the AM 3D scaffolds did not influence the lamin A or C expression (Fig. 3b). Similar to 2D TCP, however, increasing cell seeding density significantly increased lamin A expression in 3D ESP scaffolds, with 2.5 ± 0.1 ($p<0.001$) and 3.7 ± 1.0 ($p<0.05$) times more lamin A from 30k and 120k cells/scaffold, respectively, compared to 10k cells/scaffold (Fig. 3c). Lamin C expression was not significantly changed by cell density on the ESP 3D scaffold, with 2.1 ± 1.0 and 1.9 ± 0.87 times more lamin C expression from 30k and 120k cells/scaffold compared to the 10k cells/scaffold.

At 5k/cm^2, cells don't reach full confluency on 2D films after 7 days, while cells are fully confluent after seeding at 120k/scaffold (Fig. 3d). Lamin A and C expression was still much higher on 2D films than on ESP seeded at this high cell density, regardless of the increase in lamin A and C with increased cell density. This shows that even though lamin A and C increase with increased cell density, it does not explain the differences observed here between 2D and 3D cell culture systems.

Fewer focal adhesions in 3D environments
To understand why lamin A and C expression and the actin organization change in response to dimensionality, we looked at focal adhesion formation of cells cultured on 3D AM- or ESP scaffolds, compared to 2D films. As expected, many large focal adhesions were found on flat films, visualized by zyxin staining, a marker for mature focal adhesions (Fig. 4a). Very few and faint focal adhesions were observed in cells cultured in the 3D AM- and ESP scaffolds. hMSCs cultured in 3D AM- or ESP scaffolds displayed 76.0±16.3% ($p<0.0001$) and 85.8±8.4% ($p<0.0001$) fewer zyxin positive focal adhesions per cell area than 2D films (Fig. 4b). The same trend was observed for paxillin positive focal adhesions, an early focal adhesion marker (Supplementary Fig. 5a). Interestingly, total protein expression of zyxin did not change between 2D films and 3D scaffolds (Fig. 4c). However, expression of paxillin was reduced in both 3D AM- and 3D ESP scaffolds, 75% ± 18% ($p<0.05$) and 57% ± 11% ($p<0.05$), respectively (Supplementary Fig. 5b).
Fewer focal adhesions in response to dimensionality correlated to the reduced lamin A and C expression in the 3D scaffolds. In 2D, lamin A and C increased with higher cell seeding densities. To see whether focal adhesion formation also follows the same correlation in 2D, focal adhesion formation and zyxin and paxillin expression were analyzed with different cell seeding densities in 2D TCP, after 7 days of culture. Indeed, at a lower cell seeding density (625 cells/cm^2), 65.9±0.1% ($p<0.0001$) fewer zyxin positive focal adhesions formed than at higher cell seeding density (20k/cm^2) (Fig. 4d-e). Stainings for paxillin revealed a similar trend (Supplementary Fig. 5c). Total zyxin expression was increased 2.3±0.3, 2.6±0.5 and 2.1±0.2

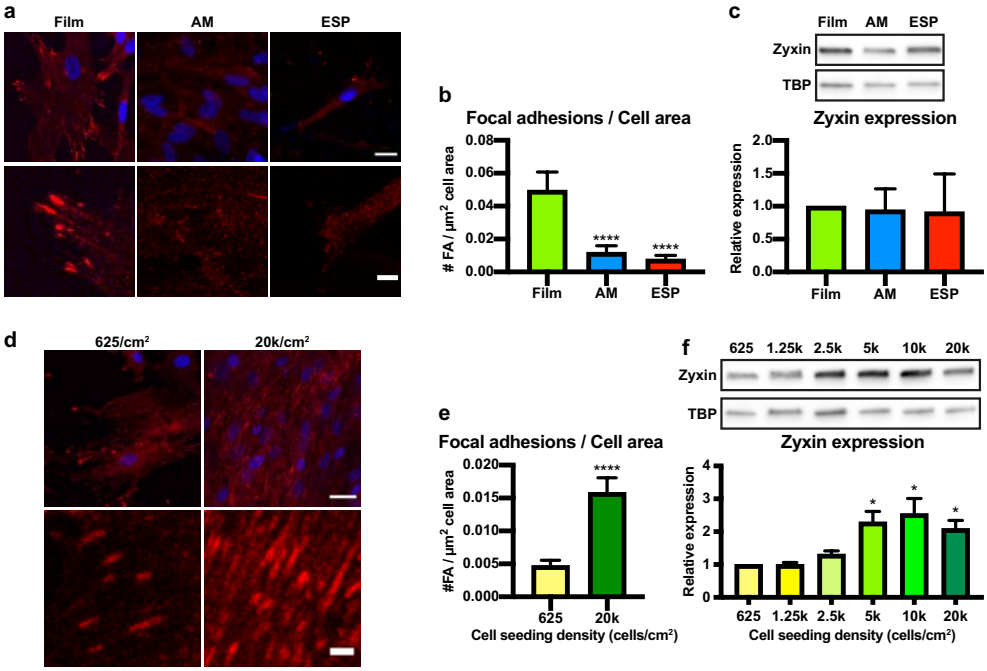

Figure 4. Decreased focal adhesions in 3D. a, hMSCs on 300PEOT55PBT45 2D films, 3D additive manufactured (AM) or electrospun (ESP) scaffolds stained for zyxin (red) and nuclei (blue). The bottom panels are magnifications (4×) of the respective images above. Scale bars represent 20 µm (top panels) and 5 µm (bottom panels). **b,** Quantification of the number of zyxin positive focal adhesions, normalized to cell area, in hMSCs grown on 300PEOT55PBT45 films, AM or ESP 3D scaffolds. One-way ANOVA. **** p<0,0001. n=20 cells for each condition. Error bars represent mean±95% CI. **c,** Zyxin expression in hMSCs cultured on 300PEOT55PBT45 2D film, 3D AM and ESP scaffolds. TBP is shown as a loading control. Graph shows western blot quantifications of zyxin/TBP, normalized to 2D films, from 4 independent experiments. Error bars represent mean±SD. **d,** hMSCs seeded on 2D TCP at different cell densities and stained for zyxin (red) and nuclei (blue), with the bottom panels showing magnifications (8×) of the respective images above. Scale bars represent 40 µm (top panels) and 5 µm (bottom panels). **e,** Quantification of the number of zyxin positive focal adhesions, normalized to cell area, in hMSCs grown on 2D TCP at different cell seeding densities. Student's t-test. **** p<0,0001. n=20 cells for each condition. Error bars represent mean±95% CI. **f,** Zyxin expression in hMSCs seeded in different cell densities and cultured on TCP for 7 days. TBP is shown as a loading control. Graphs show western blot quantification as zyxin/TBP, normalized to 625 cells/cm^2, from 3 independent. Error bars represent mean±SD. One-way ANOVA; *p<0.05 compared to 625 cells/cm^2.

times (p<0.05) in 5k, 10k and 20k cells/cm^2, compared to 625 cells/cm^2, respectively. Paxillin expression also followed this trend, where at 20k cells /cm^2 paxillin expression was 2.0 ± 0.43 times higher than at 1.25k/cm^2 (p<0.05) (Supplementary Fig. 5d).

Together, these data show that dimensionality reduces focal adhesion formation. In addition, a positive correlation between focal adhesions and lamin A and C expression was found, hinting at a possible connection between the two.

Reduced YAP1 nuclear translocation and pMLC2 in 3D cultures

YAP1 translocates to the nucleus when there is higher cellular tension[35]. To determine the behavior of YAP1 in response to dimensionality, we measured the nuclear translocation of YAP1 in hMSCs cultured on AM or ESP scaffolds, compared to flat films (Fig. 5a). From both AM and ESP scaffolds, the nuclear/cytoplasmic ratio of YAP1 was significantly lower (0.3 ± 0.1 ($p<0.0001$) and 0.7 ± 0.2 ($p<0.0001$), respectively, compared to that on 2D films 1.9 ± 0.7) (Fig. 5b); these low ratios show that more YAP1 remained in the cytoplasm than translocated to the nucleus.

In addition, we tested the phosphorylation of myosin light chain 2 (MLC2) on Thr18 and Ser19 (pMLC2). Phosphorylation of MLC2 induces contraction of the actin-myosin bundles and induces cellular tension[36]. In 2D films, clear pMLC2 staining was observed, overlapping with F-actin fibers (Fig. 5c). hMSCs in both AM and ESP scaffolds, however, displayed very little pMLC2 staining. Average staining intensity per cell was 88,9±5,3% ($p<0,0001$) and 67,4±13,1% ($p<0,0001$) lower in AM and ESP than in 2D films, respectively. Individual cells are difficult to distinguish in the 3D AM scaffolds. As the quantification was done on maximum-intensity images of Z-stacks, it is possible that the pMLC2 intensity was measured in more than one cell, slightly overestimating the intensity. However, even with this potential overestimation, pMLC2 staining intensity is still much lower in hMSCs cultured in 3D AM than 2D films.

The lack of YAP1 nuclear translocation and phosphorylation of MLC2 strongly indicates that the dimensionality of the 3D cultures causes a lower cellular tension in hMSCs. These findings are in line with the reduced focal adhesions, actin stress fibers and lamin A and C expression in response to dimensionality.

Previous work hypothesized that YAP1 regulates lamin A and C[5, 37]. To test if YAP1 plays a role in lamin A and C expression, we knocked down YAP1 in hMSCs cultured on TCP and determined the levels of lamin A and C expression. No difference in lamin A or C expression was found between scrambled control and YAP1 knockdowns (Supplementary Fig. 6). This shows that lamin A and C are not regulated through YAP1 and indicates that the lower lamin A and C levels in the 3D scaffolds are not due to a lack of YAP1 activity in the 3D scaffolds.

Zyxin influences lamin A and C expression and actin organization

The dimensionality introduced by the 3D AM and ESP scaffolds caused lower lamin A and C levels and fewer focal adhesions and actin stress fibers. We next determined whether the focal adhesions are involved in controlling the low lamin A and C expression and resulting changed actin network. Zyxin is known to be critical for focal adhesion formation and the

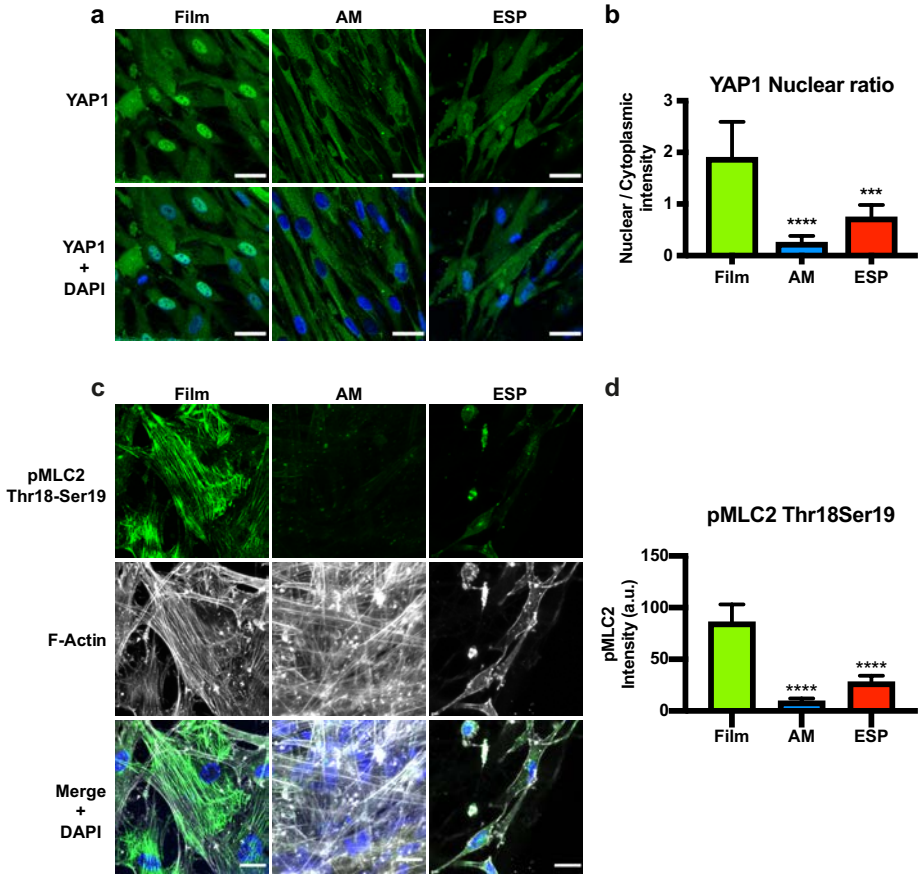

Figure 5. Reduced YAP1 nuclear localization and MLC2 phosphorylation in 3D. a, YAP1 staining (green) of hMSCs grown on 300PEOT55PBT45 2D films, 3D AM and ESP scaffolds. Top panels show YAP1 staining alone, while the bottom panels show YAP1 and nuclei (blue). Scale bars represent 30 μm. **b,** Quantification of the nuclear to cytoplasmic intensity of YAP1 staining in individual cells. Krusal Wallis test; ***p<0.001, ****p<0.0001 compared to films. Total counted cells for films: 27, AM: 28 and ESP: 22 from 4 images. **c,** Phosphorylated myosin light chain 2 (Thr18 and Ser19) (green, top panels) and F-actin staining (gray, middle panels) of hMSCs cultured on 300PEOT55PBT45 2D films, 3D AM or ESP scaffolds. Bottom panels show merge of the respective images above, plus nuclei (blue). Scalebars represent 25 μm. **d,** Quantification of average pMLC2 intensity per cell. One-way ANOVA; **** p<0.0001 compared to films. Total counted cells for films: 8, AM: 14, ESP: 17. **b, d,** Error bars represent mean±95% CI.

connection to the actin cytoskeleton[38, 39], and was therefore chosen as target to diminish the focal adhesion formation. We knocked down zyxin in hMSCs using two different ZYX-shRNAs (Supplementary Fig. 7), cultured the cells on TCP, then measured lamin A and C expression and evaluated the actin network.

Lamin A was reduced 92 ± 5% (p<0.01) and 71 ± 13% (p<0.05) and lamin C reduced 86 ± 11% and 76 ± 19% by the two ZYX-shRNAs, respectively, compared to the scrambled control (Fig. 6a).

In the ZYX knockdowns, less actin was observed in the cell center and over the nucleus, while more F-actin was found in the cell periphery compared to that of the scrambled control (Fig. 6b-d), a localization pattern similar to the LMNA knockdown and cells cultured on ESP scaffolds (Fig. 1). The reduction of central actin stress fibers after ZYX knockdown is in line with previous reports[38, 39].

Zyxin also greatly reduced the number and intensity of paxillin positive focal adhesions, although it could still be visualized (Supplementary Fig. 8), also in line with previous reports[40]. Paxillin is an important protein for the downstream signaling of focal adhesions[41]. To test if lamin A and C expression are influenced by paxillin, we knocked paxillin down. No difference was observed in lamin A or C expression, demonstrating that the reduction of lamin A and C following zyxin knock down does not occur through paxillin (Supplementary Fig. 6). Indeed, also the actin distribution in the cells was not affected by paxillin knock down (Supplementary Fig. 9).

To test whether the influence of zyxin on lamin A and C expression is bidirectional, we looked at zyxin expression in LMNA knockdowns. Zyxin expression and focal adhesion formation were similar in LMNA knockdowns and scrambled controls (Fig. 6e and f), demonstrating that lamin A and C expression does not affect zyxin levels. Furthermore, these data suggest that the faint focal adhesions we observed from hMSCs on 3D scaffolds (Fig. 4a) were not due to the low lamin A and C expression.

Interestingly, in both ZYX and LMNA knockdowns, YAP1 was still located mainly in the nucleus (Supplementary Fig. 10). This indicates that the lack of YAP1 nuclear localization in 3D is through a mechanism independent of lamin A and C or zyxin.

Osteogenic preference for hMSCs in 2D and 3D

In 2D, higher expression of lamin A and C, YAP1 nuclear translocation and more focal adhesion, stress fibers and p-MLC2 have all been linked to increased osteogenesis, while a reduction in these have been shown to favor adipogenesis[20, 23-26, 37, 42-45]. To test whether the dimensionality-induced reduction in these proteins has an effect lineage commitment of hMSCs, we cultured hMSCs in 2D films, 3D AM and ESP scaffolds in bipotential medium (mixed osteo- and adipogenic medium) for 21 days. hMSCs differentiated to osteoblasts were visualized with osteocalcin, while peroxisome proliferator-activated receptor gamma (PPAR-γ) staining was used for adipogenic cells (Supplementary Fig. 11). As expected, all cells committed to the osteoblast lineage when cultured on 2D films (Fig. 7a). Surprisingly, however, also all cells cultured in 3D AM and ESP scaffolds committed to the osteoblast lineage, and no PPAR-γ positive cells were found in any of the culture platforms.

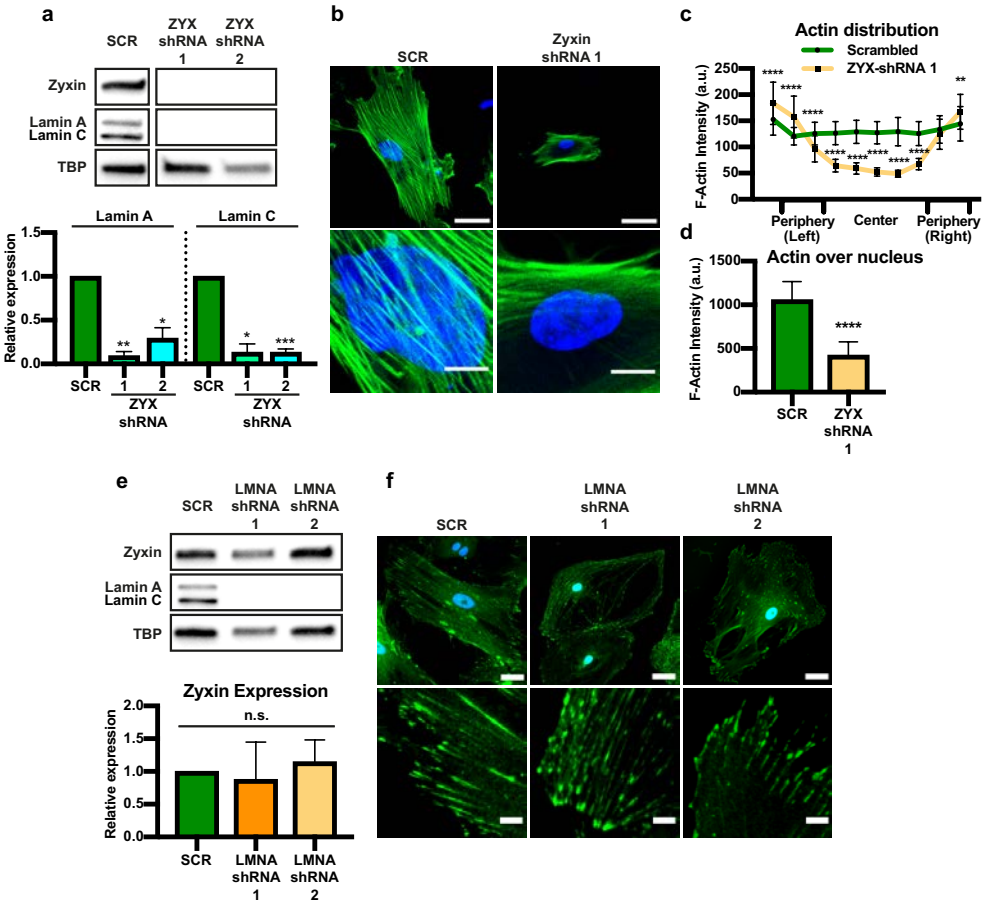

Figure 6. Zyxin influences lamin A and C expression, but not vice versa. a, e, Western blots of zyxin and lamin A and C expression in hMSCs transduced with scrambled or two different ZYX-shRNAs (a) or two different LMNA-shRNAs (e). Graphs show the quantification of lamin A/TBP (a) and zyxin/TBP (e) expression averaged from 4 biological replicates and normalized to expression from SCR-shRNA. Error bars represent mean ± SD. One-way ANOVA; **p<0.01 compared to SCR. **b,** hMSCs transduced with scrambled or ZYX-shRNA, stained for F-actin (green) and nuclei (blue). The bottom panels show 5× magnifications of the respective images above. Scale bars represent 50 µm (top) and 10 µm (bottom). **c,** Quantification of the F-actin intensity distribution in hMSCs transduced with scrambled or ZYX-shRNA. n=33 cells analyzed for SCR and n=32 for ZYX-shRNA from 3 biological replicates. Two-way ANOVA; ****p<0.0001. **d,** Quantification of F-actin intensity that overlaps with nuclei staining in hMSCs transduced with scrambled or ZYX-shRNA cultured on 2D TCP. n=25 cells analyzed for SCR and n=26 for ZYX from 3 biological replicates. Mann-Whitney test, ****p<0.0001. **c, d,** Error bars represent mean ± 95% CI. **f,** hMSCs transduced with scrambled or LMNA-shRNAs stained for zyxin (green) and nuclei (blue). Bottom panels show 5× magnifications of the respective images above. Scale bars represent 50 µm (top panels) and 10 µm (bottom panels). **a-f,** All cells were cultured on 2D TCP for 7 days.

A model for actin fiber formation mediated by lamin A and C and zyxin in 2D v. 3D

Our data comes together in the model depicted in Fig. 7b. In 3D, dimensionality prevents focal adhesion formation, which leads to a decrease in lamin A and C. The lack of both zyxin and lamin A and C then shapes the actin network and does not allow for the formation of actin stress fibers through the cell center. In 2D, the lack of dimensionality allows for the formation of many large focal adhesions, leading to an increase in lamin A and C. High zyxin and lamin A and C expression then allow for the formation of high cellular tension and large actin stress fibers. This mechanism is independent of both YAP1 and paxillin.

Discussion

In this study, we show that hMSCs cultured in 3D ESP or AM scaffolds show a decrease in focal adhesions, lamin A and C expression, YAP nuclear localization, actin stress fibers and MLC2 phosphorylation, compared to 2D films of the same material. We show that zyxin influences lamin A and C expression, but not vise-versa. Both zyxin and lamin A and C play a role in the formation of stress fibers in the cell center and are partly responsible for the different actin organization in 3D.

Fraley et al. also showed a decrease in focal adhesions in response to dimensionality in or on hydrogels[27]. Also, in a 3D *in vivo* environment, focal adhesions were found to be very different in shape and composition from 2D cultures[46]. How dimensionality initiates a difference in the focal adhesion protein zyxin and focal adhesion formation has not been studied here and remains unclear. Potential mechanisms include a difference in force distribution. On concave surfaces, focal adhesion formation and lamin A and C have been shown to decrease when compared to flat surfaces, while they increase on convex surfaces[47]. This indicates that the force distribution within the cell and the angle at which it is connected to the environment partly determines focal adhesion formation and lamin A and C expression. We hypothesize that because of the dimensionality, forces are not distributed over the nucleus like in 2D, but more throughout the whole cell and along the cell periphery, which could explain the more peripheral actin network in 3D environments. The knock down of lamin A and C could mimic what happens in a 3D environment, where forces can no longer be distributed to the nucleus, which leads to the lack of actin stress fibers near the nucleus. Indeed, stress fibers and focal adhesions can still be found in the LMNA knock downs but are then located almost exclusively in the cell periphery (Fig. 2b, 2c, 5f).

We found that YAP1 was excluded from the nucleus on ESP and AM scaffolds, in contrast to 2D films. However, in LMNA and ZYX knockdowns, YAP1 was still located in the nucleus. The opening of nuclear pores due to force on the nucleus has been shown to allow YAP1 to enter the nucleus[35]. A possible explanation is that because of lower nuclear stiffness in both LMNA and ZYX knockdowns (due to lack of lamin A and C), YAP1 can enter the nucleus even if the cell is under less tension[35]. In 3D, the nucleus might be under less tension, as forces are

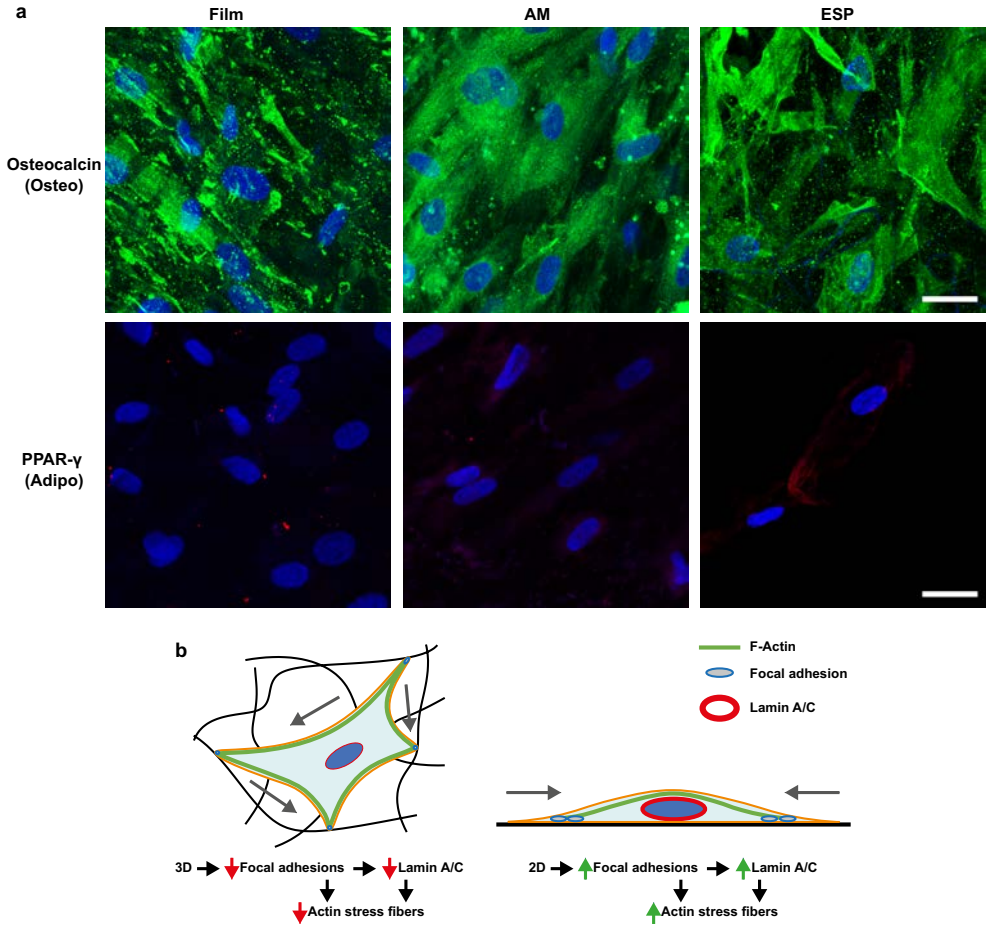

Figure 7. Osteogenic preference of hMSCs in 2D and 3D. a, hMSCs were expanded for 7 days on 300PEOT55PBT45 2D films, 3D AM or 3D ESP scaffolds and then differentiated for 21 days in bipotential medium (osteo and adipogenic differentiation medium mix). Cells were stained for osteocalcin (green, top panels), to identify osteogenic cells, or for PPAR-γ (red, bottom panels) to identify adipogenic cells. Nuclei are stained in blue. Scalebars represent 30 μm. **b,** Model showing differences in actin fiber formation, focal adhesion and lamin A and C in 3D (left) v 2D (right.) In 3D, cellular tension forces (grey arrows) are distributed in multiple directions and focal adhesions (light grey ovals) stay small and few. The reduction of focal adhesions then leads to a reduction in lamin A and C expression (red oval). Together, small and few focal adhesions and low lamin A and C expression then lead to the lack of actin stress fibers (green lines) through the cell center. In 2D, cellular tension forces (grey arrows) are distributed along a single plane, allowing for the build-up tension and large focal adhesions (light grey ovals). This leads to an increase in lamin A and C expression (red oval). Large focal adhesions and high lamin A and C expression then enable the formation of actin stress fibers (green lines) through the cell center.

distributed in all 3 dimensions, whereas in 2D forces are concentrated in a single plane. In 2D, a large portion of the forces are going over the nucleus and pushing down on it[35]. This lack of tension on the nucleus in 3D could potentially result in avoiding YAP1 to enter the nucleus in 3D.

Here, we have presented a link between lamin A and C and the actin cytoskeleton, and lamin A and C and focal adhesions, specifically zyxin. Others have found a similar link between lamin A and C and the actin cytoskeleton, more specifically with actin-cap fibers[33], or total actin[30, 48], while our results focus F-actin distribution in the cell. We have found that this process is not mediated by YAP1. Other mechanosensitive (co-)transcription factors could be inhibited to look at the effect on lamin A and C and zyxin, to find the signaling pathway involved in orchestrating the differences in expression in 3D environments.

Decoupling individual variables in 2D vs 3D in stiff materials remains challenging. Local and bulk material properties can change when creating scaffolds, potentially affecting cell behavior. Also, ECM produced by cells can be influenced, directly changing the environment. Using hydrogels, 2D vs 3D can be more strictly controlled, while even there the introduction of the third dimension inevitably introduces changes in nutrient diffusion, cell density, adhesion ligand density, among other factors. This makes the study of dimensionality difficult, but not less valuable. In our research presented here we have decoupled the observed effects of dimensionality from cell density by testing different cell densities on the different scaffolds. Also, we have decoupled material chemistry by using polystyrene as another material. However, there are other scaffold design variables that could affect the results. In the case of 3D AM scaffolds this includes fiber diameter, fiber spacing, layer thickness, pore size and shape, and total porosity. For 3D ESP scaffolds it includes fiber diameter, pore size, total porosity, pore interconnectivity, among others. Rather than decoupling each variable in each system to see if it can explain the observed effects, we have used these two very different 3D systems in a more holistic manner. In both 3D systems we find reduced lamin A and C, cytoplasmic retention of YAP1, fewer focal adhesions, less p-MLC2, compared to 2D. Combining all this data, we show here that dimensionality is responsible for the reduction in important mechanosensing proteins. These results are in line with a study on the effect of dimensionality on focal adhesions in 2D vs 3D hydrogels[27].
In 2D, YAP, focal adhesions, actin-myosin and lamin A and C have all been shown to increase osteogenic commitment, while a reduction in these proteins pushes hMSCs towards adipogenesis[20, 23-26, 37, 42-45]. We have tested the lineage differentiation preference in hMSCs cultured on 300PEOT55PBT45 2D films, 3D AM or 3D ESP scaffolds. Interestingly, even though in 3D these important osteogenic proteins were heavily downregulated, cells still exclusively committed to osteogenesis. This data is contrary to most of the literature on 2D but is in line with a small but growing body of evidence that suggests a different role for these proteins

in 3D. For example, cell morphology, a very important factor in 2D differentiation and greatly influenced by the above mentioned proteins[20, 42, 49], has been fully decoupled from differentiation in 3D[50-52]. In addition, the lack of both YAP nuclear localization and focal adhesions in 3D hydrogels did not limit osteogenic commitment[50]. The data presented here adds to the small body of research of mechanobiology in 3D, which can have important implications for future tissue engineering scaffold design. Further research is required to decouple the different factors that influence differentiation and lineage commitment in 3D environments.

Conclusion

Here, we study the effect of dimensionality on cellular tension of hMSCs in two common 3D tissue engineering constructs: ESP and AM scaffolds. We demonstrate that dimensionality causes fewer stress fibers, fewer focal adhesion, lower lamin A and C expression, less YAP1 nuclear localization. Cell density influences lamin A and C expression and focal adhesion formation in 2D and 3D, but it is not responsible for the observed differences between 2D and 3D, further proving that dimensionality is an important environmental factor. Lamin A and C or zyxin knock down result resulted in fewer stress fibers in the cell center and over the nucleus. Zyxin knock down also reduced lamin A and C expression, but not vice versa, showing that this signal chain starts from the outside of the cell. In bipotential differentiation medium, all cells in 2D and 3D committed to osteogenesis. This shows that the reduction in these osteogenic mechanosensing factors did not limit osteogenic potential, contrary to literature on 2D substrates. Taken together, our study shows dimensionality changes the actin cytoskeleton through lamin A and C and zyxin and decreases cellular tension, even on stiff materials. Understanding how these key proteins are influenced and further dictate cell behavior and differentiation can have important implications for future scaffold design.

Materials and Methods

Scaffold production

Poly(ethylene oxide terephthalate) and poly(butylene terephthalate) random block co-polymer (PEOT/PBT, 300PEOT55PBT45, PolyActive™) with 300 Da PEO and a PEOT/PBT weight ratio of 55/45 was acquired from PolyVation. Polystyrene (PS, 350 kDa) was acquired from Sigma-Aldrich. PEOT/PBT or PS films were produced by melting the polymer in a circular 23-mm mold between two silicon wafers (Si-mat, Kaufering, Germany) and two hot plates under slight pressure (~100 kg) to ensure films were fully flat. PEOT/PBT was processed at 180 °C and PS at 210 °C.

AM scaffolds were produced by means of screw-extrusion–based fused deposition modeling (FDM) (Bioscaffolder SYSENG, Germany). The FDM extrusion is controlled by the screw rotation and assisted by N_2 (5 bar) gas pressure allowing fine control over deposition of the molten polymer. The manufacturing of the 20×20×4 mm scaffolds was achieved following a layer-by-layer manufacturing with 90° rotation between deposited layers. The 3D scaffold CAD models were uploaded into PrimCAM software (Primus Data, Switzerland) and the deposition patterns were calculated. The fiber spacing, defined as the distance between successive fibers in the same layer was defined as 650 µm, the layer thickness was set to 170 µm, and the fiber diameter obtained was according to the nozzle diameter used, the polymer selected and the processing parameters. The parameters that influence the production of the 3D scaffolds are temperature, screw rotation and deposition velocity. PEOT/PBT or PS pellets were loaded in the reservoir and molten at a temperature of 195 °C or 220 °C, respectively. The screw rotation for the polymers was 200 rpm. The molten polymer was extruded through a nozzle with G25 (I.D. = 250 µm). The deposition velocity was optimized to 20 and 200 mm/min for PS and PEOT/PBT, respectively.

To produce ESP scaffolds, 20% (w/v) 300PEOT55PBT45 was dissolved in a mixture of 70% chloroform (Sigma-Aldrich) and 30% 1.1,1.3,3.3-Hexafluoro-2-propanol AR (HFIP; Bio-Solve) overnight under agitation at room temperature. Electrospinning was done on a mandrel (diameter: 19 cm) slowly rotating at 100 rpm to produce many scaffolds with randomly oriented fibers at the same time under exactly the same conditions. The following conditions were maintained: 15 cm working distance, 1 ml/h flow rate, 23–25 °C and 40% humidity. The mandrel was charged between -2 and -5 kV and the needle between 10–15 kV. ESP scaffolds were spun on aluminum foil over a polyester mesh with 12-mm holes. After spinning, ESP scaffolds with a diameter of 15 mm were punched out and scaffolds were removed from the aluminum foil. This method yielded ESP scaffolds of 12 mm with a 1.5-mm supporting ring of polyester mesh around them to improve handleability. Fibers were deposited randomly with a diameter of 0.99 ± 0.18 µm, creating mats of approximately 50 µm thick.

Before cell culture, films, AM and ESP scaffolds were sterilized with 70% ethanol for 15 min and dried until visually dry. The films and scaffolds were then coated by absorption with 1 mg/ml rat-tail collagen I solution for 16 h at 37 °C. After coating, they were washed twice with

water and air-dried before cell seeding. All experiments on TCP were done without collagen coating.

Mechanical tests

To test the mechanical properties of 300PEOT55PBT45 films, AM and ESP scaffolds, and polystyrene films and AM scaffolds, a TA Electroforce 3200 mechanical tester was used with a 450 N (for film and AM scaffolds) or a 45 N (for ESP scaffolds) load cell. For films and ESP scaffolds, samples were elongated at 1% strain/s and the force and displacement were recorded. AM scaffolds were compressed at 1% strain/s. The elastic moduli were calculated using the slope of the initial linear region, after the toe region.

Cell culture

hMSCs were isolated from bone marrow by aspiration from a 24-year old female by Texas A&M Health Science Center[53] after ethical approval from the local and national authorities and written consent from the donor. Briefly, mononuclear cells were isolated by centrifugation and expanded hMSCs were tested for differentiation potential, to be received at passage 1. For expansion, hMSCs were cultured on TCP at 1000 cells/cm^2 in αMEM + Glutamax + 10% fetal bovine serum (basic medium) (Thermo-Fisher Scientific), until 70–80% confluent. All experiments were performed at passage 5. Films were punched with a diameter of 22 mm and cultured in non-treated, 12-well plates at 5k cells/cm^2, unless stated otherwise. ESP scaffolds were 15 mm and cultured in 24-well plates at 30k cells/scaffold, unless stated otherwise, with a rubber O-ring (outer diameter 15 mm, inner diameter 12 mm) to prevent the scaffolds from floating and to cover the polyester ring on which the scaffolds were produced. AM scaffolds were square blocks of 5×5×3 mm (width, length, height) and cells were seeded in a drop of 50 µl containing 400k cells, unless stated otherwise. Two hours after seeding, the AM scaffold was flipped upside down to increase cell distribution. After a total of 4 h after seeding, scaffolds were transferred to a non-treated, 12-well plate for further culture. Film and scaffold cultures were done in basic medium supplemented with 1 ng/ml FGF-2 (Neuromics), 200 µM L-Ascorbic acid 2-phosphate (ASAP) (Sigma-Aldrich) and 100 U/ml penicillin-streptomycin (P/S), and were harvested after 7 d of culture, unless stated otherwise. For differentiation experiments, hMSCs were cultured for 7 days after seeding on films, AM or ESP scaffolds, before switching to bipotential medium for 21 days. Bipotential medium was a 1:1 mix of osteo- and adipogenic medium. Osteogenic medium: Basic medium+1% P/S, 200 µM ASAP and 10 nM dexamethasone (Sigma-Aldrich). Adipogenic medium: Basic medium+1% P/S, 0.2 mM indomethacin (Sigma-Aldrich), 1 µM dexamethasone, 0.5 mM 3-Isobutyl-1-methylxanthine (Sigma-Aldrich), 2,5 µg/ml Insulin (Sigma-Aldrich).

Protein isolation and western blot

Proteins were isolated from cells cultured on films or scaffolds in RIPA buffer (Sigma-Aldrich), supplemented with cOmplete™, Mini, EDTA-free Protease Inhibitor Cocktail (Sigma-Aldrich). To get sufficient proteins, 6–12 films, 15–20 ESP scaffolds or 2–4 AM scaffolds were mixed into 300–400 µl lysis buffer for a single protein isolate. Experiments were repeated 3 or 4 times for replicates. For TCP and films, surfaces were scraped with cell scrapers to ensure cell lysis. AM scaffolds were cut into four smaller pieces and submerged in lysis buffer. ESP scaffolds were removed from the polyester supporting ring and submerged in lysis buffer. Samples were spun down at 10.000 *g*, and the supernatant was used for further processing.

Protein quantification was done using the Pierce BCA protein assay kit (Thermo Fisher Scientific). 20 µg protein was incubated with laemmli loading buffer (Bio-Rad) and 10% 2-Mercaptoethanol (Sigma-Aldrich) for 5 min at 95 °C and loaded into a 4–15% polyacrylamide gel (Bio-Rad). Proteins were transferred to a 0.45 µm PVDF membrane (Bio-Rad) using the semi-dry transfer method. Membranes were blocked for 1 h with 5% fat free milk powder (Bio-Rad) in TBS + 0.05% tween-20 (Sigma-Aldrich). All primary antibody incubations were performed overnight at 4 °C in blocking buffer. All antibodies (lamin A and C: ab108595; paxillin: ab32084; zyxin: ab58210; YAP1: ab52771; TBP: ab51841) were ordered from Abcam and diluted 1/1000, except for YAP1 which was diluted 1/500. Blots were subsequently incubated with 0.33 µg/ml goat-anti-rabbit or mouse horseradish peroxidase (Bio-Rad) in blocking buffer for 1 h at room temperature. Protein bands were then visualized using Clarity Western ECL (Bio-Rad). Quantifications of band intensity were done in Fiji using the gel quantification tool.

Immunofluorescence and imaging

Prior to staining, hMSCs were fixed in 3.6% (v/v) paraformaldehyde (Sigma-Aldrich) in PBS for 20 min at room temperature. Cells were permeabilized and blocked in 2% bovine serum albumin (BSA) (VWR) and 0.1% triton X (VWR) in PBS for 1 h at room temperature. Antibodies mentioned above in the same dilution, or osteocalcin (Abcam, ab93876, 1/250) or PPAR-γ (ThermoFisher Scientific, PA1-824, 1/250) were incubated overnight at 4 °C in 2% BSA and 0.05% tween-20 in PBS (incubation buffer). Secondary antibodies goat-anti-rabbit or mouse Alexa Fluor 488 (Thermo Fisher Scientific) were then incubated overnight at 4 °C in incubation buffer. Instead of antibody staining, F-actin staining was done with phalloidin Alexa Fluor 488 (Thermo Fisher Scientific) at room temperature for 20 min in PBS+0.05% tween-20. Nuclei were stained with DAPI (Sigma-Aldrich). Images were taken on a widefield fluorescence microscope, or confocal microscope. In culture conditions in 3D and where necessary in 2D, Z-stacks were taken to ensure the entire cell was imaged from bottom to top, to ensure equal quantification in the different substrates. To allow for quantitative comparison between

images, all images within an experiment were taken with the same settings and on the same day.
Actin quantification was done using a custom-built Fiji macro *(paper in press)*. A line was drawn through the cell perpendicular to the long axis of the cell, and the intensity over that line was measured. The intensity distribution was divided into 10 equal bins to correct for differences in cell size. The total F-actin intensity overlapping with the nucleus was also measured.
For YAP1 quantification, the nucleus and an area in the cytoplasm were selected and the overall pixel intensity in each area was measured using Fiji. The ratio between nuclear and cytoplasmic intensity was then calculated per cell.

Migration assay
As an indication for nuclear stiffness[32], hMSCs were allowed to migrate directly from films or ESP scaffolds through a Fluoroblok 24-well transwell with 3 µm or 8 µm pores. hMSCs were first cultured on 6-mm films or ESP scaffolds for 7 days in standard scaffold culture conditions (see 'Cell culture') and then transferred upside down on the transwell membrane. αMEM without serum was added to the top compartment and basic medium was added to the bottom compartment, to induce cell migration. A screw and nut were placed on top of the film or ESP scaffold as a weight to ensure proper contact between the substrate and transwell. After fixation (see 'Immunofluorescence and imaging'), the film or ESP scaffold was removed, and the transwells were stained with Syto14 (Thermo Fisher Scientific). The whole transwell was imaged, top and bottom, and cells were quantified using particle analysis in Fiji.

Lentiviral production for shRNA delivery
To deliver shRNA for gene knock-down, we produced lentiviruses using TRC pLKO.1 constructs from Dharmacon. We used the following clone IDs for LMNA-shRNA 1 and 2: TRCN0000061833 and TRCN0000061836; ZYX-shRNA 1 and 2: TRCN0000074204 and TRCN0000074205; PXN-shRNA 1 and 2: TRCN0000123134 and TRCN0000123136; YAP-shRNA 1 and 21: TRCN0000107265 and TRCN0000107266. To produce the lentiviral particles, human embryonic kidney 293FT (HEK) cells were seeded at 60k cells/cm^2 in a TCP dish in DMEM + 10% FBS. The next day, HEK cells were transfected with pMDLg pRRE, pMD2.G, pRSV Rev (Addgene) and one of the pLKO.1 plasmids containing the shRNA, using lipofectamine 2000 (Thermo Fisher Scientific) in ratio of 5:1 (µl:µg of DNA). After overnight incubation, the medium was changed to basic medium for hMSCs. Viral particles were harvested after 24 and 48 h and filtered through a 0.45 µm filter.

The day before transduction, hMSCs were thawed at 1k cells/cm^2 in a 10-cm dish. 3 milliliters of unconcentrated virus was added to the dish and incubated overnight. The medium was

changed for basic medium the following day, and the medium was changed for basic medium + 2 µg/ml puromycin at 48–72 h later. Cells were treated for 72 h with puromycin. At 9–10 days after initial thawing, cells were passaged at 1k cells/cm^2 and cultured for 7 days in basic medium before protein harvest or fixation.

Statistical analysis

The number of biological replicates and repeated experiments are indicated in the figure captions, as well as the statistical test used. All individual films and scaffolds used in one experiment were randomly assigned to an experimental group. Cells that were imaged for quantification were also randomly picked. All data was tested for normal distribution using the Shapiro-Wilk test. To test the significance of relative expression data with one comparison, a two-tailed ratio t-test was performed, or the Mann-Whitney test as non-parametric equivalent. For relative expression data with multiple comparisons, the log of each value was used for a repeated measures ANOVA, with Tukey's post hoc to compare individual groups. For non-relative comparisons, a One-way ANOVA with Tukey's post hoc, or Two-way ANOVA with Sidak's post-hoc was used, or the Kruskal-Wallis test with Dunn's post hoc as non-parametric equivalent. Statistical significance was set at $p<0.05$. Statistical tests were performed with GraphPad Prism 8.

Acknowledgements

We would like to thank Jos Broers for valuable discussions on the lamin A and C data. We are grateful to the European Research Council starting grant "Cell Hybridge" for financial support under the Horizon2020 framework program (Grant #637308). Some of the materials used in this work were provided by the Texas A&M Health Science Center College of Medicine Institute for Regenerative Medicine at Scott & White through a grant from NCRR of the NIH (Grant #P40RR017447).

References

1. M.A. Wozniak, K. Modzelewska, L. Kwong, and P.J. Keely, *Focal adhesion regulation of cell behavior.* Biochim Biophys Acta, 2004. **1692**(2-3): p. 103-19.
2. M.J. Stroud, *Linker of nucleoskeleton and cytoskeleton complex proteins in cardiomyopathy.* Biophys Rev, 2018. **10**(4): p. 1033-1051.
3. K.N. Dahl, S.M. Kahn, K.L. Wilson, and D.E. Discher, *The nuclear envelope lamina network has elasticity and a compressibility limit suggestive of a molecular shock absorber.* J Cell Sci, 2004. **117**(Pt 20): p. 4779-86.
4. J. Lammerding, L.G. Fong, J.Y. Ji, K. Reue, C.L. Stewart, S.G. Young, and R.T. Lee, *Lamins A and C but not lamin B1 regulate nuclear mechanics.* J Biol Chem, 2006. **281**(35): p. 25768-80.
5. J. Swift, I.L. Ivanovska, A. Buxboim, T. Harada, P.C. Dingal, J. Pinter, J.D. Pajerowski, K.R. Spinler, J.W. Shin, M. Tewari, F. Rehfeldt, D.W. Speicher, and D.E. Discher, *Nuclear lamin-A scales with tissue stiffness and enhances matrix-directed differentiation.* Science, 2013. **341**(6149): p. 1240104.
6. A. Buxboim, J. Irianto, J. Swift, A. Athirasala, J.W. Shin, F. Rehfeldt, and D.E. Discher, *Coordinated increase of nuclear tension and lamin-A with matrix stiffness outcompetes lamin-B receptor that favors soft tissue phenotypes.* Mol Biol Cell, 2017. **28**(23): p. 3333-3348.
7. R. Al-Saaidi and P. Bross, *Do lamin A and lamin C have unique roles?* Chromosoma, 2015. **124**(1): p. 1-12.
8. K. Weber and U. Groeschel-Stewart, *Antibody to myosin: the specific visualization of myosin-containing filaments in nonmuscle cells.* Proc Natl Acad Sci U S A, 1974. **71**(11): p. 4561-4.
9. Y.C. Yeh, J.Y. Ling, W.C. Chen, H.H. Lin, and M.J. Tang, *Mechanotransduction of matrix stiffness in regulation of focal adhesion size and number: reciprocal regulation of caveolin-1 and beta1 integrin.* Sci Rep, 2017. **7**(1): p. 15008.
10. R.J. Pelham, Jr. and Y. Wang, *Cell locomotion and focal adhesions are regulated by substrate flexibility.* Proc Natl Acad Sci U S A, 1997. **94**(25): p. 13661-5.
11. D.E. Discher, P. Janmey, and Y.L. Wang, *Tissue cells feel and respond to the stiffness of their substrate.* Science, 2005. **310**(5751): p. 1139-43.
12. M. Prager-Khoutorsky, A. Lichtenstein, R. Krishnan, K. Rajendran, A. Mayo, Z. Kam, B. Geiger, and A.D. Bershadsky, *Fibroblast polarization is a matrix-rigidity-dependent process controlled by focal adhesion mechanosensing.* Nat Cell Biol, 2011. **13**(12): p. 1457-65.
13. S. Tavares, A.F. Vieira, A.V. Taubenberger, M. Araujo, N.P. Martins, C. Bras-Pereira, A. Polonia, M. Herbig, C. Barreto, O. Otto, J. Cardoso, J.B. Pereira-Leal, J. Guck, J. Paredes, and F. Janody, *Actin stress fiber organization promotes cell stiffening and proliferation of pre-invasive breast cancer cells.* Nat Commun, 2017. **8**: p. 15237.
14. S. Ankam, B.K.K. Teo, G. Pohan, S.W.L. Ho, C.K. Lim, and E.K.F. Yim, *Temporal Changes in Nucleus Morphology, Lamin A/C and Histone Methylation During Nanotopography-Induced Neuronal Differentiation of Stem Cells.* Front Bioeng Biotechnol, 2018. **6**: p. 69.
15. M. Azatov, X. Sun, A. Suberi, J.T. Fourkas, and A. Upadhyaya, *Topography on a subcellular scale modulates cellular adhesions and actin stress fiber dynamics in tumor associated fibroblasts.* Phys Biol, 2017. **14**(6): p. 065003.
16. B.G. Keselowsky, D.M. Collard, and A.J. Garcia, *Surface chemistry modulates focal adhesion composition and signaling through changes in integrin binding.* Biomaterials, 2004. **25**(28): p. 5947-54.
17. S. Dupont, L. Morsut, M. Aragona, E. Enzo, S. Giulitti, M. Cordenonsi, F. Zanconato, J. Le Digabel, M. Forcato, S. Bicciato, N. Elvassore, and S. Piccolo, *Role of YAP/TAZ in mechanotransduction.* Nature, 2011. **474**(7350): p. 179-83.

18. A.J. Engler, S. Sen, H.L. Sweeney, and D.E. Discher, *Matrix elasticity directs stem cell lineage specification.* Cell, 2006. **126**(4): p. 677-89.
19. I. Han, B.S. Kwon, H.K. Park, and K.S. Kim, *Differentiation Potential of Mesenchymal Stem Cells Is Related to Their Intrinsic Mechanical Properties.* Int Neurourol J, 2017. **21**(Suppl 1): p. S24-31.
20. R. McBeath, D.M. Pirone, C.M. Nelson, K. Bhadriraju, and C.S. Chen, *Cell shape, cytoskeletal tension, and RhoA regulate stem cell lineage commitment.* Dev Cell, 2004. **6**(4): p. 483-95.
21. J.S. Park, J.S. Chu, A.D. Tsou, R. Diop, Z. Tang, A. Wang, and S. Li, *The effect of matrix stiffness on the differentiation of mesenchymal stem cells in response to TGF-beta.* Biomaterials, 2011. **32**(16): p. 3921-30.
22. M. Sun, G. Chi, P. Li, S. Lv, J. Xu, Z. Xu, Y. Xia, Y. Tan, J. Xu, L. Li, and Y. Li, *Effects of Matrix Stiffness on the Morphology, Adhesion, Proliferation and Osteogenic Differentiation of Mesenchymal Stem Cells.* Int J Med Sci, 2018. **15**(3): p. 257-268.
23. P.S. Mathieu and E.G. Loboa, *Cytoskeletal and focal adhesion influences on mesenchymal stem cell shape, mechanical properties, and differentiation down osteogenic, adipogenic, and chondrogenic pathways.* Tissue Eng Part B Rev, 2012. **18**(6): p. 436-44.
24. B. Zhang, Y. Yang, R. Keyimu, J. Hao, Z. Zhao, and R. Ye, *The role of lamin A/C in mesenchymal stem cell differentiation.* J Physiol Biochem, 2019. **75**(1): p. 11-18.
25. Y. Tang, T. Feinberg, E.T. Keller, X.Y. Li, and S.J. Weiss, *Snail/Slug binding interactions with YAP/TAZ control skeletal stem cell self-renewal and differentiation.* Nat Cell Biol, 2016. **18**(9): p. 917-29.
26. Y. Tang, R.G. Rowe, E.L. Botvinick, A. Kurup, A.J. Putnam, M. Seiki, V.M. Weaver, E.T. Keller, S. Goldstein, J. Dai, D. Begun, T. Saunders, and S.J. Weiss, *MT1-MMP-dependent control of skeletal stem cell commitment via a beta1-integrin/YAP/TAZ signaling axis.* Dev Cell, 2013. **25**(4): p. 402-16.
27. S.I. Fraley, Y. Feng, R. Krishnamurthy, D.H. Kim, A. Celedon, G.D. Longmore, and D. Wirtz, *A distinctive role for focal adhesion proteins in three-dimensional cell motility.* Nat Cell Biol, 2010. **12**(6): p. 598-604.
28. L. Moroni, J.R. de Wijn, and C.A. van Blitterswijk, *3D fiber-deposited scaffolds for tissue engineering: influence of pores geometry and architecture on dynamic mechanical properties.* Biomaterials, 2006. **27**(7): p. 974-85.
29. M. Gupta, B.R. Sarangi, J. Deschamps, Y. Nematbakhsh, A. Callan-Jones, F. Margadant, R.M. Mege, C.T. Lim, R. Voituriez, and B. Ladoux, *Adaptive rheology and ordering of cell cytoskeleton govern matrix rigidity sensing.* Nat Commun, 2015. **6**: p. 7525.
30. A. Buxboim, J. Swift, J. Irianto, K.R. Spinler, P.C. Dingal, A. Athirasala, Y.R. Kao, S. Cho, T. Harada, J.W. Shin, and D.E. Discher, *Matrix elasticity regulates lamin-A,C phosphorylation and turnover with feedback to actomyosin.* Curr Biol, 2014. **24**(16): p. 1909-17.
31. V. Kochin, T. Shimi, E. Torvaldson, S.A. Adam, A. Goldman, C.G. Pack, J. Melo-Cardenas, S.Y. Imanishi, R.D. Goldman, and J.E. Eriksson, *Interphase phosphorylation of lamin A.* J Cell Sci, 2014. **127**(Pt 12): p. 2683-96.
32. T. Harada, J. Swift, J. Irianto, J.W. Shin, K.R. Spinler, A. Athirasala, R. Diegmiller, P.C. Dingal, I.L. Ivanovska, and D.E. Discher, *Nuclear lamin stiffness is a barrier to 3D migration, but softness can limit survival.* J Cell Biol, 2014. **204**(5): p. 669-82.
33. J.K. Kim, A. Louhghalam, G. Lee, B.W. Schafer, D. Wirtz, and D.H. Kim, *Nuclear lamin A/C harnesses the perinuclear apical actin cables to protect nuclear morphology.* Nat Commun, 2017. **8**(1): p. 2123.
34. D.H. Kim, B. Li, F. Si, J.M. Phillip, D. Wirtz, and S.X. Sun, *Volume regulation and shape bifurcation in the cell nucleus.* J Cell Sci, 2015. **128**(18): p. 3375-85.
35. A. Elosegui-Artola, I. Andreu, A.E.M. Beedle, A. Lezamiz, M. Uroz, A.J. Kosmalska, R. Oria, J.Z. Kechagia, P. Rico-Lastres, A.L. Le Roux, C.M. Shanahan, X. Trepat, D. Navajas, S. Garcia-Manyes, and

P. Roca-Cusachs, *Force Triggers YAP Nuclear Entry by Regulating Transport across Nuclear Pores.* Cell, 2017. **171**(6): p. 1397-1410 e14.

36. M. Vicente-Manzanares, X. Ma, R.S. Adelstein, and A.R. Horwitz, *Non-muscle myosin II takes centre stage in cell adhesion and migration.* Nat Rev Mol Cell Biol, 2009. **10**(11): p. 778-90.
37. J. Swift and D.E. Discher, *The nuclear lamina is mechano-responsive to ECM elasticity in mature tissue.* J Cell Sci, 2014. **127**(Pt 14): p. 3005-15.
38. E. Griffith, A.S. Coutts, and D.M. Black, *RNAi knockdown of the focal adhesion protein TES reveals its role in actin stress fibre organisation.* Cell Motil Cytoskeleton, 2005. **60**(3): p. 140-52.
39. M.A. Smith, E. Blankman, M.L. Gardel, L. Luettjohann, C.M. Waterman, and M.C. Beckerle, *A zyxin-mediated mechanism for actin stress fiber maintenance and repair.* Dev Cell, 2010. **19**(3): p. 365-76.
40. Z. Sun, S. Huang, Z. Li, and G.A. Meininger, *Zyxin is involved in regulation of mechanotransduction in arteriole smooth muscle cells.* Front Physiol, 2012. **3**: p. 472.
41. N.O. Deakin and C.E. Turner, *Paxillin comes of age.* J Cell Sci, 2008. **121**(Pt 15): p. 2435-44.
42. J. Fu, Y.K. Wang, M.T. Yang, R.A. Desai, X. Yu, Z. Liu, and C.S. Chen, *Mechanical regulation of cell function with geometrically modulated elastomeric substrates.* Nat Methods, 2010. **7**(9): p. 733-6.
43. J.X. Pan, L. Xiong, K. Zhao, P. Zeng, B. Wang, F.L. Tang, D. Sun, H.H. Guo, X. Yang, S. Cui, W.F. Xia, L. Mei, and W.C. Xiong, *YAP promotes osteogenesis and suppresses adipogenic differentiation by regulating beta-catenin signaling.* Bone Res, 2018. **6**: p. 18.
44. B. Sen, G. Uzer, R.M. Samsonraj, Z. Xie, C. McGrath, M. Styner, A. Dudakovic, A.J. van Wijnen, and J. Rubin, *Intranuclear Actin Structure Modulates Mesenchymal Stem Cell Differentiation.* Stem Cells, 2017. **35**(6): p. 1624-1635.
45. C. Yang, M.W. Tibbitt, L. Basta, and K.S. Anseth, *Mechanical memory and dosing influence stem cell fate.* Nat Mater, 2014. **13**(6): p. 645-52.
46. E. Cukierman, R. Pankov, D.R. Stevens, and K.M. Yamada, *Taking cell-matrix adhesions to the third dimension.* Science, 2001. **294**(5547): p. 1708-12.
47. M. Werner, S.B. Blanquer, S.P. Haimi, G. Korus, J.W. Dunlop, G.N. Duda, D.W. Grijpma, and A. Petersen, *Surface Curvature Differentially Regulates Stem Cell Migration and Differentiation via Altered Attachment Morphology and Nuclear Deformation.* Adv Sci (Weinh), 2017. **4**(2): p. 1600347.
48. C.Y. Ho, D.E. Jaalouk, M.K. Vartiainen, and J. Lammerding, *Lamin A/C and emerin regulate MKL1-SRF activity by modulating actin dynamics.* Nature, 2013. **497**(7450): p. 507-11.
49. Y. Yang, X. Wang, Y. Wang, X. Hu, N. Kawazoe, Y. Yang, and G. Chen, *Influence of Cell Spreading Area on the Osteogenic Commitment and Phenotype Maintenance of Mesenchymal Stem Cells.* Sci Rep, 2019. **9**(1): p. 6891.
50. O. Chaudhuri, L. Gu, D. Klumpers, M. Darnell, S.A. Bencherif, J.C. Weaver, N. Huebsch, H.P. Lee, E. Lippens, G.N. Duda, and D.J. Mooney, *Hydrogels with tunable stress relaxation regulate stem cell fate and activity.* Nat Mater, 2016. **15**(3): p. 326-34.
51. S. Khetan, M. Guvendiren, W.R. Legant, D.M. Cohen, C.S. Chen, and J.A. Burdick, *Degradation-mediated cellular traction directs stem cell fate in covalently crosslinked three-dimensional hydrogels.* Nat Mater, 2013. **12**(5): p. 458-65.
52. N. Huebsch, P.R. Arany, A.S. Mao, D. Shvartsman, O.A. Ali, S.A. Bencherif, J. Rivera-Feliciano, and D.J. Mooney, *Harnessing traction-mediated manipulation of the cell/matrix interface to control stem-cell fate.* Nat Mater, 2010. **9**(6): p. 518-26.
53. C.M. Digirolamo, D. Stokes, D. Colter, D.G. Phinney, R. Class, and D.J. Prockop, *Propagation and senescence of human marrow stromal cells in culture: a simple colony-forming assay identifies samples with the greatest potential to propagate and differentiate.* Br J Haematol, 1999. **107**(2): p. 275-81.

Supplementary figures

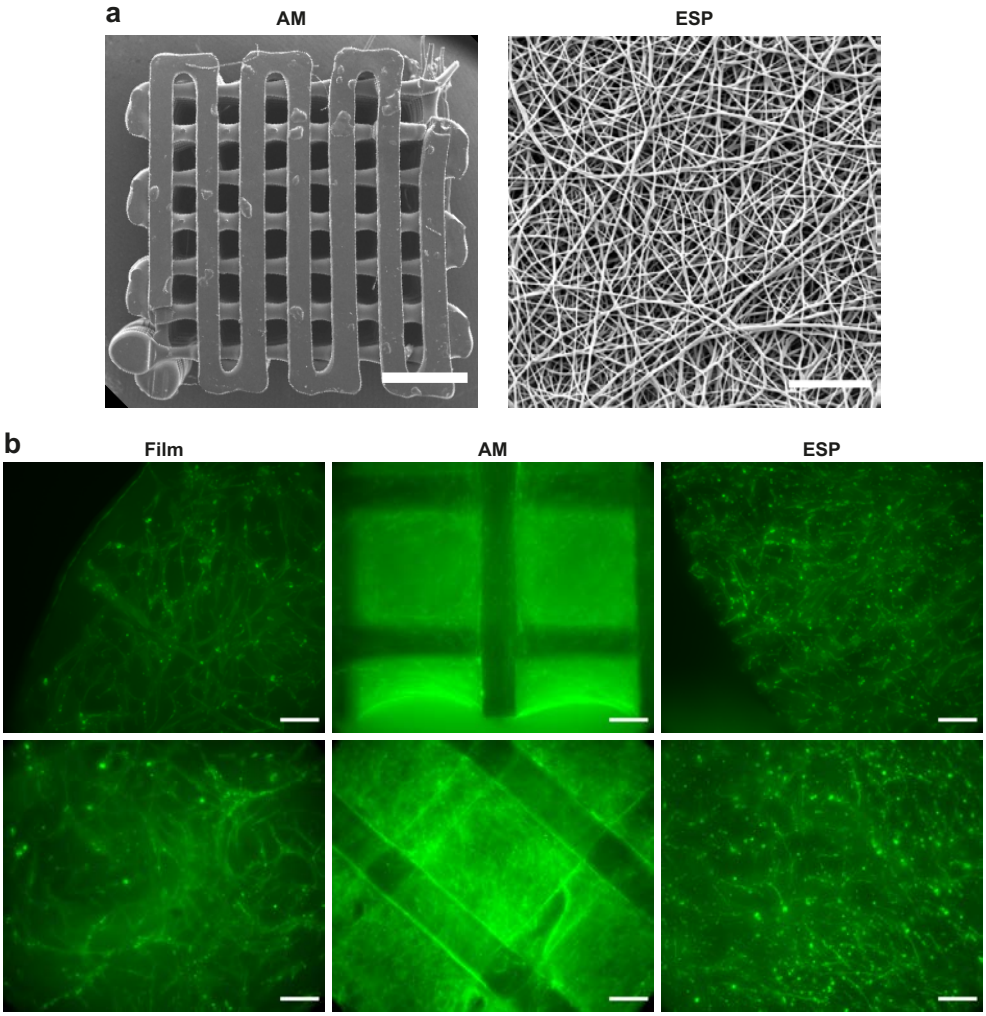

Supplementary Figure 1. Overview of the different culture platforms. a, SEM image of 300PEOT55PBT45 (300PEOT55PBT45) AM (left) and ESP (right) scaffold. Scalebar of AM 1 mm (left), scale bar of ESP 20 µm (right). b, hMSCs after 7 days of culture on 300PEOT55PBT45 2D films, AM, or ESP scaffolds, stained for F-actin (green). All images are maximum projection images to include multiple planes of focus in the 3D (AM and ESP) scaffolds. Scale bars 200 µm.

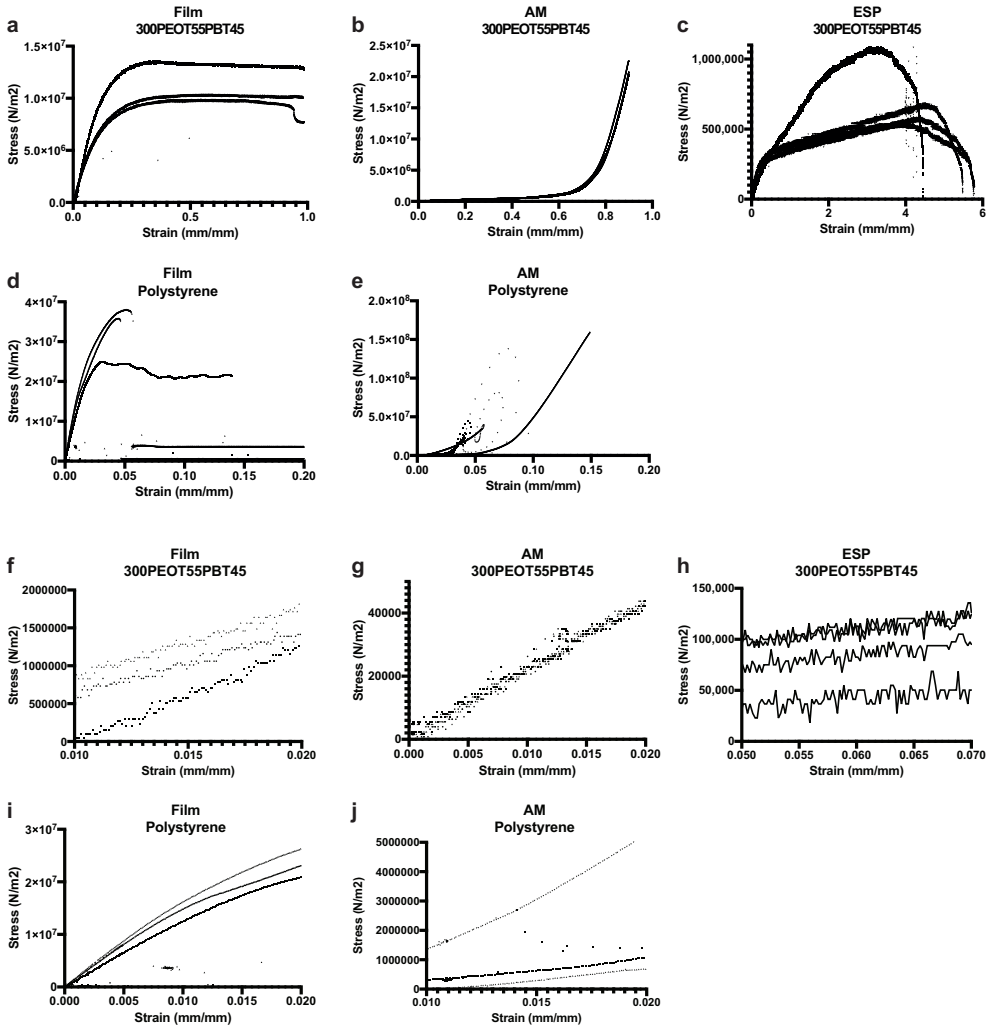

Supplementary Figure 2. Mechanical tests of different culture platforms. a, b, c Tensile **(a, c)** or compression **(b)** tests of 300PEOT55PBT45 films and scaffolds. **d, e** Tensile **(d)** or compression **(e)** tests for polystyrene films and scaffolds. n=3 for each condition. **f-j** Display a zoomed in region of the respective graphs in a-e; the region in which the Young's modulus was calculated. Calculations were done at 0-2% strain after the samples were slightly loaded.

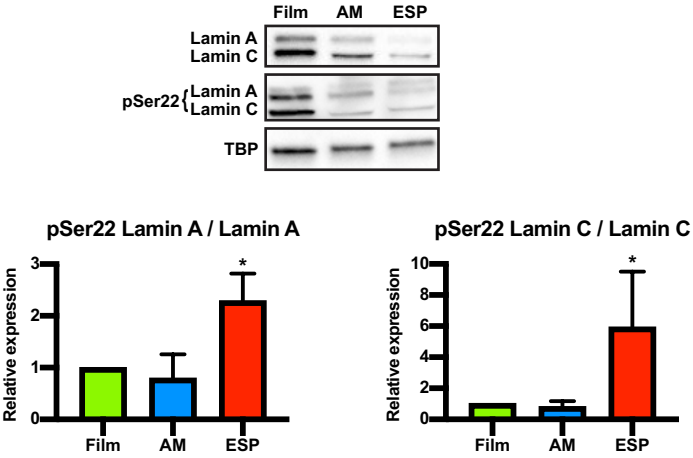

Supplementary Figure 3. Ratio of phosphorylated lamin A and C (at Ser22) to total lamin A and C. Quantification by western blot of hMSCs cultured on films, 3D AM or 3D ESP. n=3 per condition. Graphs show mean±SD of the ratio of phosphorylated lamin A or C to total lamin A or C, normalized to films. One-way ANOVA. * p<0.05 compared to films.

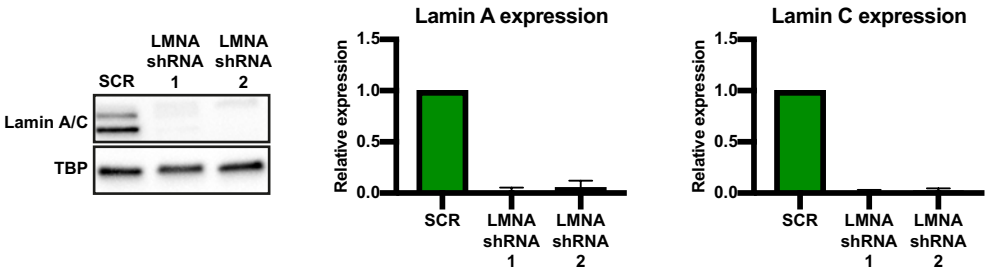

Supplementary Figure 4. Proof of LMNA knock downs. Quantification by western blot of Lamin A and C of hMSCs transduced with scrambled-, or 2 different LMNA shRNA's, cultured on TCP. TBP is shown as loading control. Graphs show the average expression of lamin A or C/TBP, normalized to SCR of 4 biological replicates. Error bars represent mean±SD.

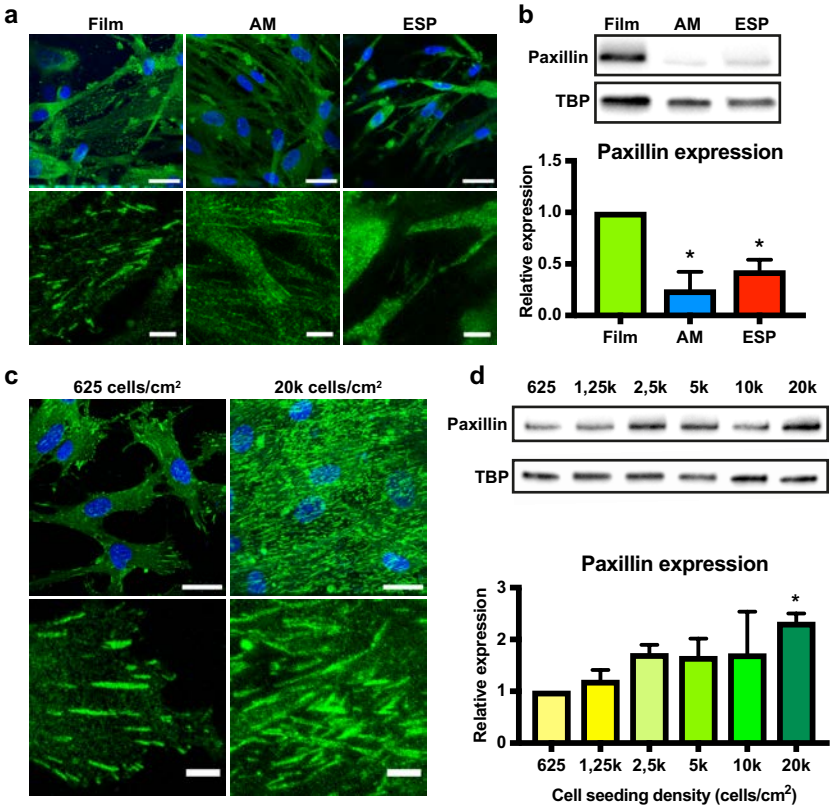

Supplementary Figure 5. Decreased focal adhesions in 3D. a, hMSCs on 300PEOT55PBT45 2D films, 3D additive manufactured (AM) or electrospun (ESP) scaffolds stained for paxillin (green) and nuclei (blue). The bottom panels are magnifications (5×) of the respective images above. Scale bars represent 30 µm (top panels) and 5 µm (bottom panels). **b,** Paxillin expression in hMSCs cultured on 2D film, 3D AM and ESP scaffolds. TBP is shown as a loading control. Graph shows western blot quantifications of paxillin/TBP, normalized to 2D films, from 4 independent experiments. Error bars represent mean±SD. One-way ANOVA; *p<0.05 compared to 2D films. **c, d,** Paxillin expression in hMSCs seeded on 2D TCP at different cell densities. **c**, Images show paxillin staining (green), with the bottom panels showing magnifications (5×) of the respective images above. Scale bars represent 30 µm (top panels) and 5 µm (bottom panels). **d**, Western blots and quantification of western blots from 3 independent experiments show paxillin expression. TBP is shown as a loading control. Values are normalized to 625 cells/cm^2. Error bars represent mean±SD. One-way ANOVA; *p<0.05 compared with 1250 cells/cm^2.

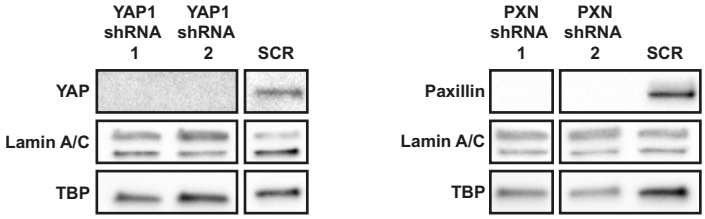

Supplementary Figure 6. Lamin A and C expression is not regulated by YAP1 or Paxillin. Western blot of hMSCs cultured on TCP, knocked down for YAP1 (left), or paxillin (right). TBP is shown as loading control. Representative western blot of two independent experiments.

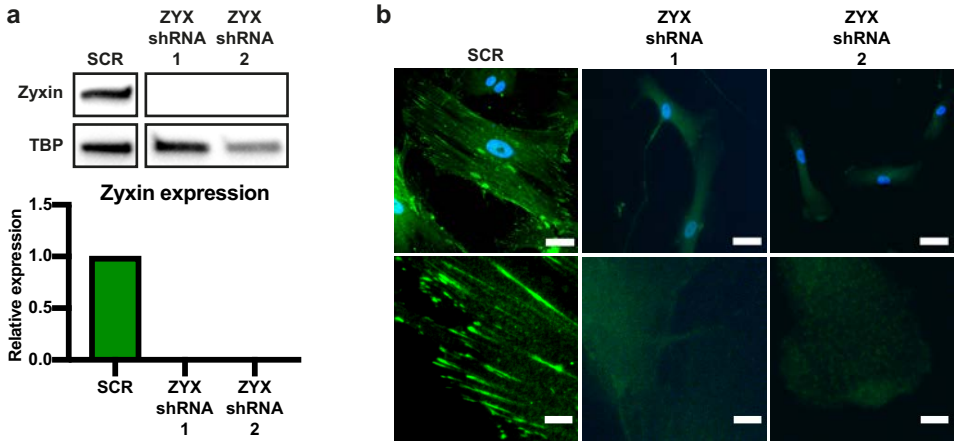

Supplementary Figure 7. Proof of zyxin knockdowns. a, Quantification by western blot of zyxin of hMSCs transduced with scrambled-, or 2 different ZYX shRNA's cultured on TCP. TBP is shown as loading control. Graphs show the average expression of Zyxin/TBP, normalized to SCR of 4 biological replicates. **b,** Staining of zyxin (green) and nuclei(blue) in scramble- or zyxin knockdown-hMSCs cultured on TCP. Bottom panel shows a 5x magnification of the respective image above. Scalebars 50 µm (top panel) and 10 µm (bottom panel).

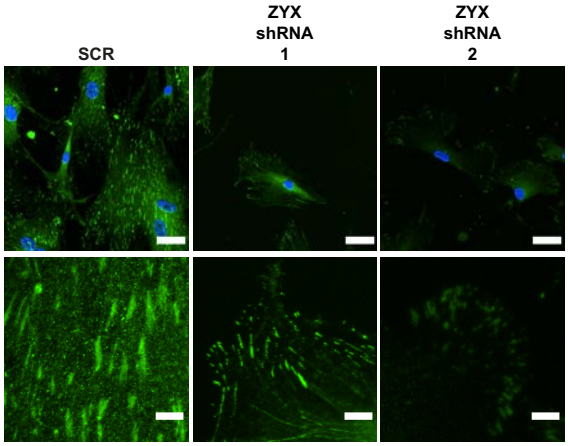

Supplementary Figure 8. Reduction of paxillin positive focal adhesions in ZYX knockdowns. Staining of paxillin (green) and nuclei (blue) in scramble- or zyxin knockdown-hMSCs, cultured on TCP. Bottom panel shows a 5x magnification of the respective image above. Scalebars 50 µm (top panel) and 10 µm (bottom panel).

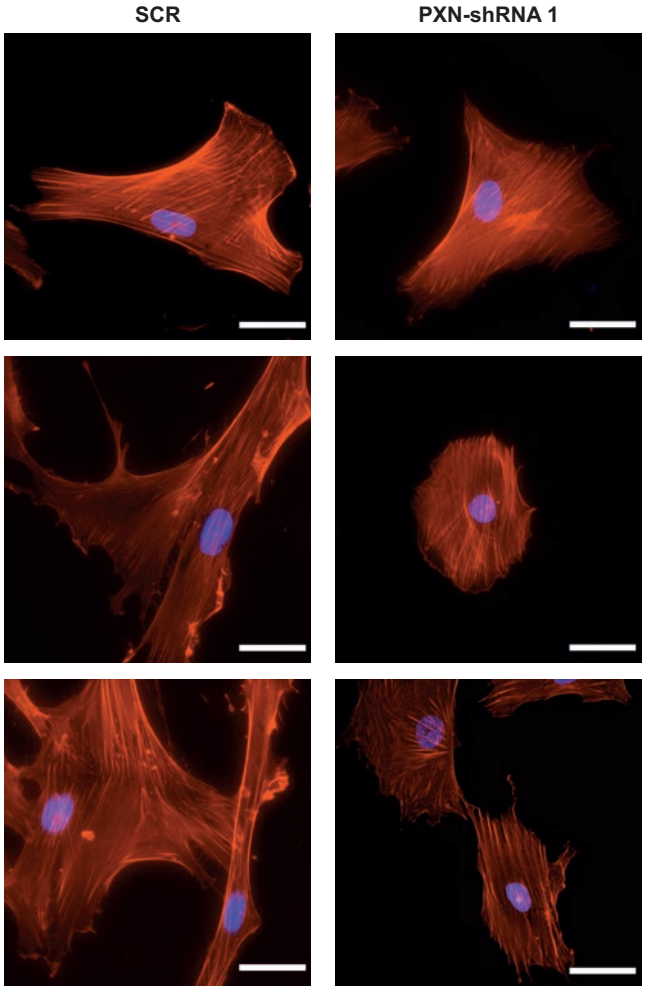

Supplementary Figure 9. No change in actin after paxillin knockdown. F-Actin (red) and nuclei (blue) staining in hMSCs with SCR (left) or PXN-shRNA (right), cultured for on 2D TCP.

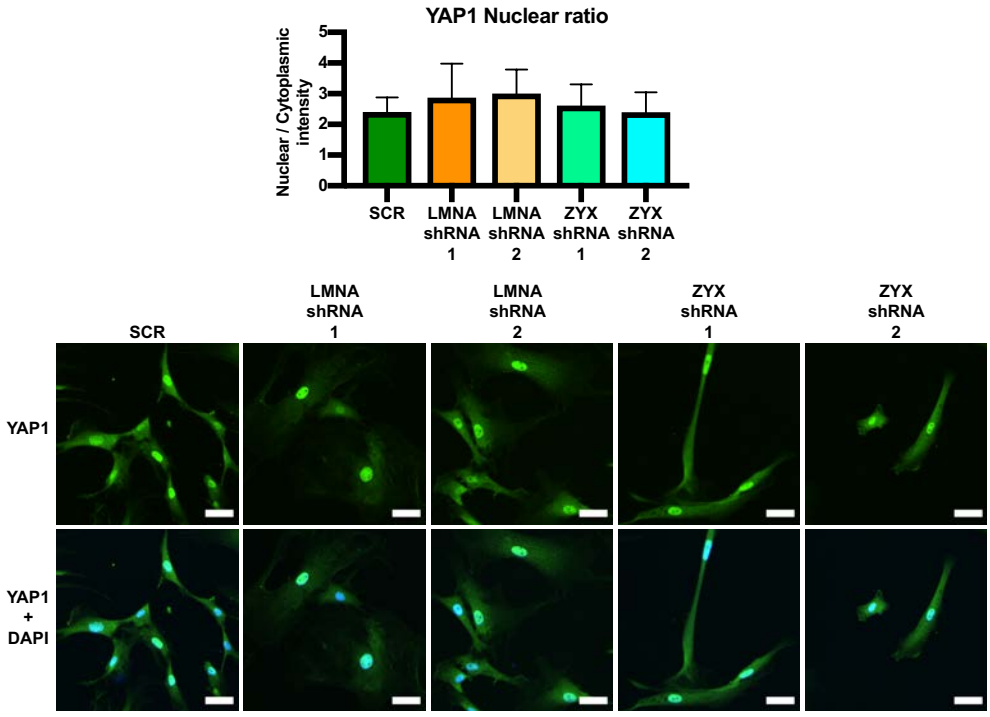

Supplementary Figure 10. Lamin A and C and Zyxin do not regulate YAP1 nuclear localization. YAP1 staining (green) and nuclei (blue) of hMSCs transduced with scrambled-, LMNA- or ZYX-shRNA cultured on TCP. Top panel shows YAP1 staining alone, while the bottom panel shows YAP1 and nuclei (blue). Scalebars 30 µm. Graph shows the corresponding quantification of. Total cells analyzed for SCR: 20, LMNA-shRNA-1: 15, LMNA-shRNA-2: 21, ZYX-shRNA-1: 21, ZYX-shRNA-2: 17. One-way ANOVA, not significant. Error bars represent mean±SD.

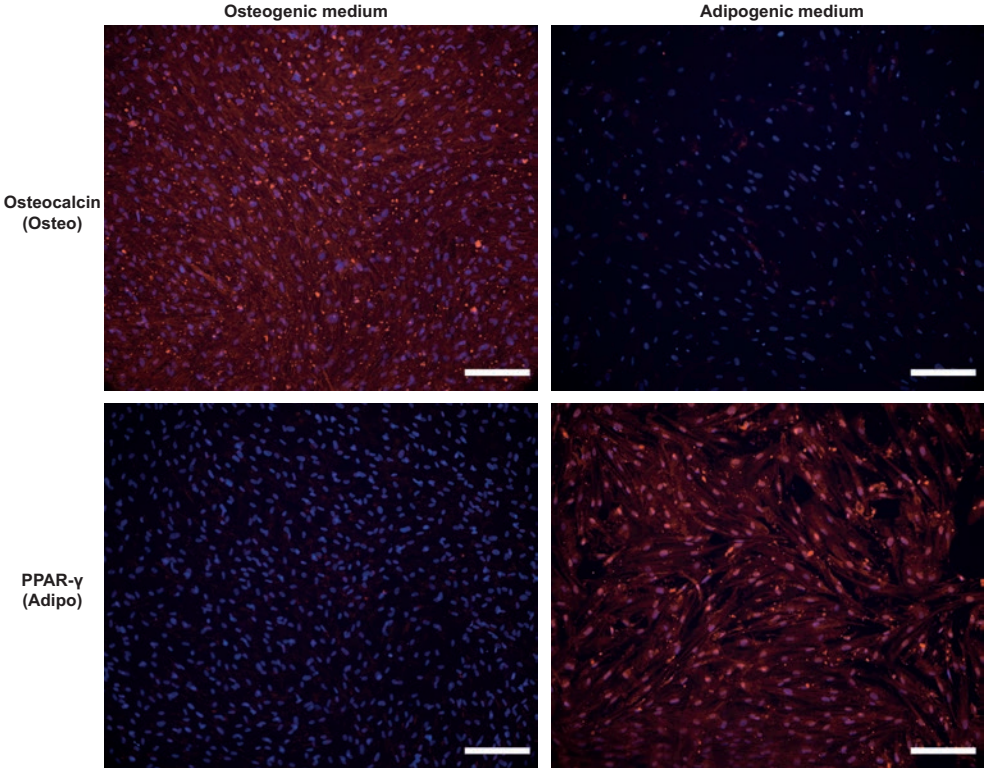

Supplementary Figure 11. Control of differentiation markers. hMSCs were cultured in osteogenic (left panels) or adipogenic (right panels) medium for 21 days and stained for osteocalcin (red, top panels) or PPAR-γ (red, bottom panels) and nuclei. Scalebars represent 250 µm.

Chapter 3 appendix

A quantitative method to analyze F-Actin distribution in cells

Jip Zonderland, Paul Wieringa, Lorenzo Moroni

Complex Tissue Regeneration Department, MERLN Institute for Technology-Inspired Regenerative Medicine, Maastricht University, Maastricht, the Netherlands.

Abstract

Changes in actin structure and distribution are involved in many cellular processes, such as differentiation, proliferation and migration. Differences in cell shape and size make the analysis of actin distribution difficult. Here, we have developed a Fiji macro that analyzes the distribution of actin within the cell, regardless of cell size or shape. The staining intensity is measured along an automatically drawn line over the cell. The intensity data is divided in equal bins, making the analysis insensitive to changes in cell size or shape. We have also created an R script that further processes the acquired data. Together, final data can be acquired within minutes from a set of images, with freely available software. We demonstrate our method with F-actin staining of cytochalasin D treated cells. The advantages of our methods are:

- The analysis is not influenced by cell shape or size
- All steps in the analysis are shown, and can therefore easily be verified for each image
- All software required for the analysis is freely available

Graphical abstract

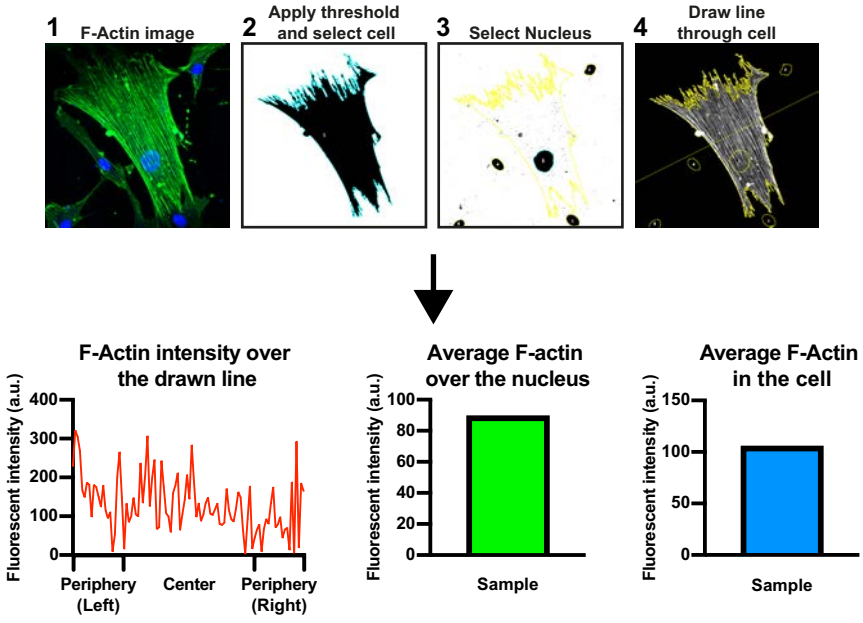

Method details

We have analyzed the F-actin distribution in human mesenchymal stromal cells (hMSCs) using a Fiji macro that we have developed. The macro could be used to test any staining intensity distribution within any cell type. Images were acquired using a confocal microscope with a 25x objective at 512x512 pixels and 8-bit. Depending on the desired resolution, other imaging parameters can be used. To ensure fair quantification among conditions, all images should be taken with the same objective and microscope settings. For optimal post-processing, cells should not be in contact with each other. Z-stacks were taken to ensure the whole cell was in focus. The image analysis was then done in Fiji.

To install the Fiji macro, install Fiji (see useful links), and drag the Fiji macro file (see supplementary data) into the Fiji window, save it and press run.
When the Fiji macro is started, it first asks to choose a folder to save the output data file. After this is selected, a window with several options is opened. There is the option for fully automated cell selection, manual cell selection, or to manually draw a line. In addition, there is an option to perform a maximum intensity projection of a Z-stack, as the macro does not work with Z-stacks. The maximum intensity images are automatically saved in a separate folder in the folder of the original files.
The second set of options is about the line creation. A line can be drawn perpendicular or parallel with the long axis of the cell or the nucleus. Select the option that is most relevant to your research question. In this paper, we were interested in the actin distribution of hMSCs. In our experiments with hMSCs presented here, most actin fibers that formed were in line with the major axis of the cells. To best analyze the actin distribution, we therefore analyzed the cells with lines drawn perpendicular to the major (long) axis of the cell. The reader is kindly referred to the "additional information" section for a more detailed discussion on the different line options.
In the window, the slice (channel) number that contains the nuclear or actin staining (or other staining of interest) and the name of the data group should be filled in.
Lastly, there is the option to analyze all files in a folder for rapid image processing, or to analyze an image that is already opened. The last option runs the macro on the last active image.

After selecting the desired options, the macro will run as follows:
Step 1. Clearing background around cell of interest
A threshold is made using the 'Default' threshold method. (See tips and tricks on how to adjust and optimize this process)
The 'Fill Holes' function is run.
The 'Analyze particles' function is run on the actin image slice, minimal size 200μm^2. (See tips and tricks on how to adjust the minimal cell size)

If manual selection was selected, the ROI's are displayed and the cell of interest can be selected manually, if there is more than one cell present in the image. If automated selection is selected, the largest ROI in the image is considered the cell of interest.
The 'Clear Outside' function clears everything outside of the cell of interest.

Step 2. Selecting the nucleus
The 'Analyze particles' function is run on the nucleus image slice, minimal size 25μm^2. (See tips and tricks on how to adjust the minimal nuclear size)
If manual selection was selected, the ROI's are shown and the nucleus of interest can be selected manually, if there are multiple nuclei in the image. For automated selection, the largest ROI within the cell of interest is considered the nucleus.

Step 3. Measuring average actin intensity over the nucleus and in the whole cell
For the actin intensity over the nucleus, the nucleus of interest is selected and the mean gray value (mean pixel intensity) in this ROI is measured in the actin slice (channel).
For the average actin intensity in the cell, the cell of interest is selected and the mean gray value (mean pixel intensity) in the actin slice (channel) is measured.

Step 4. Measuring actin intensity over the line
A line can be drawn through the cell or through the nucleus, depending on what was selected in the main window.
The center of mass and fit ellipse functions are used on the ROI of the selected cell to determine the middle and the shape of the ROI, respectively.
A line is then drawn through the middle of the ROI, parallel, or perpendicular to the long axis of the fitted ellipse of the ROI.
The line is drawn through the whole image.
When the manually drawn line option is selected, the macro skips the previous steps and starts here.
The pixel intensity along the line is measured using the getProfile() function.
The line is trimmed on both ends until the first value higher than 0, to measure only the cell of interest.
As cells are not equally sized, the pixel intensity data from the line is split up into equally sized bins. The average is taken of all data points within each bin. Because pixel intensity is only measured where the line goes over the cell, the cell shape and size determine the size of each bin and will be different between different cells. The standard bin size is set to 10, so the first bin always contains the outer 10% of the cells, and the last bin the outer 10% of the other side of the cell. See tips and tricks on how to change the bin size.

Step 5. Exporting data to .csv

The actin intensity over the nucleus, within the whole cell and within each bin is exported into a single .csv file. When the macro is started, a folder is selected where the data file will be stored. If a data file already exists in the folder, the new data will be added to that file. If the added data has the same data group name, the R script (see step 6) will treat it all as one data group. This allows for measurements to be done at different times and all data can be selected in a single file.

Step 1-5 are done automatically by the macro in Fiji. To automatically analyze the data, we have written a script in R.

Step 6. Data analysis with R

To run the code, install R (see useful links), File -> New document; copy the code in this window, save as Unicode(UTF-8) file. Follow the instructions in the code to set the right working folder. Copy the code in the R console window and press enter.

The data is separated per data group and the values for each bin are averaged using the aggregate function.

The standard deviation and the n are also determined using the aggregate function.

These values, along with the actin intensity over the nucleus and within the whole cell, are exported to a new .csv file.

This file gives a clear overview of the different measurements per data group. See tips and tricks on how to calculate the 95% confidence interval, as is used in Fig. 1, from these values.

To validate our method, we have treated bone-marrow derived human mesenchymal stromal cells (hMSCs) with cytochalasin D (cytoD) (Sigma-Aldrich), an inhibitor of actin polymerization[1] (Fig. 1a). hMSCs were isolated from the bone-marrow by Texas A&M Health Science Center[2]. hMSCs were seeded on glass coverslips at passage 5 at 1000 cells/cm^2 in growth medium (αMEM+Glutamax+10% FBS). 1µM cytoD was added to the medium for 24 hours and cells were fixed the following day in 3,6% (v/v) paraformaldehyde. Permeabilization and blocking was done using 2% (w/v) bovine serum albumin in PBS+0,1% Triton-X for 1 hour at room temperature. After one PBS+0.05% Tween-20 wash, actin and nuclei were visualized using 66nM phalloidin-488 (ThermoFisher Scientific) and 0,14µg/ml DAPI (Sigma-Aldrich) in PBS+0.05% Tween-20 (Sigma-Aldrich), for 20 minutes at room temperature, followed by three PBS+0.05% Tween-20 washes. The unmounted cells on coverslips were imaged using a confocal microscope with a 25x objective (Numerical aperture: 0.95; working distance: 2.4 mm) at 512x512 pixels and 8-bit, pinhole 1 Airy unit (55,87µm). Z-stacks were made with a z step size of 1µm between images and typically 5 to 10 images, depending on cell shape, to image the cell from top to bottom. Using the Fiji macro and R script we analyzed the F-actin distribution in the cell. The line over which the actin intensity was measured was

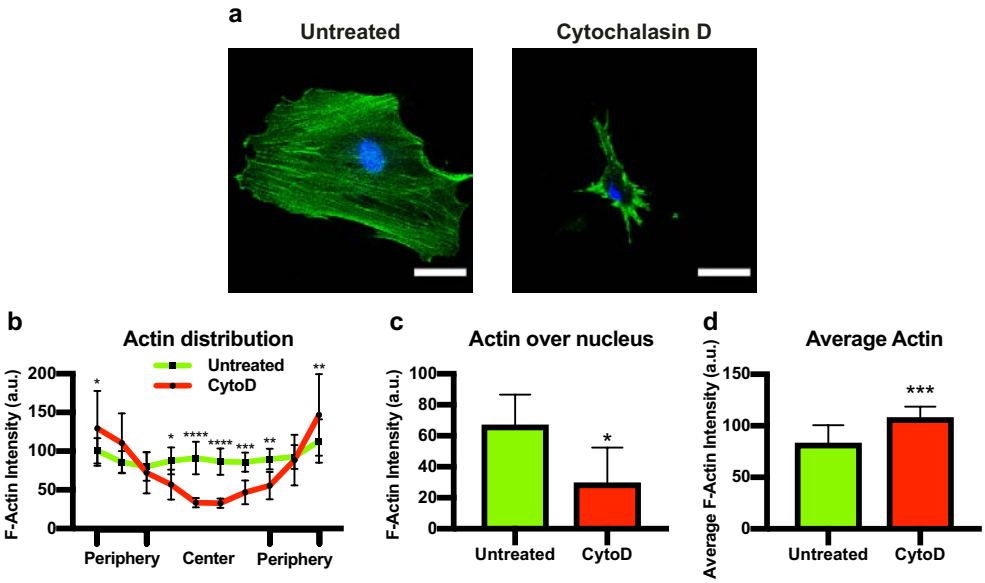

Figure 1. F-Actin distribution in hMSCs treated with Cytochalasin D. hMSCs were cultured for 24 h on coverslips and then incubated with 1 µM cytochalasin D for 24 h. **(a)** Cells were stained for F-actin (phalloidin, green) and nuclei (DAPI, blue). Scale bars 50 µm. **(b-d)** Graphs show mean + 95% CI. Statistical differences were calculated using Graphpad Prism 8. **(b)** A two-way ANOVA with Sidak's multiple comparisons for each bin was performed. Stars indicate statistically significant difference between the two groups within the same bin. **(c, d)** An unpaired t-test was performed. * p<0.05, ** p<0.01, *** p<0.001, **** p<0.0001. N=15 for Untreated, N=13 for CytoD.

perpendicular to the major (long) axis of the cell and through the cell center. As expected, the distribution of F-actin changed upon treatment with cytoD (Fig. 1b). In the untreated hMSCs, actin was distributed equally over the cell. In the cytoD treated hMSCs, F-actin intensity was higher on the cell border than in the cell center due to a lack of stress fibers. Less F-actin was found over the nucleus (Fig. 1c). Interestingly, on average more F-actin per cell was observed in the CytoD treated hMSCs, probably due to strong decrease in cell size (Fig. 1d).

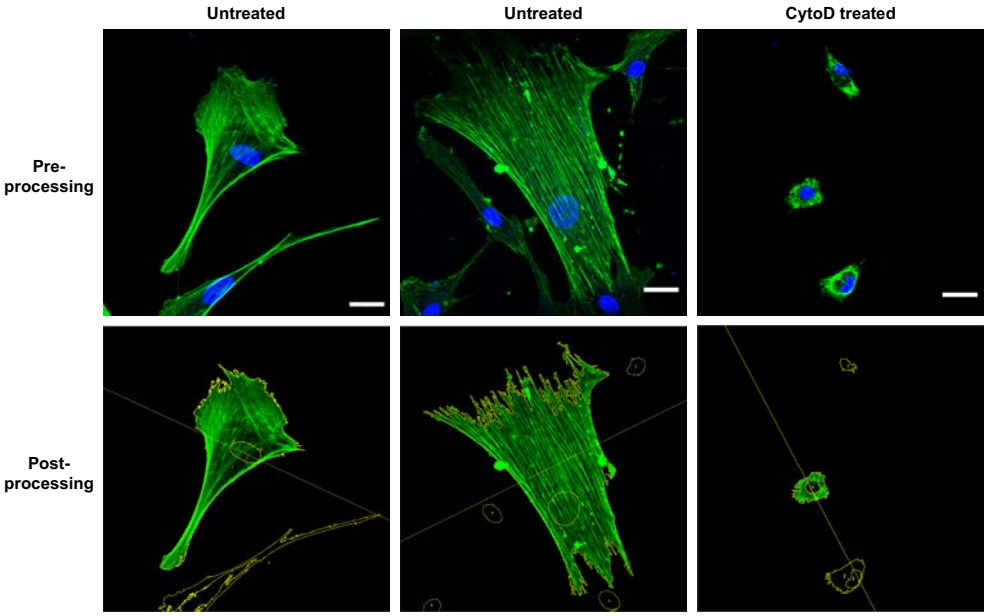

Figure 2. Images of hMSCs pre- and post-processing by the macro. The macro was run on the images in the top panel with automatic cell selection and line perpendicular to the major (long) axis of the cell. When multiple cells are present in the image, but they are not touching, the macro is able to select the cell of interest and remove the others (bottom panel). hMSCs were untreated (left and middle panel) or treated for 24 h with 1 µM cytoD (right panel) and stained for phalloidin (green) and DAPI (blue). Scalebars 30 µm.

Tips and tricks:

Image type requirements

Image files should be .tiff or .tif files, the macro does not work with other image files. The images should contain a µm scale. If images do not contain a scale, then a scale should be set (Analyze->Set Scale). There should be at least a channel with a nuclear staining and a channel with actin or another staining. Image files can contain more than these two channels, but the macro can only analyze two channels. In case of Z-stacks, use the macro to create maximum projection images before proceeding.

Cell-cell contact

As will all image processing, it's difficult to distinguish between different cells if they are in contact. The macro can also not distinguish between different cells if there is too much cell contact. See Fig. 2 for examples of images with multiple cells that the macro is still able to handle properly. Avoid taking images of cells that are in contact with other cells. If this cannot be avoided, the macro can be run as normal, but afterwards the line can then be adjusted manually to the region of interest in the cell of interest, and the line measured manually by

the macro. In case of a manually drawn line, the macro will not have the information on average cellular actin or average actin over the nucleus.

Cell shape

The macro shortens the drawn line to when it first reaches the border of the cell. If a cell is a particular shape so that the line goes through a cell multiple times, it can happen that the inter-cell space is being measured in part of the line. In this case, the measurement will not be reliable. A line can be drawn manually through the cell and this line can be measured by the macro. In case of a manually drawn line, the macro will not have the information on average cellular actin or average actin over the nucleus.

Threshold

The thresholding method should be optimized if the 'Default' method does not work well. Use the 'Auto Threshold' function with 'Method: Try all', to try all automatic thresholding settings and determine which works best for your image acquisition. Ideally, the thresholding is optimized before taking all images for quantification to ensure that a good automatic threshold can be made with the researcher's image set. To change the method the macro uses, look for: 'method=Default white' and change 'Default' into the name of the preferred method,

Adjust minimal cell or nucleus size

The minimal surface area of what the macro will detect as a cell is 200μm^2, the minimal size of a nucleus is 25μm^2. If cells or objects smaller than 200μm^2 are to be analyzed, the minimal detection size can easily be adjusted. Search for '200' in the code, there are two locations where 200 is used. Change this number to the desired cell size in both locations. To change the minimal size of the nuclei: search for '25', there are three locations where 25 is used. Change all three into the desired minimal nuclear size.

Changing bin number and maximum number of bins

The standard number of bins is 10. To change this, search for: 'bin = 10', and change 10 into the desired number. There is no upper limit for the number of bins in the macro, but keep in mind that the number of pixels in the cell where the line passes is the theoretical maximum number of bins.

Changing data in the .csv file

In case measurements need to be deleted or edited, open the .csv file in a TextEdit (mac) or Notepad (windows), and not in excel. Changing the file in excel will damage the file beyond repair and all measurements will have to be done again, before the R script can process the file.

Calculate the confidence interval

The R code gives the average and standard deviation of the measurements. To calculate the confidence interval, as was done for the results in Fig. 1, the following formula can be used: $Z*\sqrt{(s^2/n)}$. Z is the confidence interval factor, which is 1.96 for 95% confidence interval. s is the standard deviation. n is the number of samples.

Additional information

To our knowledge, only one other method has been described to quantify actin distribution within cells, regardless of cell shape[3]. Elosegui-Artola et al. use a Matlab script to transform cells into circles and measure the actin intensity radially. The difference with our method is that we measure the intensity over a line, and not radially over the whole cell. This can be an advantage or a disadvantage, depending on the use. It can be advantageous to measure over a line rather than the whole radius in a number of different situations: 1. If there is interest in a particular distribution of the staining in the cell. An example of this is front to end polarization of actin of migrating cells. 2. The line over which staining intensity is analyzed can be drawn perpendicular to, or in line with the cell. Analyzing cells using both options can give more information of the distribution of the staining through the cell. 3. When analyzing actin distribution in cells with many long protrusions, analyzing staining distribution over a line can be advantageous over measuring radially over the whole. The line could be placed over the exact region of interest, while a radial distribution could give unreliable results because of the protrusions. Lastly, our method can be done with freely available software and we have developed a fully automated pipeline, from image to final analysis. Other researchers have looked at characterizing individual actin stress fibers, or different actin structures within cell, but not distribution[4-7].

Acknowledgements

We are grateful to the European Research Council starting grant "Cell Hybridge" for financial support under the Horizon2020 framework program (Grant # 637308)

References

1. J.F. Casella, M.D. Flanagan, and S. Lin, Cytochalasin D inhibits actin polymerization and induces depolymerization of actin filaments formed during platelet shape change. Nature, 1981. **293**(5830): p. 302-5.
2. C.M. Digirolamo, D. Stokes, D. Colter, D.G. Phinney, R. Class, and D.J. Prockop, Propagation and senescence of human marrow stromal cells in culture: a simple colony-forming assay identifies samples with the greatest potential to propagate and differentiate. Br J Haematol, 1999. **107**(2): p. 275-81.
3. A. Elosegui-Artola, A. Jorge-Penas, O. Moreno-Arotzena, A. Oregi, M. Lasa, J.M. Garcia-Aznar, E.M. De Juan-Pardo, and R. Aldabe, Image analysis for the quantitative comparison of stress fibers and focal adhesions. PLoS One, 2014. **9**(9): p. e107393.
4. F. Kunz, H. Rebl, A. Quade, C. Matschegewski, B. Finke, and J.B. Nebe, Osteoblasts with impaired spreading capacity benefit from the positive charges of plasma polymerised allylamine. Eur Cell Mater, 2015. **29**: p. 177-88; discussion 188-9.
5. S. Lockett, C. Verma, A. Brafman, P. Gudla, K. Nandy, Y. Mimaki, P.L. Fuchs, J. Jaja, K.M. Reilly, J. Beutler, and T.J. Turbyville, Quantitative analysis of F-actin redistribution in astrocytoma cells treated with candidate pharmaceuticals. Cytometry A, 2014. **85**(6): p. 512-21.
6. C. Matschegewski, S. Staehlke, H. Birkholz, R. Lange, U. Beck, K. Engel, and J.B. Nebe, Automatic Actin Filament Quantification of Osteoblasts and Their Morphometric Analysis on Microtextured Silicon-Titanium Arrays. Marterials (Basel), 2012. **5(7)**: p. 1176-1195.
7. J. Weichsel, N. Herold, M.J. Lehmann, H.G. Krausslich, and U.S. Schwarz, A quantitative measure for alterations in the actin cytoskeleton investigated with automated high-throughput microscopy. Cytometry A, 2010. **77**(1): p. 52-63.

Chapter 4

Mechanosensitive regulation of stanniocalcin-1 by actin-myosin in human mesenchymal stromal cells

Jip Zonderland*, David Boaventura Gomes*, Yves Palada, Ivan Lorenzo Moldero, Sandra Camarero Espinosa, Lorenzo Moroni
*These authors contributed equally to this work

Complex Tissue Regeneration Department, MERLN Institute for Technology-Inspired Regenerative Medicine, Maastricht University, Maastricht, the Netherlands.

Abstract

Stanniocalcin-1 (STC1) secreted by mesenchymal stromal cells (MSCs) has anti-inflammatory functions, reduces apoptosis and aids in angiogenesis, both *in vitro* and *in vivo*. However, little is known about the molecular mechanisms of its regulation. Here, we show that STC1 secretion is increased only under specific cell-stress conditions. We find that this is due to a change in actin stress fibers and actin-myosin tension. Abolishment of stress fibers by blebbistatin, inhibition of ROCK and knockdown of the focal adhesion protein zyxin lead to an increase in STC1 secretion. To also study this connection in 3D, where few focal adhesions and actin stress fibers are present, STC1 expression was analyzed in 3D alginate hydrogels and 3D electrospun scaffolds. Indeed, STC1 secretion was increased in these low cellular tension 3D environments. Together, our data shows that STC1 does not directly respond to cell-stress, but that it is regulated through mechanotransduction. This research takes a step forward in the fundamental understanding of STC1 regulation and can have implications for cell based regenerative medicine, where cell survival, anti-inflammatory factors and angiogenesis are critical.

Introduction

Stanniocalcin-1 (STC1) is a widely expressed hypocalcemic 50-kDa homodimeric glycoprotein hormone originally found in teleost fish, and more recently in mammals. STC1 is released into the bloodstream and regulates blood calcium levels by influencing renal and intestinal calcium and phosphate transport through paracrine signaling[1]. In addition, STC1 has recently been reported to be involved in cellular responses to several cell-stress inducing stimuli such as hypoxia[2-4], inflammation[3], oxidative stress[5, 6] and cancer[7]. STC1 expression increases in hypoxia, regulated by hypoxia-inducible factor (HIF)[4] and promotes angiogenesis *in vitro* and *in vivo* by increasing expression of vascular endothelial growth factor (VEGF)[7]. In addition, STC1 secreted by human mesenchymal stromal cells (hMSCs) has been proposed as an important anti-apoptotic factor in the MSC secretome[8-10]. Several studies have shown that STC1 is related with cell survival. In a co-culture model, hMSCs increased STC1 secretion when fibroblasts were UV-irradiated, which in turn enhanced their survival by reducing apoptosis[11]. Similarly, hMSCs upregulated STC1 expression when cancer cells were treated with reactive oxygen species (ROS), increasing their survival by reducing intracellular ROS[5]. The reduction of intracellular ROS by hMSC-secreted STC1 has also been shown for endothelial cells[12]. *In vivo*, STC1 secreted by injected hMSCs reduced fibrosis and ROS in a mouse pulmonary fibrosis model[13]. STC1 has also been reported to increase in 3D culture platforms, such as spheroids and 3D-additive manufactured scaffolds, compared to 2D cultures such as tissue culture polystyrene (TCP)[14-17]. Despite these efforts, the molecular mechanisms by which STC1 expression and secretion are regulated are still unclear.

Here, we show that STC1 secretion is increased in hMSCs challenged with stress conditions[18-21] such as hypotonic shock or nutrient deprivation, but not in hypertonic shock. Our data shows that the regulation of STC1 secretion is not directly related with apoptosis and cell survival, but rather regulated by mechanotransduction. We demonstrate that the actin structure changes in hypotonic and nutrient deprivation conditions, but not with hypertonic treatment. This change in actin is, at least partly, responsible for the increased STC1 secretion, demonstrated by an increase in STC1 secretion after treatment with blebbistatin, ROCK inhibitor or zyxin knockdown. This shows that STC1 is regulated by mechanotransduction, an observation not previously reported.

Results

Increased STC1 release in certain cell-stress conditions

STC1 has been shown to be involved in apoptosis both *in vitro* and *in vivo*[5, 7, 11-13], but its regulation is largely unknown. To start investigating how STC1 is regulated, we treated hMSCs for 8 h in different cell-stress inducing conditions: hypertonic medium (200 mM NaCl in basic medium), hypotonic medium (90% water in basic medium), or nutrient deprivation (phosphate buffered saline (PBS)). After 8 h, apoptosis, measured by caspase 3/7 activity, was significantly increased 9.1±1.2x ($p<0.001$) and 1.5±0.05x ($p<0.01$) in the

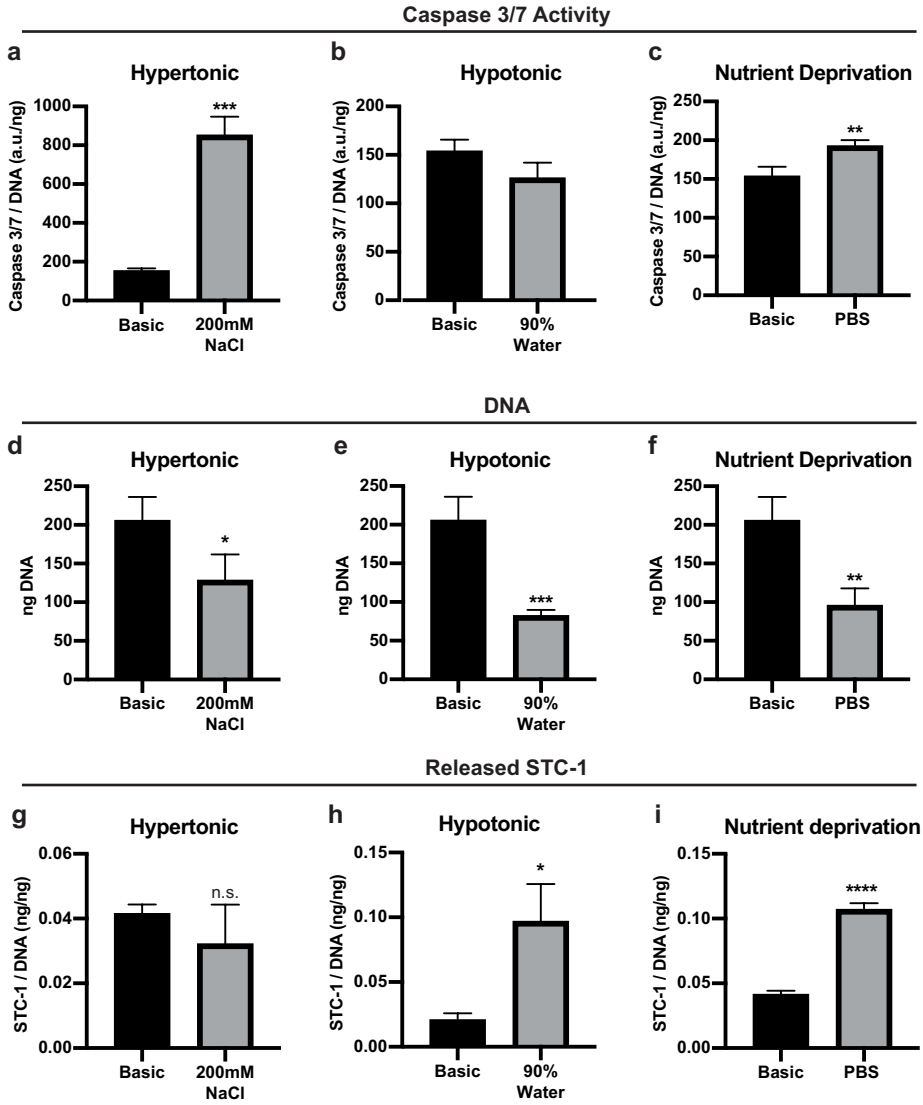

Figure 1. Caspase 3/7 activity, DNA and STC1 release in specific cell-stress conditions. (a-c) Caspase 3/7 activity, normalized by total DNA, of hMSCs treated for 8 h in **(a)** hypertonic medium (Basic medium+200 mM NaCl), **(b)** hypotonic medium (90% water in basic medium), or **(c)** nutrient deprivation medium (PBS). **(d-f)** Total DNA of hMSCs after 8 h in **(d)** hypertonic medium, **(e)** hypotonic medium, or **(f)** PBS. **(g-i)** Total released STC1, measured by ELISA, over an 8 h period of hMSCs treated with **(g)** hypertonic medium, **(h)** hypotonic medium, or **(i)** PBS. N=3 for each condition. Students t-test; n.s. not-significant, * p<0.05, ** p<0.01, *** p<0.001, **** p<0.0001, compared to Basic. Error bars represent mean±SD.

hypertonic (Fig. 1a) and nutrient deprivation conditions (Fig. 1c), respectively, compared to the basic (untreated) condition. Caspase 3/7 activity was not affected in the hypotonic condition (Fig. 1b). Total DNA was significantly reduced in all conditions, by 38±16% ($p<0.05$) in the hypertonic condition (Fig. 1d), by 60±4% ($p<0.001$) in the hypotonic condition (Fig. 1e) and by 54±11% ($p<0.01$) in the nutrient deprivation condition (Fig. 1f). Together, these results show that the different cell-stress inducing conditions successfully induced cell death in a large portion, but not all of the treated cells. Interestingly, STC1 secretion was not significantly different in the hypertonic condition but was significantly increased in both the hypotonic and nutrient deprivation conditions (Fig. 1g-i). In the hypotonic and nutrient deprivation conditions, STC1 secretion increased 4.6±1.4x ($p<0.05$) and 2.6±0.1x ($p<0.0001$) compared to the untreated condition, respectively. To exclude a potential effect of differences in proliferation in the 8 h of various cell-stress conditions, we analyzed STC1 release in different proliferation inhibited conditions. When proliferation was inhibited by culturing cells for 6 days with 0.5% FBS, STC1 secretion increased (Supplementary Fig. 1a, b). However, when proliferation was inhibited for 24 h with 1% DMSO, STC1 secretion decreased (Supplementary Fig. 1c, d). Other proliferation inhibitors did not influence STC1 secretion (high cell seeding density, actinomycin D, CDK4 inhibitor, valproic acid, AZD5438) (Supplementary Fig. 1e, f). Also, increasing proliferation by the addition of bFGF to the medium did not affect STC1 secretion. DNA significantly decreased in the 0.5% FBS, 1% DMSO condition and AZD5438 condition, but not in the other conditions. This suggests that proliferation is not directly correlated with STC1 secretion. Knock down of STC1, however, lead to a decrease in proliferation and adding recombinant STC1 increased proliferation (Supplementary Fig. 1g-i). Together, this shows that STC1 can influence proliferation, but proliferation does not influence STC1 secretion.

Specific cell-stress conditions induce change in actin network

The STC1 secretion was increased by hypotonic- and nutrient deprivation treatment, but not by hypertonic treatment. Clear differences in cell morphology were observed in the different cell-stress conditions. To understand if this could be correlated to the increased STC1 secretion, we stained hMSCs for F-actin after 8 h in the hypertonic, hypotonic and nutrient deprivation conditions (Fig 2a). Interestingly, hypertonic treatment did not greatly affect the actin structure, cell area or number of actin stress fibers in the cells that remained alive (Fig. 2a-c). Hypotonic treatment reduced cell size 71±30% ($p<0.001$) and the number of stress fibers by 86±25% ($p<0.001$), compared to the untreated condition. While the nutrient deprivation treatment did not significantly affect cell area, it completely abolished the actin stress fibers in the cells.

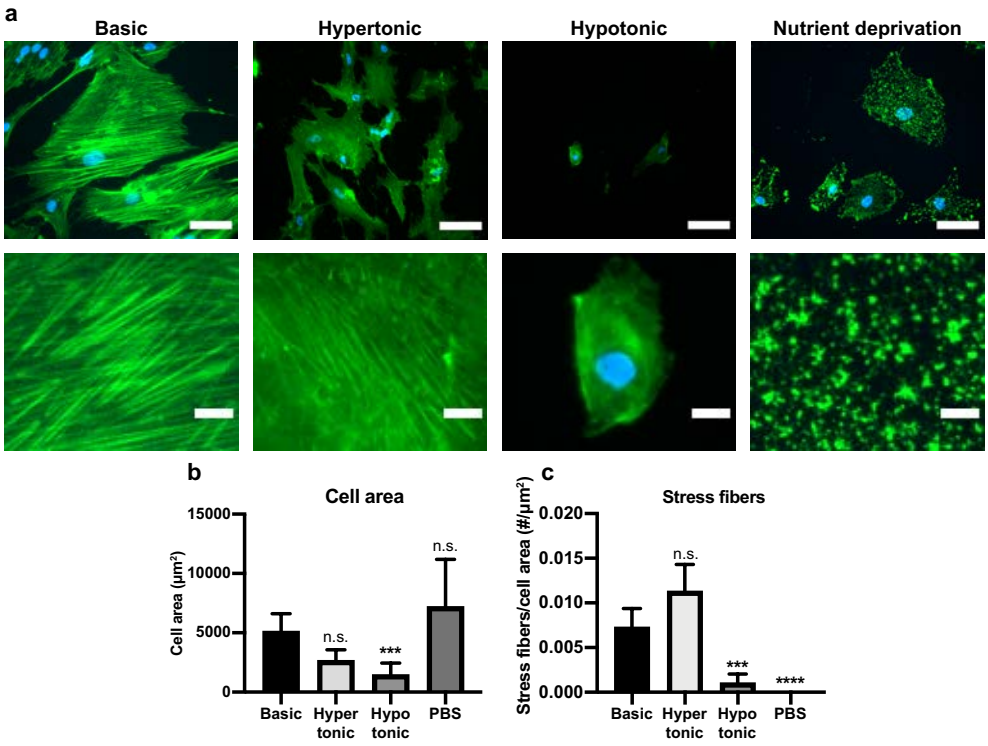

Figure 2. Reduced actin stress fibers in specific cell-stress conditions. (a) F-actin (green) and nulcei (blue) staining of hMSCs incubated for 8 hours with hypertonic medium (200 mM NaCl in basic medium), or hypotonic medium (90% water in basic medium), or nutrient deprivation medium (PBS). Bottom panel shows a 7x magnification of the respective image above. Scalebar 75 µm (top) and 10 µm (bottom). **(b)** Quantification of cell area in the respective cell-stress conditions. Average cell area was measured in 12 different images for each condition. **(c)** Quantification of the number of stress fibers per cell area in the different stress conditions. n=15 cells per condition. **(b, c)** One-way ANOVA; n.s. not-significant, *** p<0.001, **** p<0.0001 compared to Basic. Error bars represent mean±95% CI.

STC1 secretion is regulated through mechanotransduction

Hypotonic and nutrient deprivation treatments decreased actin stress fibers and increased STC1 secretion, while the hypertonic treatment did not affect actin stress fibers or STC1 secretion. To test whether there is a functional link between the actin network and STC1 secretion, we treated hMSCs for 24 h with blebbistatin, a potent actin-myosin inhibitor[22]. Indeed, a 3.1±0.9x ($p<0.01$) increase of released STC1 was observed when actin-myosin tension was inhibited (Fig. 3a). Focal adhesions are directly connected to the actin network and play an important role in mechanotransduction pathways[23]. To understand their role in the regulation of STC1, we knocked down paxillin or zyxin in hMSCs (Supplementary Fig. 1a-b), two important focal adhesion proteins. No change in STC1 secretion was observed after knockdown of paxillin (Fig. 3b). However, STC1 secretion increased by 5.0±1.0x and

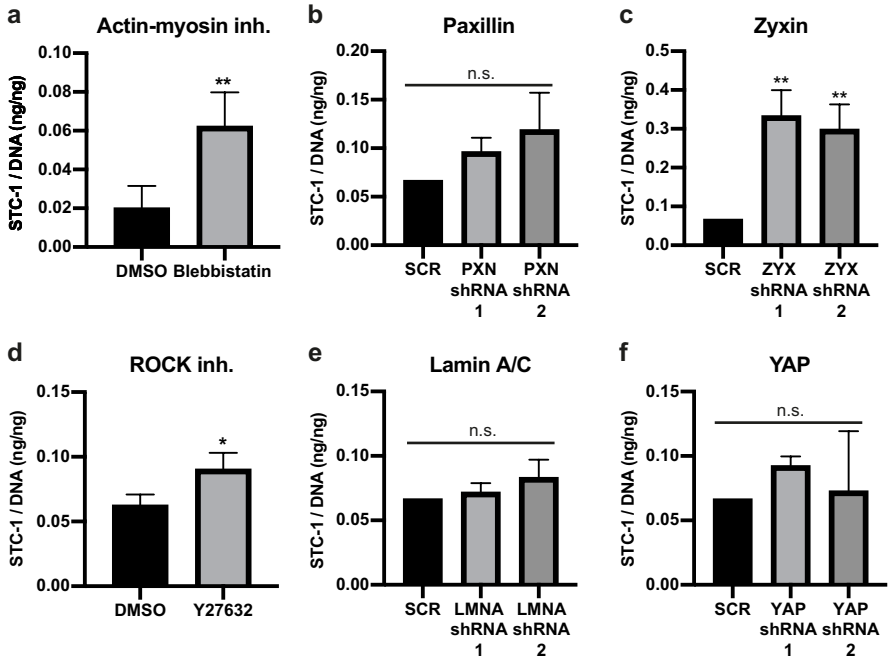

Figure 3. Increased STC1 release after specific interference in mechanotransduction pathways. (a) Total excreted STC1 in the medium over 24 h culture period measured by ELISA, normalized by total DNA in each sample. STC1/DNA was measured in hMSCs treated with blebbistatin (n=4) **(a)**, or ROCK inhibitor Y27632 (n=3) **(d)**, or in hMSCs transduced with shRNA against PXN **(b)**, ZYX **(c)**, LMNA **(e)** or YAP **(f)** (n=3). Student's t-test **(a, d)**, or one-way ANOVA **(b, c, e, f)**; n.s. not-significant, * p<0.05, ** p<0.01 compared to DMSO **(a, d)** or SCR **(b, c, e, f)**. Error bars represent mean±SD.

4.5±1.0x (p<0.01 for both) in zyxin knockdowns 1 and 2, respectively (Fig 3c). Zyxin plays an important role in linking the focal adhesions to the actin network and forming stress fibers[24, 25], as opposed to paxillin [26-28], further hinting at the importance of actin-myosin tension in the regulation of STC1. ROCK activation induces actin-myosin tension[29, 30] and stabilizes actin stress fibers [31, 32]. To further investigate the link between actin-myosin and STC1, we treated hMSCs for 24 h with the ROCK inhibitor Y27632. As expected, STC1 secretion increased 29±18% (p<0.05) after ROCK inhibition, showing that ROCK plays a role in the regulation of STC1 (Fig. 3d). Lamin A/C, a nuclear skeleton protein, is also connected to the actin network and transduces signals to the inside of the nucleus[33]. After knockdown of lamin A/C (Supplementary Fig. 1c), no difference in STC secretion was observed (Fig. 3e), demonstrating that it is not involved in this process. Lastly, we knocked down YAP (Supplementary Fig. 1d), an important mechanosensitive transcription factor. Again, no change in STC1 secretion was observed (Fig. 3f). Together, these results demonstrate that STC1 secretion is mechanosensitive, a signal going through focal adhesions, actin-myosin and ROCK, but not through Lamin A/C or YAP.

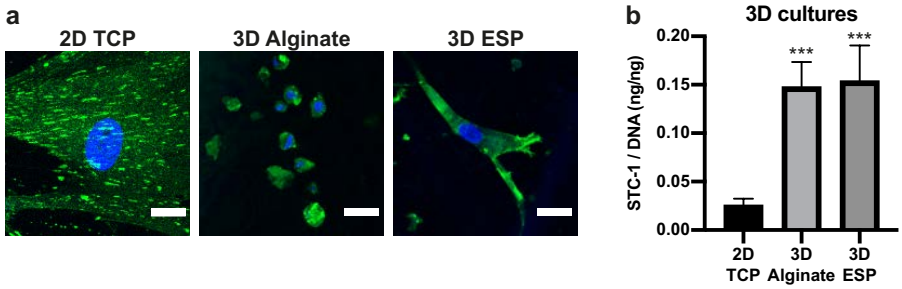

Figure 4. Less zyxin and more STC1 secretion in 3D cultures. (a) Zyxin (green) and nuclei (blue) immunofluorescent staining of hMSCs cultured in 2D TCP, 3D Alginate and 3D ESP. Scalebar represents 30 µm. **(b)** Total excreted STC1 in the medium over 24 h culture period, measured by ELISA, normalized by total DNA in each sample (n=4 for 2D TCP; n=3 for 3D alginate and 3D ESP). One-way ANOVA; ******* p<0.001 compared to 2D TCP. Error bars represent mean±SD.

Increased STC1 secretion in 3D cultures

Previous reports have shown that STC1 is upregulated in different 3D culture systems[14-17]. Also, hMSCs in hydrogels have previously been reported to have fewer stress fibers and focal adhesions[34-42], and we and others have recently shown similar results for electrospun (ESP) scaffolds[43, 44]. To confirm these observations, we stained hMSCs cultured in 3D RGD-modified alginate hydrogels or 3D ESP scaffolds for zyxin (Fig. 4a). Indeed, very few zyxin positive focal adhesions were observed in the hydrogels of ESP scaffolds, while many large focal adhesions were observed in 2D TCP. STC1 secretion was increased 5.7±1.0x ($p<0.001$) in 3D alginate and 6.0±1.4x ($p<0.001$) in 3D ESP. These results further demonstrate the mechanosensitive regulation of STC1 and show that a 3D environment can influence STC1 secretion.

Discussion

Acting as a paracrine protein, STC1 has been shown to promote angiogenesis, reduce apoptosis and enhance overall cell survival[5, 7, 11-13]. STC1 is known to be upregulated in different stress conditions[4, 11-13], but the molecular mechanisms behind this are still poorly understood. This was used as a starting point and treated hMSCs were treated with different stress inducing conditions (hypo- and hypertonic and nutrient deprivation). STC1 secretion only increased in specific stress-inducing conditions and only in the conditions where the actin cytoskeleton was greatly affected (hypotonic and nutrient deprivation). We found a reduction in actin stress fibers and cell size after 8 h of hypotonic treatment, in line with previous reports[19] and an aberration of actin stress fibers in cells treated following nutrient deprivation, also in line with previous reports[18, 20]. The increase in STC1 secretion in these conditions, as well as the change in the actin cytoskeleton, has not been previously reported and led us to investigate a causal link between the two. Indeed, by inhibiting actin-myosin tension with blebbistatin, we showed that the change in actin structure was responsible for

the increased STC1 secretion. The hypertonic treatment did not change the actin cytoskeleton, and even though it induced cell death and apoptosis, STC1 secretion remained unchanged. This suggests that the increase in STC1 release after induced cell-stress might be due to a change in actin cytoskeleton, rather than being a direct response to cell-stress, apoptosis or cell death. When zyxin was knocked down, we also found an increase in STC1 secretion. Zyxin is known to play an important role in stress fiber formation[24, 25]. Paxillin knockdown, however, did not result in an increase in STC1 secretion, in line with the fact that paxillin is not required for stress fiber formation[26-28]. ROCK activation induces actin-myosin contraction[29, 30] and stabilizes actin filaments[31, 32]. Indeed, when ROCK was inhibited, STC1 secretion was also increased. Together, these results show an influence of mechanotransduction pathways on the regulation of STC1 secretion and highlight the role of focal adhesions and actin-myosin tension. Interestingly, lamin A/C knock down, critical in the transduction of mechanical signals to the nucleus, did not affect the STC1 secretion. Also, YAP knockdown did not affect STC1 secretion. This suggests that the reduced STC1 secretion due to actin-myosin tension might not be regulated through the nucleus, or through YAP. Block et. al.[11] have shown that STC1 and vinculin staining colocalize in hMSCs, A549 lung epithelial cells and mouse embryonic fibroblasts. Interestingly, when fibroblasts were UV-irradiated they increased STC1 expression, changed their morphology and decreased focal adhesion staining[11]. However, when cocultured with hMSCs, UV-irradiated fibroblast restored their shape as well as their vinculin and STC1 expression, with both proteins colocalizing. In addition, Ylostalo et al. have demonstrated an upregulation of STC1 gene expression when hMSCs are cultured in 3D spheroids, compared to spread hMSCs cultured on TCP[45]. When 3T3-L1 fat cells undergo adipogenic differentiation, they become more spherical and upregulate STC1 gene and protein expression[46]. These results are in line with ours and hinted at a mechanosensitive regulation of STC1. Here, we have shown that STC1 is indeed regulated through mechanotransduction pathways, specifically through zyxin, actin-myosin and ROCK. In line with this, in 3D environments (alginate hydrogels and ESP scaffolds), fewer focal adhesions formed and STC1 secretion increased. Reduced number of focal adhesions and actin stress fibers have been previously reported in a number of studies in both hydrogels[34-42] and ESP scaffolds[43, 44]. The increase of STC1 in 3D cultures has been shown before in different 3D culture systems[14-17]. Our data suggests that this might be due to a reduction in focal adhesions and/or actin-myosin tension. Together, these new findings pave the way to understand the regulation of STC1 as a paracrine factor secreted by hMSCs. As STC1 can aid cell survival and angiogenesis *in vitro* and *in vivo*[5, 7, 11-13], a better understanding of STC1 regulation could aid future cell-based regenerative medicine.

Materials and Methods

Cell culture

Bone marrow hMSCs were isolated from a 22-year old male by aspiration by Texas A&M Health Science Center[47] after ethical approval from the local and national authorities and written consent from the donor. Mononuclear cells were isolated by centrifugation. Isolated hMSCs were verified for differentiation capacity and were received at passage 1. For further expansion, hMSCs were seeded at 1000 cells/cm^2 in αMEM+Glutamax medium (Thermo Fisher Scientific) supplemented with 10% (V/V) fetal bovine serum (FBS) (Sigma-Aldrich) (basic medium) at 37° C in 5% CO_2. Upon reaching 70-80% confluency, cells were trypsinized in 0.05% Trypsin and 0.53 mM EDTA (ThermoFisher Scientific) and used for experiments at passage 5.

Cell-stress conditions

Prior to the cell-stress treatments, hMSCs were expanded for seven days to get sufficient cell numbers. For the hypertonic condition, basic medium was supplemented with 200 mM NaCl (Sigma-Aldrich); for the hypotonic condition, Basic medium was diluted in miliQ water to get 90% water and 10% basic medium; for the nutrient deprivation condition, pure PBS (Sigma-Aldrich) was used. Basic medium was used as control. hMSCs were incubated in the various media for 8 h on the 7^{th} day of culture. After these 8 h, medium and cells were harvested for Caspase 3/7 assay, DNA and STC1 ELISA (discussed below).

Proliferation inhibition conditions

hMSCs were seeded at 1,000 cells/cm^2 and cultured for 5 days in basic medium before starting the different proliferation inhibiting conditions. On day 5, the medium was replaced with basic medium containing 1% (v/v) DMSO, 1 µg/ml actinomycin D, 2 µg/ml CDK4 inhibitor, 166 µg/ml valproic acid, or 0.74 µg/ml AZD5438. Cells were cultured for 6 days with basic medium + 10 ng/ml bFGF, medium with 0.5% FBS (instead of 10%), or seeded at 20,000 cells/cm^2 (instead of 1,000) and cultured in basic medium. The medium replaced 24 h before harvesting and cells were harvested at the end of the experiment to measure STC1 released in the medium and DNA, respectively. Cells were cultured for 7 days with basic medium supplemented with recombinant STC1 (0.5 µg/ml, BioVendor) to measure the effect of STC1 on proliferation.

Lentiviral production and transduction, Actin-myosin and ROCK inhibition

Lentivirus was produced in human embryonic kidney 293FT (HEK) cells. HEK cells were seeded at 60k cells/cm^2 in a 10 cm-TCP dish in DMEM + 10% FBS. HEK cells were transfected with pMDLg pRRE, pMD2.G, pRSV Rev (Addgene) and one of the pLKO.1 shRNA plasmids using lipofectamine 2000 (Thermo Fisher Scientific) in a ratio of 5:1 (µl lipofectamine 2000:µg DNA) 24 h after seeding. TRC pLKO.1 constructs (Dharmacon) with the following Clone ID's were used: PXN: TRCN0000123134 and TRCN0000123136; ZYX: TRCN0000074204 and

TRCN0000074205; LMNA: TRCN0000061833 and TRCN0000061836; YAP1: TRCN0000107265 and TRCN0000107266; STC: TRCN0000154599 and TRCN0000155141; and a non-targeting shRNA as control (RHS6848). The medium was changed 16 h after transfection to basic medium. Lentiviral particles were harvested 24 and 48 h after the change to basic medium and filtered through a 0.45 µm filter. hMSCs were thawed at 1000 cells/cm^2 in a 10 cm-TCP dish 24 h before transduction. 3 ml unconcentrated filtered medium containing the lentiviral particles was added and incubated overnight at 37° C. After 16-24 h, the medium was changed to basic medium and 24-48 h after, medium was replaced with selection medium (basic medium + 2 µg/ml puromycin (Sigma-Aldrich)) for 72 h. After a total of 9-10 days after thawing, the cells were passaged at 1000 cells/cm^2 and used for subsequent experiments. To test the effect of actin-myosin tension and ROCK on STC1 secretion, 100 µM blebbistatin (Sigma-Aldrich) or 10 µM Y27632 in basic medium was added to untransduced hMSCs.

Hydrogel and scaffold production and culture

Food grade alginate was purified according to a protocol previously published by Neves et al.[48]. Briefly, alginate with 70% "GG blocks", kindly provided by FMC polymers, was dissolved overnight in ultrapure water (18 MΩ, Milli-Q UltraPure Water System, Millipore) at a final concentration of 1% (w/v). After dissolution, activated charcoal (2% (w/v), Sigma- Aldrich) was added under agitation for 1 h at RT. The obtained suspension was then centrifuged for 1 h at 27 000×g (Beckman centrifuges). Afterwards, the supernatant passed through a series of filters (1.2, 0.45 and 0.22 µm membrane pores, VWR) and was freeze-dried and stored at –20 °C until further use. The alginate was then modified with (Glycine)4-Arginine-Glycine-Aspartic acid-Serine-Proline (abbreviated as G4RGDSP, Genscript, Piscataway, NJ, USA) to allow cell adhesion by using aqueous carbodiimide chemistry (EDC chemistry). Briefly, as described previously[49], a 1% (w/v) solution was prepared in 0.1 M 2-(N-morpholino) ethanesulfonic acid (MES) buffer solution (0.1 M MES buffering salt, 0.3 M NaCl, pH adjusted to 6.5 using 1 M NaOH, Sigma). N-Hydroxy-sulfosuccinimide (sulfo-NHS, Pierce Chemical) and 1-ethyl-(dimethylaminopropyl)-carbodiimide (EDC, Sigma, 27.40 mg per g alginate), at a molar ratio of 1:2, were sequentially added to the solutions, followed by the addition of 65.9 µmol RGD per gram alginate. The solution was then left stirring for 20 h and quenched with 18 mg of hydroxylamine hydrochloride (Sigma) per gram alginate. The final product was dialyzed (MWCO 3500, Spectra/Por®, VWR) against decreasing concentrations of ultrapure water with NaCl for three days at 4 °C and freeze-dried and stored at -20 °C. For encapsulation, 100,000 hMSCs were pelleted by centrifugation at 500 *xg* for 5 min and cells were embedded in 10 µl 1% alginate-RGD (w/v) (10^6 cells/ml). The alginate hydrogels were crosslinked in a bath of 100 mM $BaCl_2$ (Sigma-Aldrich) for 5 min, to be subsequently cultured in basic medium.

Electrospun (ESP) scaffolds were produced using 300PEOT55PBT45 (PolyVation), made from a starting 300 kDa poly(ethylene glycol) in the synthesis reaction, with a PEOT/PBT weight ratio of 55/45. A 20% (w/v) solution of 300PEOT55PBT45 was made by dissolving the

copolymer in a mixture of 30% (v/v) 1,1,1,3,3,3-Hexafluoro-2-propanol AR (HFIP) (Bio-Solve) and 70% (v/v) Chloroform (Sigma-Aldrich), overnight at room temperature under agitation. ESP scaffolds were produced on a 19 cm diameter mandrel at 100 RPM rotation on a polyester mesh (FinishMat 6691 LL (40 g/m^2), generously provided by Lantor B.V.) with 12 mm holes, on top of aluminum foil. After electrospinning, the collected ESP scaffolds were punched out with a diameter of 15 mm and the aluminum foil was removed. Using this method, 12 mm ESP scaffolds were created with a 1.5 mm supporting polyester ring to improve handleability. Processing parameters were: 1 ml/h flow rate, 15 cm working distance, 40% humidity and 23-25° C. The needle was charged between 10-15 kV, while the collector was charged between -2 and -5 kV. For sterilization, ESP scaffolds were submerged in 70% ethanol for 15 min and subsequently dried until visually dry. The ESP scaffold were then seeded with 30,000 hMSCs and cultured in basic medium.

Stanniocalcin ELISA

STC1 secreted into the medium by hMSCs was quantified using a STC1 ELISA kit (Antibodies-online, kit no. ABIN852096). Medium was changed 24 h before harvest to an exact volume on the 6th day of culture. For the cell-stress experiments, medium was changed on the 7th day and only incubated for 8 h. The ELISA was performed according to the manufacturer's instructions. STC1 concentration was normalized to total DNA in each sample to correct for differences in cell numbers.

Caspase 3/7 activity assay

Caspase 3/7 activity was measured using the Caspase-Glo 3/7 assay (Promega). Caspase 3/7 assay solution was mixed 1:1 with alpha-MEM without phenol red (ThermoFisher Scientific) (caspase 3/7 lysis buffer) and added to the cells at the moment of harvest. After 30 min incubation, light intensity was measured at 520 nm on a CLARIOstar® Plus plate reader.

DNA quantification

hMSCs were washed 2x with PBS to remove dead cells and medium before stored dry at -80 for later DNA quantification. Samples were freeze-thawed twice before either RLT lysis buffer (Qiagen) or the caspase lysis 3/7 buffer was added. Samples were freeze-thawed three times again in lysis buffer (after caspase 3/7 assay, if applicable) to ensure full lysis. TCP samples were scraped and hydrogel and ESP scaffolds were left in the lysis buffer. Samples were then diluted 50x in Tris-EDTA buffer (10 mM Tris-HCl, 1 mM EDTA, pH 7.5 (Sigma-Aldrich)) and a DNA standard curve was made in the same final solution (2% RLT or caspase lysis 3/7 buffer in Tris-EDTA buffer). Pico green assay (ThermoFisher Scientific) was used to quantify DNA, according to the manufacturer's protocol.

Protein isolation and western blot

To validate the knockdowns, protein was isolated from transduced cells with RIPA buffer (Sigma-Aldrich), supplemented with cOmplete™, Mini, EDTA-free Protease Inhibitor Cocktail (Sigma-Aldrich). Cells were grown in TCP dishes and after scraping with lysis buffer, the samples were spun down at 10,000 *xg* and the supernatant was used for further analysis. Total protein concentration was quantified using the Pierce BCA protein assay kit (Thermo Fisher Scientific). 20 µg protein of each sample was incubated in 10% 2-Mercaptoethanol (Sigma-Aldrich) in laemmli loading buffer (Bio-Rad) at 95 ˚C for 5 min before loading into a 4–15% polyacrylamide gels (Bio-Rad). The semi-dry transfer method was used to blot proteins from the gel to a 0.45 µm PVDF membrane (Bio-Rad). Membranes were blocked in 5% (w/v) fat free milk (Bio-Rad) in TBS + 0.05% (v/v) tween-20 (Sigma-Aldrich) for 1 h. Primary antibodies were incubated in blocking buffer overnight at 4˚ C. All antibodies were ordered from Abcam and diluted 1/1000, except for YAP1 which was diluted 1/500. Lamin A/C: ab108595; Paxillin: ab32084; Zyxin: ab58210; YAP1: ab52771; TBP: ab51841. The following day, blots were incubated for 1 h at room temperature in 0.33 µg/ml Goat-anti-rabbit or -mouse HRP (Bio-Rad) in blocking buffer. Membranes were incubated in Clarity Western ECL (Bio-Rad) for 1-5 min to visualize protein bands on a Bio-Rad ChemiDoc™.

Immunofluorescence and imaging

hMSCs were fixed at room temperature for 20 min in 3.6% (v/v) paraformaldehyde (Sigma-Aldrich) in PBS. Blocking and permeabilization was done for 1 h at room temperature in 2% bovine serum albumin (BSA) (VWR) with 0.1% (v/v) triton X (VWR) in PBS. Zyxin antibody (mentioned above in the western blot section) was used in the same dilution for immunofluorescent staining. Incubation was done overnight at 4˚ C in 2% (w/v) BSA and 0.05% (v/v) tween-20 in PBS (incubation buffer). Goat-anti-mouse Alexa Fluor 488 (Thermo Fisher Scientific) in incubation buffer was incubated overnight at 4˚ C. F-actin was visualized using phalloidin Alexa Fluor 488 (Thermo Fisher Scientific). After blocking and permeabilization, phalloidin (1/100 in PBS+0.05% (v/v) tween-20) was incubated at room temperature for 20 min. DAPI (Sigma-Aldrich, 0.14 µg/ml in PBS+0.05% (v/v) tween-20) was used as nuclear staining. Actin images were taken on a wide-field fluorescence microscope (Nikon-Ti); zyxin images on an SP8 confocal (Leica) microscope. All images within an experiment were captured on the same day and using the same settings, so quantitative comparisons could be made.

Cell area was quantified using Fiji. Total cell area was divided by the number of cells to get the average cell area per image. 12 individual images, taken from three different biological replicates, were used for quantification. Actin stress fibers were manually counted in 15 cells per condition and normalized to cell area.

Statistics

Number of biological replicates and statistical tests used are stated in figure subtext. At least three biological replicas were used for each assay. Cells selected for quantification of cell size and actin stress fibers were selected randomly. Normal distribution of each data set was tested using the Shapiro-Wilk test. For multiple comparisons within one experiment, a One-way ANOVA with Tukey's post hoc was performed, or Kruskal-Wallis with Dunn's post hoc as nonparametric equivalent. Experiments with one comparison were tested using a two-tailed student's t-test. Significance was set at $p<0.05$. Statistical analysis was performed using GraphPad Prism 8.

Acknowledgements

We are grateful to the European Research Council starting grant "Cell Hybridge" for financial support under the Horizon2020 framework program (Grant #637308). Some of the materials used in this work were provided by the Texas A&M Health Science Center College of Medicine Institute for Regenerative Medicine at Scott & White through a grant from NCRR of the NIH (Grant #P40RR017447).

References

1. M.E. Gerritsen and G.F. Wagner, *Stanniocalcin: no longer just a fish tale.* Vitam Horm, 2005. **70**: p. 105-35.
2. Y. Ito, R. Zemans, K. Correll, I.V. Yang, A. Ahmad, B. Gao, and R.J. Mason, *Stanniocalcin-1 is induced by hypoxia inducible factor in rat alveolar epithelial cells.* Biochem Biophys Res Commun, 2014. **452**(4): p. 1091-7.
3. J.A. Westberg, M. Serlachius, P. Lankila, M. Penkowa, J. Hidalgo, and L.C. Andersson, *Hypoxic preconditioning induces neuroprotective stanniocalcin-1 in brain via IL-6 signaling.* Stroke, 2007. **38**(3): p. 1025-30.
4. A.Y. Law, L.Y. Ching, K.P. Lai, and C.K. Wong, *Identification and characterization of the hypoxia-responsive element in human stanniocalcin-1 gene.* Mol Cell Endocrinol, 2010. **314**(1): p. 118-27.
5. S. Ohkouchi, G.J. Block, A.M. Katsha, M. Kanehira, M. Ebina, T. Kikuchi, Y. Saijo, T. Nukiwa, and D.J. Prockop, *Mesenchymal stromal cells protect cancer cells from ROS-induced apoptosis and enhance the Warburg effect by secreting STC1.* Mol Ther, 2012. **20**(2): p. 417-23.
6. Y. Wang, L. Huang, M. Abdelrahim, Q. Cai, A. Truong, R. Bick, B. Poindexter, and D. Sheikh-Hamad, *Stanniocalcin-1 suppresses superoxide generation in macrophages through induction of mitochondrial UCP2.* J Leukoc Biol, 2009. **86**(4): p. 981-8.
7. L.F. He, T.T. Wang, Q.Y. Gao, G.F. Zhao, Y.H. Huang, L.K. Yu, and Y.Y. Hou, *Stanniocalcin-1 promotes tumor angiogenesis through up-regulation of VEGF in gastric cancer cells.* J Biomed Sci, 2011. **18**: p. 39.
8. R.H. Lee, J.Y. Oh, H. Choi, and N. Bazhanov, *Therapeutic factors secreted by mesenchymal stromal cells and tissue repair.* J Cell Biochem, 2011. **112**(11): p. 3073-8.
9. M. Mirotsou, T.M. Jayawardena, J. Schmeckpeper, M. Gnecchi, and V.J. Dzau, *Paracrine mechanisms of stem cell reparative and regenerative actions in the heart.* J Mol Cell Cardiol, 2011. **50**(2): p. 280-9.
10. D.J. Prockop, *Concise review: two negative feedback loops place mesenchymal stem/stromal cells at the center of early regulators of inflammation.* Stem Cells, 2013. **31**(10): p. 2042-6.
11. G.J. Block, S. Ohkouchi, F. Fung, J. Frenkel, C. Gregory, R. Pochampally, G. DiMattia, D.E. Sullivan, and D.J. Prockop, *Multipotent stromal cells are activated to reduce apoptosis in part by upregulation and secretion of stanniocalcin-1.* Stem Cells, 2009. **27**(3): p. 670-681.
12. M. Shi, Y. Yuan, J. Liu, Y. Chen, L. Li, S. Liu, X. An, R. Luo, D. Long, B. Chen, X. Du, J. Cheng, and Y. Lu, *MSCs protect endothelial cells from inflammatory injury partially by secreting STC1.* Int Immunopharmacol, 2018. **61**: p. 109-118.
13. M. Ono, S. Ohkouchi, M. Kanehira, N. Tode, M. Kobayashi, M. Ebina, T. Nukiwa, T. Irokawa, H. Ogawa, T. Akaike, Y. Okada, H. Kurosawa, T. Kikuchi, and M. Ichinose, *Mesenchymal stem cells correct inappropriate epithelial-mesenchyme relation in pulmonary fibrosis using stanniocalcin-1.* Mol Ther, 2015. **23**(3): p. 549-60.
14. T.J. Bartosh and J.H. Ylostalo, *Efficacy of 3D Culture Priming is Maintained in Human Mesenchymal Stem Cells after Extensive Expansion of the Cells.* Cells, 2019. **8**(9).
15. G.A. Higuera, H. Fernandes, T.W. Spitters, J. van de Peppel, N. Aufferman, R. Truckenmueller, M. Escalante, R. Stoop, J.P. van Leeuwen, J. de Boer, V. Subramaniam, M. Karperien, C. van Blitterswijk, A. van Boxtel, and L. Moroni, *Spatiotemporal proliferation of human stromal cells adjusts to nutrient availability and leads to stanniocalcin-1 expression in vitro and in vivo.* Biomaterials, 2015. **61**: p. 190-202.
16. T.J. Bartosh, J.H. Ylostalo, A. Mohammadipoor, N. Bazhanov, K. Coble, K. Claypool, R.H. Lee, H. Choi, and D.J. Prockop, *Aggregation of human mesenchymal stromal cells (MSCs) into 3D spheroids enhances their antiinflammatory properties.* Proc Natl Acad Sci U S A, 2010. **107**(31): p. 13724-9.

17. D.A. Cantu, P. Hematti, and W.J. Kao, *Cell encapsulating biomaterial regulates mesenchymal stromal/stem cell differentiation and macrophage immunophenotype.* Stem Cells Transl Med, 2012. **1**(10): p. 740-9.
18. S. Kameshima, M. Okada, and H. Yamawaki, *Eukaryotic elongation factor 2 (eEF2) kinase/eEF2 plays protective roles against glucose deprivation-induced cell death in H9c2 cardiomyoblasts.* Apoptosis, 2019. **24**(3-4): p. 359-368.
19. S.L. Romano, G.P. Raaphorst, and W.C. Dewey, *The effects of various salt and sucrose solutions on the U.V.L. sensitivity of CHO cells.* Int J Radiat Biol Relat Stud Phys Chem Med, 1979. **35**(5): p. 401-15.
20. P. Vasicova, M. Rinnerthaler, D. Haskova, L. Novakova, I. Malcova, M. Breitenbach, and J. Hasek, *Formaldehyde fixation is detrimental to actin cables in glucose-depleted S. cerevisiae cells.* Microb Cell, 2016. **3**(5): p. 206-214.
21. A. Criollo, L. Galluzzi, M.C. Maiuri, E. Tasdemir, S. Lavandero, and G. Kroemer, *Mitochondrial control of cell death induced by hyperosmotic stress.* Apoptosis, 2007. **12**(1): p. 3-18.
22. M. Kovacs, J. Toth, C. Hetenyi, A. Malnasi-Csizmadia, and J.R. Sellers, *Mechanism of blebbistatin inhibition of myosin II.* J Biol Chem, 2004. **279**(34): p. 35557-63.
23. M.A. Wozniak, K. Modzelewska, L. Kwong, and P.J. Keely, *Focal adhesion regulation of cell behavior.* Biochim Biophys Acta, 2004. **1692**(2-3): p. 103-19.
24. M.A. Smith, E. Blankman, M.L. Gardel, L. Luettjohann, C.M. Waterman, and M.C. Beckerle, *A zyxin-mediated mechanism for actin stress fiber maintenance and repair.* Dev Cell, 2010. **19**(3): p. 365-76.
25. E. Griffith, A.S. Coutts, and D.M. Black, *RNAi knockdown of the focal adhesion protein TES reveals its role in actin stress fibre organisation.* Cell Motil Cytoskeleton, 2005. **60**(3): p. 140-52.
26. A.A. Birukova, I. Cokic, N. Moldobaeva, and K.G. Birukov, *Paxillin is involved in the differential regulation of endothelial barrier by HGF and VEGF.* Am J Respir Cell Mol Biol, 2009. **40**(1): p. 99-107.
27. H. Ngu, Y. Feng, L. Lu, S.J. Oswald, G.D. Longmore, and F.C. Yin, *Effect of focal adhesion proteins on endothelial cell adhesion, motility and orientation response to cyclic strain.* Ann Biomed Eng, 2010. **38**(1): p. 208-22.
28. T. Watanabe-Nakayama, M. Saito, S. Machida, K. Kishimoto, R. Afrin, and A. Ikai, *Requirement of LIM domains for the transient accumulation of paxillin at damaged stress fibres.* Biol Open, 2013. **2**(7): p. 667-74.
29. M. Amano, M. Ito, K. Kimura, Y. Fukata, K. Chihara, T. Nakano, Y. Matsuura, and K. Kaibuchi, *Phosphorylation and activation of myosin by Rho-associated kinase (Rho-kinase).* J Biol Chem, 1996. **271**(34): p. 20246-9.
30. K. Burridge and M. Chrzanowska-Wodnicka, *Focal adhesions, contractility, and signaling.* Annu Rev Cell Dev Biol, 1996. **12**: p. 463-518.
31. S.H. Zigmond, *Formin-induced nucleation of actin filaments.* Curr Opin Cell Biol, 2004. **16**(1): p. 99-105.
32. E.C. Lessey, C. Guilluy, and K. Burridge, *From mechanical force to RhoA activation.* Biochemistry, 2012. **51**(38): p. 7420-32.
33. Y. Gruenbaum and R. Foisner, *Lamins: nuclear intermediate filament proteins with fundamental functions in nuclear mechanics and genome regulation.* Annu Rev Biochem, 2015. **84**: p. 131-64.
34. S.A. Ferreira, M.S. Motwani, P.A. Faull, A.J. Seymour, T.T.L. Yu, M. Enayati, D.K. Taheem, C. Salzlechner, T. Haghighi, E.M. Kania, O.P. Oommen, T. Ahmed, S. Loaiza, K. Parzych, F. Dazzi, O.P. Varghese, F. Festy, A.E. Grigoriadis, H.W. Auner, A.P. Snijders, L. Bozec, and E. Gentleman, *Bi-directional cell-pericellular matrix interactions direct stem cell fate.* Nat Commun, 2018. **9**(1): p. 4049.
35. H.P. Lee, R. Stowers, and O. Chaudhuri, *Volume expansion and TRPV4 activation regulate stem cell fate in three-dimensional microenvironments.* Nat Commun, 2019. **10**(1): p. 529.

36. N. Huebsch, P.R. Arany, A.S. Mao, D. Shvartsman, O.A. Ali, S.A. Bencherif, J. Rivera-Feliciano, and D.J. Mooney, *Harnessing traction-mediated manipulation of the cell/matrix interface to control stem-cell fate.* Nat Mater, 2010. **9**(6): p. 518-26.
37. O. Chaudhuri, L. Gu, D. Klumpers, M. Darnell, S.A. Bencherif, J.C. Weaver, N. Huebsch, H.P. Lee, E. Lippens, G.N. Duda, and D.J. Mooney, *Hydrogels with tunable stress relaxation regulate stem cell fate and activity.* Nat Mater, 2016. **15**(3): p. 326-34.
38. X. Tong and F. Yang, *Sliding Hydrogels with Mobile Molecular Ligands and Crosslinks as 3D Stem Cell Niche.* Adv Mater, 2016. **28**(33): p. 7257-63.
39. S.H. Parekh, K. Chatterjee, S. Lin-Gibson, N.M. Moore, M.T. Cicerone, M.F. Young, and C.G. Simon, Jr., *Modulus-driven differentiation of marrow stromal cells in 3D scaffolds that is independent of myosin-based cytoskeletal tension.* Biomaterials, 2011. **32**(9): p. 2256-64.
40. S. Nam, R. Stowers, J. Lou, Y. Xia, and O. Chaudhuri, *Varying PEG density to control stress relaxation in alginate-PEG hydrogels for 3D cell culture studies.* Biomaterials, 2019. **200**: p. 15-24.
41. S. Khetan, M. Guvendiren, W.R. Legant, D.M. Cohen, C.S. Chen, and J.A. Burdick, *Degradation-mediated cellular traction directs stem cell fate in covalently crosslinked three-dimensional hydrogels.* Nat Mater, 2013. **12**(5): p. 458-65.
42. C.P. Chaires-Rosas, X. Ambriz, J.J. Montesinos, B. Hernandez-Tellez, G. Pinon-Zarate, M. Herrera-Enriquez, E. Hernandez-Estevez, J.R. Ambrosio, and A. Castell-Rodriguez, *Differential adhesion and fibrinolytic activity of mesenchymal stem cells from human bone marrow, placenta, and Wharton's jelly cultured in a fibrin hydrogel.* J Tissue Eng, 2019. **10**: p. 2041731419840622.
43. S.J. Sequeira, D.A. Soscia, B. Oztan, A.P. Mosier, R. Jean-Gilles, A. Gadre, N.C. Cady, B. Yener, J. Castracane, and M. Larsen, *The regulation of focal adhesion complex formation and salivary gland epithelial cell organization by nanofibrous PLGA scaffolds.* Biomaterials, 2012. **33**(11): p. 3175-86.
44. J. Zonderland, I. Moldero Lorenzo, C. Mota, and L. Moroni, *Dimensionality changes actin network through lamin A/C and zyxin.* BioRxiv https://doi.org/10.1101/752691, 2019.
45. J.H. Ylostalo, T.J. Bartosh, A. Tiblow, and D.J. Prockop, *Unique characteristics of human mesenchymal stromal/progenitor cells pre-activated in 3-dimensional cultures under different conditions.* Cytotherapy, 2014. **16**(11): p. 1486-1500.
46. M. Serlachius and L.C. Andersson, *Upregulated expression of stanniocalcin-1 during adipogenesis.* Exp Cell Res, 2004. **296**(2): p. 256-64.
47. C.M. Digirolamo, D. Stokes, D. Colter, D.G. Phinney, R. Class, and D.J. Prockop, *Propagation and senescence of human marrow stromal cells in culture: a simple colony-forming assay identifies samples with the greatest potential to propagate and differentiate.* Br J Haematol, 1999. **107**(2): p. 275-81.
48. S.C. Neves, D.B. Gomes, A. Sousa, S.J. Bidarra, P. Petrini, L. Moroni, C.C. Barrias, and P.L. Granja, *Biofunctionalized pectin hydrogels as 3D cellular microenvironments.* Journal of Materials Chemistry B, 2015. **3**(10): p. 2096-2108.
49. J.A. Rowley, G. Madlambayan, and D.J. Mooney, *Alginate hydrogels as synthetic extracellular matrix materials.* Biomaterials, 1999. **20**(1): p. 45-53.

Supplementary Figures

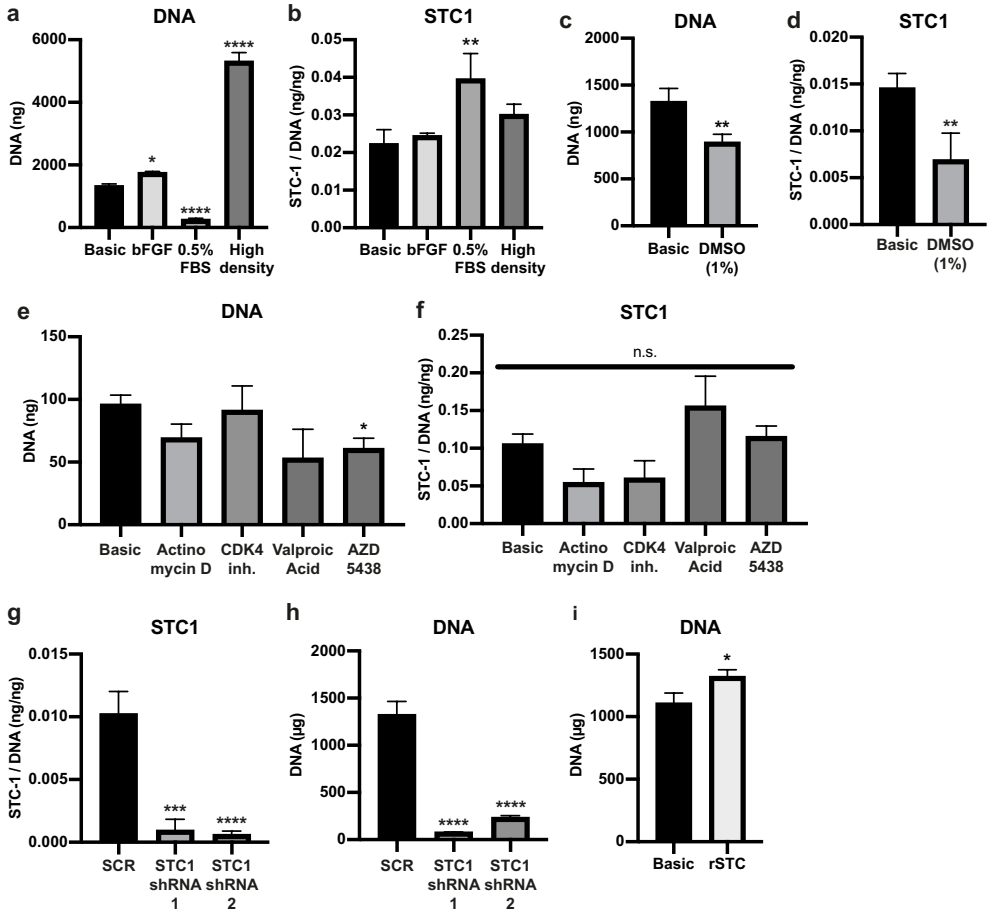

Supplementary figure 1. Exploring the link between proliferation and STC1. DNA **(a)** and STC1 release in 24 h, normalized to DNA **(b)**, in proliferative cells: basic (untreated), and basic +bFGF, or non-proliferative cells: medium with 0.5% FBS and high cell seeding density (20,000 cells/cm^2), 1% DMSO **(c, d)**, actinomycin D, CDK4 inhibitor, valproic acid, or AZD5438 (**e, f**). **(g)** STC1 release in 24 h of hMSCs transduced with scrambled shRNA, or two different STC1 shRNA. **(h)** DNA analysis after 7 days of culture in basic medium. **(i)** DNA analysis after 7 days of culture in basic medium, or basic medium supplemented with recombinant STC1. **(c, d, i)** student's t-test, **(a, b, e-h)** One-way Anova. * p<0.05, ** p<0.01, *** p<0.001, **** p<0.0001, compared to basic or SCR. Error bars represent mean±SD.

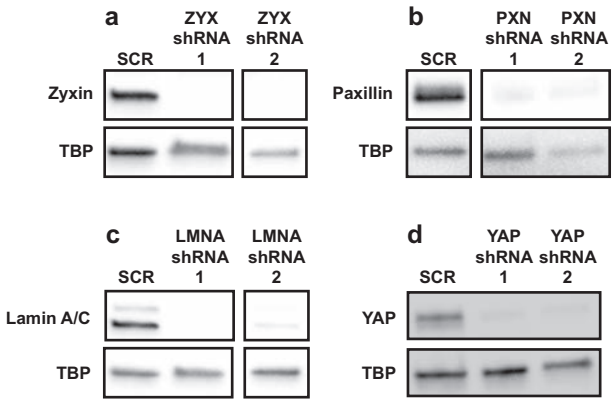

Supplementary figure 2. Validation of knock downs. Western blots of hMSCs transduced with shRNA for PXN **(a)**, ZYX **(b)**, LMNA **(c)**, YAP **(d)**. TBP is shown as loading control.

Chapter 5

Mechanosensitive regulation of FGFR1 through the MRTF-SRF pathway

Jip Zonderland, Silvia Rezzola, Lorenzo Moroni

Complex Tissue Regeneration Department, MERLN Institute for Technology-Inspired Regenerative Medicine, Maastricht University, Maastricht, the Netherlands.

Abstract

Controlling basic fibroblast growth factor (bFGF) signaling is important for both tissue-engineering purposes, controlling proliferation and differentiation potential, and for cancer biology, influencing tumor progression and metastasis. Here, we observed that human mesenchymal stromal cells (hMSCs) no longer responded to soluble or covalently bound bFGF when cultured on microfibrillar substrates, while fibroblasts did. This correlated with a downregulation of FGF receptor 1 (FGFR1) expression of hMSCs on microfibrillar substrates, compared to hMSCs on conventional tissue culture plastic (TCP). hMSCs also expressed less SRF on ESP scaffolds, compared to TCP, while fibroblasts maintained high FGFR1 and SRF expression. Inhibition of actin-myosin tension or the MRTF/SRF pathway decreased FGFR1 expression in hMSCs, fibroblasts and MG63 osteosarcoma cells. This downregulation was functional, as hMSCs became irresponsive to bFGF in the presence of MRTF/SRF inhibitor. Together, our data show that hMSCs, but not fibroblasts, are irresponsive to bFGF when cultured on microfibrillar substrates by downregulation of FGFR1 through the MRTF/SRF pathway. This is the first time FGFR1 expression has been shown to be mechanosensitive and adds to the sparse literature on FGFR1 regulation. These results could open up new targets for cancer treatments and could aid designing tissue engineering constructs that better control cell proliferation.

Introduction

Guiding cell behavior is a critical aspect for cell-based tissue engineering constructs. Among the different tissue engineering scaffolds, electrospun (ESP) scaffolds are being widely studied and are particularly interesting for defects of limited depth, but with a large surface area. Examples include cartilage repair[1], skin patches[2], corneal regeneration[3], nerve guides[4] and vascular grafts[5], among others.

Electrospinning is a technique where synthetic or natural polymers are dissolved in volatile solvents and deposited onto a collector using a highly charged electric field. While traveling from the needle to the collector, the polymer solution becomes highly unstable and is elongated significantly. The solvents evaporate and the polymer is deposited on the collector, resulting in a highly porous fibrous mesh with individual fiber diameters typically ranging 100 nm-10 µm, depending on processing parameters.

Sufficient number of cells and the right cell density is highly important for tissue engineering applications, so cell proliferation is a key aspect to control. Several growth factors are well known for their proliferation inducing abilities. Arguably, the most well-studied of these is basic fibroblast growth factor (bFGF). bFGF is known to increase proliferation rates in a wide variety of cell types and has anti-apoptotic effects, while maintaining or enhancing differentiation- and regeneration potential[6].

In solution, bFGF, like most growth factors, is highly unstable and loses activity after 24-48 hours[6, 7]. Covalently coupling bFGF to scaffolds has been shown to enhance stability while maintaining signaling activity[8-10]. Nur et al. showed that covalently coupled bFGF to electrospun fibers maintained activity for 6 months when stored dry[10]. When bFGF was covalently coupled to a heparin-mimicking polymer, it maintained increased stability under normal storage conditions[9], and under several stress conditions such as heat or acidic conditions , as opposed to bFGF in solution[8].

bFGF can bind to 7 FGF receptors (coming from 4 FGFR genes, FGFR1-4); tyrosine kinase receptors that can activate a variety of pathways, including the RAS-MAPK, PI3K-Akt, PLCγ and STAT pathways[11]. Using next generation sequencing to analyze 4853 tumors, Helsten T. et al. found aberrations in FGFR's in 7.1% of all tumors[12]. In addition, increased expression of FGFR's has been correlated with a bad prognosis, increased metastasis and tumor progression in a large variety of cancers[13-17]. Indeed, animal studies and clinical trials are currently ongoing to test the effects of FGFR inhibitors on cancer treatment, showing promising initial results[18-23]. This highlights the importance of understanding how FGFR expression is regulated. Very little is known about the regulation of any FGFR, while a better understand could advance the understanding of tumor development and open up new therapeutic targets.

Besides the role in cancer development, FGFR's are also interesting for tissue engineering purposes. FGFR1 and 2 have been shown to be involved in adipo- and osteogenic differentiation in hMSCs[24, 25]. FGFR3 is highly expressed in chondrocytes and is involved in

chondrogenesis[26]. Only FGFR1 has been shown to be involved in hMSCs proliferation[27], while the other receptors remain unstudied in this regard. For this reason, here we focused on the regulation of FGFR1 expression.

Cells adhere to their surrounding matrix or culture substrate through integrins[28]. When enough force can be applied, integrin clusters can bind to the actin cytoskeleton through large protein complexes called focal adhesions[29]. On the other end, actin filaments can be attached to other focal adhesions, or to the nucleus[30]. Between these attachment points, force can be generated by actin-myosin filaments to generate cellular tension[31]. A large variety of cellular processes are regulated by cellular tension, including proliferation[32-35], differentiation[36-38] and migration[39]. Different transcription factors have been shown to orchestrate these changes in behaviors, of which serum response factor (SRF) is a well-studied example. When globular actin concentrations are low in the cytoplasm, myocardin related transcription factor (MRTF) A or B enters the nucleus and binds to SRF to start transcribing target genes[40].

Here, we have found that hMSCs don't respond to soluble or covalently bound bFGF when cultured on microfibrillar substrates such as those created by ESP, while fibroblasts do. hMSCs, but not fibroblasts, downregulate FGFR1 expression when cultured on ESP scaffolds. We show that FGFR1 expression is mechanosensitive and works through actin-myosin tension and the MRTF/SRF pathway. Inhibition of the MRTF/SRF pathway made hMSCs irresponsive to bFGF on tissue culture plastic (TCP) and downregulated FGFR1 in hMSCs, fibroblasts and MG63 osteosarcoma cells.

Results

Fibroblasts, but not hMSCs, respond to bFGF functionalized ESP scaffolds

Cell-laden ESP scaffolds have been shown to aid tissue repair by hMSCs[41-43] and fibroblasts[44-46] in vivo. bFGF is known to enhance proliferation while maintaining differentiation potential in hMSCs, fibroblasts and many other cell types[6], but is highly unstable in solution[6, 7]. To potentially enhance the regeneration capacity, we set out to covalently couple bFGF to ESP scaffolds.

300PEOT45PBT55 was used to produce 50 µm thick ESP scaffolds with 0.99±0.18 µm average fiber diameter (Supplementary Fig. 1). The ester bond in the polymer was opened using 0.5M NaOH to expose carboxyl groups on the surface of the scaffold. EDC-NHS chemistry was used to covalently couple the free amine groups of proteins to the surface of the scaffold. As a model protein, FITC labeled bovine serum albumin (BSA) was coupled to the ESP scaffolds. A ~27 fold (26.4±0.8x, $p<0.001$) higher fluorescent signal was observed when BSA was added after EDC-NHS, than when BSA was added after water control (Fig. 1a). After washing with SDS, to wash away non-covalently bound BSA, the fluorescent signal was 39.8±14.5x higher ($p<0.001$) in the EDC-NHS group compared to BSA only. Together, this strongly suggests that covalent coupling of BSA was achieved.

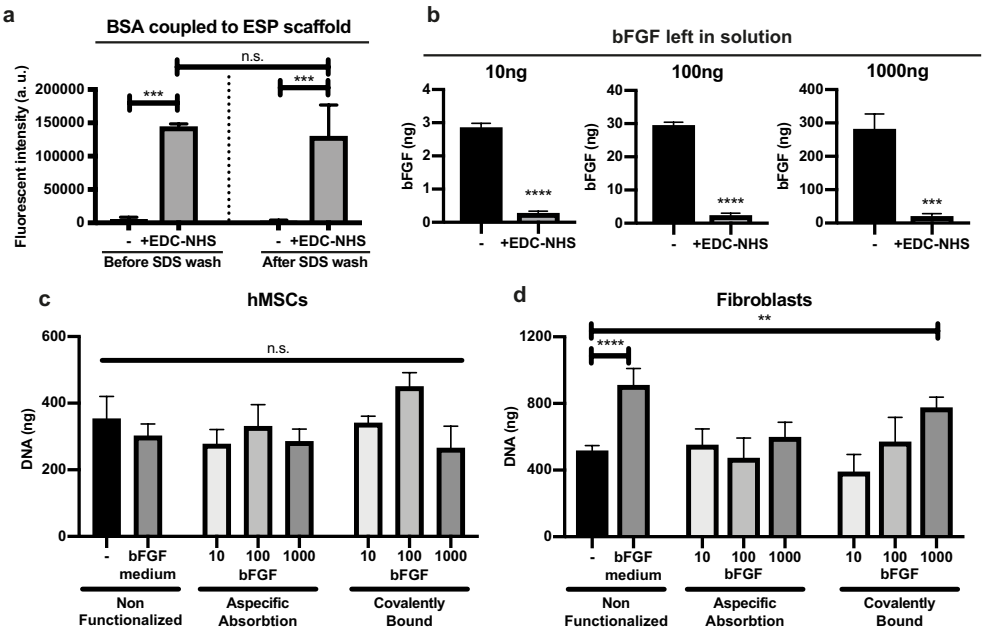

Figure 1. Functional coupling of bFGF to ESP scaffold. a, Fluorescent model protein BSA coupled to ESP scaffold using EDC-NHS, or water (-). Right bars are the same scaffolds after overnight wash with 1% (w/v) SDS in water. n=3 scaffolds per condition. **b,** Measurement of bFGF left in solution by ELISA after functionalization of 10, 100 or 1000 ng bFGF per scaffold, using EDC-NHS+bFGF, or water+bFGF(-). n=3 scaffolds per condition. **c, d,** DNA quantification of hMSCs **(c)** or human dermal fibroblasts **(d)** cultured on ESP scaffolds functionalized with 10, 100 or 1000 ng bFGF per scaffold using bFGF+EDC-NHS (covalently bound, right 3 bars), bFGF+water (aspecific absorption, middle 3 bars), or non-functionalized scaffolds (left two bars). Cells were cultured in basic medium, or in medium supplemented with 10 ng/ml bFGF (bFGF medium condition). n=3 scaffolds per condition for **(c)**, and n=5 scaffolds per condition for **(d)**. **a, c, d,** One-way ANOVA with Tukey's post-hoc test. **b,** Student's t-test. **a-d,** n.s. $p > 0.05$; ** $p<0.01$; *** $p<0.001$; **** $p<0.0001$. Error bars indicate mean±SD.

Next, bFGF was coupled to ESP scaffolds, using the same strategy. As opposed to bFGF in solution, cell response to covalently coupled bFGF has not been widely studied. In an attempt to find the right concentration range, we coupled three different amounts of bFGF to ESP scaffolds. bFGF left over in solution after coupling was measured by ELISA (Fig. 1b). Without the addition of EDC-NHS, around 70% of the bFGF adhered aspecifically to the scaffolds in all three concentrations. With the addition of EDC-NHS, around 98% of bFGF was bound to the scaffolds, aspecifically or covalently. Before cell culture, scaffolds were thoroughly washed in water and PBS, to wash away most of the aspecifically bound bFGF.

To test whether the bound bFGF was still functional, proliferation of hMSCs cultured on the ESP scaffolds was assessed after 7 days (Fig. 1c). Interestingly, the hMSCs did not respond to either bFGF bound to the ESP scaffold, or bFGF in solution. In 2D tissue culture plastic, hMSCs did increase proliferation over 7 days in response to bFGF in solution, displaying 45±11% more

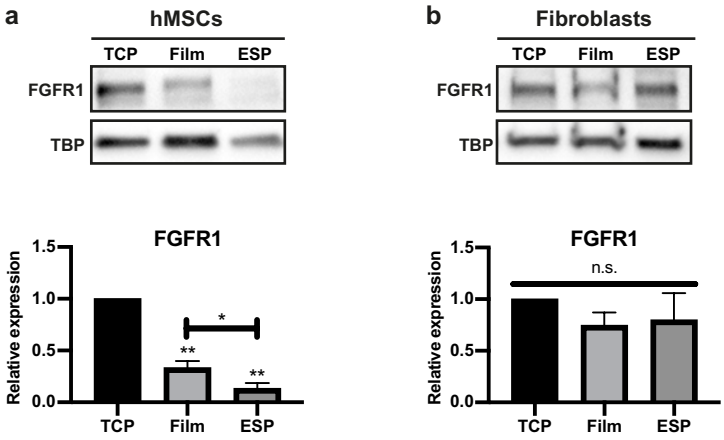

Figure 2. FGFR1 expression of hMSCs and fibroblasts on TCP, films and ESP scaffolds. a, b, Western blot of FRFR1 and TBP (as loading control) of hMSCs **(a)** or human dermal fibroblasts **(b)** on TCP, films or ESP scaffolds. Graphs depict quantification of western blots of FGFR1/TBP from 4 **(a)**, or 3 **(b)** independent experiments, normalized to TCP. **a, b,** Repeated measures ANOVA with Tukey's post-hoc test. Stars above bars indicate significance compared to TCP. n.s. $p>0.05$; * $p<0.05$; ** $p<0.01$. Error pars indicate mean±SD.

DNA, demonstrating that the ESP scaffold environment influenced the hMSC's response to bFGF (Supplementary Fig. 2).

Fibroblasts are particularly well studied for their increase in proliferation in response to bFGF. To test whether this lack of response to bFGF when cultured on ESP scaffolds was specific to hMSCs, human dermal fibroblasts were cultured for 7 days on the ESP scaffolds. On non-functionalized scaffolds, 76.5±19.6% more ($p<0.0001$) DNA was found after 7 days of culture in the presence of bFGF in the medium. On the 1000 ng covalently coupled bFGF scaffolds, 50.2±12.5% more ($p<0.01$) DNA was found compared to non-functionalized scaffolds, showing that the covalently bound bFGF was still functional.

Heparin is known to bind and stabilize bFGF and increase efficacy[47]. To covalently couple heparin to ESP scaffolds, PEG-NH_2 was incorporated into the electrospinning polymer solution to introduce amino groups on the surface of the ESP scaffold. The carboxyl groups of heparin were then bound to the ESP scaffolds by EDC-NHS chemistry (Supplementary Fig. 3a). bFGF was then bound to the heparin-functionalized scaffolds by overnight incubation. As the heparin interfered with the bFGF ELISA (data not shown), the amount of absorbed bFGF could not be measured. After 7 days of culture, no differences were observed between hMSCs cultured on heparin+bFGF scaffolds and the heparin only- or non-functionalized scaffolds (Supplementary Fig. 3b). This further demonstrates that hMSCs don't respond to bFGF on ESP scaffolds, also not when bound to heparin.

Together, these results show that the covalently coupled bFGF was still functional, and that hMSCs do not respond to bFGF when cultured on ESP scaffolds, but fibroblasts do.

Reduced FGFR1 expression on ESP scaffolds in hMSCs, but not fibroblasts

To test why fibroblasts did, but hMSCs did not, respond to bFGF when cultured on such microfibrillar substrates, we analyzed FGF receptor 1 (FGFR1) expression of hMSCs and fibroblasts cultured on TCP, ESP scaffolds, and on 2D films made up of the same material as the ESP scaffolds. Interestingly, when cultured on ESP scaffolds, hMSCs expressed 86.5±5.3% less ($p<0.01$) FGFR1 than when cultured on TCP (Fig. 2a). On films, hMSCs displayed 66.7±6.6% less ($p<0.01$) FGFR1 expression than on TCP, showing that part of the reduction of FGFR1 expression on ESP scaffolds comes from the material properties. However, on ESP scaffolds the FGFR1 expression was still 59.5±15.8% lower ($p<0.05$) than on films, showing that regardless of material properties, the microfibrillar environment influenced FGFR1 expression.

Fibroblasts, however, did not display a difference in FGFR1 expression between the different culture substrates (Fig. 2b). The reduced FGFR1 expression of hMSCs on ESP scaffolds, and the high FGFR1 expression of fibroblasts on ESP scaffolds, potentially explains the difference in bFGF response of hMSCs and fibroblasts on ESP scaffolds.

hMSCs, but not fibroblasts, display fewer focal adhesions on ESP scaffolds

To understand why hMSCs, but not fibroblasts, reduced FGFR1 expression on ESP scaffolds, we investigated the difference in adhesion to the different substrates in hMSCs and fibroblasts by looking at focal adhesions. The expression of zyxin, an important focal adhesion protein, was reduced in both hMSCs and fibroblasts, respectively by 65.6±7.0% ($p<0.01$) and 79.4±10.9% ($p<0.05$) compared to TCP (Fig. 3a, b). Paxillin expression, another well studied focal adhesion protein, was significantly reduced in both hMSCs and fibroblasts on ESP scaffolds, compared to TCP; respectively 73.2±5.2% ($p<0.01$) and 65±7.9% ($p<0.05$) (Supplementary Fig. 4a, b). On films, hMSCs also displayed reduced zyxin and paxillin expression, respectively 63.1±16.7% and 41.4±11.4% compared to TCP. Fibroblasts did not show a significant difference in zyxin or paxillin expression on films, compared to TCP.

When looking at the formation of zyxin positive focal adhesions, a reduction of 46.0±18.4% ($p<0.01$) of focal adhesions per cell area was observed when hMSCs were cultured on ESP scaffolds, compared to TCP (Fig. 3c, d). When compared to films, hMSCs on ESP scaffolds displayed 54.1±15.7% ($p<0.0001$) less zyxin positive focal adhesions per cell area. Interestingly, no significant difference was found between fibroblasts cultured on the different substrates (Fig. 3c, e). Indeed, when compared to fibroblasts grown on ESP scaffolds, hMSCs on ESP scaffolds displayed 60.4±13.5% ($p<0.0001$) fewer focal adhesions per cell area. The same trend was observed for paxillin positive focal adhesions, where hMSCs displayed far fewer paxillin positive focal adhesions on ESP scaffolds than on films or TCP, while fibroblasts contained many paxillin positive focal adhesions on all three substrates (Supplementary Fig. 4c, d).

These results demonstrate that the microfibrillar environment of ESP scaffolds changes focal adhesion formation in hMSCs, but not in fibroblasts. This shows that hMSCs adhere

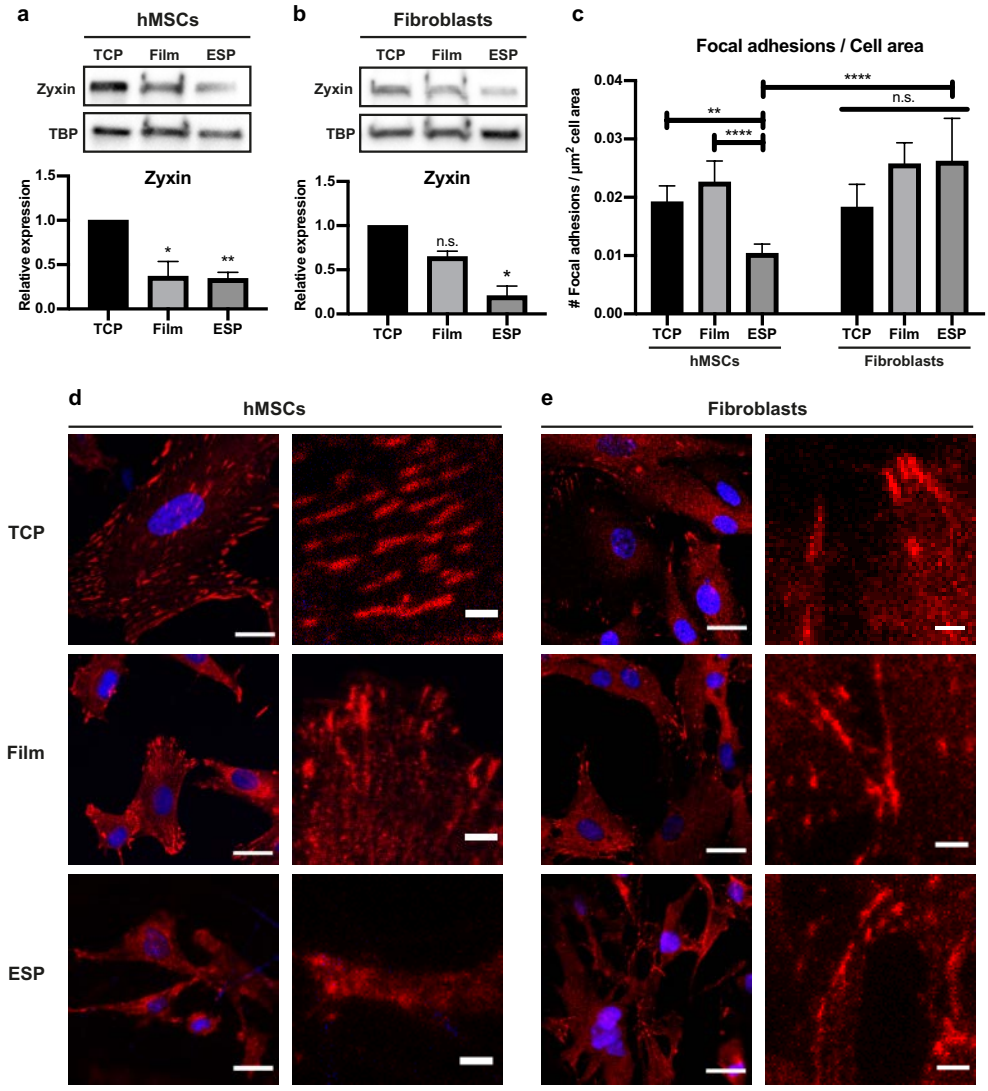

Figure 3. Zyxin expression and focal adhesion analysis of hMSCs and fibroblasts on TCP, films and ESP scaffolds. a, b, Western blot of zyxin and TBP (as loading control) of hMSCs **(a)** or human dermal fibroblasts **(b)** on TCP, films or ESP scaffolds. Graphs depict quantification of western blots of zyxin/TBP from 4 **(a)**, or 3 **(b)** independent experiments, normalized to TCP. Stars indicate significance compared to TCP. Repeated measured ANOVA with post-hoc test. Error bars indicate mean±SD. **c,** quantification of number of zyxin positive focal adhesions per µm2 cell area of hMSCs or human dermal fibroblasts grown on TCP, films or ESP scaffolds. n=17-27 cells, quantified in 5-10 different images from biological triplicates. One-way ANOVA with post-hoc test. Error bars indicate mean±95% CI. **a, b, c,** n.s. $p>0.05$; * $p<0.05$; ** $p<0.01$; **** $p<0.0001$. **d, e,** Representative images of hMSCs **(d)** or human dermal fibroblasts **(e)** stained for zyxin (red) and nuclei (blue). Right panels represent a 5x magnification of the respective left panel. Scalebars represent 25 µm (left panels) and 4 µm (right panels).

differently to the ESP scaffolds than fibroblasts, potentially explaining the difference in FGFR1 expression.

FGFR1 is not regulated through zyxin or paxillin

As the lower FGFR1 expression correlated with fewer focal adhesions of hMSCs on ESP scaffolds, we knocked down paxillin and zyxin. Interestingly, neither paxillin nor zyxin depletion resulted in a change in FGFR1 expression, demonstrating that the differential expression of these proteins by hMSCs on ESP scaffolds is not the reason for the reduced FGFR1 expression (Figure 4a-b).

Even though focal adhesions didn't influence the FGFR1 expression, the reduction in focal adhesions of hMSCs on ESP suggests a difference in mechanosensitive signaling. An important mechanosensitive pathway is the MRTF/SRF pathway. MRTF translocates to the nucleus when actin is incorporated into actin filaments and globular actin is low, where it activates SRF to transcribe target genes. To investigate this pathway, we looked at the expression of SRF. Indeed, compared to TCP, the SRF expression was 73.1±10.7% ($p<0.05$) lower on films and 91.9±5.9% ($p<0.01$) lower on ESP scaffolds in hMSCs. Compared to films, SRF expression was 69.7±21.8% ($p<0.05$) lower on ESP scaffolds (Fig. 4c). For fibroblasts, expression of SRF was 24.9±79% ($p>0.05$) and 50±20.3% ($p>0.05$) lower on films and ESP respectively, but this difference was not statistically significant (Fig. 4d). To further investigate the MRTF/SRF pathway, we looked at the localization of MRTF-A in hMSCs and fibroblasts, on TCP, films and ESP scaffolds. MRTF-A was mainly located in the nucleus in fibroblasts, regardless of the culture substrate (Supplementary Fig. 5). In hMSCs, however, MRTF-A was located in the nucleus when cultured on TCP, but mainly in the cytoplasm when cultured on films. Surprisingly, hMSCs on ESP scaffolds also showed nuclear localization of MRTF-A. Together with the SRF expression, these results suggest activity of the MRTF/SRF pathway in fibroblasts on all substrates and of hMSCs on TCP, but not of hMSCs on films or ESP scaffolds. The activity of the MRTF/SRF pathway correlates with the reduced FGFR1 expression of hMSCs on films or ESP scaffolds.

Actin-myosin and MRTF/SRF pathway regulate FGFR1 expression

To investigate the role of the MRTF/SRF pathway in the regulation of FGFR1 in hMSCs, we inhibited the pathway using CCG203971[48, 49]. Indeed, in both hMSCs and fibroblasts, inhibition of the MRTF/SRF pathway reduced FGFR1 expression by 59.6±7.0% ($p<0.01$) and 61.5±2.9% ($p<0.01$), respectively (Fig 5a, c). This shows that MRTF/SRF directly or indirectly regulates FGFR1 expression in both hMSCs and fibroblasts. We observed a strong decrease in SRF expression in hMSCs on ESP scaffolds (Fig. 4c), strongly suggesting that the reduced FGFR1 expression of hMSCs on ESP scaffolds is due to a decrease in SRF expression. Fibroblasts maintained a high expression of SRF on ESP scaffolds (Fig. 4d), explaining the high expression of FGFR1 on ESP scaffolds.

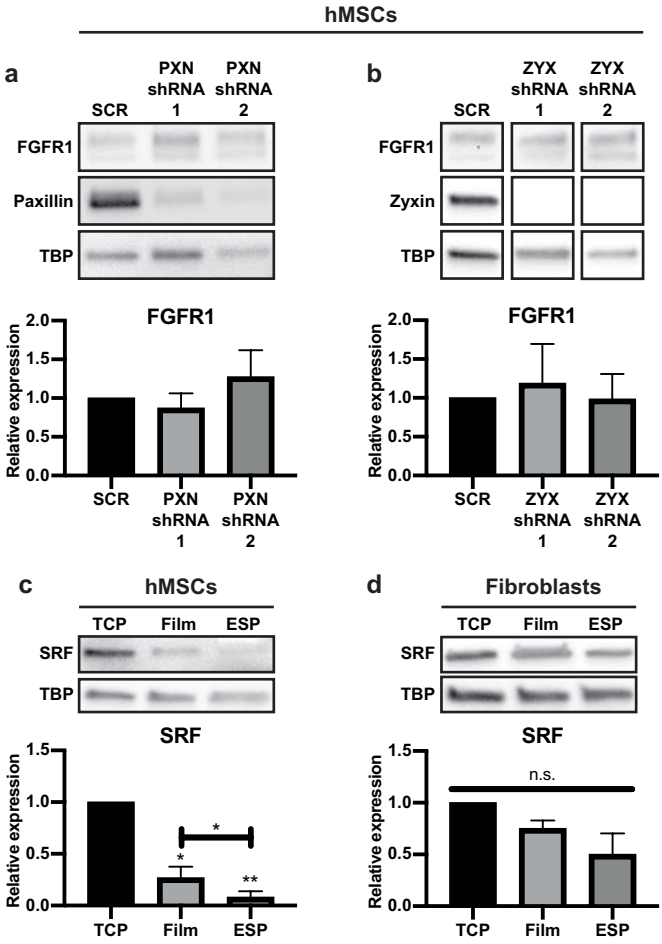

Figure 4. No role of paxillin or zyxin in regulation of FGFR1. a, b, Western blot of FGFR1, paxillin, zyxin and TBP (as loading control) of hMSCs transduced with PXN-shRNA **(a)** or ZYX-shRNA **(b)** cultured on TCP. Graphs depict quantification of western blots of FGFR1/TBP from 4 biological replica's, normalized to TCP. **c, d,** Western blot of SRF and TBP (as loading control) of hMSCs **(c)** or human dermal fibroblasts **(d)** cultured on TCP, films or ESP scaffolds. Graphs depict quantification of western blots of SRF/TBP from 4 **(c)** or 3 **(d)** independent experiments, normalized to TCP. Stars above bars indicate significance compared to TCP. **a, b, c, d,** Repeated measures ANOVA with Tukey's post-hoc test. n.s. $p>0.05$; * $p<0.05$; **** $p<0.0001$. Error bars indicate mean±SD.

When most actin monomers are assembled into filaments and globular actin is low, the MRTF/SRF pathway is activated. To determine the role of the actin cytoskeleton in the regulation of FGFR1, we treated hMSCs and fibroblasts with blebbistatin, an inhibitor of actin-myosin interaction. Expression of FGFR1 reduced 48.4±10.2% ($p<0.05$) in hMSCs and

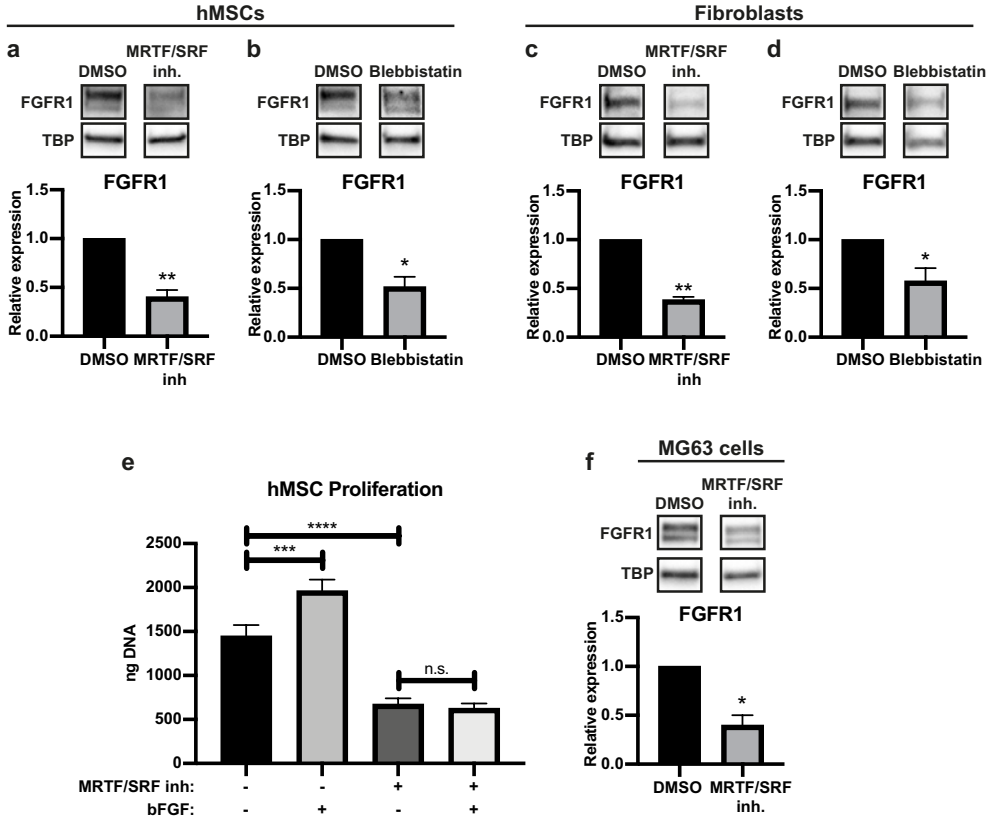

Figure 5. Actin-myosin and MRTF/SRF inhibitors change FGFR1 expression in hMSCs, fibroblasts and MG63 cells. a, b, c, d, Western blot of FGFR1 and TBP (as loading control) of hMSCs **(a, b)** or human dermal fibroblasts **(c, d)**, cultured on TCP and treated with MRTF/SRF inhibitor CCG203971 **(a, c)** or blebbistatin **(b, d)**. Graphs depict quantification of western blots of FGFR1/TBP from 3 biological replica's, normalized to TCP. **e,** DNA quantification of hMSCs cultured for 7 days on TCP in the presence of MRTF/SRF inhibitor and/or 10 ng/ml bFGF. n=3 for each condition. One-way ANOVA with Tukey's post-hoc test. n.s. $p>0.05$; *** $p<0.001$; **** $p<0.0001$; Error bars indicate mean±SD. **f,** Western blot of FGFR1 and TBP (as loading control) of MG63, an osteosarcoma cell-line cultured on TCP and treated with MRTF/SRF inhibitor CCG203971. Graph depicts quantification of western blots of FGFR1/TBP from 3 biological replicas, normalized to TCP. **a, b, c, d, f,** ratio paired t-test. * $p<0.05$; ** $p<0.01$. Error bars indicate mean±SD.

42.4±13.3% in fibroblasts (Fig. 5b, d). Together, this demonstrates that FGFR1 is regulated by the actin cytoskeleton, directly or indirectly through the MRTF/SRF pathway.

Another important mechanosensitive co-transcription factor is Yes activated protein 1 (YAP), entering the nucleus when a cell experiences high cellular tension[33]. To investigate if YAP plays a role in FGFR1 regulation, we knocked down YAP in hMSCs. No difference was observed in FGFR1 expression between YAP-knock down and control-shRNA groups (Supplementary Fig. 6), demonstrating that YAP does not play a role in FGFR1 regulation in hMSCs.

To further investigate the link between the MRTF/SRF pathway and the FGF pathway, we investigated the response to bFGF of hMSCs cultured with MRTF/SRF inhibitor. After 7 days of culture on TCP in the presence of bFGF and/or MRTF/SRF inhibitor, total DNA was analyzed. As expected, 35.5±8.9% more DNA was found when bFGF was added to the medium, compared to basic medium (Fig. 5e). In the presence of MRTF/SRF inhibitor, 53.4±4.6% less DNA was found than in basic medium. Interestingly, in the presence of MRTF/SRF inhibitor, hMSCs did not increase proliferation when bFGF was added. This shows that the MRTF/SRF pathway regulates the response to bFGF, in confirmation with the reduced FGFR1 expression. Aberrant FGFR regulation in cancer cells has been linked to metastasis, tumor progression and a worse diagnosis. To test whether the MRTF/SRF pathway is also responsible for FGFR1 regulation in cancer cells, we treated the osteosarcoma cell line MG63 with the MRTF/SRF inhibitor. Similar to hMSCs and fibroblasts, FGFR1 expression was reduced by 60.2±10.3% ($p<0.05$) when MRTF/SRF was inhibited (Fig. 5f). MRTF/SRF inhibition decreased FGFR1 expression in all three tested human cell types, suggesting that the MRTF/SRF pathway could be a regulator of the FGFR1 pathway in many different cell types.

Discussion

Here, we have functionalized 300PEOT45PBT55 ESP scaffolds by coupling bFGF to the surface. The covalent binding of bFGF to ESP scaffolds made of other polymers has been shown before to retain the growth factor bioactivity[10, 50]. Similarly, the covalently coupled bFGF was still active on our ESP scaffolds and could be used as a method to increase cell proliferation rate on ESP scaffolds. This could be useful for *in vivo* approaches, but it can also be used as a cell culture substrate *in vitro*. bFGF is highly unstable in solution and covalent binding to a surface has been shown to increase its stability[10].

Unlike fibroblasts, hMSCs did not increase proliferation in response to bFGF (in solution or covalently bound) on ESP scaffolds. We found that this was due to reduced SRF expression, which caused decreased FGFR1 expression. SRF expression is known to be regulated by itself through a positive feedback loop[51]. The observed difference in SRF expression between TCP, films and ESP scaffolds highlight the difference in SRF activity on the different substrates. The positive feedback loop can increase the differences in SRF expression, but the origin of the initial difference in SRF expression remains unclear. MRTF-A was located in the nucleus of fibroblasts on all substrates, and of hMSCs on TCP, strongly suggesting together with high SRF activity that the MRTF/SRF pathway was active. hMSCs on films did not show nuclear localization of MRTF-A, which together with the low SRF expression suggests that the pathway is inactive, explaining the low FGFR1 expression. On ESP, however, MRTF-A was located in the nucleus. Even though MRTF-A was located in the nuclei, the low SRF expression of hMSCs on ESP scaffolds could prevent active transcription of the FGFR1 gene, or of genes that (indirectly) regulate FGFR1.

Through actin-myosin inhibition by blebbistatin, we found that FGFR1 expression is reduced with less actin-myosin tension. The MRTF/SRF pathway is dependent on the actin cytoskeleton, but also plays a role in shaping the actin network[52]. Whether the effect of actin-myosin inhibition went through MRTF/SRF, or vise-versa, we did not investigate. It is possible that no clear cause and effect between these two players exists, because there is a positive feedback look between the two. MRTF/SRF activity increases stress fiber formation, thereby also increasing MRTF nuclear localization and increasing MRTF/SRF activity[52].

hMSCs grown on ESP scaffolds displayed fewer focal adhesions than on films or TCP. In contrast, fibroblasts formed similar numbers of focal adhesions per cell area on ESP scaffold as on films or TCP. On TCP and films, the number of zyxin positive focal adhesions was the same between hMSCs and fibroblasts. The reason for the difference between fibroblasts and hMSCs was not investigated here. Different cell types exhibit different cell spreading and traction forces in response to different substrate stiffnesses[53-55]. Indeed, the optimal stiffness for differentiation and proliferation defer per cell type[56, 57]. We have previously shown that hMSCs experience the ESP scaffolds used here as a soft substrate, demonstrated by fewer focal adhesions, less lamin A/C and less YAP nuclear translocation[58]. The difference in focal adhesion formation between hMSCs and fibroblasts observed here potentially derives from a different response to matrix stiffness. Perhaps fibroblasts are able to form focal adhesions on softer substrates than hMSCs. Side by side comparison of hMSCs and fibroblasts on different stiffnesses has not yet been reported but could shed light on the differences observed here.

Knockdown of either zyxin or paxillin did not affect FGFR1 expression. In contrast to paxillin, zyxin knockdown is known to diminish stress fibers[59-61]. While actin-myosin inhibition by blebbistatin did decrease FGFR1 expression, zyxin knockdown did not. Although fewer than normally, zyxin knockdown cells still form focal adhesions[62]. Our data suggests that the actin-myosin tension between these focal adhesions is still sufficient to maintain a higher FGFR1 expression, as full inhibition of actin-myosin by blebbistatin reduced FGFR1.

The regulation of FGFR1 expression is poorly studied. YAP knockdown has been shown to decrease FGFR1 expression in lung cancer cells[63] and neurospheres[64]. Also, integrin α6 has been shown to regulate FGFR1[64]. We found that YAP knockdown didn't alter FGFR1 expression in hMSCs, suggesting a different role for YAP in different cell types. YAP and integrin α6 regulation of FGFR1 does, however, hint at the mechanosensitive regulation of FGFR1, in accordance with what we've shown here. Other mechanisms of FGFR1 regulation include regulation by Pdx-1[65, 66] and ZEB1[64]. The regulation of FGFR1 by MRTF/SRF and actin-myosin tension presented here adds to the sparse literature on FGFR1 regulation. These novel findings can give insight in tumor development, as aberrant FGFR1 regulation is important in a wide variety of cancers[12, 17]. FGFR inhibitors are already being used in clinical trials as novel anti-cancer drugs[18-23]. Our study opens up new potential targets for FGFR1 regulation in cancer cells. Also, as an important regulator of proliferation in hMSCs[27] and other cell

types[67, 68], this can have implications for scaffold designs. We show here that the scaffold design itself, as well as material properties, can influence the FGFR1 expression. Optimizing scaffold design to influence MRTF/SRF activity and FGFR1 expression could be crucial for certain tissue regeneration applications.

Conclusion

ESP scaffolds were successfully functionalized with bFGF, which increased the proliferation of fibroblasts, but not hMSCs. hMSCs responded to bFGF on TCP, but reduced FGFR1 expression on ESP scaffolds, explaining their irresponsiveness to bFGF on ESP scaffolds. Fibroblasts maintained a high expression of FGFR1 on ESP scaffolds, explaining the difference in bFGF responsiveness between hMSCs and fibroblasts. hMSCs, but not fibroblasts, displayed fewer focal adhesions and expressed less SRF on ESP scaffolds than on TCP or 2D film controls. In hMSCs and fibroblasts, the inhibition of actin-myosin interaction and MRTF/SRF activity decreased FGFR1 expression. In osteosarcoma MG63 cells, MRTF/SRF inhibition also led to decreased FGFR1 expression. Together, our data shows that hMSCs become irresponsive to bFGF on ESP scaffolds because of a downregulation of SRF, which leads to a decrease in FGFR1. Fibroblasts maintain a high SRF and FGFR1 expression and remain responsive to bFGF on ESP scaffolds.

Materials and Methods

Film and ESP scaffold production

Random block co-polymer of poly(ethylene oxide terephthalate) (PEOT) and poly(butylene terephthalate) (PBT), with 300 Da PEO and PEOT/PBT ratio (w/w) of 55/45 (300PEOT55PBT45, acquired from PolyVation) was used to produce films and ESP scaffolds. 300PEOT55/PBT45 granules were melted at 180 ˚C under slight pressure (~100 kg) in a circular 23 mm mold between two silicon wafers (Si-mat, Kaufering, Germany) to produce flat films. Films were punched out using a 22 mm punch to fit in a 12 well plate.

The electrospinning polymer solution was prepared by dissolving 20% (w/v) 300PEOT55PBT45 in 3:7 1,1,1,3,3,3,-Hexafluoro-2-propanol (HFIP):chloroform, overnight at room temperature under agitation. For heparin functionalization, 2% (w/v) poly(ethylene glycol) (PEG) with 2 NH_2 end-groups (Mw: 3350 kDa) (PEG-NH_2), was added to the polymer solution and mixed for 4 hours before electrospinning.

ESP scaffolds were produced on a slowly rotating (100 RPM) 19 cm diameter mandrel by electrospinning on a polyester mesh (FinishMat 6691 LL (40 gr/m2), generously provided by Lantor B.V.) with 12 mm holes, on top of aluminum foil. The following parameters were maintained: 15 cm working distance between needle and rotating mandrel, 1 ml/h flow rate, 23-25 ˚C and 40% relative humidity, a needle charge between 10-15 kV and collector charge between -2 and -5 kV. Individual ESP scaffolds were punched out with a diameter of 15 mm over the 12 mm holes in the polyester mesh and removed from the aluminum foil. This resulted in 15 mm ESP scaffolds with a 12 mm diameter surface for cell culture and a 1.5 mm polyester ring around it to improve handleability. Using this method, up to 100 ESP scaffolds were produced under exactly equal parameters.

Before cell culture, ESP scaffolds and films were sterilized in 70% ethanol for 15 min and dried at room temperature until visually dry. The 1.5 mm polyester ring was covered with a rubber 15 mm outer- and 12 mm inner-diameter O-ring (Eriks) to keep the scaffolds from floating in tissue culture well plates.

Functionalization of ESP scaffolds with BSA or bFGF

Before coupling of bovine serum albumin (BSA)-FITC conjugate (ThermoFisher Scientific) or basic fibroblast growth factor (bFGF) (Neuromics), ethanol sterilized ESP scaffolds were incubated in 0.5 M NaOH for 30 min at room temperature to open the ester bond of the 300PEOT55PBT45 polymer. Scaffolds were thoroughly washed 5 times with water and then incubated with 4 mg/ml N-(3-Dimethylaminopropyl)-N′-ethylcarbodiimide hydrochloride (EDC) (Sigma-Aldrich) and 10 mg/ml N-hydroxysuccinimide (NHS) (Sigma-Aldrich) in milliQ water, or in milliQ water only, without EDC-NHS, as negative control, for 30 min at room temperature on a rocking plate. EDC-NHS solution was removed and 500 µl of 1 µg/ml BSA or 20, 200, or 2000 ng/ml bFGF in water was added to the scaffolds in a 24 well-plate well and incubated overnight at 4 ˚C on a rocking plate. The following day, BSA-FITC scaffolds were

washed 5 times with water and scaffold fluorescence was measured in the fluorescein channel on a Clariostar plate reader (BMG Labtech). For sodium dodecyl sulfate (SDS) wash, 1% (w/v) in water was added to the functionalized scaffolds and incubated under agitation at room temperature overnight. The following day, scaffolds were thoroughly washed 5 times with water and measured on the plate reader as described before.
For bFGF functionalized scaffolds, bFGF solution was harvested to be analyzed by bFGF ELISA, and the scaffolds were washed 5 times with water, once with PBS and once with medium. For the bFGF scaffolds, all solutions were sterilized by filtration through at 0.2 µm filter. bFGF was quantified using a bFGF ELISA kit (Abcam), according to manufacturer's protocol.

Heparin functionalization of ESP scaffolds
1.5 mg/ml heparin sodium salt from porcine intestinal mucosa (Sigma-Aldrich) was mixed with 4 mg/ml EDC and 10 mg/ml NHS in water (or water only, without EDC-NHS, as negative control) and directly added to the 300PEOT55PBT45+PEG-NH_2 ESP scaffolds and incubated overnight at 4 ˚C.
To measure bound heparin, scaffolds were washed with 5 times with milliQ water and stained for 30 min with alcian blue staining solution (0.1% alcian blue, 10% ethanol, 0.1% acetic acid, 0.03 M $MgCl_2$ in water (all Sigma-Aldrich)). Scaffolds were washed once with MQ water and incubated for 30 min at room temperature in destaining solution (10% ethanol, 0.1% acetic acid, 0.03 M $MgCl_2$ in water). Scaffolds were washed again once with water and then incubated for 30 min in 1% SDS to extract the heparin-bound alcian blue from the scaffolds. The absorbance of this solution was measured in a Clariostar plate reader.
For cell culture, the heparin functionalized scaffolds were washed 5 times with milliQ water and incubated overnight at 4 ˚C with 500 µl 2000 ng/ml bFGF. The following day scaffolds were washed 5 times with water, once with PBS and once with medium. All solutions were sterilized by filtration through at 0.2 µm filter.

Cell culture
Human dermal fibroblasts (Lonza) were expanded at 2000 cells/cm^2 in DMEM+Glutamax medium (Thermo Fisher Scientific) supplemented with 10% (V/V) fetal bovine serum (FBS) (Sigma-Aldrich).) Bone marrow derived hMSCs were isolated by Texas A&M Health Science Center[69]. Briefly, aspirated bone marrow was centrifuged to isolate mononuclear cells. The hMSCs were further expanded and tested for differentiation potential. hMSCs were received at passage 1 and were further expanded at 1000 cells/cm^2 in α-MEM+Glutamax medium (Thermo Fisher Scientific) supplemented with 10% FBS. MG63 cells (ATCC) were expanded at 5000 cells/cm^2 in DMEM+Glutamax+10% FBS medium. All cells were cultured in 37 ˚C in 5% CO_2 until reaching 70-80% confluency. Cells were trypsinised in 0.05% Trypsin and 0.53 mM EDTA

(ThermoFisher Scientific) and hMSCs and fibroblasts were used for experiments at passage 5. MG63 cells were used at passage 90.
Unless otherwise stated, all experiments were harvested at day 7. For scaffold experiments, hMSCs and fibroblasts were cultured at 1000 cells/cm^2 in TCP and films, and 30.000 cells/ESP scaffold in growth medium with and 100 U/ml penicillin-streptomycin. All other experiments were done in medium without penicillin-streptomycin. In bFGF medium conditions, 10 ng/ml bFGF was added to the medium.
For blebbistatin and MRTF/SRF inhibitor experiments, hMSCs and fibroblasts cells were seeded at 1000 cells/cm^2 on TCP and cultured for 6 days. MG63 cells were seeded at 5000 cells/cm^2 cultured for 2 days, because of a very high proliferation rate. After the initial culture period in growth medium, 100 µM blebbistatin (Sigma-Aldrich) in 0.2% DMSO in growth medium, or 12.2 µM MRTF/SRF inhibitor CCG203971 in 0.1% DMSO in growth medium, or respective DMSO control was added to the cells for 24 h.
To test the responsiveness of hMSCs to bFGF in the presence of MRTF/SRF inhibitor, hMSCs were seeded at 1000 cells/cm^2 in TCP and cultured for 7 days in 0.1% DMSO control, 0.1% DMSO + 10 ng/ml bFGF, 24.4 µM MRTF/SRF in 0.1% DMSO or 24.4 µM MRTF/SRF in 0.1% DMSO + 10 ng/ml bFGF, all in hMSC growth medium.

DNA quantification
To lyse cells for DNA quantification, cells were washed 2x with PBS and freeze-thawed dry twice before RLT lysis buffer (Qiagen) was added. ESP scaffolds were removed from the polyester ring after the last PBS wash. Samples were then freeze-thawed 3x in lysis buffer. TCP plates and films were scraped with a cell scraper after the first freeze-thaw in lysis buffer. ESP scaffolds were left in lysis buffer. Samples were diluted 100-400x, depending on expected number of cells per samples, in Tris-EDTA buffer (10 mM Tris-HCl, 1 mM EDTA, pH 7.5) and λ-DNA standard was made in the same final solution (0.25-1% RLT in Tris-EDTA buffer). Pico green assay (ThermoFisher Scientific) was then used to quantify DNA, according to manufacturer's protocol.

Protein isolation and western blot
Protein was isolated in a custom lysis buffer to allow for the detection of membrane proteins with western blot. Other buffers, such as RIPA buffer, were tried for FGFR1 western blot without success (data not shown). The buffer consisted of 150 mM NaCl, 0.5% sodium deoxycholate, 1% SDS, 1% NP-40 and 50 mM Tris-HCl in water, set to pH 7.4. The buffer was supplemented with cOmplete™ Mini EDTA-free Protease Inhibitor Cocktail (Sigma-Aldrich).
Samples were washed in cold PBS twice before lysis. ESP scaffolds were removed from the supporting polyester ring. To get sufficient proteins, 6–12 films or 15–20 ESP scaffolds were combined in 300-400 µl for a single protein isolate. Experiments were repeated 3 or 4 times to obtain sufficient replicates. 6 or 10 cm dishes were used for TCP samples. TCP and film

conditions were scraped in lysis buffer with cell scrapers. ESP scaffolds were submerged in lysis buffer and incubated for around 30 min in lysis buffer because the scaffolds were removed from the protein isolate. Samples were not spun down to maintain potentially non-dissolved membrane proteins in solution.
Pierce BCA protein assay kit (Thermo Fisher Scientific) was used to quantify total protein concentration. 20 µg protein was incubated in 10% 2-Mercaptoethanol (Sigma-Aldrich) in laemmli loading buffer (Bio-Rad) for 37 ˚C for 20 min for FGFR1 western blots and at 95 ˚C for 5 min for all other western blots. Samples were loaded into 4–15% polyacrylamide gels (Bio-Rad) and blotted to 0.45 µm PVDF membranes (Bio-Rad) using semi-dry transfer. Membranes were blocked in 5% (w/v) fat free milk (Bio-Rad) in TBS + 0.05% (v/v) tween-20 (Sigma-Aldrich) for 1 hour, except for SRF western blots, which had to be blocked in 2% (w/v) BSA (VWR) + 0.05% tween-20 in PBS to work (data not shown). Primary antibodies were incubated in their respective blocking buffer overnight at 4 ˚C. All antibodies were ordered from Abcam: FGFR1: ab76464 1/500; Paxillin: ab32084 1/1000; Zyxin: ab58210 1/1000; YAP1: ab52771 1/1000; SRF: ab53147 1/250; TBP: ab51841 1/1000. Blots were incubated the following day with 0.33 µg/ml Goat-anti-rabbit or -mouse HRP (Bio-Rad) in blocking buffer for 1 h at room temperature. To visualize the protein bands, blots were incubated with Clarity Western ECL (Bio-Rad) for 1-5 min right before imaging.

Immunofluorescence and imaging
Cells were fixed with 3.6% (v/v) paraformaldehyde (Sigma-Aldrich) in PBS for 20 min at room temperature. To block and permeabilize, fixed cells were incubated in 2% (w/v) BSA+0.1% (v/v) triton X (VWR) in PBS. Zyxin or paxillin (Abcam, ab58210 and ab32084, respectively, both 1/1000) were incubated in 2% (w/v) BSA+0.05% (v/v) tween-20 in PBS overnight at 4 ˚C. The following day, 1/1000 Goat-anti-mouse Alexa Fluor 568 or Goat-anti-rabbit Alexa Fluor 488 was incubated overnight at 4 ˚C in 2% (w/v) BSA+0.05% (v/v) tween-20 in PBS. The next day, samples were stained with DAPI (Sigma-Aldrich, 0.14 µg/ml in PBS+0.05% (v/v) tween-20) to stain nuclei. Images were taken on a confocal microscope.
Focal adhesions were quantified manually by counting the number of focal adhesions per cell using Fiji. Between 17 and 27 cells were counted per condition, from 5-10 different images from biological triplicates. Cell area was measured by manually outlining the cells and measuring surface area using Fiji. The number of focal adhesions was normalized to the cell area.

Lentiviral production and transduction
To produce lentiviral particles, human embryonic kidney 293FT (HEK) cells were seeded at 60.000 cells/cm^2 in DMEM+Glutamax+10% FBS. Cells were transfected with pMDLg pRRE, pMD2.G, pRSV Rev (Addgene) and one of the pLKO.1 shRNA plasmids using 5:1 lipofectamine 2000 (Thermo Fisher Scientific):DNA (v/w) 24 h after seeding. The following TRC pLKO.1

constructs (Dharmacon) were used: ZYX: TRCN0000074204 and TRCN0000074205; PXN: TRCN0000123134 and TRCN0000123136; YAP1: TRCN0000107265 and TRCN0000107266; and non-targeting shRNA control (RHS6848). Medium was changed 16 h post-transfection to hMSC growth medium. Lentivirus was harvested and filtered through a 0.45 µm filter 24 h and 48 h after the change to hMSC growth medium.
24 h after thawing at 1000 cells/cm^2, hMSCs were transduced with the lentiviral medium for 16 h. Medium was replaced with growth medium the following day. 48-72 h post transduction, medium was replaced with growth medium + 2 µg/ml puromycin for 72 hours. A total of 9-10 days after thawing, hMSCs were passaged and seeded at 1000 cells/cm^2 on TCP for 7 days in growth medium before protein harvest.

Statistics
The statistical tests and number of biological replicates and/or experiments are stated in the figure subtexts. Each experiment used at least 3 biological replicas. Cells selected for quantification of focal adhesions were selected randomly. Films and electrospun scaffolds were also randomly assigned to different experimental groups. Shapiro-Wilk test was used to test for normal distribution of each experimental group before further statistical analysis. To test for significance of absolute differences in experiments with multiple comparisons between groups, a One-way ANOVA with Tukey's post hoc was performed. For relative differences between multiple experimental groups, log values were used for repeated measures ANOVA, with Tukey's post-hoc test. For experiments with a single comparison, two-tailed student's t-test was used for absolute differences, and ratio-paired t-test for relative differences. Significance was set at $p<0.05$. Statistical analysis was done using Graphpad Prism 8.

Acknowledgements

We would like to thank Matt Baker and Paul Wieringa for the valuable discussions about the functionalization strategy of the electrospun scaffolds. We are grateful to the European Research Council starting grant "Cell Hybridge" for financial support under the Horizon2020 framework program (Grant #637308). Some of the materials used in this work were provided by the Texas A&M Health Science Center College of Medicine Institute for Regenerative Medicine at Scott & White through a grant from NCRR of the NIH (Grant #P40RR017447).

References

1. G. Li, S. Shi, S. Lin, T. Zhou, X. Shao, Q. Huang, B. Zhu, and X. Cai, *Electrospun Fibers for Cartilage Tissue Regeneration.* Curr Stem Cell Res Ther, 2018. **13**(7): p. 591-599.
2. S.P. Zhong, Y.Z. Zhang, and C.T. Lim, *Tissue scaffolds for skin wound healing and dermal reconstruction.* Wiley Interdiscip Rev Nanomed Nanobiotechnol, 2010. **2**(5): p. 510-25.
3. B. Kong and S. Mi, *Electrospun Scaffolds for Corneal Tissue Engineering: A Review.* Materials (Basel), 2016. **9**(8).
4. E. Biazar, M.T. Khorasani, N. Montazeri, K. Pourshamsian, M. Daliri, M. Rezaei, M. Jabarvand, A. Khoshzaban, S. Heidari, M. Jafarpour, and Z. Roviemiab, *Types of neural guides and using nanotechnology for peripheral nerve reconstruction.* Int J Nanomedicine, 2010. **5**: p. 839-52.
5. K.A. Rocco, M.W. Maxfield, C.A. Best, E.W. Dean, and C.K. Breuer, *In vivo applications of electrospun tissue-engineered vascular grafts: a review.* Tissue Eng Part B Rev, 2014. **20**(6): p. 628-40.
6. A. Bikfalvi, S. Klein, G. Pintucci, and D.B. Rifkin, *Biological roles of fibroblast growth factor-2.* Endocr Rev, 1997. **18**(1): p. 26-45.
7. S. Lotz, S. Goderie, N. Tokas, S.E. Hirsch, F. Ahmad, B. Corneo, S. Le, A. Banerjee, R.S. Kane, J.H. Stern, S. Temple, and C.A. Fasano, *Sustained levels of FGF2 maintain undifferentiated stem cell cultures with biweekly feeding.* PLoS One, 2013. **8**(2): p. e56289.
8. T.H. Nguyen, S.H. Kim, C.G. Decker, D.Y. Wong, J.A. Loo, and H.D. Maynard, *A heparin-mimicking polymer conjugate stabilizes basic fibroblast growth factor.* Nat Chem, 2013. **5**(3): p. 221-7.
9. S.J. Paluck, T.H. Nguyen, J.P. Lee, and H.D. Maynard, *A Heparin-Mimicking Block Copolymer Both Stabilizes and Increases the Activity of Fibroblast Growth Factor 2 (FGF2).* Biomacromolecules, 2016. **17**(10): p. 3386-3395.
10. E.K.A. Nur, I. Ahmed, J. Kamal, A.N. Babu, M. Schindler, and S. Meiners, *Covalently attached FGF-2 to three-dimensional polyamide nanofibrillar surfaces demonstrates enhanced biological stability and activity.* Mol Cell Biochem, 2008. **309**(1-2): p. 157-66.
11. D.M. Ornitz and N. Itoh, *The Fibroblast Growth Factor signaling pathway.* Wiley Interdiscip Rev Dev Biol, 2015. **4**(3): p. 215-66.
12. T. Helsten, S. Elkin, E. Arthur, B.N. Tomson, J. Carter, and R. Kurzrock, *The FGFR Landscape in Cancer: Analysis of 4,853 Tumors by Next-Generation Sequencing.* Clin Cancer Res, 2016. **22**(1): p. 259-67.
13. H.S. Kim, J.H. Kim, H.J. Jang, B. Han, and D.Y. Zang, *Pathological and Prognostic Impacts of FGFR2 Overexpression in Gastric Cancer: A Meta-Analysis.* J Cancer, 2019. **10**(1): p. 20-27.
14. M.N. Fletcher, M.A. Castro, X. Wang, I. de Santiago, M. O'Reilly, S.F. Chin, O.M. Rueda, C. Caldas, B.A. Ponder, F. Markowetz, and K.B. Meyer, *Master regulators of FGFR2 signalling and breast cancer risk.* Nat Commun, 2013. **4**: p. 2464.
15. S. Tang, Y. Hao, Y. Yuan, R. Liu, and Q. Chen, *Role of fibroblast growth factor receptor 4 in cancer.* Cancer Sci, 2018. **109**(10): p. 3024-3031.
16. R. Fuller, *Cardiac function and the neonatal EKG. Part I: Introduction to neonatal EKGs.* Neonatal Netw, 1989. **7**(4): p. 47-51.
17. J. Wesche, K. Haglund, and E.M. Haugsten, *Fibroblast growth factors and their receptors in cancer.* Biochem J, 2011. **437**(2): p. 199-213.
18. Y.K. Chae, K. Ranganath, P.S. Hammerman, C. Vaklavas, N. Mohindra, A. Kalyan, M. Matsangou, R. Costa, B. Carneiro, V.M. Villaflor, M. Cristofanilli, and F.J. Giles, *Inhibition of the fibroblast growth factor receptor (FGFR) pathway: the current landscape and barriers to clinical application.* Oncotarget, 2017. **8**(9): p. 16052-16074.

19. D. Piasecka, M. Braun, K. Kitowska, K. Mieczkowski, R. Kordek, R. Sadej, and H. Romanska, *FGFs/FGFRs-dependent signalling in regulation of steroid hormone receptors - implications for therapy of luminal breast cancer.* J Exp Clin Cancer Res, 2019. **38**(1): p. 230.
20. N. Sobhani, A. Ianza, A. D'Angelo, G. Roviello, F. Giudici, M. Bortul, F. Zanconati, C. Bottin, and D. Generali, *Current Status of Fibroblast Growth Factor Receptor-Targeted Therapies in Breast Cancer.* Cells, 2018. **7**(7).
21. S.K. Pal, J.E. Rosenberg, J.H. Hoffman-Censits, R. Berger, D.I. Quinn, M.D. Galsky, J. Wolf, C. Dittrich, B. Keam, J.P. Delord, J.H.M. Schellens, G. Gravis, J. Medioni, P. Maroto, V. Sriuranpong, C. Charoentum, H.A. Burris, V. Grunwald, D. Petrylak, U. Vaishampayan, E. Gez, U. De Giorgi, J.L. Lee, J. Voortman, S. Gupta, S. Sharma, A. Mortazavi, D.J. Vaughn, R. Isaacs, K. Parker, X. Chen, K. Yu, D. Porter, D. Graus Porta, and D.F. Bajorin, *Efficacy of BGJ398, a Fibroblast Growth Factor Receptor 1-3 Inhibitor, in Patients with Previously Treated Advanced Urothelial Carcinoma with FGFR3 Alterations.* Cancer Discov, 2018. **8**(7): p. 812-821.
22. C. Heinzle, Z. Erdem, J. Paur, B. Grasl-Kraupp, K. Holzmann, M. Grusch, W. Berger, and B. Marian, *Is fibroblast growth factor receptor 4 a suitable target of cancer therapy?* Curr Pharm Des, 2014. **20**(17): p. 2881-98.
23. L. Lang and Y. Teng, *Fibroblast Growth Factor Receptor 4 Targeting in Cancer: New Insights into Mechanisms and Therapeutic Strategies.* Cells, 2019. **8**(1).
24. T.E. Kahkonen, K.K. Ivaska, M. Jiang, K.G. Buki, H.K. Vaananen, and P.L. Harkonen, *Role of fibroblast growth factor receptors (FGFR) and FGFR like-1 (FGFRL1) in mesenchymal stromal cell differentiation to osteoblasts and adipocytes.* Mol Cell Endocrinol, 2018. **461**: p. 194-204.
25. H. Miraoui, K. Oudina, H. Petite, Y. Tanimoto, K. Moriyama, and P.J. Marie, *Fibroblast growth factor receptor 2 promotes osteogenic differentiation in mesenchymal cells via ERK1/2 and protein kinase C signaling.* J Biol Chem, 2009. **284**(8): p. 4897-904.
26. X. Wen, X. Li, Y. Tang, J. Tang, S. Zhou, Y. Xie, J. Guo, J. Yang, X. Du, N. Su, and L. Chen, *Chondrocyte FGFR3 Regulates Bone Mass by Inhibiting Osteogenesis.* J Biol Chem, 2016. **291**(48): p. 24912-24921.
27. C. Dombrowski, T. Helledie, L. Ling, M. Grunert, C.A. Canning, C.M. Jones, J.H. Hui, V. Nurcombe, A.J. van Wijnen, and S.M. Cool, *FGFR1 signaling stimulates proliferation of human mesenchymal stem cells by inhibiting the cyclin-dependent kinase inhibitors p21(Waf1) and p27(Kip1).* Stem Cells, 2013. **31**(12): p. 2724-36.
28. M. Barczyk, S. Carracedo, and D. Gullberg, *Integrins.* Cell Tissue Res, 2010. **339**(1): p. 269-80.
29. M.A. Wozniak, K. Modzelewska, L. Kwong, and P.J. Keely, *Focal adhesion regulation of cell behavior.* Biochim Biophys Acta, 2004. **1692**(2-3): p. 103-19.
30. M.J. Stroud, *Linker of nucleoskeleton and cytoskeleton complex proteins in cardiomyopathy.* Biophys Rev, 2018. **10**(4): p. 1033-1051.
31. K. Weber and U. Groeschel-Stewart, *Antibody to myosin: the specific visualization of myosin-containing filaments in nonmuscle cells.* Proc Natl Acad Sci U S A, 1974. **71**(11): p. 4561-4.
32. C.S. Chen, M. Mrksich, S. Huang, G.M. Whitesides, and D.E. Ingber, *Geometric control of cell life and death.* Science, 1997. **276**(5317): p. 1425-8.
33. S. Dupont, L. Morsut, M. Aragona, E. Enzo, S. Giulitti, M. Cordenonsi, F. Zanconato, J. Le Digabel, M. Forcato, S. Bicciato, N. Elvassore, and S. Piccolo, *Role of YAP/TAZ in mechanotransduction.* Nature, 2011. **474**(7350): p. 179-83.
34. D.R. Croft and M.F. Olson, *The Rho GTPase effector ROCK regulates cyclin A, cyclin D1, and p27Kip1 levels by distinct mechanisms.* Mol Cell Biol, 2006. **26**(12): p. 4612-27.
35. N. Takeda, M. Kondo, S. Ito, Y. Ito, K. Shimokata, and H. Kume, *Role of RhoA inactivation in reduced cell proliferation of human airway smooth muscle by simvastatin.* Am J Respir Cell Mol Biol, 2006. **35**(6): p. 722-9.

36. L.C. Boraas, E.T. Pineda, and T. Ahsan, *Actin and myosin II modulate differentiation of pluripotent stem cells.* PLoS One, 2018. **13**(4): p. e0195588.
37. C.P. Heisenberg and Y. Bellaiche, *Forces in tissue morphogenesis and patterning.* Cell, 2013. **153**(5): p. 948-62.
38. A.J. Steward and D.J. Kelly, *Mechanical regulation of mesenchymal stem cell differentiation.* J Anat, 2015. **227**(6): p. 717-31.
39. A.C. Callan-Jones and R. Voituriez, *Actin flows in cell migration: from locomotion and polarity to trajectories.* Curr Opin Cell Biol, 2016. **38**: p. 12-7.
40. E.N. Olson and A. Nordheim, *Linking actin dynamics and gene transcription to drive cellular motile functions.* Nat Rev Mol Cell Biol, 2010. **11**(5): p. 353-65.
41. N. Su, P.L. Gao, K. Wang, J.Y. Wang, Y. Zhong, and Y. Luo, *Fibrous scaffolds potentiate the paracrine function of mesenchymal stem cells: A new dimension in cell-material interaction.* Biomaterials, 2017. **141**: p. 74-85.
42. J. Haj, T. Haj Khalil, M. Falah, E. Zussman, and S. Srouji, *An ECM-Mimicking, Mesenchymal Stem Cell-Embedded Hybrid Scaffold for Bone Regeneration.* Biomed Res Int, 2017. **2017**: p. 8591073.
43. M.P. Prabhakaran, L. Ghasemi-Mobarakeh, and S. Ramakrishna, *Electrospun composite nanofibers for tissue regeneration.* J Nanosci Nanotechnol, 2011. **11**(4): p. 3039-57.
44. P.P. Bonvallet, M.J. Schultz, E.H. Mitchell, J.L. Bain, B.K. Culpepper, S.J. Thomas, and S.L. Bellis, *Microporous dermal-mimetic electrospun scaffolds pre-seeded with fibroblasts promote tissue regeneration in full-thickness skin wounds.* PLoS One, 2015. **10**(3): p. e0122359.
45. Y. Xu, W. Cui, Y. Zhang, P. Zhou, Y. Gu, X. Shen, B. Li, and L. Chen, *Hierarchical Micro/Nanofibrous Bioscaffolds for Structural Tissue Regeneration.* Adv Healthc Mater, 2017. **6**(13).
46. M. Pezeshki-Modaress, H. Mirzadeh, M. Zandi, S. Rajabi-Zeleti, N. Sodeifi, N. Aghdami, and M.R.K. Mofrad, *Gelatin/chondroitin sulfate nanofibrous scaffolds for stimulation of wound healing: In-vitro and in-vivo study.* J Biomed Mater Res A, 2017. **105**(7): p. 2020-2034.
47. M.A. Nugent and R.V. Iozzo, *Fibroblast growth factor-2.* Int J Biochem Cell Biol, 2000. **32**(2): p. 115-20.
48. K.M. Hutchings, E.M. Lisabeth, W. Rajeswaran, M.W. Wilson, R.J. Sorenson, P.L. Campbell, J.H. Ruth, A. Amin, P.S. Tsou, J.R. Leipprandt, S.R. Olson, B. Wen, T. Zhao, D. Sun, D. Khanna, D.A. Fox, R.R. Neubig, and S.D. Larsen, *Pharmacokinetic optimitzation of CCG-203971: Novel inhibitors of the Rho/MRTF/SRF transcriptional pathway as potential antifibrotic therapeutics for systemic scleroderma.* Bioorg Med Chem Lett, 2017. **27**(8): p. 1744-1749.
49. E.M. Lisabeth, D. Kahl, I. Gopallawa, S.E. Haynes, S.A. Misek, P.L. Campbell, T.S. Dexheimer, D. Khanna, D.A. Fox, X. Jin, B.R. Martin, S.D. Larsen, and R.R. Neubig, *Identification of Pirin as a Molecular Target of the CCG-1423/CCG-203971 Series of Antifibrotic and Antimetastatic Compounds.* ACS Pharmacology & Translational Science, 2019. **2 (2)**: p. 92-100.
50. H. Lee, S. Lim, M.S. Birajdar, S.H. Lee, and H. Park, *Fabrication of FGF-2 immobilized electrospun gelatin nanofibers for tissue engineering.* Int J Biol Macromol, 2016. **93**(Pt B): p. 1559-1566.
51. J.A. Spencer and R.P. Misra, *Expression of the SRF gene occurs through a Ras/Sp/SRF-mediated-mechanism in response to serum growth signals.* Oncogene, 1999. **18**(51): p. 7319-27.
52. D. Gau and P. Roy, *SRF'ing and SAP'ing - the role of MRTF proteins in cell migration.* J Cell Sci, 2018. **131**(19).
53. H.B. Wang, M. Dembo, and Y.L. Wang, *Substrate flexibility regulates growth and apoptosis of normal but not transformed cells.* Am J Physiol Cell Physiol, 2000. **279**(5): p. C1345-50.
54. P.C. Georges and P.A. Janmey, *Cell type-specific response to growth on soft materials.* J Appl Physiol (1985), 2005. **98**(4): p. 1547-53.
55. S.Y. Tee, A.R. Bausch, and P.A. Janmey, *The mechanical cell.* Curr Biol, 2009. **19**(17): p. R745-8.

56. H. Lv, L. Li, M. Sun, Y. Zhang, L. Chen, Y. Rong, and Y. Li, *Mechanism of regulation of stem cell differentiation by matrix stiffness.* Stem Cell Res Ther, 2015. **6**: p. 103.
57. R.G. Wells, *The role of matrix stiffness in regulating cell behavior.* Hepatology, 2008. **47**(4): p. 1394-400.
58. J. Zonderland, I. Moldero Lorenzo, C. Mota, and L. Moroni, *Dimensionality changes actin network through lamin A/C and zyxin.* BioRxiv https://doi.org/10.1101/752691, 2019.
59. E. Griffith, A.S. Coutts, and D.M. Black, *RNAi knockdown of the focal adhesion protein TES reveals its role in actin stress fibre organisation.* Cell Motil Cytoskeleton, 2005. **60**(3): p. 140-52.
60. M.A. Smith, E. Blankman, M.L. Gardel, L. Luettjohann, C.M. Waterman, and M.C. Beckerle, *A zyxin-mediated mechanism for actin stress fiber maintenance and repair.* Dev Cell, 2010. **19**(3): p. 365-76.
61. A.A. Birukova, I. Cokic, N. Moldobaeva, and K.G. Birukov, *Paxillin is involved in the differential regulation of endothelial barrier by HGF and VEGF.* Am J Respir Cell Mol Biol, 2009. **40**(1): p. 99-107.
62. Z. Sun, S. Huang, Z. Li, and G.A. Meininger, *Zyxin is involved in regulation of mechanotransduction in arteriole smooth muscle cells.* Front Physiol, 2012. **3**: p. 472.
63. T. Lu, Z. Li, Y. Yang, W. Ji, Y. Yu, X. Niu, Q. Zeng, W. Xia, and S. Lu, *The Hippo/YAP1 pathway interacts with FGFR1 signaling to maintain stemness in lung cancer.* Cancer Lett, 2018. **423**: p. 36-46.
64. A. Kowalski-Chauvel, V. Gouaze-Andersson, L. Baricault, E. Martin, C. Delmas, C. Toulas, E. Cohen-Jonathan-Moyal, and C. Seva, *Alpha6-Integrin Regulates FGFR1 Expression through the ZEB1/YAP1 Transcription Complex in Glioblastoma Stem Cells Resulting in Enhanced Proliferation and Stemness.* Cancers (Basel), 2019. **11**(3).
65. H. Wang, M. Iezzi, S. Theander, P.A. Antinozzi, B.R. Gauthier, P.A. Halban, and C.B. Wollheim, *Suppression of Pdx-1 perturbs proinsulin processing, insulin secretion and GLP-1 signalling in INS-1 cells.* Diabetologia, 2005. **48**(4): p. 720-31.
66. A.W. Hart, N. Baeza, A. Apelqvist, and H. Edlund, *Attenuation of FGF signalling in mouse beta-cells leads to diabetes.* Nature, 2000. **408**(6814): p. 864-8.
67. K. Wang, W. Ji, Y. Yu, Z. Li, X. Niu, W. Xia, and S. Lu, *FGFR1-ERK1/2-SOX2 axis promotes cell proliferation, epithelial-mesenchymal transition, and metastasis in FGFR1-amplified lung cancer.* Oncogene, 2018. **37**(39): p. 5340-5354.
68. C. Fumarola, N. Bozza, R. Castelli, F. Ferlenghi, G. Marseglia, A. Lodola, M. Bonelli, S. La Monica, D. Cretella, R. Alfieri, R. Minari, M. Galetti, M. Tiseo, A. Ardizzoni, M. Mor, and P.G. Petronini, *Expanding the Arsenal of FGFR Inhibitors: A Novel Chloroacetamide Derivative as a New Irreversible Agent With Anti-proliferative Activity Against FGFR1-Amplified Lung Cancer Cell Lines.* Front Oncol, 2019. **9**: p. 179.
69. C.M. Digirolamo, D. Stokes, D. Colter, D.G. Phinney, R. Class, and D.J. Prockop, *Propagation and senescence of human marrow stromal cells in culture: a simple colony-forming assay identifies samples with the greatest potential to propagate and differentiate.* Br J Haematol, 1999. **107**(2): p. 275-81.

Supplementary Figures

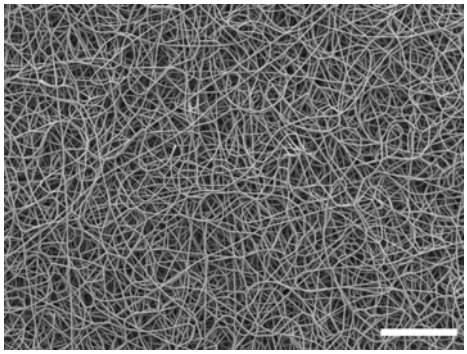

Supplementary Figure 1. Overview of ESP scaffold. Scalebar 100 µm.

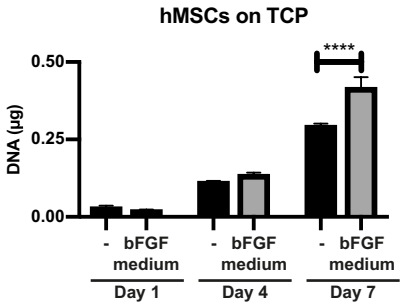

Supplementary Figure 2. Increased proliferation of hMSCs in response to bFGF. DNA quantification of hMSCs cultured on TCP in basic medium (-) or basic medium + 10 ng/ml bFGF harvested on day 1, 4 or 7. n=3 for each condition. One-way ANOVA with Tukey's post-hoc test. **** p<0.0001. Error bars indicate mean±SD.

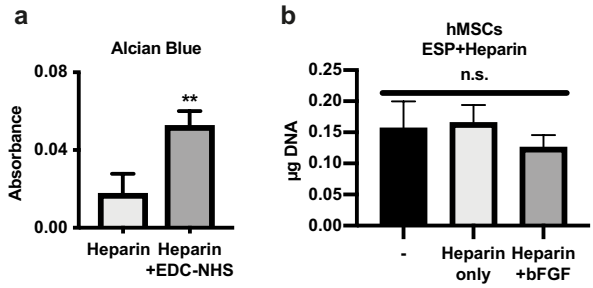

Supplementary Figure 3. No effect heparin bound bFGF on hMSC proliferation. a, Alcian blue analysis of heparin bound to ESP scaffolds with incorporated PEG-NH_2 by EDC-NHS chemistry, or aspecifically absorbed heparin, without EDC-NHS. Student's t-test. ****** $p<0.01$. **b,** DNA quantification of hMSCs cultured for 7 days on unfunctionalized scaffolds (-), or scaffolds functionalized with heparin and with or without absorbed bFGF. One-way ANOVA with Tukey's post-hoc test. n.s. $p>0.05$. **a, b,** n=3 for each condition. Error bars indicate mean±SD.

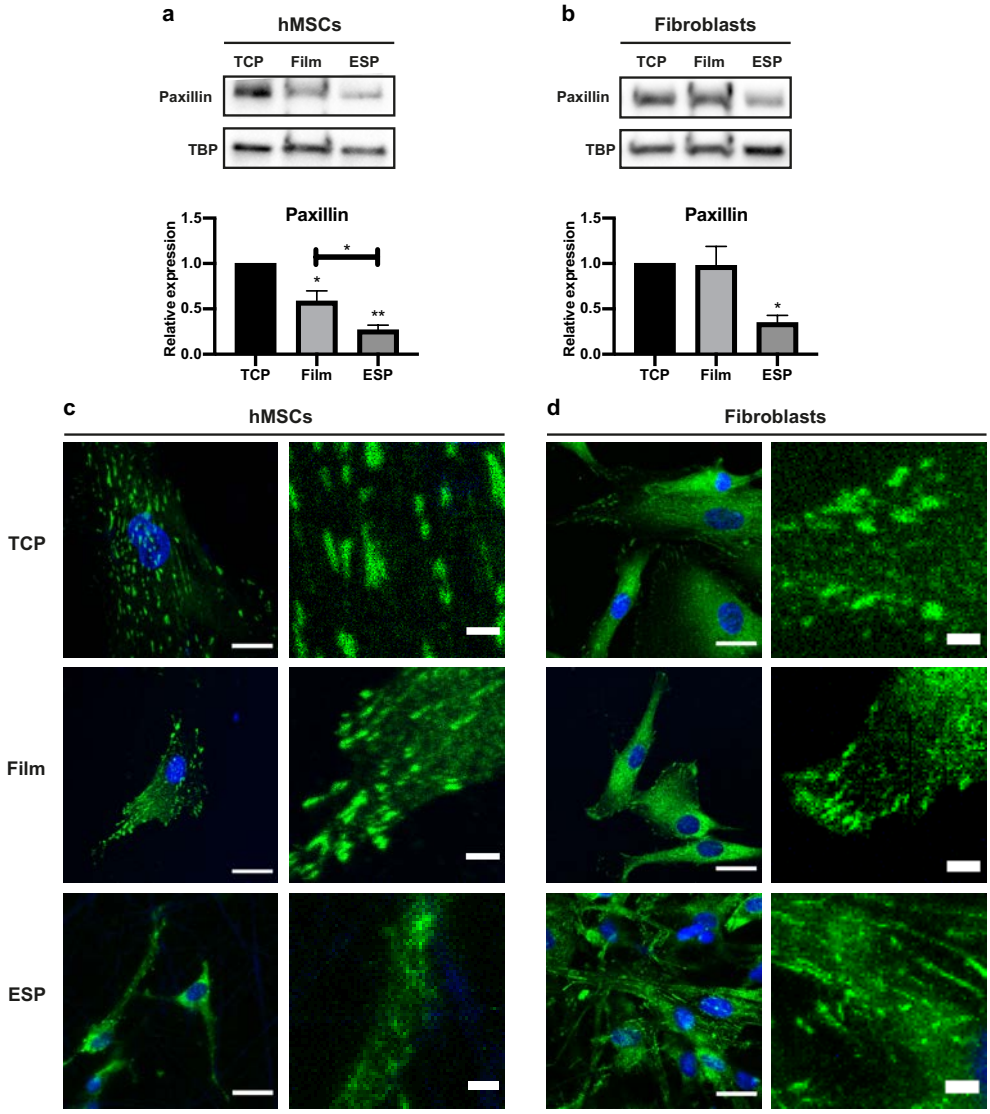

Supplementary Figure 4. Reduced paxillin expression on ESP scaffolds. a, b, Western blot of paxillin and TBP (as loading control) of hMSCs **(a)** or human dermal fibroblasts **(b)** on TCP, films or ESP scaffolds. Graphs depict quantification of western blots of paxillin/TBP from 4 **(a)**, or 3 **(b)** independent experiments, normalized to TCP. Stars above bars indicate significance compared to TCP. Repeated measures ANOVA with Tukey's post-hoc test. * $p<0.05$; ** $p<0.01$. Error bars indicate mean±SD. **c, d,** Representative images of hMSCs **(c)** or human dermal fibroblasts **(d)** stained for paxillin (green) and nuclei (blue). Right panels represent a 5x magnification of the respective left panel. Scalebars represent 25 µm (left panels) and 4 µm (right panels).

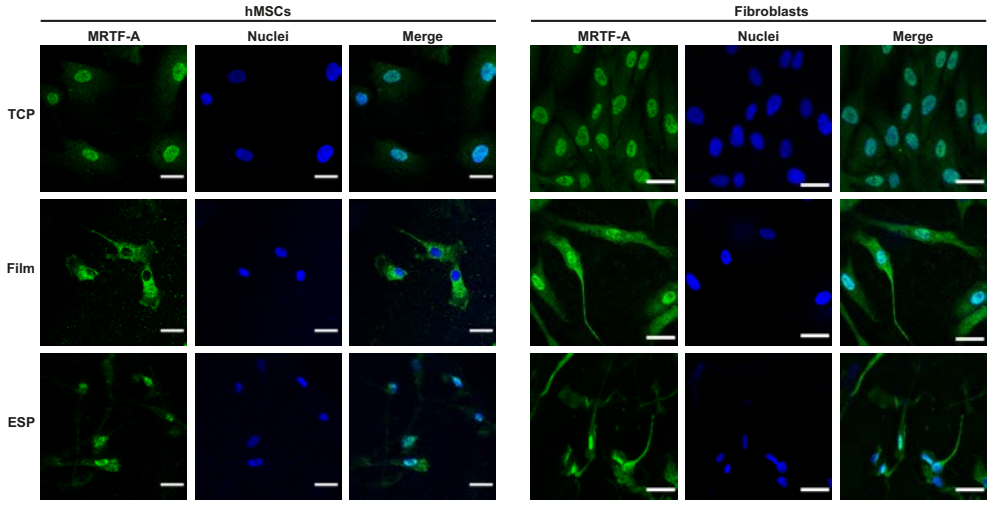

Supplementary Figure 5. MRTF-A localization in hMSCs and fibroblasts on different culture substrates. hMSCs and fibroblasts were grown for 7 days on TCP, Films or ESP scaffolds and stained for MRTF-A (green) and nuclei (blue). Scalebars represent 30 µm.

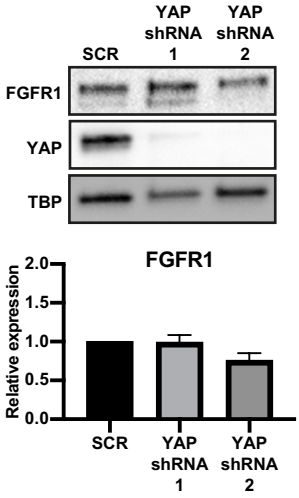

Supplementary Figure 6. YAP does not regulate FGFR1 expression. a, b, Western blot of FGFR1, YAP and TBP (as loading control) of hMSCs transduced with YAP shRNA, cultured on TCP. Graphs depict quantification of western blots of FGFR1/TBP from 4 biological replica's, normalized to TCP. Error bars indicate mean±SD. Repeated measures ANOVA with Tukey's post-hoc test.

Chapter 6

Full cell infiltration and thick tissue formation *in vivo* in tailored electrospun scaffolds

Jip Zonderland[1], Silvia Rezzola[1], David Boaventura Gomes[1], Sandra Camarero Espinosa[1], Ana Henriques Ferreira Lourenço[1], Andrada Serafim[2], Izabela Cristina Stancu[2], David Koper[1, 3, 4, 5], Hong Liu[6, 7], Pamela Habibovic[3], Peter Kessler[4, 5], Marloes Peters[1, 8], Peter Emans[8], Nicole Bouvy[6, 7], Paul Wieringa[1], Lorenzo Moroni[1]

[1] Department of Complex Tissue Regeneration, MERLN Institute for Technology-Inspired Regenerative Medicine, Maastricht University, Maastricht, the Netherlands
[2] Advanced Polymer Materials Group, University Politehnica of Bucharest, Romania
[3] Department of Instructive Biomaterials Engineering, MERLN Institute for Technology-Inspired Regenerative Medicine, Maastricht University, Maastricht, the Netherlands
[4] Department of Cranio-Maxillofacial Surgery, Maastricht University Medical Center, Maastricht, the Netherlands.
[5] GROW School for Oncology and Developmental Biology, Maastricht University, Maastricht, the Netherlands.
[6] Department of Surgery, Maastricht University Medical Centre, Maastricht, the Netherlands
[7] NUTRIM School of Nutrition and Translational Research in Metabolism, Maastricht University, Maastricht, the Netherlands
[8] Department of Orthopaedic Surgery and Laboratory for Experimental Orthopedics, Maastricht University Medical Center, the Netherlands

Abstract

Electrospun (ESP) scaffolds are a promising type of tissue engineering constructs for large defects with limited depth. To form new functional tissue, the scaffolds need to be infiltrated with cells, which will deposit extracellular matrix. However, due to dense fiber packing and small pores, cell and tissue infiltration of ESP scaffolds is limited. Here, we combine two established methods, increasing fiber diameter and co-spinning sacrificial fibers, to create a porous ESP scaffold that allows robust tissue infiltration. Full cell infiltration across 2 mm thick scaffolds is seen 3 weeks after subcutaneous implantation in rats. After 6 weeks, the ESP scaffolds are almost fully filled with *de novo* tissue. Cell infiltration and tissue formation *in vivo* in this thickness has not been previously achieved. In addition, we propose a novel method for *in vitro* cell seeding to improve cell infiltration and a model to study 3D migration through a fibrous mesh. This easy approach to facilitate cell infiltration further improves previous efforts and could greatly aid tissue engineering approaches utilizing ESP scaffolds.

Statement of significance

Electrospinning creates highly porous scaffolds with nano- to micrometer sized fibers and are a promising candidate for a variety of tissue engineering applications. However, smaller fibers also create small pores which are difficult for cells to penetrate, restricting cells to the top layers of the scaffolds. Here, we have improved the cell infiltration by optimizing fiber diameter and by co-spinning a sacrificial polymer. We developed novel culture technique that can be used to improve cell seeding and to study cytokine driven 3D migration through fibrous meshes. After subcutaneous implantation, infiltration of tissue and cells was observed up to throughout up to 2 mm thick scaffolds. This depth of infiltration *in vivo* had not yet been reported for electrospun scaffolds. The scaffolds we present here can be used for *in vitro* studies of migration, and for tissue engineering in defects with a large surface area and limited depth.

Introduction

Electrospun (ESP) scaffolds are highly porous and consist of nano- or micrometer sized fibers of natural or synthetic polymers, mimicking the fibrous composition of tissue extra cellular matrix (ECM)[1-3]. ESP scaffolds provide more mechanical support than hydrogels and are more flexible than scaffolds produced by additive manufacturing, making them interesting for tissue engineering approaches[4]. Large ESP mats are easily produced but are often limited to a thickness of several mm due to delamination and charge distribution. This makes ESP scaffolds particularly interesting for defects with a large surface area, but limited depth. This includes skin patches[5], corneal repair[6], cartilage regeneration[7], vascular grafts[8] and nerve guides[9], among others. However, due to dense fiber packing and small pores, deep cell infiltration in ESP scaffolds remains a challenge[10, 11]. To create new fully functional tissue, ESP scaffolds first need to be fully infiltrated with cells. Several approaches have been developed to increase the cellular infiltration of ESP scaffolds, including increasing fiber diameter[12, 13], incorporating sacrificial salt-[14] or ice crystals[15, 16] or co-spinning sacrificial polymer particles or fibers[17-20]. However, tissue infiltration *in vivo* has been limited to approximately 1 mm scaffold thickness. Increasing infiltration in a reliable and reproducible manner in scaffolds thicker than 1 mm remains a challenge[17, 19].

Here, we combined two approaches to improve scaffold infiltration, by increasing fiber diameter and co-spinning sacrificial poly(ethylene glycol) (PEG) fibers. Using this method, we optimized porosity *in vitro* and achieved cell and tissue infiltration in up to 2 mm thick scaffolds *in vivo*. In addition, we propose a novel method to improve *in vitro* ESP scaffold cell seeding, and a novel 3D migration platform. Traditional methods to investigate migration are mostly limited to 2D substrates or 3D hydrogels[21]. We developed a transwell system that can guide cell migration to improve cell loading of ESP scaffolds, which could also be used to research cytokine-driven 3D cell migration through a fibrous mesh.

Results

Optimizing scaffold porosity by increasing fiber diameter

Increasing fiber diameter has been shown to increase ESP scaffold porosity and pore size[12, 13]. To increase the fiber diameter of the 300PEOT55PBT45 ESP scaffolds, we evaluated the effect of working distance, flow rate and polymer concentration. The fiber diameter increased most by increasing the polymer concentration (Fig 1a, b). Flow rate had a small effect on the fiber diameter (Fig. 1a), while the working distance had no effect (Supplementary Fig. 1). Fiber diameter increased from 1.1±0.3 µm with 20% at 3 ml/h to 3.3±0.4 with 35% at 3ml/h. These scaffolds were used for further analysis. Pore size on the surface of the scaffolds was analyzed and showed an increase from 8.3±2.3 μm^2 in the 20% to 19.5±5.4 μm^2 in the 35% scaffolds (Fig. 1c). Next, cell migration through 50 µm thick scaffolds was analyzed. hMSCs were seeded on top of the scaffolds and were cultured for 1, 4 and 7 days. Cells were fixed, stained with DAPI and the number of cells on the bottom of the scaffold was quantified. On day 1, no cells were found at the bottom of the 20% or 35% scaffolds, showing that cells did not fall through the scaffold and could only reach the bottom by migration. On day 4 and 7, almost no cells (<1 cell/mm^2) were found on the bottom of the 20% scaffolds. However, 47.1±6.4 and 50.7±12.8 cells/mm^2 were found on day 4 and 7 on the bottom of the 35% scaffolds, respectively. This demonstrates that by increasing the fiber diameter, the pore space could be sufficiently increased to allow migration through the 50 µm scaffolds. As no difference was found between day 4 and 7, and no cells were observed on day 1, all migration experiments after this were measured at day 4.

Further increasing porosity by co-spinning sacrificial fibers

Scaffold porosity has previously been increased by co-spinning sacrificial electrospun fibers[17-20]. These fibers take up space during the electrospinning process and are later dissolved, leaving extra empty space in the scaffolds. To further improve the porosity of our scaffolds, we spun 20% and 35% 300PBT55PBT45 with one needle, and a PEG solution with a second needle. The PEG fibers were approximately 3 µm in diameter. After dissolving the PEG in water, surface pore area increased in both the 20% and 35% scaffolds (Fig. 2a, b). In the 20% scaffolds, pore size increased from 8.3±2.3 μm^2 to 27.6±5.0 μm^2 ($p<0.0001$), and from 19.5±5.4 μm^2 to 43.5±10.2 μm^2 ($p<0.0001$) in the 35% scaffolds. Mechanical properties were lower for the scaffolds created with PEG fibers (&PEG) (~2-3MPa), compared to the scaffolds created without PEG (~4-5MPa) (Supplementary Fig. 2a-c). This reduction in mechanical properties could be due to less inter-fiber linking in the scaffolds created with PEG fibers. We then analyzed the migration of hMSCs through 50 µm thick scaffolds 4 days after seeding. Interestingly, for both the 20% and 35% scaffolds, no difference in cell infiltration was found between the scaffolds created with or without PEG. Similar cell numbers were found on the bottom of both 35% scaffolds (35% and 35% &PEG), while very few cells were found on the bottom of the both 20% scaffolds (20% and 20% &PEG).

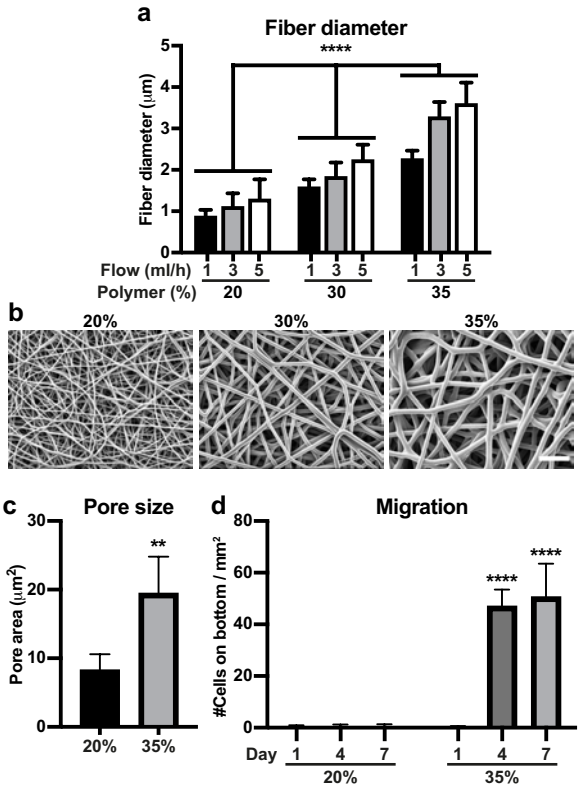

Figure 1. Optimizing fiber diameter and scaffold porosity for cell migration. a, Different concentrations of 300PEOT45PBT55 (w/v) were electrospun at different flow rates. Significance indicates differences between polymer concentrations at the same flow rate. **b,** SEM images of 20%, 30% and 35% (w/v) 300PEOT45PBT55 concentration spun at 3 ml/h. Scalebar 20 μm. **c,** Estimation of pore size on the surface of the ESP scaffolds, analyzed from SEM images (average of 10-20 pores from 10 different images). **d,** Number of hMSCs on the bottom of 20% or 35% (w/v) 300PEOT45PBT55 scaffolds 1, 4 or 7 days after cell seeding on top of the scaffolds. Cells were counted on 5 different images of each of 3 scaffolds. Significance indicates statistical differences between 35% day 1, and the same day of 20%. **b, d,** One-way Anova and **c,** Student's t-test. ** $p<0.01$, **** $p<0.0001$. Error bars indicate mean±SD.

Guided migration reveals differences between scaffolds created with or without sacrificial fibers

To further investigate the differences between the 35% scaffolds created with or without sacrificial fibers and to investigate the limits of cell infiltration, we created scaffolds with thicknesses of 50, 100 and 150 μm. Scaffolds were placed on the bottom of a normal cell culture well, as with the previous migration experiments, or on top of a transwell. In the normal cell culture well, cells migrated to the bottom of the 50 μm scaffolds and no difference was found between the 35% and 35% &PEG scaffolds(Fig. 3a). No hMSCs migrated to the bottom of 100 μm or 150 μm thick scaffolds. In the transwell system, medium

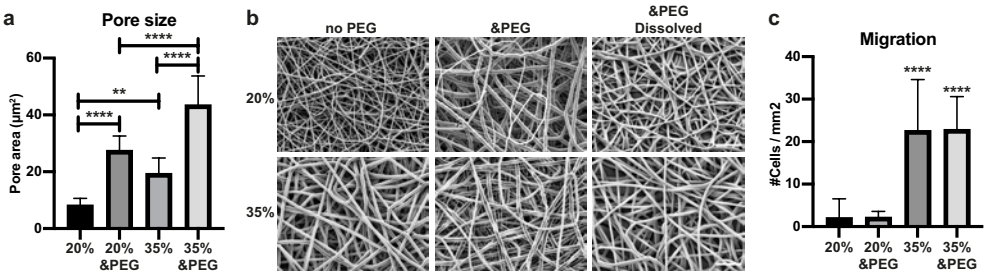

Figure 2. Improving scaffold porosity using a sacrificial polymer. a, Estimation of pore size on the surface, or **b,** SEM images, of ESP scaffolds created with 20% or 35% (w/v) 300PEOT45PEG55 with or without a second needle spinning a mixture of high and low Mw PEG. The PEG fibers were later dissolved in water. Analyzed from SEM images (average of 10-20 pores from 10 different images). Scalebar 20 µm. **c,** Number of hMSCs on the bottom of the different scaffolds 4 days after cell seeding on top of the scaffolds. Cells were counted on 5 different images of each of 3 scaffolds. Stars indicate significant difference with both 20% and 20% &PEG. **a, c,** One-way Anova. ** p<0.05, **** p<0.0001. Error bars indicate mean±SD.

containing FBS was put in the bottom compartment and medium without FBS was put in the top compartment, creating a gradient to guide cell migration. Medium was refreshed every day to maintain the FBS gradient and the bottom of the scaffolds was analyzed after 4 days of migration. Interestingly, cells were found at the bottom of the 100 µm thick 35% scaffolds (Fig. 3b). Still, no cells migrated to the bottom of the 150 µm thick 35% scaffolds. In the 35% scaffolds created with PEG fibers, migration to the bottom of the scaffolds was increased for all thicknesses, compared to 35% scaffolds. Also, many cells were found on the bottom of the 150 µm thick scaffolds. These results show that the FBS gradient guided cell migration towards the bottom of the scaffold. This method revealed the differences in the scaffolds' ability to allow infiltration. In addition, this novel method could be used to increase cell infiltration of ESP scaffolds, or as a tool to study cell migration through a fibrous mesh.

Nano-CT analysis does not explain differences in scaffold infiltration

It is not fully understood what key aspects of an electrospun scaffold allow deep cell infiltration. To better describe our scaffolds, we analyzed the 20% and 35% scaffolds created with or without PEG fibers with nano-CT (Supplementary Fig. 3). Interestingly, the pore size distribution was different between the scaffolds with or without PEG, but not different between 20% and 35%, or between 20% &PEG and 35% &PEG (Fig. 4a). In the 20% and 35% scaffolds without PEG, most pores were in the 5 µm diameter range, while both scaffolds with PEG had many pores with 10-15 µm diameter. The volume and percentage of closed pores was significantly reduced in the 20% &PEG, 35% and 35% &PEG scaffolds, compared to the 20% scaffold (Fig. 4b, c). However, the percentage of closed pores was lower than 0.0005% of total volume in all scaffolds, so unlikely to greatly affect the cell migration. Lastly, the total pore volume and porosity was slightly higher in the 20% &PEG and 35% &PEG scaffolds, but all scaffolds had a porosity of around 70-80% (Fig. 4d, e). While a big difference

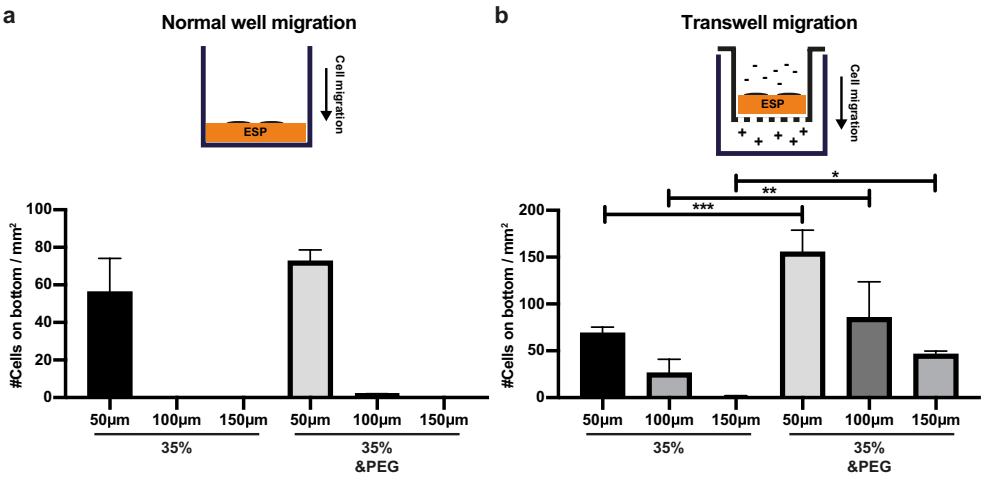

Figure 3. Migration through ESP scaffolds with and without cytokine attraction. a, b hMSCs on bottom of 50, 100 or 150 µm thick ESP scaffolds, created with or without sacrificial PEG fibers, 4 days after seeding on top of the scaffolds. Cells were counted on 5 different images of each of 3 scaffolds. **a,** hMSCs were seeded on top of an ESP scaffold in the bottom of a normal 48-well cell culture well with medium containing FBS on top. **b,** hMSCs were seeded on top of an ESP scaffold placed inside a 3 µm transwell system, with medium without FBS on top and medium with FBS in the bottom compartment. One-way Anova. * p<0.05, ** p<0.01, *** p<0.001, **** p<0.0001. Error bars indicate mean±SD.

in cell infiltration was found between the different scaffolds (Fig. 2c, Fig. 3a, b), no correlation was found with the nano-CT results. This highlights that porosity and pore size alone cannot explain the ability of an electrospun scaffold to allow cell infiltration.

Full cell infiltration and tissue formation in subcutaneously implanted scaffolds

To further test the ability of the ESP scaffolds to allow for cell infiltration, we implanted 300 µm thick 35% and 35% &PEG scaffolds in subcutaneous pockets of immunodeficient rats. We seeded the scaffolds with hMSCs and compared to cell-free scaffolds, to see the effect of the hMSCs on tissue infiltration. After 3 weeks, cells were present throughout the whole thickness of all scaffolds (Fig. 5a, b). The amount of tissue formation, however, was significantly increased in the 35% &PEG scaffolds, compared to the 35% scaffolds (Fig. 5c). Around 50% of the 35% &PEG scaffolds was filled with *de novo* tissue, compared to ~25% in the 35% scaffolds. No difference was found between hMSC-seeded scaffolds and cell-free scaffolds. After 6 weeks, the differences were even more pronounced, and tissue formation increased for both the 35% and 35% &PEG scaffolds, compared to 3 weeks. The 35% &PEG scaffolds were on average filled with >80% tissue, compared to the <50% of the 35% scaffolds. Again, no difference was found between cell-laden and cell-free scaffolds. Interestingly, the thickness of all scaffolds significantly increased after implantation. While 300 µm thick scaffolds were implanted, scaffolds were up to 2 mm thick after explantation (Supplementary Fig. 4). No significant differences in scaffold thickness were found between

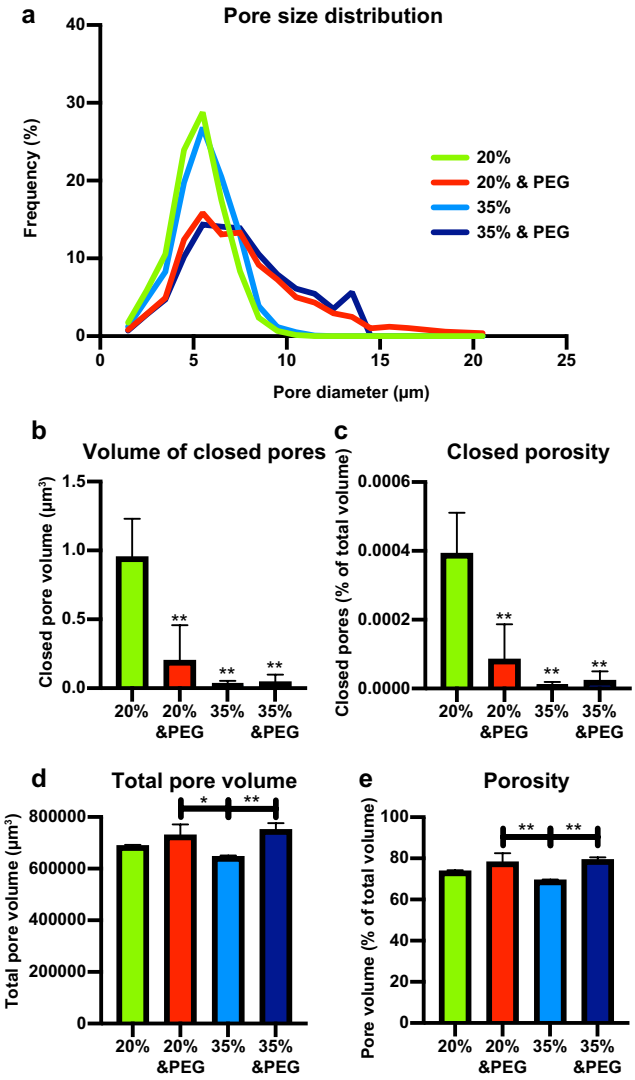

Figure 4. Nano-CT analysis of the ESP scaffolds. 20% and 35% 300PEOT45PBT55 scaffolds, created with or without sacrificial PEG fibers, were analyzed with nano-CT for **a,** pore size distribution, **b,** closed pore volume and **c,** closed porosity, **d,** total pore space and **e,** porosity. n=3 scaffolds for each condition.

3- and 6 weeks post-implantation, nor between different scaffold types, with or without cells. All groups averaged between 1.1 and 1.5 mm. This shows that these scaffolds allowed for great cell infiltration and tissue formation to up to 2 mm, something not previously reported for electrospun scaffolds.

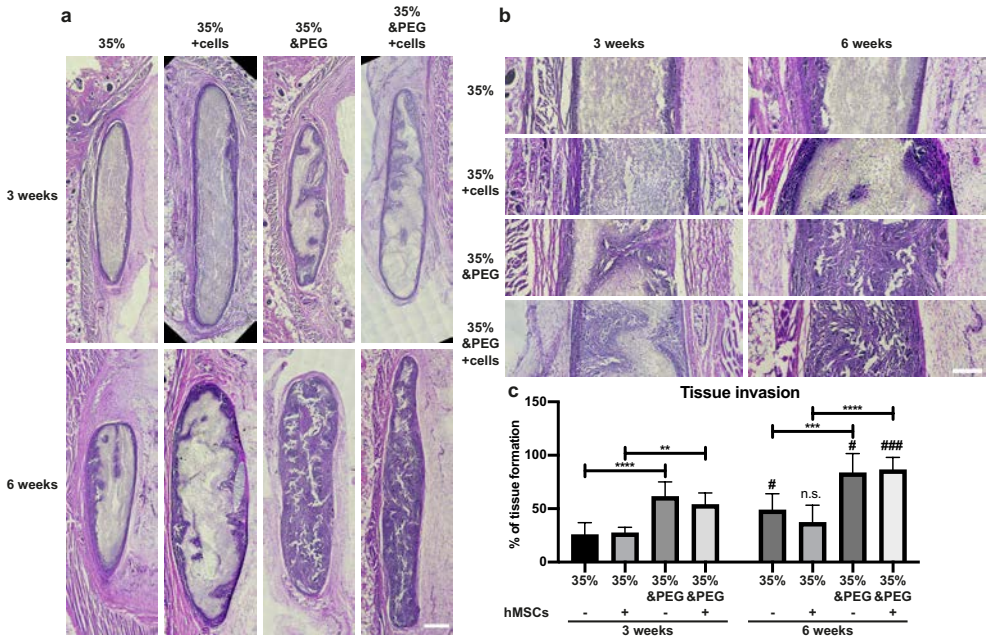

Figure 5. Cell infiltration and tissue formation of subcutaneously implanted ESP scaffolds. a, 35% 300PEOT45PBT55 scaffolds, created with or without sacrificial PEG fibers, were implanted in subcutaneous pockets and analyzed for infiltration after 3 (top panels) or 6 (bottom panels) weeks. Scaffolds were seeded with hMSCs 24h prior to implantation and compared to scaffolds without cells. Scalebar 500 µm. **b,** Detail of the ESP scaffolds from the respective images in **a**. **c,** Quantification of tissue formation in the different scaffolds 3- and 6 weeks post-implantation. Asterisks indicate statistical difference between the indicated groups. Number signs indicate differences between 3- and 6 weeks of the same scaffold type. n=6-8 rats for each group. One-way Anova. ** p<0.01, *** p<0.001, **** p<0.0001. Error bars indicate mean±SD.

Discussion

Scaffold porosity was optimized here by combing two established methods, e.g. increasing fiber diameter and adding sacrificial polymer fibers[12, 13, 17-20]. The Nano-CT analysis revealed differences in overall porosity, closed porosity and pore size distribution, but did not correlate with the scaffolds' performance on the cell migration tests. This showed that these parameters do not fully describe the essential properties of ESP scaffolds that allow cells to migrate through them. Other attributes likely describe this better, such as the minimal pore size of a series of interconnected pores, and the complexity of this maze. We have recently shown that hMSCs coming from electrospun scaffolds can migrate through 3 µm pores[22]. The minimal pore size that cells can migrate through in electrospun scaffolds could be in a similar range. However, even using nano-CT, these scaffold attributes are difficult to quantify. Novel algorithms and imaging techniques could improve this, greatly aiding ESP scaffold optimization and characterization.

Other reports have also shown robust ESP infiltration *in vitro* and *in vivo*. This includes the use of salt crystals[14], ice crystals[15, 16] PEG fibers[18], and PEG microparticles[20] and wet spinning[23]. Infiltration of 150 µm, as we've demonstrated here, has been achieved by the addition of salt crystals after 3 weeks of culture[14]. However, we report 150 µm infiltration already after 4 days. Other reports demonstrate limited cell infiltration of 50-100 µm[15, 16, 18, 24]. 150 µm infiltration *in vitro* using PEG fibers has not been previously reported, but using PEG microparticles, 400 µm infiltration of fibroblasts was achieved after 4 days of culture[20]. However, different cell types have different migration properties[21] and hMSCs have not been previously shown to deeply infiltrate an ESP scaffold in only 4 days, as we have shown. ~250 µm infiltration of hMSCs after 3 weeks of culture has been reported[25].

Dynamic seeding of ESP scaffolds has resulted in the filling of 2.5 mm scaffolds *in vitro*[23]. This cannot be considered cell infiltration but could be a useful tool to increase cell distribution in ESP scaffolds before seeding. The transwell method presented here can also be used to increase cell infiltration before implantation. In addition, this method could be used to study cell migration through fibrous meshes. Cell migration is often studied in 2D, or in 3D hydrogels[21]. However, natural ECM is a fibrous matrix with fiber diameters ranging from nano- to micrometer sized fibers[1-3]. ESP scaffolds could be an interesting tool to study 3D migration, more closely mimicking the natural ECM.

Several attempts have previously been made to improve scaffold infiltration *in vivo*. Many ESP scaffolds only allow limited infiltration of 200-400 µm[15, 16]. Using PEG fibers, others have shown infiltration of tissue up to 1 mm[17, 19]. The greatest infiltration of tissue in ESP scaffolds reported in literature is of 1.3 mm thick scaffolds, using PEG microparticles[20]. Here, we report infiltration of ESP scaffolds of up to 2 mm thick *in vivo*. The increase in size from 300 µm thick scaffolds upon implantation to 1-2 mm thick after 3 weeks could be attributed to cell infiltration and tissue formation that expand the scaffold. Seeding cells in a thinner scaffold that will later expand could be beneficial, as cells can be distributed through a 300 µm thick scaffold more easily than a thicker scaffold. The expansion in size would still allow for a thick layer of tissue to form. Others have also reported a slight change in scaffold size after implantation[19], but not as significant of an increase as we report here. Scaffold properties such as fiber stiffness and strength of inter-fiber connections could, among others, potentially influence this expansion in size. Further research into this phenomenon could improve the tissue engineering approaches utilizing ESP scaffolds.

Here, we show the optimization of ESP scaffold porosity using an increase in fiber diameter and sacrificial PEG fibers. We propose a novel *in vitro* method to research cytokine-attracted 3D migration through fibrous meshes. Also, the ESP scaffolds created here allowed for cell infiltration *in vivo* of up to 2 mm, a thickness that has not previously been reported for ESP scaffolds.

Materials and Methods

Scaffold production

Electrospun (ESP) scaffolds were produced using the 300PEOT55PBT45 (PolyVation) polymer. 300PEOT55PBT45 was made by PolyVation from a starting 300 kDa poly(ethylene glycol) in the synthesis reaction, with a PEOT/PBT weight ratio of 55/45. A 20, 30 or 35% (w/v) 300PEOT55PBT45 solution was prepared in a mixture of 30% (v/v) 1,1,1,3,3,3-Hexafluoro-2-propanol AR (HFIP) (Bio-Solve) and 70% (v/v) Chloroform (Sigma-Aldrich) and dissolved under agitation overnight at room temperature. The PEG solution was 1.5% poly(ethylene oxide) (PEO) (Mw: 900,000 Da, Sigma-Aldrich) and 50% PEG (Mw: 3350 Da, Sigma-Aldrich) in a mixture of 25% (v/v) milliQ water and 75% (v/v) methanol (Sigma-Aldrich). Unless stated otherwise, the processing parameters for 300PEOT55PBT45 were: 3 ml/h flow rate, 15 cm working distance, 40% humidity and 23-25˚ C. The needle of both the 300PEOT55PBT45 and PEG were charged between 10-25 kV. The collector was charged between -1 and -10 kV. For the PEG solution, the flowrate was 3 ml/h and 25 cm working distance. For *in vitro* analysis, ESP scaffolds were produced on a 19 cm diameter mandrel at 100 RPM rotation on a polyester mesh (FinishMat 6691 LL (40 g/m^2), generously provided by Lantor B.V.) with 8 mm diameter circular holes, on top of aluminum foil. After electrospinning, the aluminum foil was removed and circular ESP scaffolds were punched out with a diameter of 12 mm. Using this method, 12 mm ESP scaffolds were produced with a surrounding 1.5 mm polyester support ring to improve handleability. Unless stated otherwise, the ESP scaffolds used for *in vitro* analysis were 50 µm thick. Different thicknesses were prepared by increasing the spinning time. Thickness was analyzed by cutting scaffolds in liquid nitrogen and analyzing the cross-section with SEM. The scaffolds for *in vivo* implantation were 300 µm thick and were produced on aluminum foil, without the polyester mesh. The aluminum foil was removed and discs were punched out with an 8 mm diameter. To dissolve the PEG solution, the scaffolds (and the 300PEOT55PBT45 only scaffolds to which they were compared) were incubated overnight in milliQ water at 50 ˚C. The next day, scaffolds were washed 5 times with water.

For sterilization for *in vitro* experiments, ESP scaffolds were submerged in 70% ethanol for 15 min and subsequently dried until visually dry. For sterilization for *in vivo* experiments, scaffolds were submitted to 254 nm UV light for 2 hours in vacuum.

Pore and fiber size quantification

Fiber size and pore area were manually measured using a custom-built Fiji script. 10-20 fibers or pores were selected in 5 different images of at least 2 different scaffolds. For pore area analysis, high contrast images were taken to create a dark background of pores deeper than a few fiber layers. The pore area of these pores on the surface of the scaffolds were measured in the biggest pores in each image.

Nano-CT

Nano-CT scans were recorded on a SkyScan 2211 high-resolution X-Ray nanotomograph (Bruker MicroCT, Belgium). The membranes were fixed on the sample holder with dental clay. All samples were scanned in nanofocus mode, using a CCD camera with a resolution of 4032 x 2688 and a pixel size of 0.5 µm. The source voltage and current were set at 30kV and 450 µA, respectively. The images were registered with a rotation step of 0.1 ° and an averaging of 4 frames at an exposure time of 1300 ms, resulting in a scanning time of approximately 5 hours for each sample. The resulted cross-sections were processed using CT NRecon software and subsequently reconstructed using CTVox. DataViewer software was used for analyzing the projections of the samples. CTAn software was used in order to obtain quantitative data regarding the porosity and wall thickness distribution of the analyzed samples. The analysis was performed in triplicate, on equal volumes of interest (VOI). All scanning, reconstruction, visualization and analysis parameters were kept constant for the analyzed samples.

Mechanical tests

The traction tests were performed using a Brookfield CT3 texture analyzer equipped with a 4500 g cell and a dual grip assembly (TA-DGA). The samples were cut at approximately 60 x 15 mm and tested at a speed of 0.5 mm/s, at room temperature. All measurements were performed in triplicate. A stress versus strain graph was plotted using the dedicated software and Young's modulus was computed from the slope of the linear part of the traction curve, at 2% strain.

Cell culture

Bone marrow was isolated from a 22-year old male by aspiration by Texas A&M Health Science Center after ethical approval from the local and national authorities and written consent from the donor. Mononuclear cells were separated by centrifugation. Human mesenchymal stem cells (hMSCs) were subsequently isolated as described previously[26]. Isolated hMSCs were received at passage 1 and tested for trilineage differentiation capacity. hMSCs were further expanded by seeding at 1000 cells/cm^2 in tissue culture flasks in αMEM+Glutamax medium (Thermo Fisher Scientific) supplemented with 10% (V/V) fetal bovine serum (FBS) (Sigma-Aldrich) (basic medium) at 37 °C in 5% CO_2. Cells were passaged at 70-80% confluency using 0.05% Trypsin and 0.53 mM EDTA (Thermo Fisher Scientific) and seeded on the ESP scaffolds at passage 5.

Cell migration quantification in vitro

To analyze cell infiltration, ESP scaffolds were placed in the bottom of a 48 well, or a 12mm transwell with 3 µm pores in a polyester membrane insert (Corning). Rubber O-rings (outer diameter 12 mm, inner diameter 8 mm, Eriks) were placed on top of the scaffolds to prevent

cells from reaching the bottom in any other way than through the ESP scaffolds. 15,000 hMSCs were then seeded on top of the scaffolds in basic medium and cultured for 4 days, unless stated otherwise. For the samples on transwells, 24 hours after seeding, medium in the top compartment was changed to medium without FBS and basic medium in the bottom. The medium was changed every 24 hours to sustain an FBS gradient. Cells were fixed with 3.6% (v/v) paraformaldehyde (Sigma-Aldrich) in PBS at room temperature for 20 minutes. DAPI (Sigma-Aldrich, 0.14 µg/ml in PBS+0.05% (v/v) tween-20) was then used to visualize the cells. Quantification of cells was done in 5 separate images of each of 3 different scaffolds.

In vivo subcutaneous implantation

All experiments and protocols were approved by the Dutch Central Committee for Animal Experiments (in Dutch: Centrale Commissie Dierproeven). Female rats were obtained (Crl:NIH-Foxn1rnu, 8-10 weeks old, 140-212g) (Charles-River) and housed at 21 °C with a 12 h light/dark cycle and had ad libitum access to water and food. Prior to anesthesia, buprenorphine 0.05 mg/kg bodyweight and carprofen 4 mg/kg were administered as premedication. The animals were subsequently anesthetized with isoflurane 3-4% (v/v) for induction, and isoflurane 2% (v/v) for maintenance, adjusted according to the clinical signs during surgery. After shaving, disinfection and draping of the animal's dorsum, four 1 cm long linear skin incisions parallel to the spine were made, two on each side. Four subcutaneous pockets of maximum 10 mm x 10 mm were created. ESP scaffolds, 8mm diameter, that had been seeded on both sides of the scaffold 24h prior to implantation with a total of 15,000 hMSCs, were carefully placed inside the pockets. Scaffolds were randomly assigned to a pocket. After implantation, the skin was closed intracutaneously with Monocryl 4x0 sutures (Ethicon). Buprenorphine 0.03 mg/kg bodyweight was administered 8 hours after surgery. The morning of post-operative day 1 and 2, each animal was administered a dose of 4 mg/kg bodyweight carprofen. Thereafter, animal welfare was evaluated on a daily basis with a discomfort logbook scoring system, and appropriate medication was given only when needed. After 3- and 6 weeks, the animals were euthanized with gradual CO_2 overdose. The sample and surrounding tissues were collected and processed for histology. No animal was lost during this study.

Tissue preparation and infiltration quantification

3- or 6-weeks post-implantation, skin samples containing the scaffolds were explanted. Tissue explants were cut with surgical scissors to fit the dimensions of the silicon molds (2x2x2 cm), without disrupting the generated pocket that contained the implants. Samples were then placed in 50 mL centrifugation tubes and fixed for 24h at 4 °C in a 3.6% (v/v) solution of paraformaldehyde in TBS (tris-buffered saline). After fixation, the samples were transferred to new tubes and underwent embedding in a series of 30% (w/v) sucrose, then 50:50 volume ratio of 30 % sucrose and optimal cutting temperature compound (OCT)

(Thermo Fisher Scientific), and lastly OCT only for 24h each. The samples were maintained in OCT until freezing. Tissue explant were placed inside silicon molds and the molds were filled with OCT. Freezing was conducted on the liquid-vapor interface of a liquid nitrogen tank to avoid formation of bubbles. Cross-sections of 7 µm thick were cut on a cryotome and samples were stained with hematoxylin and eosin (H&E). Sections were hydrated in de-ionized water and placed in Gill's hematoxylin (III) (Sigma-Aldrich) for 5 min, in running water for 5 min, dehydrated and counterstained with alcoholic Eosin Y (Sigma-Aldrich) for 1 min. Sections were differentiated in 100% ethanol, allowed to air dry and mounted in DPX (Sigma-Aldrich). The percentage of tissue infiltration was quantified by measuring the area of infiltrated tissue in the scaffold, divided by the total area of the scaffold. The infiltrated area was defined as clear dark staining in the H&E staining of the sections, where cells were surrounded by ECM. Areas where cells were present, but individual cells could still be distinguished without ECM formation in between, were considered non-infiltrated. This was measured in sections of 6-8 different scaffolds per condition.

Statistical analysis

The number of replicates is stated in the figure subtexts. Quantification of fiber diameter was done on randomly selected fibers. Pore area quantification was done on the biggest pores in each image. Scaffolds from each condition were randomly assigned to a pocket for *in vivo* implantation. Normal distribution of each experimental group was tested with the Shapiro-Wilk test. Statistical significance was tested with a One-way ANOVA with Tukey's post hoc for experiments with multiple comparisons, or two-tailed student's t-test for experiments with one comparison. GraphPad Prism 8 was used to perform statistical analysis and significance was set at $p<0.05$.

Acknowledgements

We are grateful to the European Research Council starting grant "Cell Hybridge" for financial support under the Horizon2020 framework program (Grant #637308). Some of the materials that were used in this work were provided by the Texas A&M Health Science Center College of Medicine Institute for Regenerative Medicine at Scott & White through a grant from NCRR of the NIH (Grant #P40RR017447). The nano-CT analyses were possible due to European Regional Development Fund through Competitiveness Operational Program 2014-2020, Priority axis 1, ID P_36_611, MySMIS code 107066, INOVABIOMED. This research has been made possible with the support of the Dutch Research Council (NWO, Grant #16711) and the Dutch Province of Limburg (LINK project).

References

1. B.M. Baker and C.S. Chen, Deconstructing the third dimension: how 3D culture microenvironments alter cellular cues. J Cell Sci, 2012. **125**(Pt 13): p. 3015-24.
2. A. Pathak and S. Kumar, Biophysical regulation of tumor cell invasion: moving beyond matrix stiffness. Integr Biol (Camb), 2011. **3**(4): p. 267-78.
3. J.A. Pedersen and M.A. Swartz, Mechanobiology in the third dimension. Ann Biomed Eng, 2005. **33**(11): p. 1469-90.
4. T.J. Sill and H.A. von Recum, Electrospinning: applications in drug delivery and tissue engineering. Biomaterials, 2008. **29**(13): p. 1989-2006.
5. S.P. Zhong, Y.Z. Zhang, and C.T. Lim, Tissue scaffolds for skin wound healing and dermal reconstruction. Wiley Interdiscip Rev Nanomed Nanobiotechnol, 2010. **2**(5): p. 510-25.
6. B. Kong and S. Mi, Electrospun Scaffolds for Corneal Tissue Engineering: A Review. Materials (Basel), 2016. **9**(8).
7. G. Li, S. Shi, S. Lin, T. Zhou, X. Shao, Q. Huang, B. Zhu, and X. Cai, Electrospun Fibers for Cartilage Tissue Regeneration. Curr Stem Cell Res Ther, 2018. **13**(7): p. 591-599.
8. K.A. Rocco, M.W. Maxfield, C.A. Best, E.W. Dean, and C.K. Breuer, In vivo applications of electrospun tissue-engineered vascular grafts: a review. Tissue Eng Part B Rev, 2014. **20**(6): p. 628-40.
9. E. Biazar, M.T. Khorasani, N. Montazeri, K. Pourshamsian, M. Daliri, M. Rezaei, M. Jabarvand, A. Khoshzaban, S. Heidari, M. Jafarpour, and Z. Roviemiab, Types of neural guides and using nanotechnology for peripheral nerve reconstruction. Int J Nanomedicine, 2010. **5**: p. 839-52.
10. J. Wu and Y. Hong, Enhancing cell infiltration of electrospun fibrous scaffolds in tissue regeneration. Bioact Mater, 2016. **1**(1): p. 56-64.
11. J.M. Ameer, A.K. Pr, and N. Kasoju, Strategies to Tune Electrospun Scaffold Porosity for Effective Cell Response in Tissue Engineering. J Funct Biomater, 2019. **10**(3).
12. S. Soliman, S. Sant, J.W. Nichol, M. Khabiry, E. Traversa, and A. Khademhosseini, Controlling the porosity of fibrous scaffolds by modulating the fiber diameter and packing density. J Biomed Mater Res A, 2011. **96**(3): p. 566-74.
13. Y.M. Ju, J.S. Choi, A. Atala, J.J. Yoo, and S.J. Lee, Bilayered scaffold for engineering cellularized blood vessels. Biomaterials, 2010. **31**(15): p. 4313-21.
14. J. Nam, Y. Huang, S. Agarwal, and J. Lannutti, Improved cellular infiltration in electrospun fiber via engineered porosity. Tissue Eng, 2007. **13**(9): p. 2249-57.
15. M.F. Leong, W.Y. Chan, K.S. Chian, M.Z. Rasheed, and J.M. Anderson, Fabrication and in vitro and in vivo cell infiltration study of a bilayered cryogenic electrospun poly(D,L-lactide) scaffold. J Biomed Mater Res A, 2010. **94**(4): p. 1141-9.
16. M.F. Leong, M.Z. Rasheed, T.C. Lim, and K.S. Chian, In vitro cell infiltration and in vivo cell infiltration and vascularization in a fibrous, highly porous poly(D,L-lactide) scaffold fabricated by cryogenic electrospinning technique. J Biomed Mater Res A, 2009. **91**(1): p. 231-40.
17. B.M. Baker, R.P. Shah, A.M. Silverstein, J.L. Esterhai, J.A. Burdick, and R.L. Mauck, Sacrificial nanofibrous composites provide instruction without impediment and enable functional tissue formation. Proc Natl Acad Sci U S A, 2012. **109**(35): p. 14176-81.
18. A. Guimaraes, A. Martins, E.D. Pinho, S. Faria, R.L. Reis, and N.M. Neves, Solving cell infiltration limitations of electrospun nanofiber meshes for tissue engineering applications. Nanomedicine (Lond), 2010. **5**(4): p. 539-54.
19. J. Voorneveld, A. Oosthuysen, T. Franz, P. Zilla, and D. Bezuidenhout, Dual electrospinning with sacrificial fibers for engineered porosity and enhancement of tissue ingrowth. J Biomed Mater Res B Appl Biomater, 2017. **105**(6): p. 1559-1572.

20. K. Wang, M. Xu, M. Zhu, H. Su, H. Wang, D. Kong, and L. Wang, Creation of macropores in electrospun silk fibroin scaffolds using sacrificial PEO-microparticles to enhance cellular infiltration. J Biomed Mater Res A, 2013. **101**(12): p. 3474-81.
21. K.M. Yamada and M. Sixt, Mechanisms of 3D cell migration. Nature Reviews Molecular Cell Biology, 2019. **20**(12): p. 738-752.
22. J. Zonderland, I.L. Moldero, C. Mota, and L. Moroni, Dimensionality changes actin network through lamin A and C and zyxin. bioRxiv, 2019: p. 752691.
23. W. Yang, F. Yang, Y. Wang, S.K. Both, and J.A. Jansen, In vivo bone generation via the endochondral pathway on three-dimensional electrospun fibers. Acta Biomater, 2013. **9**(1): p. 4505-12.
24. M.C. Phipps, W.C. Clem, J.M. Grunda, G.A. Clines, and S.L. Bellis, Increasing the pore sizes of bone-mimetic electrospun scaffolds comprised of polycaprolactone, collagen I and hydroxyapatite to enhance cell infiltration. Biomaterials, 2012. **33**(2): p. 524-34.
25. B.M. Baker, A.O. Gee, R.B. Metter, A.S. Nathan, R.A. Marklein, J.A. Burdick, and R.L. Mauck, The potential to improve cell infiltration in composite fiber-aligned electrospun scaffolds by the selective removal of sacrificial fibers. Biomaterials, 2008. **29**(15): p. 2348-58.
26. C.M. Digirolamo, D. Stokes, D. Colter, D.G. Phinney, R. Class, and D.J. Prockop, Propagation and senescence of human marrow stromal cells in culture: a simple colony-forming assay identifies samples with the greatest potential to propagate and differentiate. Br J Haematol, 1999. **107**(2): p. 275-81.

Supplementary Figures

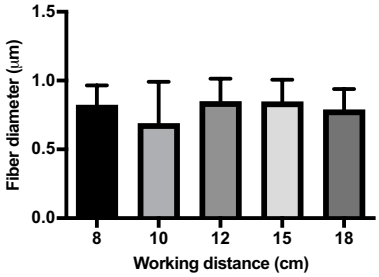

Supplementary Figure 1. Effect of working distance on fiber diameter. 20% (w/v) 300PEOT45PBT55 was spun at 1 ml/h at different distances from the collector.

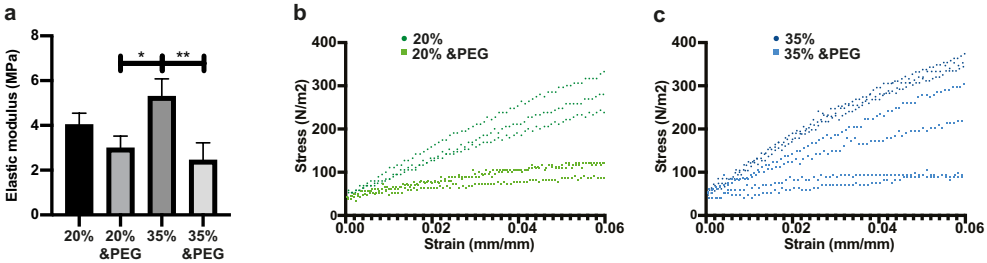

Supplementary Figure 2. Mechanical properties of ESP scaffolds. **a,** Tensile mechanical tests of 20% and 35% 300PEOT55PBT45 scaffolds, created with or without addition sacrificial PEG fibers. One-way Anova. * p<0.05, ** p<0.01. **b,** Individual data points of each replica in the first 6% strain of 20% and 20% &PEG and **c,** 35% and 35% &PEG. n=3 for 20%, 20% &PEG and 35%, n=4 for 35% &PEG.

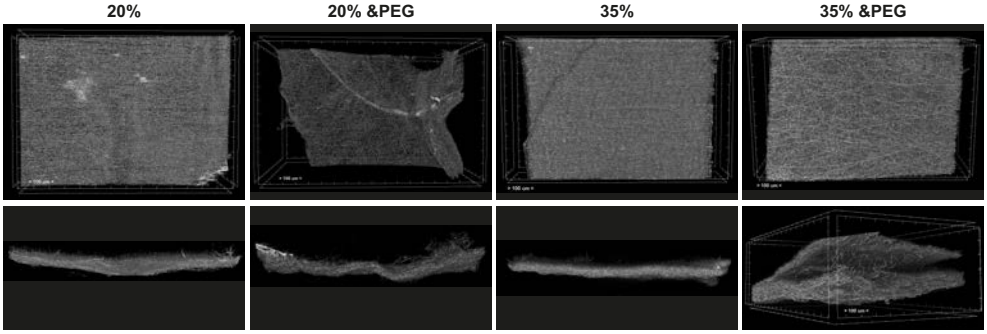

Supplementary Figure 3. Nano-CT images of the different scaffolds. Top view in the top panels and side view in the bottom panels. Delaminated areas were excluded from the measurements.

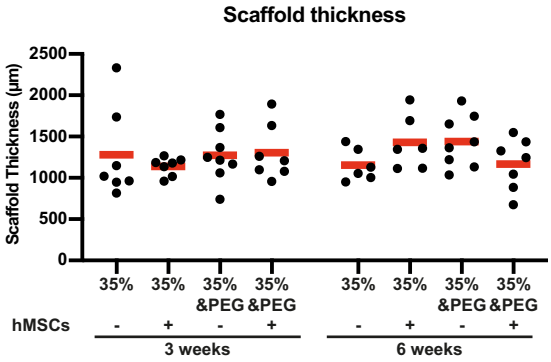

Supplementary Figure 4. Scaffold thickness after explantation. Scaffold thickness was measured at the thickest section of a cryotome section taken from a random spot in the scaffold. n=6-8 for all conditions. One-way ANOVA, no statistical differences between groups.

Chapter 7

Fiber diameter, porosity and functional group gradients in electrospun scaffolds

Jip Zonderland, Silvia Rezzola, Paul Wieringa, Lorenzo Moroni

Complex Tissue Regeneration Department, MERLN Institute for Technology-Inspired Regenerative Medicine, Maastricht University, Maastricht, the Netherlands.

Abstract

Developing, homeostatic, and regenerating tissues are full of various gradients, including mechanical, chemical, porosity and growth-factor gradients. However, it remains challenging to replicate these gradients using common tissue engineering approaches. Here, we use electrospinning to create scaffolds with in-depth gradients. We created a fiber diameter gradient and pore size gradient throughout the depth of electrospun scaffolds by a continuous gradient of polymer concentration. As an alternative to this established method, we developed a novel method to create fiber diameter gradients by changing the voltage on both needle and collector, keeping the total voltage constant. In this way, fiber diameter could be changed in a gradient matter by focusing the electrospinning spot. Using this method, we created a fiber diameter and pore size gradient, while keeping all other parameters constant. Lastly, we developed a novel method to create functional group gradients, which can potentially be used in a wide variety of polymer solutions to couple peptides and proteins to ESP scaffolds. A scaffold with an in-depth gradient of functional groups was created by adding functionalized PEG-additives to the polymer solution, a novel method with potentially wide applications. The techniques demonstrated here could be applied to a wide variety of polymers and applications and can aid in developing physiologically relevant gradient scaffolds.

Introduction

Embryonic and tissue development is steered largely through gradients[1-3]. In adult tissues, gradients are still present in, for example: cell distribution, extra-cellular matrix (ECM) proteins, physical properties and growth factors[4-8]. Regenerating tissues also use gradients in ECM remodeling and excreted growth factors[9-12]. The manufacturing of scaffolds with physiological properties has been the interest of tissue engineering researchers for the past decades. Mimicking these physiological gradient properties for tissue engineering could greatly benefit tissue function and regeneration. The creation of a wide variety of synthetic materials and isolation and characterization of biological materials allows researchers to pick materials that match the desired material properties. Also, many different proteins, peptides and minerals have been added to these materials to steer cell behavior. However, incorporating gradients in tissue engineering constructs remains challenging.

Several properties of a cell's surrounding have been shown to greatly influence cell behavior. Mechanical properties are an important factor of the cellular surroundings[13, 14]. Proliferation, differentiation, ECM production and migration have all been shown to change in response to substrate stiffness. Many different cell types have been shown to proliferate more on stiffer substrates[15-22]. Mesenchymal stromal cells are more inclined to differentiate to bone on stiffer substrates, and more likely to commit to the adipose lineage on softer substrates[16, 23, 24]. However, these material properties are mostly exploited without gradients, while developing, homeostatic and regenerating tissues consist of a wide variety of gradients[1-12]. To better recapitulate the tissue, tissue engineering scaffolds can potentially be greatly improved by incorporating gradients.

Gradients in stiffness guide cell migration in a process called durotaxis, where cells move to stiffer substrates[25-27]. Indeed, electrospun (ESP) scaffolds with an in-depth stiffness gradient have been shown to improve cellular infiltration in the scaffolds[28]. Pore size is another important aspect of the extra cellular environment. Optimal pore size for differentiation and proliferation differs per cell type[29]. Additive manufactured scaffolds with a gradient in pore size have also been shown to influence cartilage matrix deposition and bone regeneration[30, 31]. Pore shape can also affect cell behavior, shape and orientation[32, 33]. Growth factors and adhesion molecules also play an important role in controlling cell behavior. Isotropic growth factor coupling is used in the tissue engineering field[34, 35], but the use of gradients to mimic the physiological conditions is underexplored due to technical difficulties to create gradients. Several established methods to create horizontal (side to side) fiber diameter and protein gradients have been developed[36-40]. In addition, in depth fiber diameter gradients have been developed by changing polymer concentration[28]. Here, we developed a novel method to create in-depth fiber diameter gradients using a gradual change in voltage. A univocal method to create in-depth protein gradients has not yet been described. We describe a method to create in-depth functional group gradients by the addition of functionalized PEG

that could be used to create multi-directional protein or peptide gradients in a wide variety of polymers.

Results

Creating bi-directional gradients in depth of ESP scaffolds

It remains challenging to replicate the gradients found *in vivo* in tissue engineering scaffolds. Layer by layer approaches have been reported in ESP scaffolds[41], but true in-depth gradients have not been widely reported in literature. An easy approach to create gradients in ESP scaffolds is using two syringe pumps with different solutions that feed into a single spinneret. As a proof of principle, we loaded one syringe with 300PEOT55PBT45 polymer solution and a green dye, and another with the polymer solution and a red dye. Over time, the flowrate of the first syringe was decreased, while the flowrate of the second syringe was increased, keeping the total flowrate equal (Fig. 1a). As expected, the green dye decreased in intensity over time, while the intensity of the red dye increased (Fig.1 b). Using this method, we created a scaffold with bi-directional gradients: high-low concentration of green dye, and a low-high concentration of red dye.

Fiber diameter and porosity gradient by changing polymer concentration over time

Adult tissues, such as cartilage and bone, are known to have a gradient in porosity[8, 42]. Mimicking such a gradient could potentially aid in capturing tissue properties and steering cell behavior. In ESP scaffolds, the fiber size and the pore size are inherently linked[43-50]. We have previously shown that increasing the polymer concentration from 20% (w/v) 300PEOT55PBT45 to 35% results in an increase in fiber diameter and pore size (Chapter 6), in line with reports for other polymers[43, 46, 49]. Thus, to create a fiber diameter and porosity gradient in an ESP scaffold, we increased the polymer concentration from 20% to 35% over the time of spinning. Using the double syringe pump setup, ESP scaffolds with a gradient in fiber diameter were produced (Fig. 2a). At the bottom, where a 35% (w/v) 300PEOT55PBT45 polymer solution was spun, 2.4 ± 0.2 µm fibers were formed. By reducing the flowrate of the syringe containing 35% 300PEOT55PBT45 and increasing the flowrate of the 20% 300PEOT55PBT45 containing syringe, an in-depth gradient in fiber diameter was created. At the top, where a 20% (w/v) 300PEOT55PBT45 polymer solution was spun, fibers of 1.0 ± 0.1 µm were formed (Fig. 2b and c). Pore area on the bottom, with larger fiber diameter, also increased significantly ($p<0.0001$), compared to the top, with smaller fiber diameter. This demonstrates that a gradient in fiber diameter and pore size could be created by decreasing polymer concentration over time.

Fiber diameter and porosity gradient by changing voltage over time

As an alternative method to modulate fiber diameter, we attempted to focus or scatter the electrospinning spot. We hypothesized that by focusing the spot size, fibers would have less

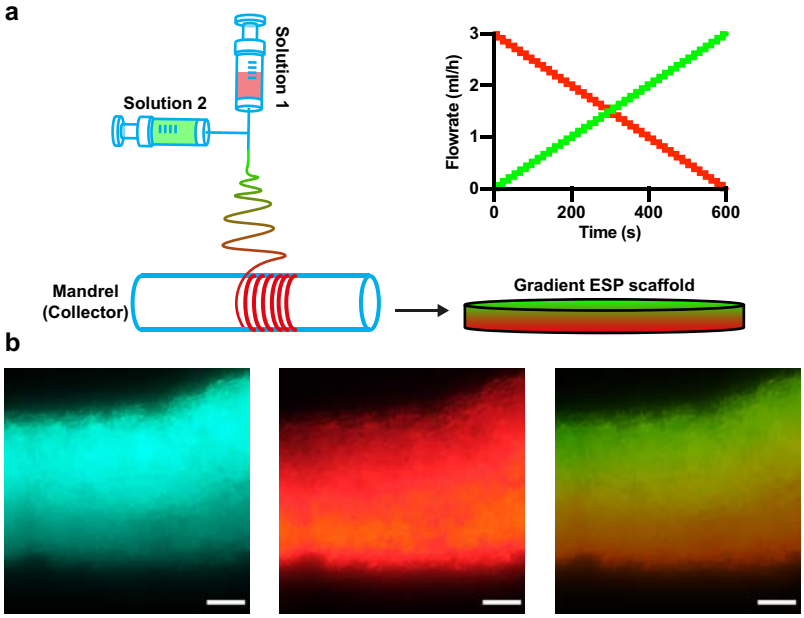

Figure 1. In depth gradient in ESP scaffolds. a, Schematic overview of electrospinning set up. Two syringes, one loaded with 300PEOT55PBT45 polymer solution and a green dye, the other with 300PEOT55PBT45 and a red dye. The solutions of each syringe flowed into a single tubing. The flowrates of each syringe were changed over time, increasing one while decreasing the other, keeping the total flow rate at 3 ml/h. **b,** Representative images of the cross-section of a scaffold with a high-low gradient of green dye (left) and a low-high gradient of red dye (middle). The right panel shows the merge of the green and red channel. Scalebars 250 µm.

time to stretch, thereby increasing the fiber diameter. Inversely, by increasing spot size we could stretch fibers more and decrease the fiber diameter. We hypothesized that by decreasing the voltage of the collector and the needle, we could focus the spinning spot. Indeed, by setting the collector voltage to -16 kV and the needle to 4 kV, the spinning spot size decreased to 32.5 ± 2.3 cm^2 (Fig. 3a). By setting the collector to 0 kV and the needle to 20 kV, we increased the spot size 4.8x to 156.6 ± 9.7 cm^2. Together with the change in spot size, a change in fiber diameter was observed. In the -16 kV charged collector condition, a scaffold with 3.2 ± 0.6 µm fibers was obtained (Fig. 3b). When the collector was left uncharged, a scaffold with 2.1 ± 0.4 µm fibers was produced. Together with fiber diameter, the pore size also increased (Fig. 3c, d). To create a gradient in fiber diameter throughout the ESP scaffold, we gradually increased both needle and collector voltage (Fig. 3f). Indeed, a scaffold with in-depth fiber diameter gradient was produced (Fig. 3e and g). This is the first time a voltage gradient is used to create an in-depth gradient scaffold. This method is likely to work for a wide variety of polymer solutions and is easy to implement in many different electrospinning setups. The elegance of this approach is that all parameters, such as polymer concentration and flowrate, are kept constant, which could be used as a tool to specifically investigate the effect of just fiber diameter.

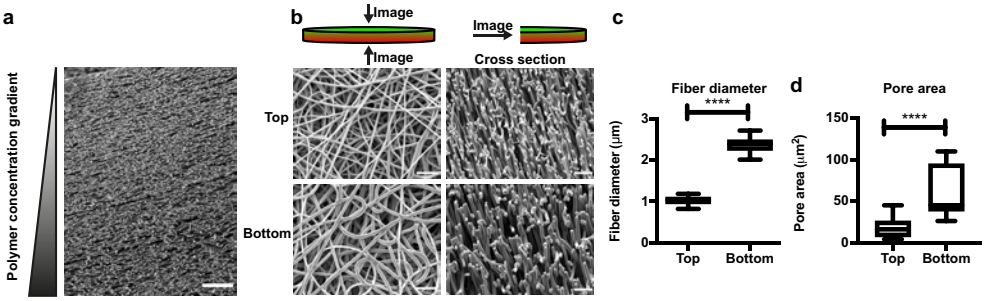

Figure 2. In depth fiber diameter gradient. a. Cross-section overview of fiber diameter gradient, made by a changing the polymer concentration over time with the two syringe set-up. Scalebar 80 µm. **b.** Top view (left panels) and cross section (right panels) of the bottom and top of the fiber diameter gradient scaffold. Scalebars 15 µm **c, d.** Quantification of fiber diameter (n=10-20) **(c)** and pore area (n=15) **(d)** of top and bottom of fiber diameter gradient scaffold. **c.** Students t-test. **d.** Mann-Whitney test ******** p<0.0001.

Functional group gradient

Besides mechanical and spatial cues, *in vivo* also many gradients of biological factors exist[9-11, 51-53]. To replicate this, we attempted to incorporate functional groups in the scaffold. Alkyne groups are a good candidate because they can be coupled very efficiently to an azide group by a copper-mediated click reaction. We have recently developed a method to present functional groups on the surface of ESP scaffolds by mixing low Mw PEG with a functional group in the polymer solution[54]. First, we tested whether different concentrations of PEG-alkyne added to the 300PEOT55PBT45 polymer solution would result in a different amount of alkyne groups at the surface of ESP scaffolds. After copper-mediated click reaction with a fluorescent azide dye, an increase in fluorescence was visible with increased PEG-Alk additive concentration (Fig. 4a). Even at 0.001% (w/v) slightly fluorescent fibers could be observed. The signal seemed to plateau around 1%. We also tested other functional groups: PEG-SH (Supplementary Fig. 1) and PEG-NH_2 (Supplementary Fig. 2) additives, which also increased the amount of available functional groups with increased concentration. To create a scaffold with an in-depth gradient of PEG-Alk, we loaded one syringe with 300PEOT55PBT45+2% PEG-Alk and the other one with 300PEOT55PBT45 alone. The flowrate of the first syringe was gradually decreased while the flowrate of the second syringe increased. After coupling the fluorescent azide dye, the in-depth alkyne functional group gradient was visualized (Fig. 4b). These experiments showed that it is possible to present different functional groups in a gradient matter on the surface of ESP fibers by adding the PEG-additives. These PEG-additives can potentially be mixed with a wide variety of polymer solutions.

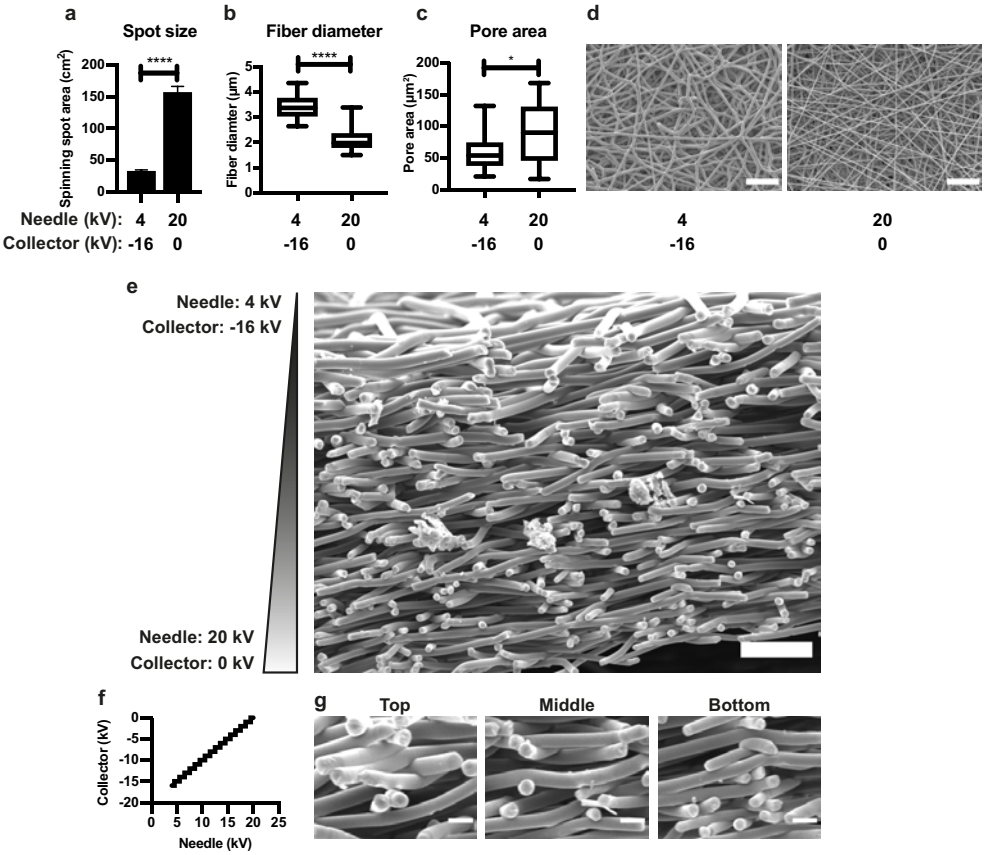

Figure 3. Fiber diameter gradient through voltage modulation. Electrospinning spot size (n=3) **(a)** fiber diameter (n=20) **(b)** and pore area (n=20-25) **(c)** quantified in scaffolds ESP with different voltages of needle and collector. Two tailed student's t-test **(a)** and Mann-Whitney test **(b, c)**, * p<0.05, **** p<0.0001. **d.** Examples of the resulting ESP scaffolds. Scalebars 50 µm. **e.** Cross-sectional overview of ESP scaffold with fiber diameter gradient created by changing the voltage of the needle and collector over time. Scalebar 25 µm **f.** Graph depicting the increase in needle and collector voltage over time. **g.** Detailed cross-sectional images of top (left panel), middle (middle panel) and bottom (right panel) of the voltage gradient scaffold. Scalebars 5 µm.

Discussion

We have used established technology and developed a new method to create in-depth gradients of fiber diameter and porosity in ESP scaffolds. A 300PEOT55PBT45 scaffold with a fiber diameter gradient going from 1 µm to approximately 2.4 µm was created by changing polymer concentration. Changing polymer concentration over the spinning time to create in-depth fiber diameter gradients has been reported previously[28, 55, 56]. Here, we have developed a novel method to create fiber diameter gradients. By gradually changing the needle and collector voltage over time, the electrospinning spot was focused and a gradient in fiber diameter was created from 2.1 µm to 3.2 µm. Changing the fiber diameter by using a

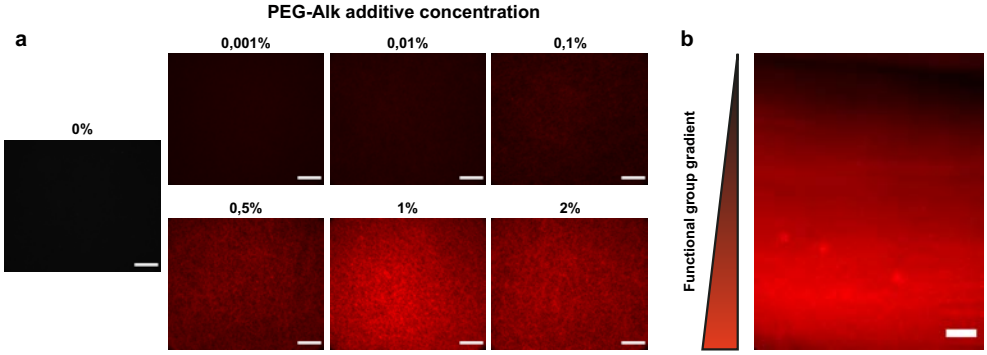

Figure 4. In depth functional group gradient. a. Fluorescent images of ESP scaffolds made with different concentrations of PEG-Alkyne additive, stained with fluorescent azide dye. Scalebars 250 µm. **b.** Cross section overview of ESP scaffold with PEG-alkyne gradient, stained with fluorescent azide dye. Scalebar 250 µm.

change in voltage over time has not yet been reported. The benefit of this novel method is that fiber diameter can be changed without changing other parameters, such as polymer concentration, allowing for the decoupling of different variables. In addition, this method could be combined with other methods, such as changing polymer concentration, to further in- or decrease the fiber diameter. Pore size has been optimized with a variety of methods, including a change in fiber diameter, but also incorporating sacrificial polymers or salt- or ice crystals[57-65]. Such methods could also be used in addition to the methods described here to further optimize pore size gradients.

In addition to the methods to create fiber diameter gradients, we created functional group gradients by adding functionalized PEG molecules to the polymer solution. While in-depth gradient of fiber diameter and pore size have been developed, as described above, in-depth functional group gradients in ESP scaffolds have not yet been reported. Methods to create functional group or protein gradients in the horizontal (side to side) direction have been developed[37, 38, 40], but these methods cannot be directly transferred to create in-depth functional group gradients. Here, we have developed a method to create in-depth functional group gradients that can potentially be used in a wide variety of polymer solutions. We've shown that different functional groups can easily be incorporated, including alkyne, thiol and amine groups. By coupling proteins or peptides to these functional groups, this method could be used to create multi-directional gradients for a wide variety of applications. An in-depth adhesive ligand gradient has been previously described[28], but the benefit of our method is that it could be univocally applied to a wide variety of proteins and peptides.

Together, these methods could be combined or used alone to create novel ESP gradient scaffolds. As regenerating tissues contain multiple forms of gradients, these scaffolds could potentially aid tissue engineering constructs for a wide variety of tissue engineering approaches. Regenerating or homeostatic tissues with gradients include nerve, heart, skin, bone and cartilage, among others[4-12, 66].

On top of the tissue-recapitulation capacity of gradient scaffolds, these scaffolds can also be used for optimizations, having a single scaffold to test a wide range of a single variable[31, 67]. Most cellular responses to gradients have been studied in 2D. A better understanding of how gradients affect cell behavior in 3D could also lead to smarter design of tissue engineering scaffolds. Both the voltage gradient method and the functionalized PEG method developed here are well suited for these kind of studies, because fiber diameter or protein incorporation can be changed while keeping other parameters equal.

Conclusion

In summary, we have created in-depth gradients of fiber diameter, porosity and functional groups in electrospun scaffolds. We have created a 300PEOT45PBT55 scaffold with a fiber diameter and pore size gradient using a change in polymer concentration, or a change in voltage. Also, we presented an easy way to create functional group gradients in a potentially wide range of polymer solutions, using PEG-Alkyne, -thiol or -amine additives. By changing the functional group on the PEG additive, a wide variety of functional groups can be presented in gradients on electrospun scaffolds. Together, the methods presented here could be used to create more physiologically relevant scaffolds with continuous physical and chemical gradients.

Materials and Methods

Electrospinning

300PEOT55PBT45 is a segmented block co-polymer of 300 Da poly(ethelyne oxide terephthalate) and poly(butylene terephthalate) with a PEOT/PBT weight ratio of 55/45 (PolyVation). 20% or 35% (w/v) 300PEOT55PBT45 was dissolved overnight under agitation at room temperature in a mixture of 70% Chloroform (Sigma-Aldrich) and 30% 1,1,1,3,3,3-Hexafluoro-2-propanol AR (HFIP) (Bio-Solve). Electrospinning was done using the Bioinicia Fluidnatek LE-100. For the dye and PEG additive experiments, a 20% polymer solution was used. For the fiber diameter gradient scaffolds, 20% and 35% 300PEOT55PBT45 were used. For the voltage gradient experiments, 35% 300PEOT45PBT was used. ESP scaffolds were produced on a 19 cm diameter mandrel rotating at 100 RPM to produce a large batch of scaffolds at the same time under exactly the same conditions. The following conditions were maintained: 15 cm working distance, 3 ml/h flow rate, 23-25 ˚C and 40% humidity. For the dye, polymer concentration and PEG additive experiments, the mandrel was uncharged and the needle was charged between 20-25 kV. For the voltage gradient scaffolds, the mandrel voltage was varied (see voltage gradient section). ESP scaffolds were collected on aluminum foil.

Flowrate gradient

In-depth gradients were created by increasing the flowrate of one syringe while decreasing the flowrate of the second syringe. To control the flowrate, a custom LabVIEW program was developed (Supplementary Fig. 3 and 4). The two syringes were connected in a 90˚ angle, with 1 m tubing after the connection point to ensure sufficient mixing of the two solutions. For the proof of concept experiment with fluorescent dyes, we mixed Macrolex fluorescent yellow 10G (Lanxess) and Macrolex fluorescent red G (Lanxess) at 1 mg/ml with the 20% 300PEOT45PBT polymer solution for 4 hours. The gradient was produced by changing the flowrates from 0-3 or 3-0 ml/h in 30 steps, over the course of 5 minutes. The polymer concentration gradient and PEG-Alk gradient were produced by changing flowrates in 40 steps over 10 minutes. The PEG-Alk, PEG-SH and PEG-NH_2 (Sigma-Aldrich) were all mixed for 4 hours before electrospinning. All PEG chains were 5000 Da with both ends functionalized. The PEG-Alk scaffolds were stained with 10 µg/ml azide Megastokes 673 (Sigma-Aldrich) in 2.5 mM copper sulfate (Sigma-Aldrich) and 25 mM sodium ascorbate (Sigma-Aldrich) in water overnight at room temperature. The PEG-SH scaffolds were stained with 10 µg/ml DyLight-488 (Thermo Fisher) overnight in PBS at room temperature. The PEG-NH_2 scaffolds were stained with 30 µg/ml fluorescamine (Sigma-Aldrich) in 10% acetone and 90% water for 5 min. After staining of each PEG-additive scaffold, scaffolds were washed 3x with water and imaged under the fluorescent microscope, or in the case of PEG-NH_2, quantified using the CLARIOstar™ platereader (BMG Labtech).

Voltage gradient

In-depth fiber diameter gradients were created by changing the voltage of both needle and collector. To control the voltage, a custom LabVIEW program was developed (Supplementary Fig. 5 and 6). In 17 steps (1 kV/step) over the course of 4 min, the voltage was changed from 4 kV on the needle and -16 kV on the mandrel to 20 kV and 0 kV, respectively.

Fiber and pore size quantification

Fiber diameter and pore area were quantified manually using a custom-built Fiji script. At least 3 different images of at least 2 different scaffolds were taken and around 20 fibers or pores were measured. To quantify pore area, images were acquired with high contrast to create a dark background within pores that were deeper than a few fiber layers. The pore area of these pores on the surface of the scaffolds were measured in the biggest pores in each image.

Statistical analysis

All data was tested for normal distribution using the Shapiro-Wilk test. Two-tailed student's t-test was performed for normally distributed samples and the Mann-Whitney test was used as non-parametric equivalent. Fiber diameter analysis was done using a custom-made macro in FIJI, while pore size was manually measured in the top layer of fibers, analyzing at least 20 fibers in 3 separate images.

Acknowledgments

We are grateful to the European Research Council starting grant "Cell Hybridge" for financial support under the Horizon2020 framework program (Grant #637308).

References

1. J.B. Gurdon and P.Y. Bourillot, *Morphogen gradient interpretation.* Nature, 2001. **413**(6858): p. 797-803.
2. J.L. Christian, *Morphogen gradients in development: from form to function.* Wiley Interdiscip Rev Dev Biol, 2012. **1**(1): p. 3-15.
3. J. Briscoe and S. Small, *Morphogen rules: design principles of gradient-mediated embryo patterning.* Development, 2015. **142**(23): p. 3996-4009.
4. C.A. Parent and P.N. Devreotes, *A cell's sense of direction.* Science, 1999. **284**(5415): p. 765-70.
5. A. Di Luca, C. Van Blitterswijk, and L. Moroni, *The osteochondral interface as a gradient tissue: from development to the fabrication of gradient scaffolds for regenerative medicine.* Birth Defects Res C Embryo Today, 2015. **105**(1): p. 34-52.
6. A.J. Sophia Fox, A. Bedi, and S.A. Rodeo, *The basic science of articular cartilage: structure, composition, and function.* Sports Health, 2009. **1**(6): p. 461-8.
7. H.J. Nieminen, T. Ylitalo, S. Karhula, J.P. Suuronen, S. Kauppinen, R. Serimaa, E. Haeggstrom, K.P. Pritzker, M. Valkealahti, P. Lehenkari, M. Finnila, and S. Saarakkala, *Determining collagen distribution in articular cartilage using contrast-enhanced micro-computed tomography.* Osteoarthritis Cartilage, 2015. **23**(9): p. 1613-21.
8. D.W. Buck, 2nd and G.A. Dumanian, *Bone biology and physiology: Part I. The fundamentals.* Plast Reconstr Surg, 2012. **129**(6): p. 1314-20.
9. A. Eichmann, F. Le Noble, M. Autiero, and P. Carmeliet, *Guidance of vascular and neural network formation.* Curr Opin Neurobiol, 2005. **15**(1): p. 108-15.
10. M. Tessier-Lavigne and C.S. Goodman, *The molecular biology of axon guidance.* Science, 1996. **274**(5290): p. 1123-33.
11. J. Goldman, K.A. Conley, A. Raehl, D.M. Bondy, B. Pytowski, M.A. Swartz, J.M. Rutkowski, D.B. Jaroch, and E.L. Ongstad, *Regulation of lymphatic capillary regeneration by interstitial flow in skin.* Am J Physiol Heart Circ Physiol, 2007. **292**(5): p. H2176-83.
12. M. Xue and C.J. Jackson, *Extracellular Matrix Reorganization During Wound Healing and Its Impact on Abnormal Scarring.* Adv Wound Care (New Rochelle), 2015. **4**(3): p. 119-136.
13. S. Li, J.L. Guan, and S. Chien, *Biochemistry and biomechanics of cell motility.* Annu Rev Biomed Eng, 2005. **7**: p. 105-50.
14. D.E. Discher, P. Janmey, and Y.L. Wang, *Tissue cells feel and respond to the stiffness of their substrate.* Science, 2005. **310**(5751): p. 1139-43.
15. R.G. Wells, *The role of matrix stiffness in regulating cell behavior.* Hepatology, 2008. **47**(4): p. 1394-400.
16. M. Sun, G. Chi, P. Li, S. Lv, J. Xu, Z. Xu, Y. Xia, Y. Tan, J. Xu, L. Li, and Y. Li, *Effects of Matrix Stiffness on the Morphology, Adhesion, Proliferation and Osteogenic Differentiation of Mesenchymal Stem Cells.* Int J Med Sci, 2018. **15**(3): p. 257-268.
17. N. Liu, M. Zhou, Q. Zhang, L. Yong, T. Zhang, T. Tian, Q. Ma, S. Lin, B. Zhu, and X. Cai, *Effect of substrate stiffness on proliferation and differentiation of periodontal ligament stem cells.* Cell Prolif, 2018. **51**(5): p. e12478.
18. L. Hui, J. Zhang, X. Ding, X. Guo, and X. Jiang, *Matrix stiffness regulates the proliferation, stemness and chemoresistance of laryngeal squamous cancer cells.* Int J Oncol, 2017. **50**(4): p. 1439-1447.
19. Y.T. Yeh, S.S. Hur, J. Chang, K.C. Wang, J.J. Chiu, Y.S. Li, and S. Chien, *Matrix stiffness regulates endothelial cell proliferation through septin 9.* PLoS One, 2012. **7**(10): p. e46889.

20. A. Shkumatov, M. Thompson, K.M. Choi, D. Sicard, K. Baek, D.H. Kim, D.J. Tschumperlin, Y.S. Prakash, and H. Kong, *Matrix stiffness-modulated proliferation and secretory function of the airway smooth muscle cells.* Am J Physiol Lung Cell Mol Physiol, 2015. **308**(11): p. L1125-35.
21. Z. Razinia, P. Castagnino, T. Xu, A. Vazquez-Salgado, E. Pure, and R.K. Assoian, *Stiffness-dependent motility and proliferation uncoupled by deletion of CD44.* Sci Rep, 2017. **7**(1): p. 16499.
22. J. Schrader, T.T. Gordon-Walker, R.L. Aucott, M. van Deemter, A. Quaas, S. Walsh, D. Benten, S.J. Forbes, R.G. Wells, and J.P. Iredale, *Matrix stiffness modulates proliferation, chemotherapeutic response, and dormancy in hepatocellular carcinoma cells.* Hepatology, 2011. **53**(4): p. 1192-205.
23. J.S. Park, J.S. Chu, A.D. Tsou, R. Diop, Z. Tang, A. Wang, and S. Li, *The effect of matrix stiffness on the differentiation of mesenchymal stem cells in response to TGF-beta.* Biomaterials, 2011. **32**(16): p. 3921-30.
24. H. Lv, L. Li, M. Sun, Y. Zhang, L. Chen, Y. Rong, and Y. Li, *Mechanism of regulation of stem cell differentiation by matrix stiffness.* Stem Cell Res Ther, 2015. **6**: p. 103.
25. C.M. Lo, H.B. Wang, M. Dembo, and Y.L. Wang, *Cell movement is guided by the rigidity of the substrate.* Biophys J, 2000. **79**(1): p. 144-52.
26. S. Kidoaki and T. Matsuda, *Microelastic gradient gelatinous gels to induce cellular mechanotaxis.* J Biotechnol, 2008. **133**(2): p. 225-30.
27. D.S. Gray, J. Tien, and C.S. Chen, *Repositioning of cells by mechanotaxis on surfaces with micropatterned Young's modulus.* J Biomed Mater Res A, 2003. **66**(3): p. 605-14.
28. H.G. Sundararaghavan and J.A. Burdick, *Gradients with depth in electrospun fibrous scaffolds for directed cell behavior.* Biomacromolecules, 2011. **12**(6): p. 2344-50.
29. S.H. Oh, I.K. Park, J.M. Kim, and J.H. Lee, *In vitro and in vivo characteristics of PCL scaffolds with pore size gradient fabricated by a centrifugation method.* Biomaterials, 2007. **28**(9): p. 1664-71.
30. T.D. Roy, J.L. Simon, J.L. Ricci, E.D. Rekow, V.P. Thompson, and J.R. Parsons, *Performance of degradable composite bone repair products made via three-dimensional fabrication techniques.* J Biomed Mater Res A, 2003. **66**(2): p. 283-91.
31. T.B. Woodfield, C.A. Van Blitterswijk, J. De Wijn, T.J. Sims, A.P. Hollander, and J. Riesle, *Polymer scaffolds fabricated with pore-size gradients as a model for studying the zonal organization within tissue-engineered cartilage constructs.* Tissue Eng, 2005. **11**(9-10): p. 1297-311.
32. S. Zmora, R. Glicklis, and S. Cohen, *Tailoring the pore architecture in 3-D alginate scaffolds by controlling the freezing regime during fabrication.* Biomaterials, 2002. **23**(20): p. 4087-94.
33. P.X. Ma and R. Zhang, *Microtubular architecture of biodegradable polymer scaffolds.* J Biomed Mater Res, 2001. **56**(4): p. 469-77.
34. R. Chen, J. Wang, and C. Liu, *Biomaterials Act as Enhancers of Growth Factors in Bone Regeneration.* Advanced Functional Materials, 2016. **26**(48): p. 8810-8823.
35. A.G. Guex, D. Hegemann, M.N. Giraud, H.T. Tevaearai, A.M. Popa, R.M. Rossi, and G. Fortunato, *Covalent immobilisation of VEGF on plasma-coated electrospun scaffolds for tissue engineering applications.* Colloids and surfaces. B, Biointerfaces, 2014. **123**: p. 724-733.
36. M. Ramalingam, M.F. Young, V. Thomas, L. Sun, L.C. Chow, C.K. Tison, K. Chatterjee, W.C. Miles, and C.G. Simon, Jr., *Nanofiber scaffold gradients for interfacial tissue engineering.* Journal of biomaterials applications, 2013. **27**(6): p. 695-705.
37. J. Shi, L. Wang, F. Zhang, H. Li, L. Lei, L. Liu, and Y. Chen, *Incorporating protein gradient into electrospun nanofibers as scaffolds for tissue engineering.* ACS applied materials & interfaces, 2010. **2**(4): p. 1025-1030.
38. M.L. Tanes, J. Xue, and Y. Xia, *A General Strategy for Generating Gradients of Bioactive Proteins on Electrospun Nanofiber Mats by Masking with Bovine Serum Albumin.* Journal of materials chemistry. B, 2017. **5**(28): p. 5580-5587.

39. S. Samavedi, C. Olsen Horton, S.A. Guelcher, A.S. Goldstein, and A.R. Whittington, *Fabrication of a model continuously graded co-electrospun mesh for regeneration of the ligament-bone interface.* Acta biomaterialia, 2011. **7**(12): p. 4131-4138.
40. T. Wu, J. Xue, H. Li, C. Zhu, X. Mo, and Y. Xia, *General Method for Generating Circular Gradients of Active Proteins on Nanofiber Scaffolds Sought for Wound Closure and Related Applications.* ACS Applied Materials & Interfaces, 2018. **10**(10): p. 8536-8545.
41. J.S. Kim, B.G. Im, G. Jin, and J.H. Jang, *Tubing-Electrospinning: A One-Step Process for Fabricating Fibrous Matrices with Spatial, Chemical, and Mechanical Gradients.* ACS Appl Mater Interfaces, 2016. **8**(34): p. 22721-31.
42. W. Bian, Q. Lian, D. Li, J. Wang, W. Zhang, Z. Jin, and Y. Qiu, *Morphological characteristics of cartilage-bone transitional structures in the human knee joint and CAD design of an osteochondral scaffold.* Biomed Eng Online, 2016. **15**(1): p. 82.
43. Q.P. Pham, U. Sharma, and A.G. Mikos, *Electrospun poly(epsilon-caprolactone) microfiber and multilayer nanofiber/microfiber scaffolds: characterization of scaffolds and measurement of cellular infiltration.* Biomacromolecules, 2006. **7**(10): p. 2796-805.
44. S. Soliman, S. Pagliari, A. Rinaldi, G. Forte, R. Fiaccavento, F. Pagliari, O. Franzese, M. Minieri, P. Di Nardo, S. Licoccia, and E. Traversa, *Multiscale three-dimensional scaffolds for soft tissue engineering via multimodal electrospinning.* Acta Biomater, 2010. **6**(4): p. 1227-37.
45. J.L. Lowery, N. Datta, and G.C. Rutledge, *Effect of fiber diameter, pore size and seeding method on growth of human dermal fibroblasts in electrospun poly(epsilon-caprolactone) fibrous mats.* Biomaterials, 2010. **31**(3): p. 491-504.
46. H.M. Powell and S.T. Boyce, *Fiber density of electrospun gelatin scaffolds regulates morphogenesis of dermal-epidermal skin substitutes.* J Biomed Mater Res A, 2008. **84**(4): p. 1078-86.
47. K. Sisson, C. Zhang, M.C. Farach-Carson, D.B. Chase, and J.F. Rabolt, *Fiber diameters control osteoblastic cell migration and differentiation in electrospun gelatin.* J Biomed Mater Res A, 2010. **94**(4): p. 1312-20.
48. J. Rnjak, Z. Li, P.K. Maitz, S.G. Wise, and A.S. Weiss, *Primary human dermal fibroblast interactions with open weave three-dimensional scaffolds prepared from synthetic human elastin.* Biomaterials, 2009. **30**(32): p. 6469-77.
49. A. Balguid, A. Mol, M.H. van Marion, R.A. Bank, C.V. Bouten, and F.P. Baaijens, *Tailoring fiber diameter in electrospun poly(epsilon-caprolactone) scaffolds for optimal cellular infiltration in cardiovascular tissue engineering.* Tissue Eng Part A, 2009. **15**(2): p. 437-44.
50. S.J. Eichhorn and W.W. Sampson, *Statistical geometry of pores and statistics of porous nanofibrous assemblies.* J R Soc Interface, 2005. **2**(4): p. 309-18.
51. H. Gerhardt, *VEGF and endothelial guidance in angiogenic sprouting.* Organogenesis, 2008. **4**(4): p. 241-6.
52. D.G. Greenhalgh, *The role of growth factors in wound healing.* J Trauma, 1996. **41**(1): p. 159-67.
53. K.A. Siwicka, H. Kitoh, M. Kawasumi, and N. Ishiguro, *Spatial and temporal distribution of growth factors receptors in the callus: implications for improvement of distraction osteogenesis.* Nagoya J Med Sci, 2011. **73**(3-4): p. 117-27.
54. P. Wieringa, A. Girao, R. Truckenmuller, A. Welle, S. Micera, R. van Wezel, and L. Moroni, *A one-step biofunctionalization strategy of electrospun scaffolds enables spatially selective presentation of biological cues.* bioRxiv, 2019: p. 850875.
55. C.P. Grey, S.T. Newton, G.L. Bowlin, T.W. Haas, and D.G. Simpson, *Gradient fiber electrospinning of layered scaffolds using controlled transitions in fiber diameter.* Biomaterials, 2013. **34**(21): p. 4993-5006.

56. A. Timnak, J.A. Gerstenhaber, K. Dong, Y.E. Har-El, and P.I. Lelkes, *Gradient porous fibrous scaffolds: a novel approach to improving cell penetration in electrospun scaffolds.* Biomed Mater, 2018. **13**(6): p. 065010.
57. S. Soliman, S. Sant, J.W. Nichol, M. Khabiry, E. Traversa, and A. Khademhosseini, *Controlling the porosity of fibrous scaffolds by modulating the fiber diameter and packing density.* J Biomed Mater Res A, 2011. **96**(3): p. 566-74.
58. Y.M. Ju, J.S. Choi, A. Atala, J.J. Yoo, and S.J. Lee, *Bilayered scaffold for engineering cellularized blood vessels.* Biomaterials, 2010. **31**(15): p. 4313-21.
59. J. Nam, Y. Huang, S. Agarwal, and J. Lannutti, *Improved cellular infiltration in electrospun fiber via engineered porosity.* Tissue Eng, 2007. **13**(9): p. 2249-57.
60. M.F. Leong, W.Y. Chan, K.S. Chian, M.Z. Rasheed, and J.M. Anderson, *Fabrication and in vitro and in vivo cell infiltration study of a bilayered cryogenic electrospun poly(D,L-lactide) scaffold.* J Biomed Mater Res A, 2010. **94**(4): p. 1141-9.
61. M.F. Leong, M.Z. Rasheed, T.C. Lim, and K.S. Chian, *In vitro cell infiltration and in vivo cell infiltration and vascularization in a fibrous, highly porous poly(D,L-lactide) scaffold fabricated by cryogenic electrospinning technique.* J Biomed Mater Res A, 2009. **91**(1): p. 231-40.
62. B.M. Baker, R.P. Shah, A.M. Silverstein, J.L. Esterhai, J.A. Burdick, and R.L. Mauck, *Sacrificial nanofibrous composites provide instruction without impediment and enable functional tissue formation.* Proc Natl Acad Sci U S A, 2012. **109**(35): p. 14176-81.
63. A. Guimaraes, A. Martins, E.D. Pinho, S. Faria, R.L. Reis, and N.M. Neves, *Solving cell infiltration limitations of electrospun nanofiber meshes for tissue engineering applications.* Nanomedicine (Lond), 2010. **5**(4): p. 539-54.
64. J. Voorneveld, A. Oosthuysen, T. Franz, P. Zilla, and D. Bezuidenhout, *Dual electrospinning with sacrificial fibers for engineered porosity and enhancement of tissue ingrowth.* J Biomed Mater Res B Appl Biomater, 2017. **105**(6): p. 1559-1572.
65. K. Wang, M. Xu, M. Zhu, H. Su, H. Wang, D. Kong, and L. Wang, *Creation of macropores in electrospun silk fibroin scaffolds using sacrificial PEO-microparticles to enhance cellular infiltration.* J Biomed Mater Res A, 2013. **101**(12): p. 3474-81.
66. E.D. Carruth, A.D. McCulloch, and J.H. Omens, *Transmural gradients of myocardial structure and mechanics: Implications for fiber stress and strain in pressure overload.* Progress in biophysics and molecular biology, 2016. **122**(3): p. 215-226.
67. C.M. Valmikinathan, J. Wang, S. Smiriglio, N.G. Golwala, and X. Yu, *Magnetically induced protein gradients on electrospun nanofibers.* Comb Chem High Throughput Screen, 2009. **12**(7): p. 656-63.

Supplementary figures

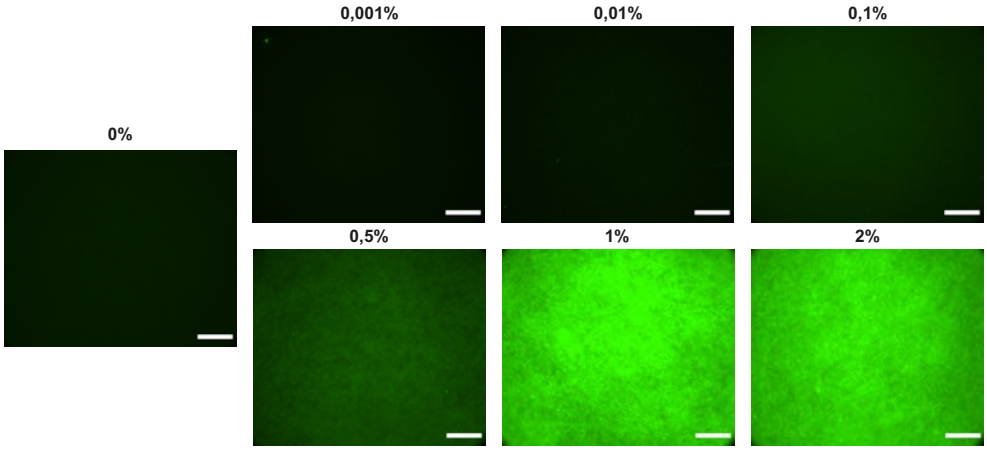

Supplementary Figure 1. ESP scaffolds with varying concentrations of PEG-SH additive. 300PEOT55PBT45 was ESP different with concentrations PEG-SH and stained with a fluorescent maleimide dye. Scalebar 250 µm.

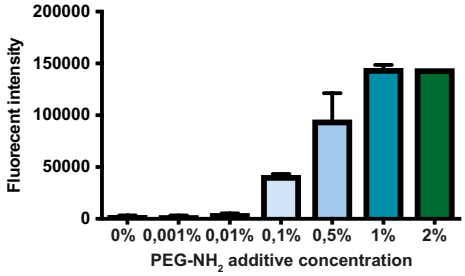

Supplementary Figure 2. ESP scaffolds with varying concentrations of PEG-NH2 additive. 300PEOT55PBT45 was ESP with different concentrations PEG-NH2 and stained with a fluorescamine (n=3).

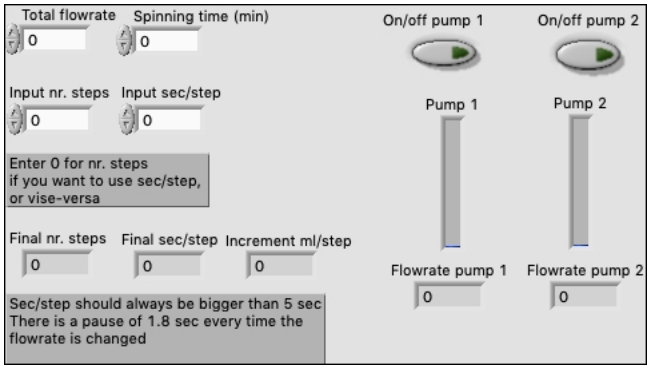

Supplementary Figure 3. LabVIEW user interface of flowrate gradient program

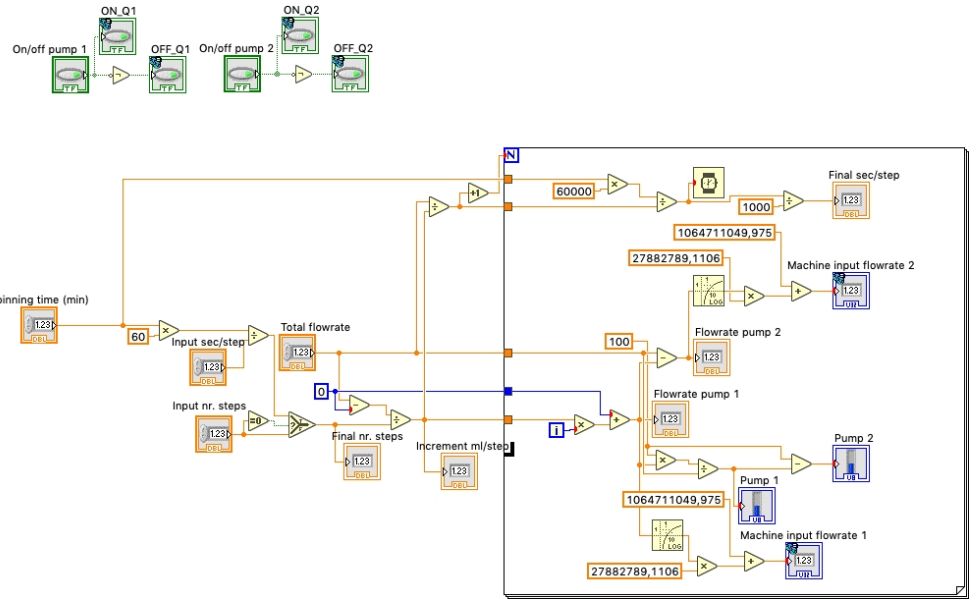

Supplementary Figure 4. LabVIEW back panel of flowrate gradient program

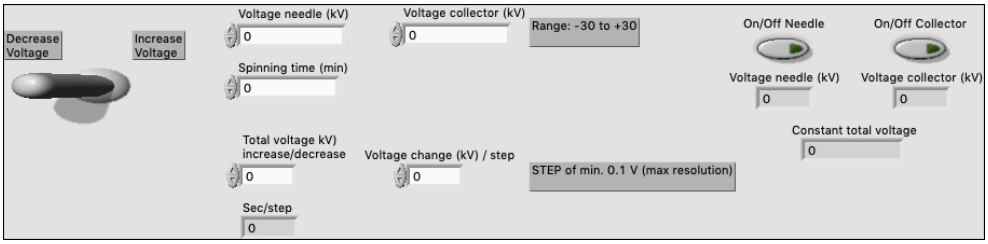

Supplementary Figure 5. LabVIEW user interface of voltage gradient program

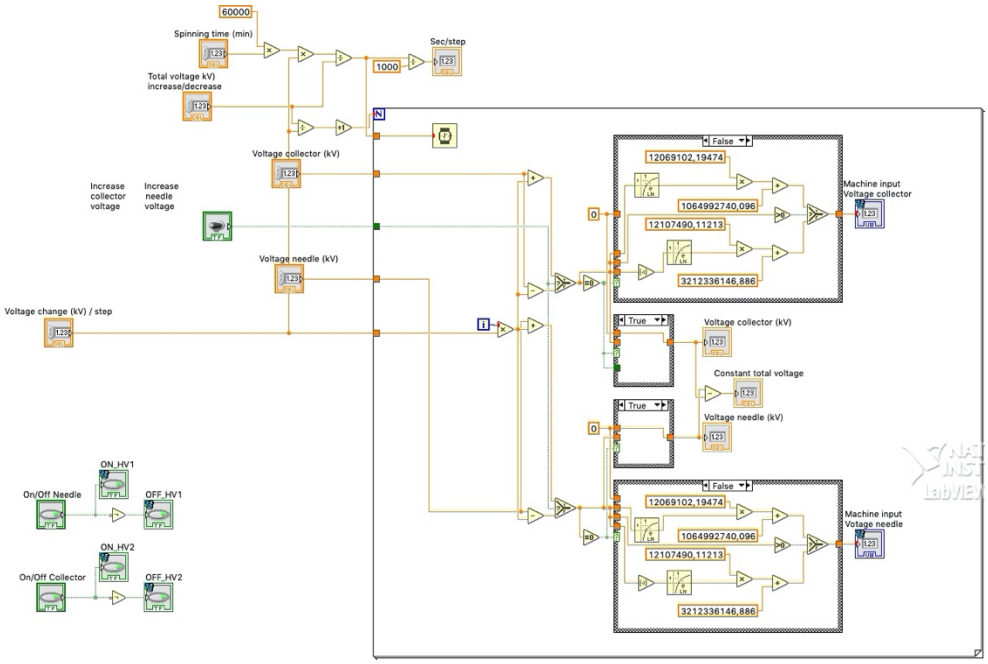

Supplementary Figure 6. LabVIEW back panel of voltage gradient program

Chapter 8

The hydrocup: a hollow electrospun scaffold for *in vivo* hydrogel delivery

Jip Zonderland[1]*, David Boaventura Gomes[1]*, Silvia Rezzola[1], Ana Henriques Ferreira Lourenço[1], Hong Liu[2, 3], Marloes Peters[1, 4], Peter Emans[4], Nicole Bouvy[2, 3], Paul Wieringa[1], Sandra Camarero Espinosa[1], Lorenzo Moroni[1]
* These authors contributed equally to this work

[1] Department of Complex Tissue Regeneration, MERLN Institute for Technology-Inspired Regenerative Medicine, Maastricht University, Maastricht, the Netherlands
[2] Department of Surgery, Maastricht University Medical Centre, Maastricht, the Netherlands
[3] NUTRIM School of Nutrition and Translational Research in Metabolism, Maastricht University, Maastricht, the Netherlands
[4] Department of Orthopaedic Surgery and Laboratory for Experimental Orthopedics, Maastricht University Medical Center, the Netherlands

Chapter 9

General discussion

Jip Zonderland

Introduction

Mechanobiology plays a very important role in differentiation and proliferation of a wide variety of cells[1, 2]. In human mesenchymal stromal cells (hMSCs) the role and regulation of mechanotransduction pathways in 2D differentiation and proliferation has been fairly well established[3, 4]. However, more and more studies show a difference in the role and regulation of mechanotransduction proteins between 2D and 3D cell cultures[5-7]. Since final *in vivo* applications of regenerative medicine and tissue engineering will inevitably be in a 3D environment, it is critical to have a thorough understanding of 3D mechanobiology.

Mechanobiology in 3D

Most studies to date investigating the role and regulation of mechanosensitive proteins on MSC differentiation and proliferation in 3D have been performed in hydrogels. This is discussed in depth in the literature review in chapter 2. In chapter 3 we set out to explore 3D mechanobiology in common tissue engineering scaffolds: additive manufactured- (AM) and electrospun (ESP) scaffolds. In 2D, hMSCs cultured on stiff substrates have a well-established profile of a combination of actin stress fibers, phosphorylated myosin light chain 2 (pMLC2), many large focal adhesions, nuclear localization of yes-associated protein (YAP) and high levels of lamin A and C[8-15]. However, we found that hMSCs in 3D scaffolds made from stiff materials exhibit few actin stress fibers, little pMLC2, few and small focal adhesions, cytoplasmic YAP and low levels of lamin A and C. This profile is similar to hMSCs cultured on soft materials[8-10, 12-16]. Chapter 3, therefore, highlights that the influence of material properties on mechanosensitive proteins cannot be directly translated from 2D to 3D, as others have also illustrated in hydrogels[5-7, 17, 18]. In 2D, low expression of the important mechanosensitive proteins named above pushes hMSCs towards adipogenesis, and not to osteogenesis[8, 9, 11, 12, 19-34]. However, efficient osteogenic- and no adipogenic- differentiation was still observed in hMSCs cultured in AM- and ESP scaffolds, despite the low expression of these important mechanosensitive proteins. Although contrary to the 2D literature, chapter 3 adds to literature that shows a difference in the role of mechanosensitive proteins in MSC differentiation in 3D hydrogels[35-39].

This raises the question why 3D is any different from 2D. In chapter 2 and 3 I speculate that the main difference could come from a difference in force distribution. In 2D, all cellular adhesions are lower than the nucleus, creating a downward force on the nucleus by actin fibers going over and attaching to the nucleus[40]. In 3D, cellular adhesions are in all directions, above and below the nucleus. This potentially also explains the reduction in lamin A and C expression observed in chapter 3, which increase with an increase of force on the nucleus[41]. This does, however, not explain why MSCs in 3D can undergo osteogenic differentiation without pronounced stress fibers or focal adhesions and cytoplasmic YAP as described in chapter 3 and in hydrogels by others[7, 17, 18, 35, 37, 38, 42-46]. Perhaps the levels of expression of these proteins is still sufficient. However, there are also potential other mechanisms through

which differentiation could occur. For example, two studies have shown the dominant role of cell volume in MSC differentiation in 3D[37, 45]. This was shown to be partly regulated by actin-myosin and by TRPV4, an ion-channel in the cell membrane[37]. When actin-myosin was inhibited osteogenic differentiation in 3D hydrogels was reduced. However, when actin-myosin was inhibited but TRPV4 activated, osteogenic differentiation still efficiently occurred. This demonstrates that there are pathways independent of actin-myosin that can induce osteogenic differentiation. Smooth muscle actin and smooth muscle myosin have also been proposed to be important for MSC osteogenesis[10, 47], proposing a potential pathway for actin-myosin independent differentiation. Whether cell volume and/or TRPV4 induce differentiation completely independent of mechanotransduction pathways, or if these pathways share similarities, remains to be explored. Investigating the effect of cell volume in ESP and AM scaffolds and establishing an optimal cell volume for each of the tri-lineage differentiations of MSCs would also be very interesting and could aid scaffold optimization.

Chapter 4 investigates stanniocalcin-1 (STC1), an understudied protein that plays an important role in cell survival. While its role in cell survival has been studied, the regulation of STC1 is almost completely unknown. Several researchers found a difference in regulation of STC1 in 3D environments, which made us investigate its regulation by mechanobiological pathways. Indeed, we found that STC1 is regulated by mechanotransduction pathways, and more STC1 is released when focal adhesions, actin-myosin, or Rho-associated protein kinase (ROCK) are inhibited. Indeed, with low levels of these proteins in 3D tissue engineering scaffolds (described in chapter 3), more STC1 is released in ESP scaffolds or alginate hydrogels. This chapter demonstrates that besides differentiation, mechanosensitive proteins can also influence the secretion of cell survival factors. Understanding the regulation of anti-apoptotic and other pro-survival factors could be important, as cell survival can be challenging in large tissue engineering constructs[48, 49]. STC1 secretion, which according to literature should result in increased cell survival of neighboring cells[50-53], was enhanced by fewer focal adhesions and less actin-myosin and ROCK. Differentiation, however, have been shown to be enhanced with higher levels of actin-myosin and ROCK in 2D[8, 12, 19-21, 25, 54-58] and in 3D[7, 35, 37], although conflicting results have been found in 3D[35, 36]. Further investigating other survival proteins and investigating whether there is a trade-off between cell survival and efficient differentiation, or proliferation, will be critical for future tissue engineering applications.

Chapter 5 investigates how ESP scaffolds impact hMSC proliferation. Specifically, we found that FGFR1 is downregulated on ESP scaffolds, compared to 2D controls or normal 2D tissue culture plates. FGFR1 is the receptor for basic fibroblast growth factor (bFGF) and important for the control of cell proliferation[59, 60]. This makes FGFR1 relevant for tissue engineering, but also to cancer biology, as 7% of all cancers have aberrations in FGFRs[61]. The downregulation of FGFR1 was caused by a reduced activity of the MRTF/SRF pathway on ESP scaffolds. It is well described that reduced cellular tension in 2D inhibits proliferation[1, 2, 44, 62,

[63], and this has also been shown in 3D hydrogels[37]. However, the mechanism by which this reduction in proliferation is regulated is largely unknown. Chapter 6 provides a potential explanation for part of this reduction in proliferation by showing that FGFR1 is regulated by mechanosensitive proteins in three different cell-types, among which human cancer cells. FGFRs are currently being tested in animal studies and clinical trials as a novel cancer treatment, with promising initial results[64-69]. How FGFRs are regulated, however, is not well known. We showed for the first time that FGFR1 is regulated through mechanotransduction, which raises questions about the mechanosensitive behavior of other FGFRs. In addition, it opens up potential targets for novel cancer treatments. Of course, a thorough understanding is required of the regulation of all FGFRs and the downstream effects of inhibiting specific mechanotransduction pathways.

Together, chapter 3, 4 and 5 describe a different behavior of hMSCs in terms of differentiation, proliferation and survival factor secretion in 3D than in 2D. In 2D, the profile of mechanosensitive proteins is often used as a predictor for MSC differentiation and proliferation. However, together these chapters show that a new profile of mechanosensitive proteins needs to be discovered that properly predicts future cell behavior in 3D. Such a profile could greatly help the optimization of scaffolds for differentiation. Differentiation experiments are often long and having a quicker read-out to optimize parameters could greatly speed up research. Even though the hMSCs in ESP scaffolds still differentiated towards osteoblasts (chapter 3), and still proliferated (chapter 5), this could potentially be optimized. In hydrogels, it has been shown that matrix remodeling is important for cellular tension, osteogenic differentiation and proliferation of MSCs[7, 17, 35]. On top of 2D fibrous matrices, matrix remodeling has also been shown to influence MSC proliferation and differentiation[70-72]. It would be interesting to investigate how matrix remodeling would affect MSC differentiation and proliferation in 3D ESP scaffolds. Optimizing the cells' ability to reorganize the ESP fibers, for example by changing fiber stiffness or inter-fiber bonding, could increase osteogenic differentiation and proliferation of MSCs in ESP scaffolds. In other more macro-sized scaffolds, such as AM scaffolds, influencing cells on the micro-level might be more challenging, as most of the cells are not in contact with the scaffold material. Hydrogels could be embedded inside the AM scaffolds to combine instructions on the micro-level with macro-level mechanical properties, for example, to bear loads in bone defects. Such a combinatorial approach of two scaffold types is also described in chapter 8, where the macro-level mechanical properties of the hollow ESP scaffold, the hydrocup, are used to fix a hydrogel in place *in vivo*. The hydrocup can keep cells in a hydrogel at the site of implantation *in vivo* and potentially protect against deforming mechanical loads on the hydrogel. As described in chapter 4, the secretion of pro-survival factor STC1 can be tuned by changing the matrix properties. It would be interesting to investigate whether other important secretion factors are also influenced by matrix properties. The hydrogel could then

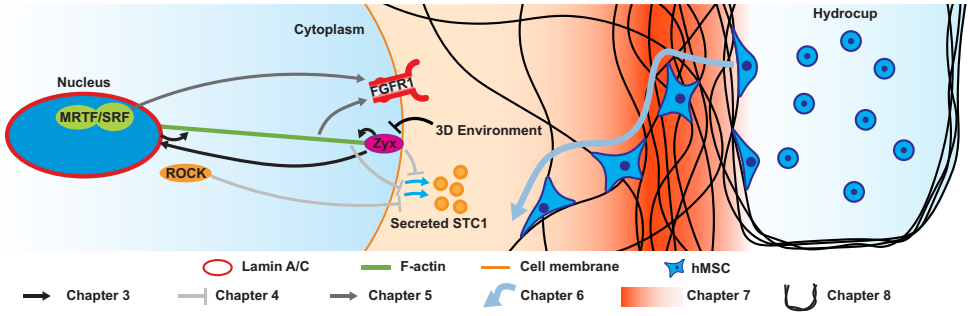

Figure 1. Summary of the novel findings of this thesis. In chapter 3, we found that the 3D environment of ESP- and AM scaffolds downregulates zyxin. The lack of zyxin then leads to a decrease in lamin A/C, and together they change the actin organization in the cell. Chapter 4 describes how this lack of zyxin and actin influence the secretion of STC1, at least partly through ROCK. The change in actin also influences the expression of FGFR1, in part through MRTF/SRF, as described in chapter 5. To further study how the 3D environment changes cell behavior, an ESP scaffold was developed that allows for cell infiltration in chapter 6. This scaffold can be used to fundamentally study 3D cell migration through a fibrous 3D environment. To aid such research, in chapter 7 multiple ways are developed to include in-depth gradients in ESP scaffolds. In chapter 8 a scaffold to deliver cell-laden hydrogels *in vivo* is developed, which can be used to study how the environment affects the MSC secretome through mechanobiology *in vivo*.

be designed to yield an optimal secretion profile of the embedded MSCs. This can have implications for regenerative medicine approaches utilizing the MSC secretome for tissue regeneration and for tissue engineering applications, as the secretome of MSCs can influence several tissue morphogenetic events, such as cell differentiation and proliferation[73, 74].

Together, chapter 3, 4 and 5 create a better understanding of how matrix properties influence MSC behavior, and the role of mechanosensitive proteins in these processes. In chapter 3 we showed how the 3D environment influences cellular tension through proteins such as zyxin, actin-myosin and lamin A/C. In chapter 4 and 5 the effects of this change in cellular tension on proliferation and cell survival are explored. FGFR1 decreased in 3D ESP scaffolds when compared to 2D, through a decrease in actin and MRTF/SRF. Interestingly, even though we have shown that lamin A/C and zyxin influence actin (chapter 3), knockdown of either of these proteins had no effect on FGFR1 expression. In chapter 4, knockdown of zyxin, or inhibition of actin-myosin or ROCK lead to increased STC1 secretion. Indeed, in 3D culture conditions, where there is less actin-myosin and zyxin (chapter 3), more STC1 was secreted. Interestingly, as with FGFR1, lamin A/C knockdown had no effect on STC1 secretion. The interplay between these proteins and the connection between the chapters is summarized in figure 1. The connection between zyxin, actin-myosin, lamin A/C, ROCK and MRTF/SRF has been relatively well established, with actin playing a central role in this. Focal adhesions (of which zyxin is a part) connect to the ECM through integrins and connect to actin fibers inside the cell. Together with proteins such as ROCK, zyxin aids in the formation of stable actin-myosin fibers. Part of these actin-myosin fibers connect to the nucleus and to

lamin A/C through the LINC (linker of nucleoskeleton and cytoskeleton complex). MRTF binds to G-actin in the cytoplasm and with the concentration decreasing by assembly in F-actin, MRTF translocates towards the nucleus and binds SRF to influence transcription.
How the 3D environment influences these proteins, and what effect this has on cell behavior has not been well studied in stiff scaffolds used in tissue engineering. For example, we found MRTF in the nucleus of hMSCs on ESP scaffolds, even though there is very little F-actin. Also, the regulation of both FGFR1 and STC1 has not been well-studied, making the discovery that they are regulated by mechanosensing pathways more impactful. It would be interesting to follow up on chapter 3 and dive deeper into how the 3D environment affects focal adhesions and actin-myosin. Also, further investigating how actin-myosin and related proteins such as lamin A/C, ROCK, MRTF/SRF and focal adhesions influence MSC differentiation in 3D could greatly improve scaffold optimization. Following up on this, one could investigate how actin-myosin then affects other important proteins for proliferation, besides FGFR1, such as other FGFRs or proliferation transcription factors. Further follow up on the influence of a 3D environment on cell survival could also be very beneficial for future scaffold design. Besides STC1, other released or intra cellular survival proteins could be influenced by the 3D environment through actin, zyxin, ROCK, and/or other mechanosensitive proteins. All of this information together would greatly aid smart designs for tissue engineering scaffolds. To design a scaffold for a specific purpose, such as osteogenic differentiation of MSCs, it is necessary to understand what MSCs need to differentiate towards the osteogenic lineage. While in 2D osteogenic MSC differentiation is aided by stiff materials and high cellular tension, in 3D this seems to be different. This has been demonstrated in hydrogels[35-39], and in this thesis in ESP and AM scaffolds in chapter 3. It could be, however, that increasing cellular tension in 3D would further improve osteogenic differentiation. This could be done, for example, by changing fiber movability by using softer materials or optimizing inter-linking of fibers is ESP. Also, to differentiate MSCs to cartilage or fat, cellular tension might have to be further reduced by reducing adhesion to the materials. Before such scaffolds can be rationally designed, however, the effects of stiffness or other material- and scaffold properties on cellular tension should be further investigated. Equally important, the role of the proteins playing a role in (or being affected by) cellular tension in MSC differentiation should be investigated, such as actin-myosin, focal adhesion proteins, lamin A/C, ROCK and YAP/TAZ. Besides MSC differentiation, proliferation and survival are also important. Cell survival can mainly be a challenge in larger tissue engineering constructs, where nutrient and oxygen supply can be hampered. Understanding that STC1 is regulated by mechanosensing and is influenced by the 3D environment could help researchers to build scaffolds that have improved cell survival. If other important cell survival proteins (secreted or intra-cellular) are also increased with low cellular tension, one could envision scaffolds where the nutrient-poor center promotes lower cellular tension, while the exterior is stiffer to ensure mechanical stability.

Similarly, understanding how the 3D environment affects cellular tension and how this influences proliferation could greatly aid to sufficiently populate tissue engineering scaffolds. FGFR1 is just one example of how cellular tension influences proliferation and many other proliferation influencing proteins are likely to be affected.

In hydrogels, improved understanding of how material properties, such as stress relaxation and degradation, influence cellular tension and MSC differentiation has already led to improved scaffolds used for *in vivo* bone formation[6, 75, 76]. For ESP or AM scaffolds, however, the fundamental research of how these properties influence cellular tension and cellular behavior is missing. A better understanding of how such individual parameters of tissue engineering scaffolds made from stiff materials influence MSC differentiation, proliferation and survival could similarly lead to superior scaffolds. For this, however, research into 3D mechanobiology should not only encompass hydrogels as a 3D cell culture system, but also stiffer porous scaffolds such as those used for tissue engineering. Chapter 3, 4 and 5 are therefore nice examples of how such fundamental research is also possible in these scaffolds and how it can result in a much better understanding of the underlying fundamental processes.

New tools to investigate 3D mechanobiology

In order to investigate cell behavior and the underlying biological processes in a 3D environment, the right tools and scaffold types need to be available. For this reason, I have developed several scaffolds that can be used for this purpose, which are summarized in figure 1.

The appendix of chapter 3 describes the development of a pipeline to analyze actin distribution. It is the first freely available tool to investigate actin distribution in cells. In chapter 3 we have used this tool to analyze the actin distribution in hMSCs on 2D films or in 3D ESP scaffolds. This tool could be used to analyze any staining distribution in a cell. For example, migration is characterized by an unequal distribution of proteins between the leading and the trailing end of the migrating cell[77, 78]. Easily quantifying the distribution of such proteins along the length of the cell could benefit migration research, in 2D and in 3D.

In chapter 6 we improved the cell infiltration of ESP scaffolds by increasing fiber diameter and co-spinning sacrificial polymers. Such techniques have previously been used to improve cell infiltration[79-84], but the *in vivo* tissue formation in 2 mm thick ESP scaffolds demonstrated in chapter 6 has not been previously reported. The ESP scaffolds developed in chapter 6 could be used for tissue engineering, particularly for defects with large surface area but limited depth. Even without any bound growth-factors or seeded cells, the scaffolds were fully infiltrated by host cells and filled with ECM. However, to form functional tissue *in vivo*, it is likely that the scaffold should be seeded with either the relevant stem cells, or with incorporated growth-factors to guide tissue formation by the host cells. The techniques developed in chapter 7 could help with guiding tissue regeneration by cells in ESP scaffolds.

Homeostatic and regenerating tissues are full of both physical and biological gradients[85-93]. Chapter 7 describes several methods that can be used to incorporate biological factors or fiber diameter and porosity gradients in ESP scaffolds. Such gradients could be used to further guide the proper regeneration of damaged tissues.

In chapter 6, we also developed a system that can be used to study guided cell migration through a 3D fibrous mesh. ESP scaffolds of tunable thickness and porosity can be seeded with cells and cultured on top of a transwell. The bottom compartment of the transwell can be filled with chemoattractant to guide cell migration through the ESP scaffolds. 2D and 3D migration is very different and is orchestrated by separate pathways[94, 95]. Currently, 3D migration and 3D tumor cell invasion are often studied in hydrogels[96-99]. However, hydrogels only partly recapitulate *in vivo* tissue environments, and the fibrous 3D matrix of ESP scaffolds can mimic the nano- to micrometer sized fibers found in natural ECM[100-102]. The ESP scaffolds could, therefore, be an interesting platform to investigate 3D cell migration or tumor invasion. Different drugs or chemoattractant can easily be mixed in the medium to study the effect of specific proteins or drugs. Additionally, with the techniques described in chapter 7, the effects of bound growth-factor gradients or physical gradients could be studied. 3D migration is virtually unstudied in 3D fibrous meshes, so using tools developed in this thesis could greatly aid understanding of 3D migration, tumor invasion and scaffold infiltration.

Future of regenerative medicine

Altogether, this thesis adds fundamental knowledge as well as novel tools to the tissue engineering field. I argue for more fundamental research into the influence of material properties on cell behavior and the underlying molecular mechanisms. Even though the mechanisms seem to be fairly well understood because of 2D mechanobiology, a 3D microenvironment is different, as others have reported and we have shown in the studies of this thesis. Intelligent scaffold design cannot be reasonably done without a thorough understanding of the influence of individual scaffolds' parameters. In my opinion, more effort should go into fundamental research to understand and decouple the effect of important scaffolds' parameters, such as matrix remodeling, stiffness, confinement and cellular force distribution.

Polystyrene 2D culture plates are being used for tissue cell culture since the '60s[103, 104]. For many years now, a continuously increasing set of studies have shown profound differences in cell behavior of 3D cell cultures compared to the 2D culture platforms from the '60s. With the end goal of aiding tissue engineering and regenerative medicine strategies, mechanobiology research solely in 2D should be of the past. Research should move to culture platforms that will be used for tissue engineering purposes, including hydrogels, but also the understudied 3D scaffolds made from stiff materials that are often used for tissue engineering and to recapitulate the macro- and micro-environment of natural extra cellular

matrix. Although translational research might seemingly give more tangible results quicker, I argue that truly functional tissues can only be engineered with a deep fundamental understanding of the biological mechanisms orchestrating the interplay between cells and biomaterials.

For these reasons, I have focused my thesis on advancing a fundamental understanding of MSC behavior in commonly used tissue engineering scaffolds, mainly ESP scaffolds. The knowledge from chapters 3, 4 and 5 add to the increasing body of literature that 3D cell behavior differs from 2D, even on the same materials. As stated before, relatively little fundamental biological research has been done in 3D ESP or AM scaffolds. Therefore, I hope that besides adding fundamental knowledge about how the 3D environment influences mechanosensing, differentiation, proliferation and survival, these chapters also encourage more fundamental research in these types of tissue engineering scaffolds. Chapters 6, 7 and 8 could also promote more fundamental research in 3D tissue engineering scaffolds. In chapter 6 we have developed a platform to relatively easily investigate 3D migration through a fibrous mesh. With the use of inhibitors, activators and knockdowns and by influencing the scaffold properties, such as described in chapter 3, 4 and 5, this platform could be of great use to advance 3D migration research. For example, knockdowns of various focal adhesion proteins in MSCs in hydrogels has shown that these proteins play a different role in 3D hydrogel migration than in 2D migration[105]. Investigating how these proteins influence 3D migration through a fibrous mesh could further increase understanding of 3D migration. Also, lamin A/C has been shown to play a role in 3D migration by influencing nuclear stiffness[106, 107]. However, this has only been studied in transwell settings, and not yet in true 3D migration platforms. Investigating what role lamin A/C plays in migration through a fibrous mesh could help to understand the role of the nucleus in guiding cell migration. Together, such knowledge can help to optimize material properties of ESP scaffolds for tissue engineering and how to most efficiently fill them with cells. In addition to this biological research, scaffold properties could be changed to understand the influence of these on cell migration. A set of such modifications, specifically to introduce a variety of gradients in ESP scaffolds, was developed in chapter 7. Lastly, in chapter 4 we have shown how mechanosensitive pathways influence STC1 secretion. The influence of mechanobiology on the MSC secretome has not been widely investigated. The hydrocup, developed in chapter 8, could be of use in this research. Hydrogel properties could be optimized to activate the right mechanobiological pathways for a certain secretome profile. Subsequently, the hydrocup can be used to test this *in vivo*, while partly isolating the hydrogel from the surrounding tissue and giving extra mechanical support.

In conclusion, this thesis has built knowledge on how a 3D environment influences processes such as differentiation, proliferation and survival and unraveled part of the underlying

biological mechanisms. In addition, novel scaffolds are developed that can be used for future fundamental research on cell migration and the MSC secretome.

References

1. A. Kumar, J.K. Placone, and A.J. Engler, *Understanding the extracellular forces that determine cell fate and maintenance.* Development, 2017. **144**(23): p. 4261-4270.
2. J.H.C. Wang and B.P. Thampatty, *Chapter 7 Mechanobiology of Adult and Stem Cells*, in *International Review of Cell and Molecular Biology*. 2008, Academic Press. p. 301-346.
3. J. Hao, Y. Zhang, D. Jing, Y. Shen, G. Tang, S. Huang, and Z. Zhao, *Mechanobiology of mesenchymal stem cells: Perspective into mechanical induction of MSC fate.* Acta Biomater, 2015. **20**: p. 1-9.
4. A.B. Castillo and C.R. Jacobs, *Mesenchymal Stem Cell Mechanobiology.* Current Osteoporosis Reports, 2010. **8**(2): p. 98-104.
5. S.R. Caliari, S.L. Vega, M. Kwon, E.M. Soulas, and J.A. Burdick, *Dimensionality and spreading influence MSC YAP/TAZ signaling in hydrogel environments.* Biomaterials, 2016. **103**: p. 314-323.
6. Y. Tang, R.G. Rowe, E.L. Botvinick, A. Kurup, A.J. Putnam, M. Seiki, V.M. Weaver, E.T. Keller, S. Goldstein, J. Dai, D. Begun, T. Saunders, and S.J. Weiss, *MT1-MMP-dependent control of skeletal stem cell commitment via a beta1-integrin/YAP/TAZ signaling axis.* Dev Cell, 2013. **25**(4): p. 402-16.
7. S. Khetan, M. Guvendiren, W.R. Legant, D.M. Cohen, C.S. Chen, and J.A. Burdick, *Degradation-mediated cellular traction directs stem cell fate in covalently crosslinked three-dimensional hydrogels.* Nat Mater, 2013. **12**(5): p. 458-65.
8. A.J. Engler, S. Sen, H.L. Sweeney, and D.E. Discher, *Matrix elasticity directs stem cell lineage specification.* Cell, 2006. **126**(4): p. 677-89.
9. J. Swift, I.L. Ivanovska, A. Buxboim, T. Harada, P.C. Dingal, J. Pinter, J.D. Pajerowski, K.R. Spinler, J.W. Shin, M. Tewari, F. Rehfeldt, D.W. Speicher, and D.E. Discher, *Nuclear lamin-A scales with tissue stiffness and enhances matrix-directed differentiation.* Science, 2013. **341**(6149): p. 1240104.
10. N.P. Talele, J. Fradette, J.E. Davies, A. Kapus, and B. Hinz, *Expression of alpha-Smooth Muscle Actin Determines the Fate of Mesenchymal Stromal Cells.* Stem Cell Reports, 2015. **4**(6): p. 1016-30.
11. M. Kuroda, H. Wada, Y. Kimura, K. Ueda, and N. Kioka, *Vinculin promotes nuclear localization of TAZ to inhibit ECM stiffness-dependent differentiation into adipocytes. J* Cell Sci, 2017. **130**(5): p. 989-1002.
12. J. Oliver-De La Cruz, G. Nardone, J. Vrbsky, A. Pompeiano, A.R. Perestrelo, F. Capradossi, K. Melajova, P. Filipensky, and G. Forte, *Substrate mechanics controls adipogenesis through YAP phosphorylation by dictating cell spreading.* Biomaterials, 2019. **205**: p. 64-80.
13. M. Guvendiren and J.A. Burdick, *Stiffening hydrogels to probe short- and long-term cellular responses to dynamic mechanics.* Nat Commun, 2012. **3**: p. 792.
14. A. Galarza Torre, J.E. Shaw, A. Wood, H.T.J. Gilbert, O. Dobre, P. Genever, K. Brennan, S.M. Richardson, and J. Swift, *An immortalised mesenchymal stem cell line maintains mechano-responsive behaviour and can be used as a reporter of substrate stiffness.* Sci Rep, 2018. **8**(1): p. 8981.
15. J. Fu, Y.K. Wang, M.T. Yang, R.A. Desai, X. Yu, Z. Liu, and C.S. Chen, *Mechanical regulation of cell function with geometrically modulated elastomeric substrates.* Nat Methods, 2010. **7**(9): p. 733-6.
16. R.J. Pelham, Jr. and Y. Wang, *Cell locomotion and focal adhesions are regulated by substrate flexibility.* Proc Natl Acad Sci U S A, 1997. **94**(25): p. 13661-5.
17. N. Huebsch, P.R. Arany, A.S. Mao, D. Shvartsman, O.A. Ali, S.A. Bencherif, J. Rivera-Feliciano, and D.J. Mooney, *Harnessing traction-mediated manipulation of the cell/matrix interface to control stem-cell fate.* Nat Mater, 2010. **9**(6): p. 518-26.
18. S.A. Ferreira, M.S. Motwani, P.A. Faull, A.J. Seymour, T.T.L. Yu, M. Enayati, D.K. Taheem, C. Salzlechner, T. Haghighi, E.M. Kania, O.P. Oommen, T. Ahmed, S. Loaiza, K. Parzych, F. Dazzi, O.P. Varghese, F. Festy, A.E. Grigoriadis, H.W. Auner, A.P. Snijders, L. Bozec, and E. Gentleman, *Bi-directional cell-pericellular matrix interactions direct stem cell fate.* Nat Commun, 2018. **9**(1): p. 4049.

19. Y.K. Wang, X. Yu, D.M. Cohen, M.A. Wozniak, M.T. Yang, L. Gao, J. Eyckmans, and C.S. Chen, *Bone morphogenetic protein-2-induced signaling and osteogenesis is regulated by cell shape, RhoA/ROCK, and cytoskeletal tension.* Stem Cells Dev, 2012. **21**(7): p. 1176-86.
20. R.J. McMurray, N. Gadegaard, P.M. Tsimbouri, K.V. Burgess, L.E. McNamara, R. Tare, K. Murawski, E. Kingham, R.O.C. Oreffo, and M.J. Dalby, *Nanoscale surfaces for the long-term maintenance of mesenchymal stem cell phenotype and multipotency.* Nature Materials, 2011. **10**(8): p. 637-644.
21. C.H. Seo, H. Jeong, Y. Feng, K. Montagne, T. Ushida, Y. Suzuki, and K.S. Furukawa, *Micropit surfaces designed for accelerating osteogenic differentiation of murine mesenchymal stem cells via enhancing focal adhesion and actin polymerization.* Biomaterials, 2014. **35**(7): p. 2245-52.
22. J. Hu, H. Liao, Z. Ma, H. Chen, Z. Huang, Y. Zhang, M. Yu, Y. Chen, and J. Xu, *Focal Adhesion Kinase Signaling Mediated the Enhancement of Osteogenesis of Human Mesenchymal Stem Cells Induced by Extracorporeal Shockwave.* Sci Rep, 2016. **6**: p. 20875.
23. W. Zheng, X. Gu, X. Sun, Q. Wu, and H. Dan, *FAK mediates BMP9-induced osteogenic differentiation via Wnt and MAPK signaling pathway in synovial mesenchymal stem cells.* Artificial Cells, Nanomedicine, and Biotechnology, 2019. **47**(1): p. 2641-2649.
24. C. Yuan, X. Gou, J. Deng, Z. Dong, P. Ye, and Z. Hu, *FAK and BMP-9 synergistically trigger osteogenic differentiation and bone formation of adipose derived stem cells through enhancing Wnt-beta-catenin signaling.* Biomed Pharmacother, 2018. **105**: p. 753-757.
25. D. Rajshankar, Y. Wang, and C.A. McCulloch, *Osteogenesis requires FAK-dependent collagen synthesis by fibroblasts and osteoblasts.* FASEB J, 2017. **31**(3): p. 937-953.
26. A.K. Kundu and A.J. Putnam, *Vitronectin and collagen I differentially regulate osteogenesis in mesenchymal stem cells.* Biochem Biophys Res Commun, 2006. **347**(1): p. 347-57.
27. S. Dupont, L. Morsut, M. Aragona, E. Enzo, S. Giulitti, M. Cordenonsi, F. Zanconato, J. Le Digabel, M. Forcato, S. Bicciato, N. Elvassore, and S. Piccolo, *Role of YAP/TAZ in mechanotransduction.* Nature, 2011. **474**(7350): p. 179-183.
28. Y. Zhu, Y. Wu, J. Cheng, Q. Wang, Z. Li, Y. Wang, D. Wang, H. Wang, W. Zhang, J. Ye, H. Jiang, and L. Wang, *Pharmacological activation of TAZ enhances osteogenic differentiation and bone formation of adipose-derived stem cells.* Stem Cell Res Ther, 2018. **9**(1): p. 53.
29. Z. Chen, Q. Luo, C. Lin, and G. Song, *Simulated microgravity inhibits osteogenic differentiation of mesenchymal stem cells through down regulating the transcriptional co-activator TAZ.* Biochem Biophys Res Commun, 2015. **468**(1-2): p. 21-6.
30. H. Pan, Y. Xie, Z. Zhang, K. Li, D. Hu, X. Zheng, Q. Fan, and T. Tang, *YAP-mediated mechanotransduction regulates osteogenic and adipogenic differentiation of BMSCs on hierarchical structure.* Colloids Surf B Biointerfaces, 2017. **152**: p. 344-353.
31. H.W. Park, Y.C. Kim, B. Yu, T. Moroishi, J.S. Mo, S.W. Plouffe, Z. Meng, K.C. Lin, F.X. Yu, C.M. Alexander, C.Y. Wang, and K.L. Guan, *Alternative Wnt Signaling Activates YAP/TAZ.* Cell, 2015. **162**(4): p. 780-94.
32. J.H. Hong, E.S. Hwang, M.T. McManus, A. Amsterdam, Y. Tian, R. Kalmukova, E. Mueller, T. Benjamin, B.M. Spiegelman, P.A. Sharp, N. Hopkins, and M.B. Yaffe, *TAZ, a transcriptional modulator of mesenchymal stem cell differentiation.* Science, 2005. **309**(5737): p. 1074-8.
33. R. Akter, D. Rivas, G. Geneau, H. Drissi, and G. Duque, *Effect of lamin A/C knockdown on osteoblast differentiation and function.* Journal of bone and mineral research : the official journal of the American Society for Bone and Mineral Research, 2009. **24**(2): p. 283-293.
34. S. Bermeo, C. Vidal, H. Zhou, and G. Duque, *Lamin A/C Acts as an Essential Factor in Mesenchymal Stem Cell Differentiation Through the Regulation of the Dynamics of the Wnt/β-Catenin Pathway.* Journal of cellular biochemistry, 2015. **116**(10): p. 2344-2353.

35. O. Chaudhuri, L. Gu, D. Klumpers, M. Darnell, S.A. Bencherif, J.C. Weaver, N. Huebsch, H.P. Lee, E. Lippens, G.N. Duda, and D.J. Mooney, *Hydrogels with tunable stress relaxation regulate stem cell fate and activity.* Nat Mater, 2016. **15**(3): p. 326-34.
36. S.H. Parekh, K. Chatterjee, S. Lin-Gibson, N.M. Moore, M.T. Cicerone, M.F. Young, and C.G. Simon, Jr., *Modulus-driven differentiation of marrow stromal cells in 3D scaffolds that is independent of myosin-based cytoskeletal tension.* Biomaterials, 2011. **32**(9): p. 2256-64.
37. H.P. Lee, R. Stowers, and O. Chaudhuri, *Volume expansion and TRPV4 activation regulate stem cell fate in three-dimensional microenvironments.* Nat Commun, 2019. **10**(1): p. 529.
38. J. Zonderland, I.L. Moldero, C. Mota, and L. Moroni, *Dimensionality changes actin network through lamin A and C and zyxin.* bioRxiv, 2019: p. 752691.
39. O. Chaudhuri, L. Gu, M. Darnell, D. Klumpers, S.A. Bencherif, J.C. Weaver, N. Huebsch, and D.J. Mooney, *Substrate stress relaxation regulates cell spreading.* Nat Commun, 2015. **6**: p. 6364.
40. M. Werner, S.B. Blanquer, S.P. Haimi, G. Korus, J.W. Dunlop, G.N. Duda, D.W. Grijpma, and A. Petersen, *Surface Curvature Differentially Regulates Stem Cell Migration and Differentiation via Altered Attachment Morphology and Nuclear Deformation.* Adv Sci (Weinh), 2017. **4**(2): p. 1600347.
41. C. Guilluy, L.D. Osborne, L. Van Landeghem, L. Sharek, R. Superfine, R. Garcia-Mata, and K. Burridge, *Isolated nuclei adapt to force and reveal a mechanotransduction pathway in the nucleus.* Nature cell biology, 2014. **16**(4): p. 376-381.
42. F.R. Maia, K.B. Fonseca, G. Rodrigues, P.L. Granja, and C.C. Barrias, *Matrix-driven formation of mesenchymal stem cell-extracellular matrix microtissues on soft alginate hydrogels.* Acta Biomater, 2014. **10**(7): p. 3197-208.
43. X.T. He, R.X. Wu, X.Y. Xu, J. Wang, Y. Yin, and F.M. Chen, *Macrophage involvement affects matrix stiffness-related influences on cell osteogenesis under three-dimensional culture conditions.* Acta Biomater, 2018. **71**: p. 132-147.
44. Y.H. Zhao, X. Lv, Y.L. Liu, Y. Zhao, Q. Li, Y.J. Chen, and M. Zhang, *Hydrostatic pressure promotes the proliferation and osteogenic/chondrogenic differentiation of mesenchymal stem cells: The roles of RhoA and Rac1.* Stem Cell Res, 2015. **14**(3): p. 283-96.
45. M. Bao, J. Xie, A. Piruska, and W.T.S. Huck, *3D microniches reveal the importance of cell size and shape.* Nature Communications, 2017. **8**(1): p. 1962.
46. C. Loebel, R.L. Mauck, and J.A. Burdick, *Local nascent protein deposition and remodelling guide mesenchymal stromal cell mechanosensing and fate in three-dimensional hydrogels.* Nat Mater, 2019. **18**(8): p. 883-891.
47. K.P. Bennett, C. Bergeron, E. Acar, R.F. Klees, S.L. Vandenberg, B. Yener, and G.E. Plopper, *Proteomics reveals multiple routes to the osteogenic phenotype in mesenchymal stem cells.* BMC Genomics, 2007. **8**: p. 380.
48. G. Rijal, B.S. Kim, F. Pati, D.H. Ha, S.W. Kim, and D.W. Cho, *Robust tissue growth and angiogenesis in large-sized scaffold by reducing H2O2-mediated oxidative stress.* Biofabrication, 2017. **9**(1): p. 015013.
49. C. Bergemann, P. Elter, R. Lange, V. Weißmann, H. Hansmann, E.-D. Klinkenberg, and B. Nebe, *Cellular Nutrition in Complex Three-Dimensional Scaffolds: A Comparison between Experiments and Computer Simulations.* International journal of biomaterials, 2015. **2015**: p. 584362-584362.
50. G.J. Block, S. Ohkouchi, F. Fung, J. Frenkel, C. Gregory, R. Pochampally, G. DiMattia, D.E. Sullivan, and D.J. Prockop, *Multipotent stromal cells are activated to reduce apoptosis in part by upregulation and secretion of stanniocalcin-1.* Stem Cells, 2009. **27**(3): p. 670-681.
51. S. Ohkouchi, G.J. Block, A.M. Katsha, M. Kanehira, M. Ebina, T. Kikuchi, Y. Saijo, T. Nukiwa, and D.J. Prockop, *Mesenchymal stromal cells protect cancer cells from ROS-induced apoptosis and enhance the Warburg effect by secreting STC1.* Mol Ther, 2012. **20**(2): p. 417-23.

52. M. Shi, Y. Yuan, J. Liu, Y. Chen, L. Li, S. Liu, X. An, R. Luo, D. Long, B. Chen, X. Du, J. Cheng, and Y. Lu, *MSCs protect endothelial cells from inflammatory injury partially by secreting STC1.* Int Immunopharmacol, 2018. **61**: p. 109-118.
53. M. Ono, S. Ohkouchi, M. Kanehira, N. Tode, M. Kobayashi, M. Ebina, T. Nukiwa, T. Irokawa, H. Ogawa, T. Akaike, Y. Okada, H. Kurosawa, T. Kikuchi, and M. Ichinose, *Mesenchymal stem cells correct inappropriate epithelial-mesenchyme relation in pulmonary fibrosis using stanniocalcin-1.* Mol Ther, 2015. **23**(3): p. 549-60.
54. R. McBeath, D.M. Pirone, C.M. Nelson, K. Bhadriraju, and C.S. Chen, *Cell shape, cytoskeletal tension, and RhoA regulate stem cell lineage commitment.* Dev Cell, 2004. **6**(4): p. 483-95.
55. L. Zhang, G. Jiang, X. Zhao, and Y. Gong, *Dimethyloxalylglycine Promotes Bone Marrow Mesenchymal Stem Cell Osteogenesis via Rho/ROCK Signaling.* Cellular Physiology and Biochemistry, 2016. **39**(4): p. 1391-1403.
56. Z. Chen, X. Wang, Y. Shao, D. Shi, T. Chen, D. Cui, and X. Jiang, *Synthetic osteogenic growth peptide promotes differentiation of human bone marrow mesenchymal stem cells to osteoblasts via RhoA/ROCK pathway.* Molecular and Cellular Biochemistry, 2011. **358**(1): p. 221-227.
57. Y.R. Shih, K.F. Tseng, H.Y. Lai, C.H. Lin, and O.K. Lee, *Matrix stiffness regulation of integrin-mediated mechanotransduction during osteogenic differentiation of human mesenchymal stem cells.* J Bone Miner Res, 2011. **26**(4): p. 730-8.
58. S.A. Ruiz and C.S. Chen, *Emergence of patterned stem cell differentiation within multicellular structures.* Stem Cells, 2008. **26**(11): p. 2921-7.
59. D.M. Ornitz and N. Itoh, *The Fibroblast Growth Factor signaling pathway.* Wiley Interdiscip Rev Dev Biol, 2015. **4**(3): p. 215-66.
60. C. Dombrowski, T. Helledie, L. Ling, M. Grunert, C.A. Canning, C.M. Jones, J.H. Hui, V. Nurcombe, A.J. van Wijnen, and S.M. Cool, *FGFR1 signaling stimulates proliferation of human mesenchymal stem cells by inhibiting the cyclin-dependent kinase inhibitors p21(Waf1) and p27(Kip1).* Stem Cells, 2013. **31**(12): p. 2724-36.
61. T. Helsten, S. Elkin, E. Arthur, B.N. Tomson, J. Carter, and R. Kurzrock, *The FGFR Landscape in Cancer: Analysis of 4,853 Tumors by Next-Generation Sequencing.* Clin Cancer Res, 2016. **22**(1): p. 259-67.
62. M. Sun, G. Chi, P. Li, S. Lv, J. Xu, Z. Xu, Y. Xia, Y. Tan, J. Xu, L. Li, and Y. Li, *Effects of Matrix Stiffness on the Morphology, Adhesion, Proliferation and Osteogenic Differentiation of Mesenchymal Stem Cells.* Int J Med Sci, 2018. **15**(3): p. 257-268.
63. B. Venugopal, P. Mogha, J. Dhawan, and A. Majumder, *Cell density overrides the effect of substrate stiffness on human mesenchymal stem cells' morphology and proliferation.* Biomater Sci, 2018. **6**(5): p. 1109-1119.
64. Y.K. Chae, K. Ranganath, P.S. Hammerman, C. Vaklavas, N. Mohindra, A. Kalyan, M. Matsangou, R. Costa, B. Carneiro, V.M. Villaflor, M. Cristofanilli, and F.J. Giles, *Inhibition of the fibroblast growth factor receptor (FGFR) pathway: the current landscape and barriers to clinical application.* Oncotarget, 2017. **8**(9): p. 16052-16074.
65. D. Piasecka, M. Braun, K. Kitowska, K. Mieczkowski, R. Kordek, R. Sadej, and H. Romanska, *FGFs/FGFRs-dependent signalling in regulation of steroid hormone receptors - implications for therapy of luminal breast cancer.* J Exp Clin Cancer Res, 2019. **38**(1): p. 230.
66. N. Sobhani, A. Ianza, A. D'Angelo, G. Roviello, F. Giudici, M. Bortul, F. Zanconati, C. Bottin, and D. Generali, *Current Status of Fibroblast Growth Factor Receptor-Targeted Therapies in Breast Cancer.* Cells, 2018. **7**(7).
67. S.K. Pal, J.E. Rosenberg, J.H. Hoffman-Censits, R. Berger, D.I. Quinn, M.D. Galsky, J. Wolf, C. Dittrich, B. Keam, J.P. Delord, J.H.M. Schellens, G. Gravis, J. Medioni, P. Maroto, V. Sriuranpong, C. Charoentum, H.A. Burris, V. Grunwald, D. Petrylak, U. Vaishampayan, E. Gez, U. De Giorgi, J.L. Lee,

J. Voortman, S. Gupta, S. Sharma, A. Mortazavi, D.J. Vaughn, R. Isaacs, K. Parker, X. Chen, K. Yu, D. Porter, D. Graus Porta, and D.F. Bajorin, *Efficacy of BGJ398, a Fibroblast Growth Factor Receptor 1-3 Inhibitor, in Patients with Previously Treated Advanced Urothelial Carcinoma with FGFR3 Alterations.* Cancer Discov, 2018. **8**(7): p. 812-821.

68. C. Heinzle, Z. Erdem, J. Paur, B. Grasl-Kraupp, K. Holzmann, M. Grusch, W. Berger, and B. Marian, *Is fibroblast growth factor receptor 4 a suitable target of cancer therapy?* Curr Pharm Des, 2014. **20**(17): p. 2881-98.
69. L. Lang and Y. Teng, *Fibroblast Growth Factor Receptor 4 Targeting in Cancer: New Insights into Mechanisms and Therapeutic Strategies.* Cells, 2019. **8**(1).
70. J. Xie, M. Bao, S.M.C. Bruekers, and W.T.S. Huck, *Collagen Gels with Different Fibrillar Microarchitectures Elicit Different Cellular Responses.* ACS Appl Mater Interfaces, 2017. **9**(23): p. 19630-19637.
71. X. Cao, E. Ban, B.M. Baker, Y. Lin, J.A. Burdick, C.S. Chen, and V.B. Shenoy, *Multiscale model predicts increasing focal adhesion size with decreasing stiffness in fibrous matrices.* Proc Natl Acad Sci U S A, 2017. **114**(23): p. E4549-E4555.
72. B.M. Baker, B. Trappmann, W.Y. Wang, M.S. Sakar, I.L. Kim, V.B. Shenoy, J.A. Burdick, and C.S. Chen, *Cell-mediated fibre recruitment drives extracellular matrix mechanosensing in engineered fibrillar microenvironments.* Nat Mater, 2015. **14**(12): p. 1262-8.
73. J. Phelps, A. Sanati-Nezhad, M. Ungrin, N.A. Duncan, and A. Sen, *Bioprocessing of Mesenchymal Stem Cells and Their Derivatives: Toward Cell-Free Therapeutics.* Stem cells international, 2018. **2018**: p. 9415367-9415367.
74. C.R. Harrell, C. Fellabaum, N. Jovicic, V. Djonov, N. Arsenijevic, and V. Volarevic, *Molecular Mechanisms Responsible for Therapeutic Potential of Mesenchymal Stem Cell-Derived Secretome.* Cells, 2019. **8**(5): p. 467.
75. H.J. Kong, D. Kaigler, K. Kim, and D.J. Mooney, *Controlling rigidity and degradation of alginate hydrogels via molecular weight distribution.* Biomacromolecules, 2004. **5**(5): p. 1720-7.
76. M. Darnell, S. Young, L. Gu, N. Shah, E. Lippens, J. Weaver, G. Duda, and D. Mooney, *Substrate Stress-Relaxation Regulates Scaffold Remodeling and Bone Formation In Vivo.* Adv Healthc Mater, 2017. **6**(1).
77. M. Vicente-Manzanares, D.J. Webb, and A.R. Horwitz, *Cell migration at a glance.* Journal of Cell Science, 2005. **118**(21): p. 4917.
78. X. Trepat, Z. Chen, and K. Jacobson, *Cell migration.* Comprehensive Physiology, 2012. **2**(4): p. 2369-2392.
79. S. Soliman, S. Sant, J.W. Nichol, M. Khabiry, E. Traversa, and A. Khademhosseini, *Controlling the porosity of fibrous scaffolds by modulating the fiber diameter and packing density.* J Biomed Mater Res A, 2011. **96**(3): p. 566-74.
80. Y.M. Ju, J.S. Choi, A. Atala, J.J. Yoo, and S.J. Lee, *Bilayered scaffold for engineering cellularized blood vessels.* Biomaterials, 2010. **31**(15): p. 4313-21.
81. B.M. Baker, R.P. Shah, A.M. Silverstein, J.L. Esterhai, J.A. Burdick, and R.L. Mauck, *Sacrificial nanofibrous composites provide instruction without impediment and enable functional tissue formation.* Proc Natl Acad Sci U S A, 2012. **109**(35): p. 14176-81.
82. A. Guimaraes, A. Martins, E.D. Pinho, S. Faria, R.L. Reis, and N.M. Neves, *Solving cell infiltration limitations of electrospun nanofiber meshes for tissue engineering applications.* Nanomedicine (Lond), 2010. **5**(4): p. 539-54.
83. J. Voorneveld, A. Oosthuysen, T. Franz, P. Zilla, and D. Bezuidenhout, *Dual electrospinning with sacrificial fibers for engineered porosity and enhancement of tissue ingrowth.* J Biomed Mater Res B Appl Biomater, 2017. **105**(6): p. 1559-1572.

84. K. Wang, M. Xu, M. Zhu, H. Su, H. Wang, D. Kong, and L. Wang, *Creation of macropores in electrospun silk fibroin scaffolds using sacrificial PEO-microparticles to enhance cellular infiltration.* J Biomed Mater Res A, 2013. **101**(12): p. 3474-81.
85. C.A. Parent and P.N. Devreotes, *A cell's sense of direction.* Science, 1999. **284**(5415): p. 765-70.
86. A. Di Luca, C. Van Blitterswijk, and L. Moroni, *The osteochondral interface as a gradient tissue: from development to the fabrication of gradient scaffolds for regenerative medicine.* Birth Defects Res C Embryo Today, 2015. **105**(1): p. 34-52.
87. A.J. Sophia Fox, A. Bedi, and S.A. Rodeo, *The basic science of articular cartilage: structure, composition, and function.* Sports Health, 2009. **1**(6): p. 461-8.
88. H.J. Nieminen, T. Ylitalo, S. Karhula, J.P. Suuronen, S. Kauppinen, R. Serimaa, E. Haeggstrom, K.P. Pritzker, M. Valkealahti, P. Lehenkari, M. Finnila, and S. Saarakkala, *Determining collagen distribution in articular cartilage using contrast-enhanced micro-computed tomography.* Osteoarthritis Cartilage, 2015. **23**(9): p. 1613-21.
89. D.W. Buck, 2nd and G.A. Dumanian, *Bone biology and physiology: Part I. The fundamentals.* Plast Reconstr Surg, 2012. **129**(6): p. 1314-20.
90. A. Eichmann, F. Le Noble, M. Autiero, and P. Carmeliet, *Guidance of vascular and neural network formation.* Curr Opin Neurobiol, 2005. **15**(1): p. 108-15.
91. M. Tessier-Lavigne and C.S. Goodman, *The molecular biology of axon guidance.* Science, 1996. **274**(5290): p. 1123-33.
92. J. Goldman, K.A. Conley, A. Raehl, D.M. Bondy, B. Pytowski, M.A. Swartz, J.M. Rutkowski, D.B. Jaroch, and E.L. Ongstad, *Regulation of lymphatic capillary regeneration by interstitial flow in skin.* Am J Physiol Heart Circ Physiol, 2007. **292**(5): p. H2176-83.
93. M. Xue and C.J. Jackson, *Extracellular Matrix Reorganization During Wound Healing and Its Impact on Abnormal Scarring.* Adv Wound Care (New Rochelle), 2015. **4**(3): p. 119-136.
94. N.R. Gough, *Moving in 2D Versus 3D.* Science Signaling, 2010. **3**(138): p. ec274.
95. K.M. Yamada and M. Sixt, *Mechanisms of 3D cell migration.* Nature Reviews Molecular Cell Biology, 2019. **20**(12): p. 738-752.
96. M. Vinci, C. Box, and S.A. Eccles, *Three-dimensional (3D) tumor spheroid invasion assay.* Journal of visualized experiments : JoVE, 2015(99): p. e52686-e52686.
97. T.J. Puls, X. Tan, M. Husain, C.F. Whittington, M.L. Fishel, and S.L. Voytik-Harbin, *Development of a Novel 3D Tumor-tissue Invasion Model for High-throughput, High-content Phenotypic Drug Screening.* Scientific Reports, 2018. **8**(1): p. 13039.
98. V. Brekhman and G. Neufeld, *A novel asymmetric 3D in-vitro assay for the study of tumor cell invasion.* BMC Cancer, 2009. **9**(1): p. 415.
99. L.T. Vu, G. Jain, B.D. Veres, and P. Rajagopalan, *Cell migration on planar and three-dimensional matrices: a hydrogel-based perspective.* Tissue engineering. Part B, Reviews, 2015. **21**(1): p. 67-74.
100. B.M. Baker and C.S. Chen, *Deconstructing the third dimension: how 3D culture microenvironments alter cellular cues.* J Cell Sci, 2012. **125**(Pt 13): p. 3015-24.
101. A. Pathak and S. Kumar, *Biophysical regulation of tumor cell invasion: moving beyond matrix stiffness.* Integr Biol (Camb), 2011. **3**(4): p. 267-78.
102. J.A. Pedersen and M.A. Swartz, *Mechanobiology in the third dimension.* Ann Biomed Eng, 2005. **33**(11): p. 1469-90.
103. *Altering bacteriological plastic petri dishes for tissue culture use.* Public Health Rep, 1966. **81**(9): p. 843-4.
104. M.J. Lerman, J. Lembong, S. Muramoto, G. Gillen, and J.P. Fisher, *The Evolution of Polystyrene as a Cell Culture Material.* Tissue Eng Part B Rev, 2018. **24**(5): p. 359-372.

105. S.I. Fraley, Y. Feng, R. Krishnamurthy, D.H. Kim, A. Celedon, G.D. Longmore, and D. Wirtz, *A distinctive role for focal adhesion proteins in three-dimensional cell motility.* Nat Cell Biol, 2010. **12**(6): p. 598-604.

106. P.M. Davidson, C. Denais, M.C. Bakshi, and J. Lammerding, *Nuclear deformability constitutes a rate-limiting step during cell migration in 3-D environments.* Cell Mol Bioeng, 2014. **7**(3): p. 293-306.

107. T. Harada, J. Swift, J. Irianto, J.W. Shin, K.R. Spinler, A. Athirasala, R. Diegmiller, P.C. Dingal, I.L. Ivanovska, and D.E. Discher, *Nuclear lamin stiffness is a barrier to 3D migration, but softness can limit survival.* J Cell Biol, 2014. **204**(5): p. 669-82.

Chapter 10

Valorization

Jip Zonderland

Should a single PhD thesis always have direct tangible benefits to society?

Complicated, fundamental biological research on its own cannot be directly valorized and translated to societal gains. This does of course not mean the research is not valuable to society in the long term. Fundamental research leading to the discovery of a protein in jellyfish that emits green light under UV light might have been hard to valorize when initially discovered in 1962. Years later, in 1994, this green fluorescent protein (GFP) was used to tag individual cells and proteins and revolutionized almost every field of biological research, resulting in the Nobel prize in 2008[1]. This is a classic among many examples, which question the need to immediately valorize fundamental research. The requirement for a direct societal and functional output of research seems productive, but, as argued for in this thesis, could actually prove to be counterproductive if this steers research away from much-needed fundamental research. A fundamental understanding of biological processes is required to design smart scaffolds for tissue engineering. From the build-up of such knowledge to results from practical use will exceed the length of a single PhD thesis, but could benefit society greatly in the long term.

Besides the fundamental research done in this thesis, chapter 8 describes the hydrocup, which could have direct practical applications. The hydrocup can be used to fix cell-laden or drug releasing hydrogels in place *in vivo* and the opportunities to commercialize these scaffolds are explored below.

Clinical relevance

Cytokines released by human mesenchymal stromal cells (hMSCs) have beneficial effects, including angiogenesis, immunomodulation, supporting tissue regeneration by local stem cells, and anti-scarring[2-4]. For this reason, MSCs are currently being widely used in clinical trials as 'secretion factories' in a wide variety of diseases[5-7]. The vast amount of ongoing clinical trials can be visualized by searching "mesenchymal stem cells" or "mesenchymal stromal cells" on clinicaltrials.gov, together resulting in over 1200 ongoing or completed clinical trials (January 2020). Many clinical trials inject MSCs, either intra-venously or directly in the tissue. However, these injected cells are difficult to hold in a specific place. On top of this, cells often die shortly after implantation by injection[8-10]. If hMSCs are to be used as secretion factories of biological factors to aid local regeneration of a specific tissue or immunomodulation, hMSCs should be maintained alive and in a specific location. For this purpose, we developed the hydrocup, a hollow electrospun (ESP) scaffold to deliver cells *in vivo*.

The hydrocup

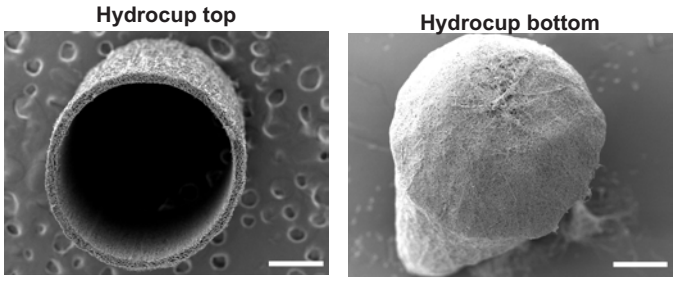

Figure 1. Scanning electron microscopy images of the hydrocup. The open end through which the hydrogel can be loaded into the hydrocup and the closed bottom that keeps the hydrogel in the hydrocup when being loaded are displayed. Scale bars are 500 µm.

The hydrocup was created by electrospinning a polymer solution on the open end of a rotating mandrel. This creates a hollow ESP scaffold with one open and one closed end (Figure 1). A hydrogel can be pipetted through the open end while the closed bottom end prevents the uncrosslinked hydrogel from leaking out. The hydrogel can then be crosslinked inside the cup and the top end is closed with sutures. The ESP scaffold wall is highly porous and, therefore, allows for cells to secrete factors out of the hydrocup, and for nutrients to diffuse in to maintain cells alive in the hydrocup. In chapter 8, we demonstrate that hMSCs release functional factors from the hydrocup and stay alive for at least 28 days. Also, 6 weeks after *in vivo* delivery, the hydrocup remained in place with the hydrogel inside. These proof of principle experiments show that the concept of the hydrocup for *in vivo* fixation of hydrogels works. However, functional *in vivo* experiments were not performed and should be the next step.

Potential applications

MSCs as secretory factories and drug releasing hydrogels are being used as potential treatment for a wide variety of diseases[2-4, 11]. The hydrocups can in principle be used for any application where cells or drug releasing hydrogels needs to be delivered and stay in a specific location. Applications of hMSCs for systemic release of immunomodulatory factors through the whole body, for example, are therefore not suited to benefit from hydrocups. Other applications where MSCs are now being delivered systemically to repair a specific tissue, such as the intervertebral disc[12], or myocardium[13], could benefit from a more local release of MSC-secreted factors. Applications where MSCs are delivered locally and are expected to stay in place by direct injection could also benefit from the hydrocup, such as heart[14], kidney[15] or radiation burns[16]. Another benefit of the hydrocups as opposed to systemic or local injection of MSCs is that the hydrocup could be removed. Unless transplanted cells die, the cells are impossible to remove from the local tissue and will therefore keep affecting the

tissue, even after regeneration would be complete. This could not be desired in tissues where MSCs normally don't reside in large numbers. To prevent potential complications, an MSC-laden hydrocup could be implanted and removed after sufficient regeneration. As briefly described, there is a wide range of potential applications. For each application, however, the efficacy of the treatment remains to be tested.

Competition

While hydrogels can be directly implanted, to our knowledge there is currently no scaffold used to fix hydrogels in place *in vivo*. Scaffolds have been developed for *in vivo* delivery of cell aggregates ([17-20] to name a few examples), but not specifically for hydrogels. Even though these cell aggregate-holding-scaffolds could theoretically also hold hydrogels, the wells are much smaller than the 1.8 mm inner-diameter and up to multiple cm long hydrocups that could be fully filled with hydrogels. Because of the large hollow interior, the hydrocup could deliver large quantities of hydrogel and cells. The lack of direct competition is a great benefit for business opportunities, but also means that the benefits of such a system still need to be proven.

Further improvements

Depending on the application of the hydrocup, further improvements could be made to the hydrocup. As described in chapter 8, the hMSCs are able to escape to the outside of the hydrocup. In chapter 6, we found that the ESP scaffold polymer solution used to create the cups indeed allows for cell migration through the scaffolds. By decreasing the ESP fiber diameter from 3 µm to 1 µm or less, the escape of MSCs could be prevent. In addition, this could prevent host cells from infiltrating the hydrocups and interacting with the MSCs.

For each application, the MSC secretome should be analyzed and the hydrogel properties should be optimized. Depending on the application, other improvements could be made to the hydrocup, such as increasing mechanical properties to protect the hydrogel, or increase the interior volume to increase total gel volume.

The hydrocup is currently made from 300PEOT55PBT45, which is not approved for clinical use. To ease the direct application of the hydrocup, it could be produced from clinically approved polymers, such as polycaprolactone (already available in medical grade).

The production process is currently quite labor intensive. An experienced user can produce 10-15 hydrocups per hour. For commercialization, this process should be fully automated. The electrospinning jet has to be positioned in a precise location, so that it hits the open end of the rotating mandrel at the right spot. However, each time the electrospinning jet started to produce a new cup, the position of the jet changes. This makes full automation difficult and required a manual process by an experienced user. Automation processes could make use of a camera focused on the electrospinning jet to calculate the position to create the hydrocup. Such an automated system could increase both scalability and reproducibility.

Another labor-intensive part of the hydrocup process is the closing of the open end of the hydrocup after loading the hydrogel. This is currently done by closing a suture tightly around each hydrocup. To improve scalability, this should also be automated.

Conclusion

The hydrocup is the first scaffold developed for *in vivo* delivery and fixation of cell-laden or drug-releasing hydrogels. It has a wide range of potential applications and the proof-of-principle experiments in chapter 8 show promising initial results. Functional *in vivo* tests should now be performed, for which the hydrocup and contained hydrogel could be modified for the specific purpose. In parallel, the production process should be automated to allow scalability. With promising *in vivo* results and a scalable production process, the hydrocups could be used to treat a wide variety of diseases and be a viable commercial opportunity.

References

1. S.J. Remington, *Green fluorescent protein: a perspective.* Protein science : a publication of the Protein Society, 2011. **20**(9): p. 1509-1519.
2. J. Xi, X. Yan, J. Zhou, W. Yue, and X. Pei, *Mesenchymal stem cells in tissue repairing and regeneration: Progress and future.* Burns Trauma, 2013. **1**(1): p. 13-20.
3. Y. Zhou, Y. Yamamoto, Z. Xiao, and T. Ochiya, *The Immunomodulatory Functions of Mesenchymal Stromal/Stem Cells Mediated via Paracrine Activity.* J Clin Med, 2019. **8**(7).
4. S. Meirelles Lda, A.M. Fontes, D.T. Covas, and A.I. Caplan, *Mechanisms involved in the therapeutic properties of mesenchymal stem cells.* Cytokine Growth Factor Rev, 2009. **20**(5-6): p. 419-27.
5. M. Wang, Q. Yuan, and L. Xie, *Mesenchymal Stem Cell-Based Immunomodulation: Properties and Clinical Application.* Stem Cells Int, 2018. **2018**: p. 3057624.
6. P. Saeedi, R. Halabian, and A.A. Imani Fooladi, *A revealing review of mesenchymal stem cells therapy, clinical perspectives and Modification strategies.* Stem Cell Investig, 2019. **6**: p. 34.
7. T. Squillaro, G. Peluso, and U. Galderisi, *Clinical Trials With Mesenchymal Stem Cells: An Update.* Cell Transplant, 2016. **25**(5): p. 829-48.
8. M. Zhang, D. Methot, V. Poppa, Y. Fujio, K. Walsh, and C.E. Murry, *Cardiomyocyte grafting for cardiac repair: graft cell death and anti-death strategies.* J Mol Cell Cardiol, 2001. **33**(5): p. 907-21.
9. C.E. Sortwell, M.R. Pitzer, and T.J. Collier, *Time course of apoptotic cell death within mesencephalic cell suspension grafts: implications for improving grafted dopamine neuron survival.* Exp Neurol, 2000. **165**(2): p. 268-77.
10. K. Malliaras, M. Kreke, and E. Marban, *The stuttering progress of cell therapy for heart disease.* Clin Pharmacol Ther, 2011. **90**(4): p. 532-41.
11. R. Narayanaswamy and V.P. Torchilin, *Hydrogels and Their Applications in Targeted Drug Delivery.* Molecules (Basel, Switzerland), 2019. **24**(3): p. 603.
12. C. Cunha, C.R. Almeida, M.I. Almeida, A.M. Silva, M. Molinos, S. Lamas, C.L. Pereira, G.Q. Teixeira, A.T. Monteiro, S.G. Santos, R.M. Goncalves, and M.A. Barbosa, *Systemic Delivery of Bone Marrow Mesenchymal Stem Cells for In Situ Intervertebral Disc Regeneration.* Stem Cells Transl Med, 2017. **6**(3): p. 1029-1039.
13. I.M. Barbash, P. Chouraqui, J. Baron, M.S. Feinberg, S. Etzion, A. Tessone, L. Miller, E. Guetta, D. Zipori, L.H. Kedes, R.A. Kloner, and J. Leor, *Systemic delivery of bone marrow-derived mesenchymal stem cells to the infarcted myocardium: feasibility, cell migration, and body distribution.* Circulation, 2003. **108**(7): p. 863-8.
14. V. Karantalis, D.L. DiFede, G. Gerstenblith, S. Pham, J. Symes, J.P. Zambrano, J. Fishman, P. Pattany, I. McNiece, J. Conte, S. Schulman, K. Wu, A. Shah, E. Breton, J. Davis-Sproul, R. Schwarz, G. Feigenbaum, M. Mushtaq, V.Y. Suncion, A.C. Lardo, I. Borrello, A. Mendizabal, T.Z. Karas, J. Byrnes, M. Lowery, A.W. Heldman, and J.M. Hare, *Autologous mesenchymal stem cells produce concordant improvements in regional function, tissue perfusion, and fibrotic burden when administered to patients undergoing coronary artery bypass grafting: The Prospective Randomized Study of Mesenchymal Stem Cell Therapy in Patients Undergoing Cardiac Surgery (PROMETHEUS) trial.* Circ Res, 2014. **114**(8): p. 1302-10.
15. M. Gregorini, V. Corradetti, E.F. Pattonieri, C. Rocca, S. Milanesi, A. Peloso, S. Canevari, L. De Cecco, M. Dugo, M.A. Avanzini, M. Mantelli, M. Maestri, P. Esposito, S. Bruno, C. Libetta, A. Dal Canton, and T. Rampino, *Perfusion of isolated rat kidney with Mesenchymal Stromal Cells/Extracellular Vesicles prevents ischaemic injury.* J Cell Mol Med, 2017. **21**(12): p. 3381-3393.
16. J.J. Lataillade, C. Doucet, E. Bey, H. Carsin, C. Huet, I. Clairand, J.F. Bottollier-Depois, A. Chapel, I. Ernou, M. Gourven, L. Boutin, A. Hayden, C. Carcamo, E. Buglova, M. Joussemet, T. de Revel, and P.

Gourmelon, *New approach to radiation burn treatment by dosimetry-guided surgery combined with autologous mesenchymal stem cell therapy.* Regen Med, 2007. **2**(5): p. 785-94.

17. G.A. Higuera, J.A. Hendriks, J. van Dalum, L. Wu, R. Schotel, L. Moreira-Teixeira, M. van den Doel, J.C. Leijten, J. Riesle, M. Karperien, C.A. van Blitterswijk, and L. Moroni, *In vivo screening of extracellular matrix components produced under multiple experimental conditions implanted in one animal.* Integr Biol (Camb), 2013. **5**(6): p. 889-98.
18. H. Blomeier, X. Zhang, C. Rives, M. Brissova, E. Hughes, M. Baker, A.C. Powers, D.B. Kaufman, L.D. Shea, and W.L. Lowe, Jr., *Polymer scaffolds as synthetic microenvironments for extrahepatic islet transplantation.* Transplantation, 2006. **82**(4): p. 452-9.
19. T. Kin, J.J. O'Neil, R. Pawlick, G.S. Korbutt, A.M. Shapiro, and J.R. Lakey, *The use of an approved biodegradable polymer scaffold as a solid support system for improvement of islet engraftment.* Artif Organs, 2008. **32**(12): p. 990-3.
20. R. Guo, C.L. Ward, J.M. Davidson, C.L. Duvall, J.C. Wenke, and S.A. Guelcher, *A transient cell-shielding method for viable MSC delivery within hydrophobic scaffolds polymerized in situ.* Biomaterials, 2015. **54**: p. 21-33.

Summary

Most tissues in the human body have a remarkable ability to regenerate. However, when damage is severe and large sections of any tissue in our body are missing, regeneration is limited. The field of tissue engineering attempts to create scaffolds to fill up this empty space and instruct cells to create new functional tissue. The properties of these scaffolds, such as the material, stiffness, architecture, topography and capacity to present specific proteins, among others, all greatly influence cell behavior. Therefore, to effectively create new tissues, a thorough understanding of how these scaffold properties influence cell behavior is crucial. In this thesis, the focus has been put on bone-marrow derived human mesenchymal stromal cells (hMSCs), which can differentiate to bone, cartilage and fat tissue. This differentiation is highly dependent on mechanobiology, the process of translating mechanical stimuli, such as those from scaffold properties, to biological signals. While mechanobiology is relatively well studied in standard 2D culture platforms, increasing evidence shows that the role and regulation of these proteins is very different in 3D. Understanding how these proteins influence hMSC behavior in 3D is critical, as any tissue engineering approach will expose cells to a 3D environment. In chapter 2 of this thesis, the current literature about mechanobiology in 3D is summarized. Most of the available literature about 3D mechanobiology has been researched in hydrogels. While this has led to valuable insights, most tissue engineering approaches use different kinds of scaffolds made from stiffer materials. In chapter 3, we have looked at how important mechanobiological proteins are regulated differently in 3D scaffolds made from stiff materials. Specifically, we've found that actin-myosin, zyxin, lamin A/C and YAP all exhibit lower expression or activation in 3D than in 2D, on the same materials. Interestingly, while this lower expression profile predicts adipogenic differentiation in 2D, in 3D we obtained efficient osteogenic differentiation, highlighting the difference in the roles of these proteins in 3D. In chapter 4 and 5, we followed up on this research by investigating the role of mechanobiology in cell survival and proliferation in 3D. In chapter 4, we found that the low expression of actin-myosin and zyxin found in chapter 3 greatly influenced the secretion of STC1, an important cell survival protein. Chapter 5 describes how the 3D environment of electrospun (ESP) scaffolds reduce the expression of an important receptor for proliferation, FGFR1, again through actin-myosin. Together, chapter 3-5 build fundamental knowledge about how the 3D environment of common tissue engineering scaffolds influences cell behavior through mechanobiology.

In chapter 6, we have optimized an ESP scaffold to allow for robust cell infiltration. The current 3D migration research has been done mostly in hydrogels. The fibrous scaffold developed in chapter 6, made from stiff materials, can be used to advance fundamental research on 3D migration. In addition, these scaffolds could be used for tissue engineering applications, as it allowed deep cell infiltration and tissue formation *in vivo*. To aid both the fundamental research and the tissue engineering applications in ESP scaffolds, in chapter 7

we developed several methods to include gradients in ESP scaffolds. These gradients could be used to guide and investigate 3D cell migration. Lastly, chapter 8 describes the hydrocup, a hollow ESP scaffold that is used to deliver cell-laden hydrogels *in vivo*. The hydrocup gives extra mechanical support to the hydrogels and partly shields it from the surrounding tissue. It can be used to investigate how environmental properties of the hydrogel affect the hMSC secretome and its effects *in vivo*.

In conclusion, this thesis adds fundamental knowledge to the understanding of cell behavior in 3D and has developed new scaffolds to further study 3D cell- migration and activity. In addition, different scaffolds are developed that could be used for regenerative medicine approaches. Together, the data in this thesis can be a steppingstone for new fundamental research and aid the smarter design of tissue engineering constructs.

Samenvatting

De meeste weefsels in het menselijk lichaam kunnen heel goed regenereren. Wanneer er echter grote stukken weefsel beschadigd zijn, is het herstel gelimiteerd. In het veld van "tissue engineering" wordt geprobeerd om scaffolds te maken die het beschadigde weefsel kunnen vervangen. Deze scaffolds moeten cellen instrueren om nieuw weefsel aan te maken. De eigenschappen van de scaffolds, zoals het materiaal, de stijfheid, de architectuur, de topografie en de mogelijkheid om specifieke eiwitten te presenteren, hebben allemaal grote invloed op het gedrag van de cellen die ermee in aanraking komen. Het is daarom van essentieel belang om goed te begrijpen hoe cellen reageren op de verschillende eigenschappen van de scaffolds. In deze thesis ligt de focus op uit beenmerg geïsoleerde menselijke mesenchymale stromacellen (MSCs), die kunnen differentiëren tot bot-, kraakbeen- of vetweefsel. Deze differentiatie wordt sterk beïnvloed door mechanobiologie, het proces dat mechanische stimuli, zoals de eigenschappen van de scaffolds, vertaalt naar biologische signalen. De mechanobiologie is relatief goed bestudeerd in standaard 2D kweekschalen, maar er komt steeds meer bewijs dat de regulatie en rol van deze eiwitten anders is in 3D kweken. Het is cruciaal om te begrijpen hoe deze eiwitten MSCs beïnvloeden in 3D, omdat cellen in scaffolds uiteindelijk altijd in een 3D omgeving terecht komen. In hoofdstuk 2 van deze thesis is de huidige literatuur over mechanobiologie in 3D samengevat. De meeste literatuur over 3D mechanobiologie is onderzocht in hydrogels. Dit heeft tot waardevolle inzichten geleid, maar de meest gebruikte tissue engineering scaffolds zijn gemaakt van stijvere materialen. In hoofdstuk 3 hebben we gekeken naar hoe belangrijke mechanobiologische eiwitten gereguleerd zijn in deze van stijve materialen gemaakte 3D scaffolds. We hebben gevonden dat actine-myosine, zyxin, lamin A/C en YAP allemaal minder tot expressie komen of geactiveerd worden in 3D kweken dan in 2D kweken van dezelfde materialen. Terwijl dit lagere expressie profiel een differentiatie naar vet zou voorspellen in 2D, differentieerde de MSCs in 3D nog efficiënt naar bot. Dit geeft de verschillende rollen van deze eiwitten weer in 3D ten opzichte van 2D. In hoofdstuk 4 en 5 zijn we verder gegaan op dit onderzoek en hebben we de rol van mechanobiologie onderzocht in de overleving en proliferatie van MSCs in 3D. In hoofdstuk 4 hebben we gevonden dat de secretie van STC1, een belangrijk eiwit voor overleving van cellen, sterk omhooggaat in 3D door de lage expressie van actine-myosine en zyxin die we in hoofdstuk 3 gevonden hebben. In hoofdstuk 5 wordt beschreven hoe de 3D omgeving van scaffolds gemaakt met electrospinning (ESP scaffolds) de expressie verlaagt van een belangrijke proliferatie receptor, FGFR1, wederom door actine-myosine. Samen voegen hoofdstuk 3-5 fundamentele kennis toe aan hoe mechanobiologie het gedrag van cellen beïnvloedt in de 3D omgeving van veel gebruikte tissue engineering scaffolds.

In hoofdstuk 6 hebben we ESP scaffolds ontwikkeld waar cellen diep in kunnen infiltreren. Het huidige onderzoek naar 3D migratie is vooral gedaan in hydrogels. De ESP scaffold van

hoofdstuk 6 is gemaakt van stijve materialen en kan gebruikt worden om fundamenteel onderzoek te doen naar 3D migratie. We hebben ook laten zien dat na implantatie *in vivo*, cellen diep kunnen infiltreren en nieuw weefsel kunnen vormen in deze scaffolds, waardoor deze scaffolds ook gebruikt kunnen worden voor tissue engineering applicaties. Om zowel fundamenteel onderzoek als tissue engineering te ondersteunen hebben we in hoofdstuk 7 meerdere methodes ontwikkeld om gradiënten te maken in ESP scaffolds. Deze gradiënten kunnen gebruikt worden om cellen in een richting te sturen en 3D migratie te onderzoeken. In hoofdstuk 8 hebben we de hydrocup ontwikkeld, een holle ESP scaffold die gebruikt kan worden om hydrogels te implanteren. De hydrocup geeft extra mechanische weerstand aan de zachte hydrogels en beschermt ze gedeeltelijk van het omringende weefsel. Het kan gebruikt worden om het effect van hydrogel-eigenschappen op het MSC secretome *in vivo* te onderzoeken.

Deze thesis voegt fundamentele kennis toe aan hoe het gedrag van cellen wordt beïnvloed in 3D. Daarnaast hebben we scaffolds ontwikkeld die zowel gebruikt kunnen worden om 3D cel-migratie en activiteit te onderzoeken, als voor tissue engineering applicaties. Samen kan de data in dez e thesis een basis zijn voor nieuw fundamenteel onderzoek en kan het helpen om slimmere tissue engineering scaffolds te ontwikkelen.

List of publications

Peer reviewed papers

Dimensionality changes actin network through lamin A/C and zyxin, Jip Zonderland, Ivan Lorenzo Moldero, Shivesh Anand, Carlos Mota, Lorenzo Moroni. *Biomaterials, 2020.*

A quantitative method to analyze F-Actin distribution in cells, Jip Zonderland, Paul Wieringa, Lorenzo Moroni. *Methods X, 2019.*

Mechanosensitive regulation of stanniocalcin-1 by zyxin and actin-myosin in human mesenchymal stromal cells, Jip Zonderland*, David Boaventura Gomes*, Yves Palada, Ivan Lorenzo Moldero, Sandra Camarero Espinosa, Lorenzo Moroni. *These authors contributed equally to this work. *Stem Cells, 2020.*

Mechanosensitive regulation of FGFR1 through the MRTF-SRF pathway, Jip Zonderland, Silvia Rezzola, Lorenzo Moroni. *Under review at Communications Biology.*

Full cell infiltration and thick tissue formation *in vivo* in tailored electrospun scaffolds, Jip Zonderland, Silvia Rezzola, David Boaventura Gomes, Sandra Camarero Espinosa, Ana Henriques Ferreira Lourenço, Andrada Serafim, Izabela Cristina Stancu, David Koper, Hong Liu, Pamela Habibovic, Peter Kessler, Marloes Peters, Peter Emans, Nicole Bouvy, Paul Wieringa, Lorenzo Moroni. *Manuscript in preparation.*

Fiber diameter, porosity and functional group gradients in electrospun scaffolds, Jip Zonderland, Silvia Rezzola, Paul Wieringa, Lorenzo Moroni. *Biomedical materials, 2020.*

The hydrocup: a hollow electrospun scaffold for *in vivo* hydrogel delivery, Jip Zonderland*, David Boaventura Gomes*, Silvia Rezzola, Ana Henriques Ferreira Lourenço, Hong Liu, Marloes Peters, Peter Emans, Nicole Bouvy, Paul Wieringa, Sandra Camarero Espinosa, Lorenzo Moroni. * These authors contributed equally to this work. *Manuscript in preparation.*

Conference presentations

A novel platform for 3D expansion and migration of hMSCs, Oral presentation, NBTE, Lunteren, The Netherlands, 2017.

A novel ECM mimicking migration platform, Oral presentation, ESB, Maastricht, The Netherlands, 2018.

The regulation of lamin A/C in a 3D environment, Poster presentation, TERMIS-World, Kyoto, Japan, 2018

Interplay between Lamin A/C and Zyxin Shapes Actin Network in 3D, Oral presentation, TERMIS-EU, Rhodos, Greece, 2019

Acknowledgements

First of all, I would like to thank Lavinia. Although you have contributed the least of all people mentioned here to the scientific content of this thesis, you have contributed the most to making these four years a great experience. Thank you for being so patient and supportive, and for always being there at the end of a very long train ride.

Lorenzo, you have been the best supervisor I could hope for. You have always been available for questions, discussions and help with any problem I've encountered during these four years. While this is a great attribute for anyone, it's even more impressive knowing that you have 20+ other students and 100+ other things to do. Thank you for always being there, for small and big problems. You've always pushed me to do more and kept me free to decide where I focused on. You've taught me a lot over the years. Thank you for giving me freedom to explore, while encouraging me to do more and always being there to guide. Thank you for being my supervisor.

David, my paranymph, during these four years of working closely together, you've become one of my best friends. Besides the two projects we've done together, I feel like we've done the whole PhD together.
Daniel, my other paranymph and good friend, thank you for being great company these four years. Although we've climbed more together than worked together, you've taught me many things about the material side of tissue engineering.
Thank you both for being there for work discussions, lunches, dinners, sports, fun, bullshit and gossip. Thank you both for being great friends and for the many good moments these four years.

Ivan, you were there at the very start of my PhD to guide me and you've taught me many things. Thank you for being a mentor, the fun times, sharing frustrations, jeans-yoga and the great pleasure of working with you.

Paul, Carlos and Matt, thank you for all the help, always answering the many questions I've asked you, valuable insights and guiding me along the way.

A special thanks to my colleagues and friends who've made these four years great and have helped me along the way: Fiona, Dani, Victor, Jasia, Clarissa, Afonso, Rabeil, Mariana and Michela.

To all other MERLN colleagues, thank you for creating a nice working environment and thank you for all the help you've given me in these four years.

Biography

Jip Zonderland was born on the 12th of September in Delft. After finishing high school, he started with a Bachelor of Applied Science in Biology and Medical Laboratory Science. His bachelor thesis research was about B-cell recombination and was nominated for best thesis of the year at the Hogeschool Leiden. He then started the Molecular Medicine research master at the Erasmus MC. As part of his thesis research he went to Stanford University to be trained in *ex vivo* muscle force measurements. He then implemented this new technique at the Erasmus MC to study develop a method for muscle stem cell transplantations in the diaphragm. He continued in academia and started a PhD in biomedical engineering at Maastricht University under the supervision of Prof. Lorenzo Moroni. This thesis describes the results of his PhD work.